

Electronic Thesis and Dissertation Repository

8-10-2022 2:15 PM

Prefrontal coding of naturalistic working memory: Mechanisms during normal maintenance and modelled disease

Megan P. Roussy, *The University of Western Ontario*

Supervisor: Martinez-Trujillo, Julio C, *The University of Western Ontario*

Co-Supervisor: Palaniyappan, L, *McGill University*

A thesis submitted in partial fulfillment of the requirements for the Doctor of Philosophy degree in Neuroscience

© Megan P. Roussy 2022

Follow this and additional works at: <https://ir.lib.uwo.ca/etd>



Part of the [Cognitive Neuroscience Commons](#), [Pharmacology Commons](#), [Systems and Integrative Physiology Commons](#), and the [Systems Neuroscience Commons](#)

Recommended Citation

Roussy, Megan P., "Prefrontal coding of naturalistic working memory: Mechanisms during normal maintenance and modelled disease" (2022). *Electronic Thesis and Dissertation Repository*. 8706. <https://ir.lib.uwo.ca/etd/8706>

This Dissertation/Thesis is brought to you for free and open access by Scholarship@Western. It has been accepted for inclusion in Electronic Thesis and Dissertation Repository by an authorized administrator of Scholarship@Western. For more information, please contact wlsadmin@uwo.ca.

Abstract

Neural activity in the primate lateral prefrontal cortex (LPFC) has been causally linked to working memory (WM) — the brief maintenance and mental manipulation of information. Primates use WM to perform tasks in complex contexts; however, neural mechanisms of WM and the pathophysiology related to WM deficits have traditionally been studied using simple tasks that deviate from naturalistic conditions. This raises the question, how is WM processed in naturalistic conditions? To explore this, I trained two macaque monkeys on a spatial WM task set in a naturalistic virtual environment. During the task, a target was presented in 1 of 9 locations in a virtual arena. The target then disappeared and following a 2-second delay period, subjects navigated to the cued target location using a joystick. I recorded single neuron activity using two 96-channel Utah Arrays implanted in LPFC (areas 9/46 & 8a).

During this task, single neurons are spatially selective for remembered target locations and neural populations contain large amounts of information about the target location over the duration of the task. Neural coding for WM is robust and distinct from signals related to perception and eye movement. Using ketamine to model the pathophysiology of schizophrenia, I demonstrate drastic deficits in WM performance. The decrease in performance is related to differential effects on putative excitatory and inhibitory neurons. Inhibitory neurons decrease their firing rate for their preferred location after ketamine injection, thus disinhibiting excitatory cells, resulting in distorted WM representations. Finally, I demonstrate a new neural code for maintaining WM in naturalistic conditions. Precise temporal patterns of population activity contain large amounts of information about target location and target trajectories in our virtual task. Ketamine distorts these neural sequences and their relationship to behavior. Together, these findings demonstrate that the LPFC relies on a robust neural code that uses firing rate and temporal information to maintain WM representations in the presence of incoming sensory signals and eye movement. These findings detail how the primate LPFC encodes WM representations in naturalistic conditions and models how WM deficits may arise in day-to-day life.

Keywords

Working Memory, Perception, Virtual Reality, Prefrontal Cortex, Non-Human Primate, Ketamine, Schizophrenia

Summary for Lay Audience

Working memory is the cognitive process that allows us to maintain information from our environment for the span of seconds to a few minutes. For example, if I were to read you a phone number to dial, you must be able to briefly remember the number to successfully make the call. However, after the call is made and the information is no longer relevant to your task, the number will fade from memory.

For this thesis, I developed a working memory task set in a virtual environment that is meant to resemble how we use working memory in real life – in complex and dynamic environments. During this task, I recorded from neurons in the prefrontal cortex of macaque monkeys, an area clearly involved in working memory.

I demonstrate that neurons in the prefrontal cortex robustly represent the locations of targets after they disappeared. Moreover, neurons that represent working memory information are separate from neurons that represent eye position and visual perception, allowing for robust memory despite eye movement or potential distractors in the environment. Next, I explore how naturalistic working memory is affected by ketamine, a drug that mimics the symptoms of schizophrenia. Here, I show that ketamine reduces the specificity of neurons for representing target location so that neurons are similarly active for all targets – limiting the ability of animals to precisely remember a location. Finally, I explore the possibility that not only is the number of action potentials that neurons fire important, but also when the action potentials are fired. I explore temporal patterns of neural activity and show that single neurons fire around the same time in each trial and that the population of neurons form complex temporal patterns that were closely related to naturalistic working memory behavior.

Overall, I demonstrate how the brain processes working memory in naturalistic conditions and how working memory deficits may occur in patients in complex environments that reflect how they would use working memory in real life.

Co-Authorship Statement

I conducted the research reported in this dissertation under the guidance of my supervisors Drs. Julio Martinez-Trujillo and Lena Palaniyappan. I sincerely thank Drs. Rogelio Luna, Roberto Gulli, and Lyle Muller for their mentorship and acknowledge their important contribution in guiding this research. I was supported through a master's scholarship from NSERC, a doctoral scholarship from NSERC (CGS-D), and a research scholarship from The Jonathan and Joshua Memorial Fund. The material presented in this dissertation has either been included in published work (Chapters 1, 2, and 3) or are in work in preparation for submission (Chapter 4). I use 'we' instead of 'I' within my data chapters to acknowledge the contributions of my research team.

Chapter 1: Megan Roussy, Diego Mendoza-Halliday, Julio C. Martinez-Trujillo. (2021). Neural Substrates of Visual Perception and Working Memory: Two Sides of the Same Coin or Two Different Coins? *Frontiers in Neural Circuits*

Sections of chapter 1 are from a recent review paper. I led this paper and was actively involved in all aspects of the project including literature review, figure creation, and manuscript writing. DM-H aided in figure creation and helped to review and edit the manuscript. JCM-T aided in figure creation and manuscript writing.

Chapter 2: Megan Roussy, Benjamin Corrigan, Rogelio Luna, Roberto A. Gulli, Adam J. Sachs, Lena Palaniyappan, Julio C. Martinez-Trujillo. (2022). Stable working memory and perceptual representations in macaque lateral prefrontal cortex during naturalistic vision. *bioRxiv, in Review at Journal of Neuroscience*

I was the lead of this study and was actively involved in all aspects of the project including experimental design, animal training, surgical planning, data collection, data processing, data analysis, figure creation, and manuscript writing. BC aided in animal training, data analysis, and manuscript editing. RL aided in animal training and data collection. RAG aided in experimental design, animal training, and surgical planning. AJS surgically implanted the Utah Array electrodes in both animals. LP aided in experimental design and manuscript editing. JCMT aided in experimental design, manuscript writing, and editing.

Chapter 3: Megan Roussy, Rogelio Luna, Lyndon Duong, Benjamin Corrigan, Roberto A. Gulli, Ramon Nogueira, Rubén Moreno-Bote, Adam J. Sachs, Lena Palaniyappan, Julio C. Martinez-Trujillo. (2021). Ketamine disrupts naturalistic coding of working memory in primate lateral prefrontal cortex networks. *Molecular Psychiatry*

I was the lead of this study and was actively involved in all aspects of the project including experimental design, animal training, surgical planning, data collection, data processing, data analysis, figure creation, and manuscript writing. RL aided in animal training and data collection. LD aided in data analysis. BC aided in animal training, and manuscript editing. RAG aided in experimental design, animal training, and surgical planning. RN aided in machine learning design and method development. RM-B aided in machine learning design and method development. AJS surgically implanted the Utah Array electrodes in both animals. LP aided in experimental design and manuscript editing. JCMT aided in experimental design, manuscript writing, and editing.

Chapter 4: Megan Roussy, Alexandra Busch, Rogelio Luna, Matthew L. Leavitt, Maryam H. Mofrad, Roberto A. Gulli, Benjamin Corrigan, Ján Mináč, Adam J. Sachs, Lena Palaniyappan, Lyle Muller, Julio C. Martinez-Trujillo

I was the lead of this study and was actively involved in all aspects of the project including experimental design, animal training, surgical planning, data collection, data processing, data analysis, figure creation, and manuscript writing. AB developed the novel dimensionality reduction analysis used in this study and aided in data analysis, figure creation, and manuscript writing. RL aided in animal training and data collection. MLL collected the ODR dataset. MHM aided in analysis design. RAG aided in experimental design, animal training, and surgical planning. BC aided in animal training, and manuscript editing. JM aided in the development of novel analyses. AJS surgically implanted the Utah Array electrodes in both animals. LP aided in experimental design and manuscript editing. LM aided in the development of novel analyses, data analysis, and manuscript writing. JCMT aided in experimental design, and manuscript writing.

Acknowledgments

The research in this dissertation would not exist without the support and dedication of my research team. I would like to recognize the critical roles played by my supervisors, lab mates, friends, and family.

- Julio Martinez-Trujillo for his mentorship and guidance and most importantly, his endless supply of excitement and enthusiasm for science.
- Lena Palaniyappan for taking a chance on me as his first PhD student in Canada and his keen insights into psychiatry
- My lab 'family' Borna, Ben, Rob, Diego, Maryam, Lyndon, Rogelio, Mat, and many others who have significantly enriched my PhD experience
- I would like to acknowledge the veterinary technicians, Kim Thomaes, Rhonda Kersten, and Kristy Gibbs who endlessly supported my research and took exceptional care of my animals. Our experiments would not have been possible without your hard work and dedication.
- My many co-authors for their contributions to this work and for sharing their expertise and knowledge with me.
- My family: my mother Patricia, father Paul, stepfather, stepmother, grandparents Helen and Claire, and my many siblings for their continued support.
- My partner Spencer for his support, ability to listen for prolonged periods, and occasional statistical advice.

Table of Contents

Abstract	ii
Summary for Lay Audience	iv
Co-Authorship Statement	v
Acknowledgments	vii
Table of Contents	viii
List of Figures	xiv
List of Appendices	xvi
List of Abbreviations	1
Chapter 1	2
1 «General Introduction»	2
1.1 « Working Memory in Non-Human Primates »	2
1.1.1 Defining Working Memory	2
1.1.2 What is the Primate Prefrontal Cortex?	3
1.1.3 How Do We Assess Working Memory in Primates?	6
1.1.4 Working Memory in the Primate Prefrontal Cortex	9
1.2 « Neural Substrates of Working Memory »	12
1.2.1 Persistent Activity Underlies Working Memory	12
1.2.2 Prefrontal Circuits Support Persistent Activity	15
1.2.3 Alternative Theories of Working Memory Coding	20
1.3 « Disorders of Working Memory »	23
1.3.1 Schizophrenia	23
1.3.2 Ketamine as a Model of Schizophrenia	26
1.4 « Dissertation Overview »	29
1.5 « References »	31

Chapter 2.....	47
2 « Stable Working Memory and Perceptual Representations in Macaque Lateral Prefrontal Cortex During Naturalistic Vision »	47
2.1 « Abstract ».....	47
2.2 « Introduction ».....	48
2.3 « Results ».....	50
2.3.1 Naturalistic Working Memory and Perception Tasks.....	50
2.3.2 Task Performance and Animal Behavior.....	52
2.3.3 Eye Behavior During Naturalistic Working Memory and Perception	54
2.3.4 Neural Spatial Selectivity	59
2.3.5 Fixation on the Target Location.....	64
2.3.6 Decoding of Gaze Position from Neural Activity in Prefrontal Neurons	68
2.3.7 Separation Between Coding for Working Memory and Perception.....	68
2.4 « Discussion »	71
2.4.1 Influence of Naturalistic Task Elements	72
2.4.2 Natural Eye Behavior and Visuospatial Working Memory.....	73
2.4.3 Perception and Working Memory in Areas 8a and 9/46.....	75
2.4.4 Conclusion	76
2.5 « Supplemental Results ».....	77
2.6 « Methods »	78
2.6.1 Ethics Statement.....	78
2.6.2 Task	78
2.6.3 Experimental Setup.....	78
2.6.4 Microelectrode Array Implant	79
2.6.5 Processing of Neuronal Data	79

2.6.6	Task Performance.....	80
2.6.7	Characterizing Eye Movement.....	80
2.6.8	Main Sequence Calculation.....	81
2.6.9	Spatial Tuning.....	81
2.6.10	Decoding Target Location from Neuronal Ensembles.....	82
2.6.11	Gaze Analysis.....	82
2.6.12	Decoding Target Location Using Eye Position.....	83
2.6.13	Decoding Eye Position from Neuronal Data.....	83
2.6.14	Decoding Target Location for Working Memory and Perception...	84
2.7	« References ».....	85
Chapter 3	89
3	« Ketamine Disrupts Naturalistic Coding of Working Memory in Primate Lateral Prefrontal Cortex Networks».....	89
3.1	« Abstract ».....	89
3.2	« Introduction ».....	89
3.3	« Results ».....	92
3.3.1	Ketamine Impairs Behavioral Performance in a Naturalistic Working Memory Task.....	92
3.3.2	Ketamine Decreases Tuning of Single Neurons for Remembered Locations.....	96
3.3.3	Ketamine Disrupts Population Decoding of Remembered Locations.....	99
3.3.4	Ketamine Has Differential Effects on Excitatory and Inhibitory Cell Types.....	101
3.3.5	Ketamine Did Not Affect Gaze Behavior.....	104
3.4	« Discussion ».....	107
3.5	« Supplementary Data ».....	111
3.6	« Methods ».....	115

3.6.1	Ethics Statement	115
3.6.2	Task and Experimental Setup	115
3.6.3	Microelectrode Array Implant	116
3.6.4	Neuronal Recordings and Spike Detection	117
3.6.5	Ketamine Injection.....	117
3.6.6	Behavioral Analysis.....	118
3.6.7	Spatial Selectivity	118
3.6.8	Ranked Target Selectivity	119
3.6.9	Plane Fitting	119
3.6.10	Neuronal Ensemble Decoding.....	120
3.6.11	Waveform Classification.....	121
3.6.12	Firing Rate for Preferred and Non-Preferred Locations.....	122
3.6.13	Gaze Analysis	122
3.7	« References »	125
Chapter 4	130
4	« Neural Sequences in Primate Prefrontal Cortex Encode Working Memory in Naturalistic Environments ».....	130
4.1	« Abstract ».....	130
4.2	« Introduction »	130
4.3	« Results ».....	132
4.3.1	Neural Sequences in Prefrontal Neurons.....	133
4.3.2	Neural Sequences are Predictive of Trajectory to Remembered Targets.....	137
4.3.3	Neural Sequences are Specific to Naturalistic Working Memory	142
4.3.4	Neuronal Sequences Represent Abstract Trajectories	145
4.3.5	Ketamine Disrupts Neuronal Sequences and Impairs Working Memory Performance.....	149

4.4 « Discussion »	151
4.4.1 Neural Sequences and Working Memory Coding	151
4.4.2 Ketamine Selectively Decreases Working Memory Performance and Disrupts Sequences	153
4.4.3 Conclusions	154
4.5 « Methods »	161
4.5.1 Ethics Statement	161
4.5.2 Experimental Setup	161
4.5.3 Task	162
4.5.4 Surgical Procedure	162
4.5.5 Task Performance	163
4.5.6 Spike Processing	163
4.5.7 Time Consistent Neurons	164
4.5.8 Complex Vector Decomposition	164
4.5.9 Projection Classification Analysis	166
4.5.10 Trajectory Analysis	166
4.6 « References »	168
5 General Discussion	172
5.1 « Overview »	172
5.2 « What Unique Role does the Prefrontal Cortex Play in Naturalistic Working Memory? »	174
5.3 « Utility of Sequential Activity »	179
5.4 « Mechanisms of Sequential Activation »	180
5.5 « Limitations in Modeling Schizophrenia using Ketamine »	182
5.6 « Future Studies »	186
5.6.1 Exploration of Cortical-Cortical and Subcortical Connections	186
5.6.2 Towards Naturalistic Research	188

5.7 « Concluding Remarks ».....	189
5.8 « References »	190
« Appendices ».....	197
« <i>Appendix A: Ethics Approval</i> »	197
« <i>Appendix B: Article Reuse Permissions</i> »	198
« <i>Appendix C: Statistical Reporting Tables</i> »	199
« Curriculum Vitae »	238

List of Figures

<i>Figure. 1.1:</i> Regions of the prefrontal cortex in humans and macaque monkeys	5
<i>Figure. 1.2:</i> Methods of measuring working memory in primates	8
<i>Figure. 1.3:</i> Summary of notable primate lesion studies that impact working memory	11
<i>Figure. 1.4:</i> Persistent activity in the prefrontal cortex	14
<i>Figure. 1.5:</i> Cellular circuits in the prefrontal cortex.....	19
<i>Figure. 1.6:</i> Ketamine blockage of NMDA receptors.....	28
<i>Figure. 2.1:</i> Experimental setup.....	51
<i>Figure. 2.2:</i> Task behavior	53
<i>Figure. 2.3:</i> Eye movement behavior	58
<i>Figure. 2.4:</i> Neural coding for remembered locations.....	60
<i>Figure. 2.5:</i> Single trial population activity	61
<i>Figure. 2.6:</i> Decoding of remembered locations	63
<i>Figure. 2.7:</i> Fixations on screen and target locations	67
<i>Figure. 2.8:</i> Neural coding for working memory and perception	70
<i>Figure. S2.9:</i> Neural recording setup.....	77
<i>Figure. 3.1:</i> Virtual working memory task and behavioral performance	95
<i>Figure. 3.2:</i> Ketamine decreases tuning of single neurons for remembered locations	98
<i>Figure. 3.3:</i> Neuronal population decoding of target locations.....	100
<i>Figure. 3.4:</i> Cell type specific effects of ketamine on working memory signals	103
<i>Figure. 3.5:</i> Effect of ketamine on gaze behavior	106
<i>Figure. S3.6:</i> Ensemble decoding for correct trials and nine target locations.....	112
<i>Figure. S3.7:</i> Changes in narrow and broad neuron firing rates per subject	113
<i>Figure. S3.8:</i> Gaze behavior.....	114
<i>Figure. 4.1:</i> Experimental design	134

<i>Figure. 4.2: Time consistent neurons underlie sequence formation</i>	136
<i>Figure. 4.3: Classification using sequential coding</i>	138
<i>Figure. 4.4: Neural sequences represent working memory content.....</i>	141
<i>Figure. 4.5: Working memory sequences are unique to naturalistic behavior</i>	144
<i>Figure. 4.6: Trajectory analysis.....</i>	148
<i>Figure. 4.7: Ketamine manipulation distorts neural sequences and working memory</i>	150
<i>Figure. S4.8: Example time consistent neurons</i>	156
<i>Figure. S4.9: Standard deviation of peak firing times</i>	157
<i>Figure. S4.10: Deviations of correlation method.....</i>	158
<i>Figure. S4.11: Temporal organization of neural activity during oculomotor delayed response task</i>	159
<i>Figure. S4.12: Ketamine and saline control analysis</i>	160
<i>Figure. 5.1: Flow of visual information in the brain</i>	176

List of Appendices

<i>Appendix A: Ethics Approval</i>	197
<i>Appendix B: Article Reuse Permissions</i>	198
<i>Appendix C: Statistics Reporting Tables</i>	199

List of Abbreviations

NHP - Non-human primate

PFC - Prefrontal cortex

LPFC - Lateral prefrontal cortex

dIPFC - Dorsolateral prefrontal cortex

FEF - Frontal eye field

V1 - Primary visual area

MT - Middle temporal visual area

MST - Middle superior temporal visual area

LIP - Lateral intraparietal cortex

HVC - High vocal center

WM - Working memory

ODR - Oculomotor delayed response

EPSCs - Excitatory postsynaptic currents

EPSPs - Excitatory postsynaptic potential

NMDA - N-methyl d-aspartate

AMPA - α -Amino-3-hydroxy-5-methyl-4-isoxazolepropionic acid

GABA - Gamma aminobutyric acid

GAD67 - Glutamate decarboxylase

Hz - Hertz

PV - Parvalbumin

CB - Calbindin

CR - Calretinin

SST - Somatostatin

VIP - Vasoactive intestinal polypeptide

LSD - Lysergic acid diethylamide

PCP - Phencyclidine

MK-801 - Dizocilpine

ANOVA - Analysis of variance

Std - Standard Deviation

Chapter 1

1 «General Introduction»

1.1 « Working Memory in Non-Human Primates »

1.1.1 Defining Working Memory

Whereas visual perception is defined as the ability to interpret the surrounding environment from signals entering the retinas, visual working memory (WM) is the ability to remember and manipulate, for short periods of time, an interpretation of the physical reality when the corresponding physical signals are no longer entering the retinas (Baddeley, 2010). WM representations persist upon the termination of sensory input and carry information about memorized objects or object properties. They are independent of sensory inputs and are resilient to distractors. They can be manipulated in mind and are independent from motor response. WM representations are also task-relevant - they are maintained long enough to guide behavior and decision-making but are not transferred to long-term storage. For example, you may use WM to maintain a phone number just long enough to dial it – this memory fades when the task is complete.

Although WM may superficially appear as a mere extension of visual perception, evidence that mnemonic representations are unique from perception and are separable in the brain originated from early investigations into patients with localized cortical damage. These case studies describe independent impairments in top-down driven mental representations or perception. Charcot and Bernard first described a patient in 1883 that could identify objects but was neither able to form mental representations of these objects nor envision them from memory (Charcot & Bernard, 1883). The opposite deficit has also been described in which patients are unable to perceive objects yet can describe them in detail based on clear mental representations. A well-known case of this, described in patient C.K, was presented by Behrmann and colleagues in the early 1990s. C.K

was unable to identify either simple or complex items but was able to produce clear and detailed drawings of those same items (Behrmann et al., 1992). Together, these studies propose that mental representations that underlie WM are unique from perception and must be processed independently in the brain.

1.1.2 What is the Primate Prefrontal Cortex?

The differentiation between perception and mental processes like WM reflects the expansion of our mental world as primates. This expansion is associated with an expansion of the primate prefrontal cortex (PFC) (Passingham & Wise, 2012; Preuss & Wise, 2022). So, what is the primate PFC?

The cerebral cortex consists of several distinct regions, subdivided based on cortical thickness, layer-specific thickness, differences in the arrangement of cells into layers, and variations in cell properties like cell packing, density, size, and type (Petrides, 2005). During primate evolution, the cerebral cortex developed along the posterior to the anterior axis with the PFC notably expanded in humans, occupying 30% of the brain's surface (Passingham & Wise, 2012; Preuss & Wise, 2022; Kolk & Rakic, 2022).

The primate PFC is often divided into the medial prefrontal, lateral PFC (LPFC), and orbitofrontal cortex. Of which, the LPFC is most associated with visuospatial WM (primarily in the dorsolateral region). The dorsolateral PFC (dlPFC) was first labeled by Brodmann in 1905 as area 9. The main division between dlPFC and other prefrontal regions was the presence or absence of a granulated cortex defined by an expanded layer IV. The increased density of this layer results from thalamic projections that terminate in the region (Tobias, 1975). dlPFC is divided in reference to the two sulci within it, the principal sulcus, and the arcuate sulcus, as well as differences in tissue composition. Walker split this region into areas 9 and 46 (Walker, 1940) since area 46 displayed a highly developed granular layer IV. Area 46 was split again, adding area 9/46 based on the discovery of large pyramidal cells in layer III (Petrides & Pandya, 1999).

In this dissertation, I refer to lateral prefrontal regions specified by Petrides and colleagues. This cortical parcellation considers comparative regions between macaques and humans (see a visual comparison in Figure. 1.1) based on similarities such as the expansion of layer IV and the presence of large pyramidal cells in layer III (Petrides, 2005; Petrides & Pandya, 1994). I consider areas adjacent to the principal sulcus and anterior to the arcuate sulcus as lateral prefrontal regions. I consider the further division of regions into dorsal (i.e., located dorsally to the mid-anterior principal sulcus) and ventral (i.e., located ventrally to the mid-anterior principal sulcus). These regions, illustrated in Figure. 1.1, include 9/46dv and 8Adv).

An equivalent of the dorsolateral PFC is notably absent in commonly used animal models like rodents (Laubach, 2018; Preuss & Wise, 2022). The evolution of this region follows a continuum within the primate taxa with humans showing the greatest expansion, followed by great apes, macaques, and new world monkeys like marmosets (Passingham & Wise, 2012; Preuss & Wise, 2022; Kolk & Rakic, 2022). This expansion of PFC in primates and the parallel increase in cognitive ability is the reason macaques are used to study prefrontal processing of WM in this dissertation.

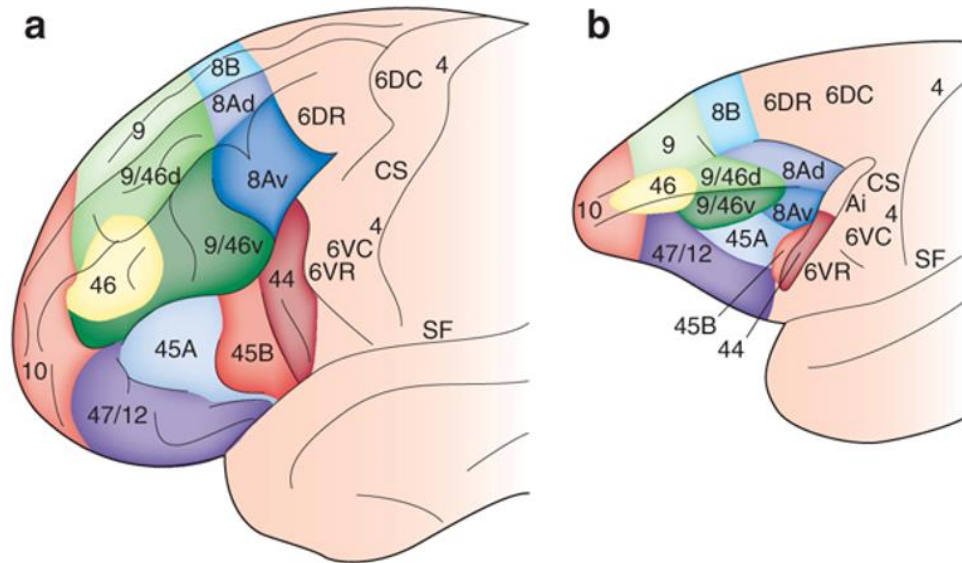


Figure. 1.1: Regions of the prefrontal cortex in humans and macaque monkeys

a, Labelled regions of human PFC. **b**, Labelled regions of macaque PFC.

1.1.3 How Do We Assess Working Memory in Primates?

Before discussing how the brain processes WM, it is important to understand how WM is measured in non-human primates (NHPs). Research into short-term memory began when scientists became interested in stimuli-associated responses that occur after a stimulus is removed. The delayed response task was created in 1913 to examine this phenomenon in different species and was later used to study visuospatial WM in NHPs using the Wisconsin General Test Apparatus (Hunter, 1913; Harlow & Bromer, 1938) (see Figure. 1.2a, b). In this task, subjects face two wells, one of which is filled with food. The wells are then covered during a delay period. After the period of delay, subjects retrieve the food by remembering in which well it is located.

The oculomotor delayed response (ODR) task was later developed to increase experimental control during the testing of visuospatial WM in NHPs. During this task, animals are typically contained in a primate chair and head-fixed in front of a computer monitor. Trials begin with fixation on a central fixation point, followed by the presentation of a cue. The cue then disappears during a delay period (Figure. 1.2c). The ODR task is still one of the most commonly used tasks for studying visuospatial WM (Dang et al., 2022; Constantinidis et al., 2018; Leavitt et al., 2017a). Another frequently used task is the delay non-match-to-sample in which the subject is shown one sample item that disappears during delay. The sample and a novel item are shown after delay and the animal must select the novel item via saccade. Alternatively, either the sample or a novel item is shown and the animal must make a response if the item is novel or make no response if the item matches the sample (response is often a saccade and/or release of a lever) (Bachevalier & Mishkin, 1986).

Recently, there has been increasing interest in developing tasks that reflect naturalistic elements of WM. WM in real life is complex. For example, when trying to remember the location of an item on a grocery store shelf, the brain must be able to maintain a mental representation of the item's location in the presence of

distracting stimuli (be it retail music or toddlers asking for treats) and changes in a visual scene caused by movement of the head and eyes. The aforementioned tasks explore WM using simple visual displays, stimuli, and responses. Contemporary studies have increased task complexity by introducing distractor stimuli during WM maintenance (Suzuki & Gottlieb, 2013; Parthasarathy et al., 2019), incorporating rule-based responses (Ma et al., 2018), and presenting multiple stimuli or sequences of stimuli to be remembered (Lundqvist et al., 2018a; Xie et al., 2022).

In this dissertation, I describe a new method of measuring WM – one which incorporates more naturalistic elements while still maintaining a high level of control. This task takes place in a visually complex virtual environment. Animals are required to make their response via 3D navigation using a joystick (Figure. 1.2 d-f).

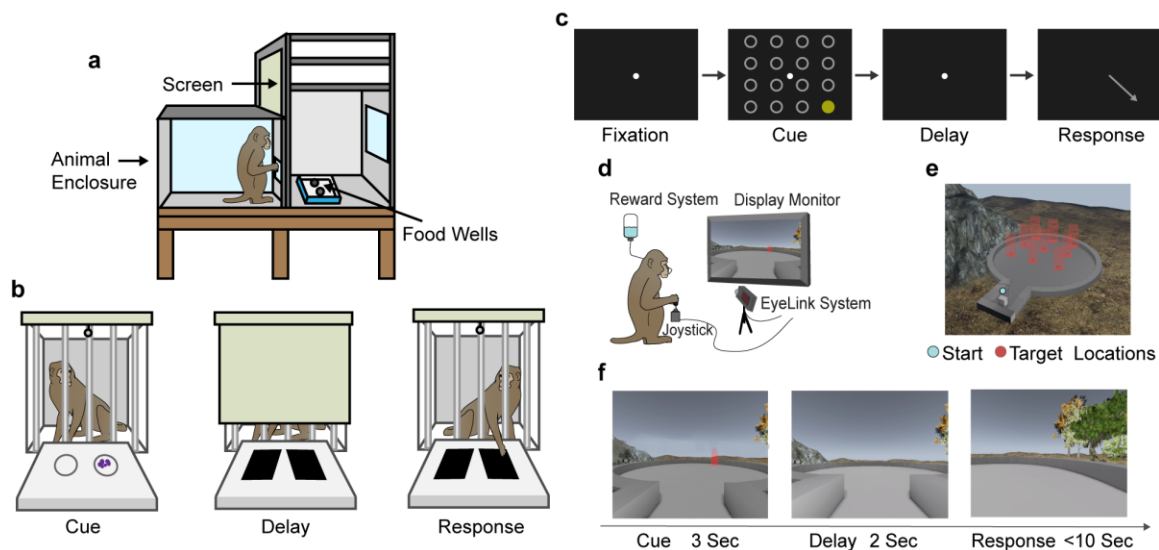


Figure. 1.2: Methods of measuring working memory in primates

a, illustration of a delayed response task being conducted in the Wisconsin General Test Apparatus. **b**, Depiction of a correct response during the delayed response task pictured in 'a'. **c**, Illustration of an oculomotor delayed response task with 16 target locations. A saccadic response to the cued location is required. **d**, Virtual reality experimental setup (primate chair and head fixation not pictured). **e**, Example of a virtual reality WM task with potential target locations outlined in the virtual arena. **f**, Timeline of a virtual WM task. Animals are required to navigate to cued targets using a joystick.

1.1.4 Working Memory in the Primate Prefrontal Cortex

There is no question that the PFC plays a pivotal role in WM processing in primates. Indeed, the importance of the PFC in WM can be traced to lesion studies conducted more than a century ago in humans and NHPs (reviewed fully in Roussy et al., 2021). These studies reported that damage to certain brain areas can produce selective deficits of WM while sparing visual perception. Jacobsen, 1936 conducted the first series of lesion experiments in the PFC using different species of NHPs [Macaca mulatta (rhesus macaque), Cercocebus torquatus (mangabey), and Papio papio (baboon)], discovering that lesions produced selective performance deficits in delayed response tasks. Importantly, the animals could perform perceptual tasks without major difficulty (Jacobsen, 1936). These results suggested that lesions of the PFC predominantly affect WM while sparing perception.

In another study, Chow, Blum, and Blum conducted lesion experiments of the posterior association areas of the parieto-occipital temporal region and the prefrontal areas close to the frontal pole in macaque monkeys (Chow et al., 1951). They found that posterior lesions did not substantially alter performance in a delayed response task. On the other hand, prefrontal lesions did decrease the animals' WM performance without significantly impairing other discrimination abilities. They also concluded that the PFC plays a selective role in the delayed aspects of the task.

In 1969, Butters and Pandya (1969) refined the lesioned areas to localize WM function more precisely within PFC. They compared the performance of lesioned and control rhesus macaques in delayed alternation tasks. Lesions included bilateral inferior parietal cortex lesions and three types of prefrontal lesions around the principal sulcus. Animals with lesions of the anterior and posterior thirds of the principal sulcus as well as periarculate and parietal lesions could re-learn the delay alternation task but animals with lesions of the central part

of the principal sulcus could not re-learn the task, thus resulting in permanent deficits.

In the second half of the twentieth century, spatially refined lesions, cooling-based inactivation, and pharmaceutical inactivation studies in the PFC of macaque monkeys further demonstrated perturbation of visuospatial WM representations and sparing of perceptual representations (Fuster & Alexander, 1970; Sawaguchi & Goldman-Rakic, 1991; Funahashi et al., 1993; Iba & Sawaguchi, 2003; Upright et al., 2018). This work introduced the concept of mnemonic scotoma, a deficit in remembering the spatial location of a target within a specific area of the visual field during a delayed response task, caused by inactivating small regions of the LPFC (Funahashi et al., 1993). However, animals with mnemonic scotomas can make saccades to the affected region when the target remains visually available. The latter not only confirmed the results of previous studies but also emphasized the major role of the PFC in visual WM and a lesser role in visual perception.

Moreover, decades earlier, Malmö, 1942 and Orbach and Fischer, 1959 first reported the unique and essential role of the PFC in maintaining WM representations in the presence of irrelevant incoming visual signals. Without PFC, stored mental representations can be disrupted by incoming sensory signals. Thus, from lesion and inactivation studies, one may conclude the PFC is needed for maintaining information in WM, but it is not essential for visual perception (i.e., when visual information remains available). Figure. 1.3 provides a graphical summary of lesion literature.

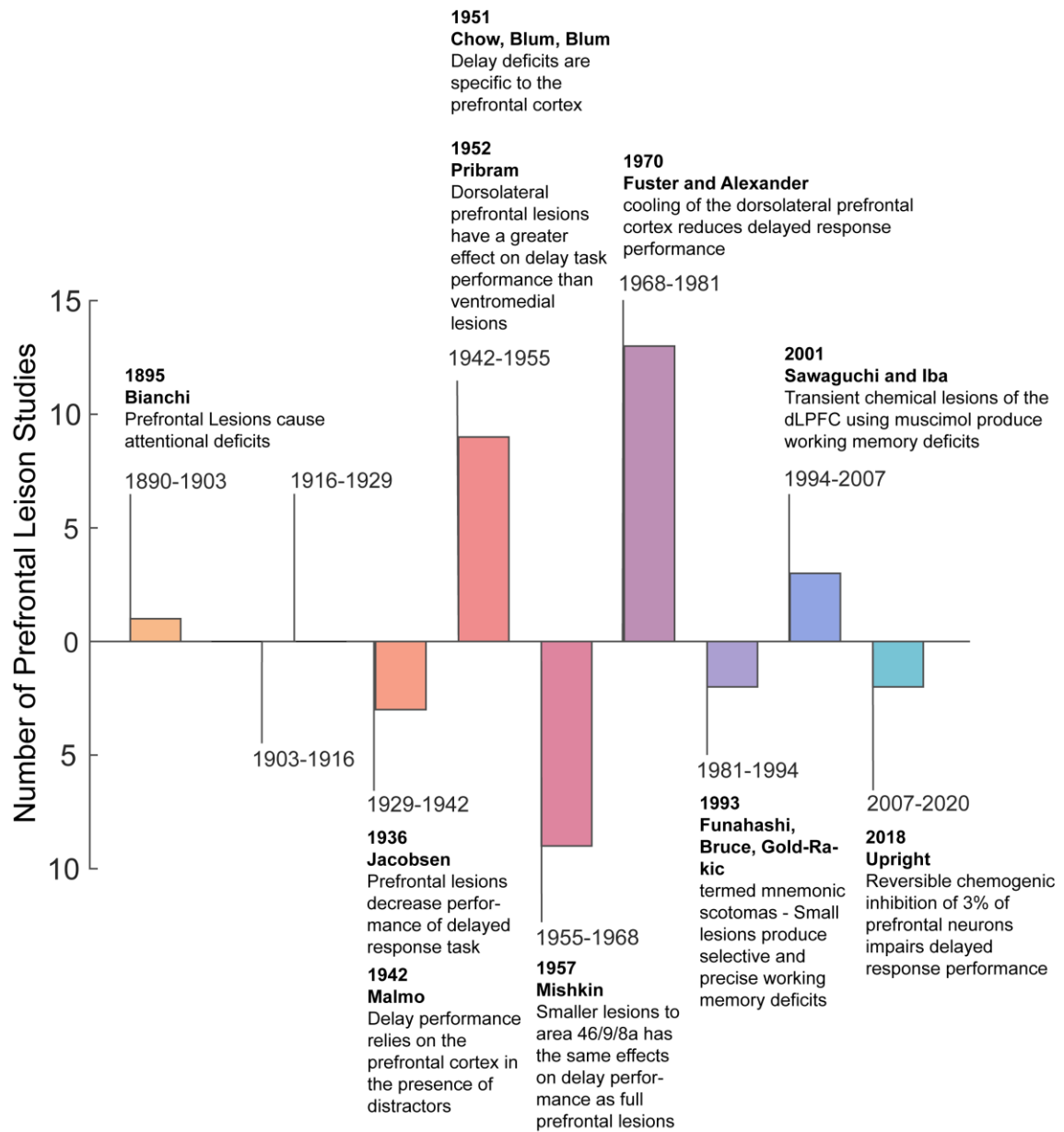


Figure. 1.3: Summary of notable primate lesion studies that impact working memory

A full summary table of lesion studies can be found in Roussy et al., 2021.

With the development of single cell recording techniques in behaving animals (Hubel, 1957), researchers began to study the neurophysiology of WM. Fuster and Alexander (1971) recorded the responses of neurons in the LPFC and mediodorsal nucleus of the thalamus in macaque monkeys during a delayed response task. They discovered neurons in the LPFC that increased their firing rate during WM delay periods, representing remembered locations and features of visual stimuli. At this same time, Kubota and Niki (1971) also observed neurons in the macaque PFC that preferentially fired during the delay period of a delayed alternation task. These initial results have since been confirmed by a multitude of studies using various WM tasks (Fuster, 1973; Kojima & Goldman-Rakic, 1982; Funahashi et al., 1989; Constantinidis et al., 2018), thus establishing the role of the LPFC in neural coding of WM.

1.2 « Neural Substrates of Working Memory »

1.2.1 Persistent Activity Underlies Working Memory

WM representations are maintained in the absence of sensory inputs when the cue or sample stimulus disappears from the visual field. From the aforementioned work starting in the 1970s, we know that neurons in PFC exhibit delay activity - increased firing rate when stimuli are removed. There is little debate that this delay activity is associated with WM performance; however, the exact neural mechanism underlying WM maintenance is more contested.

The leading mechanism proposes that prefrontal neurons maintain WM representations by continuous, (i.e., persistent) activity over delay periods. Persistent activity is characterized by an increased firing rate that spans the duration of the delay period after a stimulus is removed as well as stimuli selectivity (i.e., differential firing for specific remembered stimuli properties like color or location). See example of location selective persistent activity during an ODR task in Figure. 1.4.

Persistent activity is detached from signals for motor planning and preparation, evidenced by studies that require a separate oculomotor response from the cued target location (Takeda & Funahashi, 2002) and tasks in which the response is unknown during the delay period like in delayed match-to-sample tasks (Miller et al., 1996; Mendoza-Halliday & Martinez-Trujillo, 2017). Persistent activity is not vision-specific either – it has been documented for other sensory modalities such as somatosensory WM and auditory WM (Romo et al., 1999; Fuster et al., 2000). Persistent activity likely results from a combination of intrinsic neural properties and local circuit properties that support a controlled and task-specific state of excitability for WM maintenance.

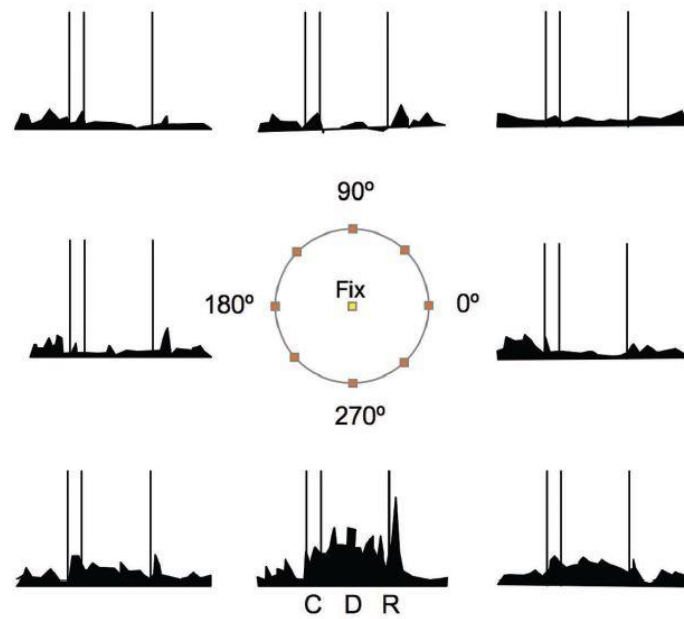


Figure. 1.4: Persistent activity in the prefrontal cortex

Firing rate of an example neuron during a classic ODR task during the cue (C), delay (D), and response (R) epochs. This neuron shows increased activity during the delay period and spatial tuning for targets presented at 270°. Figure retrieved from Arnsten, 2013

1.2.2 Prefrontal Circuits Support Persistent Activity

The primate cortex is not homogenous. Cortical architecture varies between early sensory and association areas like the PFC in terms of thickness of cortical layers, neuronal densities (Collins et al., 2010; Dombrowski et al., 2001), and proportion of different cell types (Torres-Gomez et al., 2020). Neurons differ in their morphology, receptor expression, and intracellular signaling, all of which contribute to the response and output properties of the cell (i.e., how a neuron responds to input and can interact with neurons in a network) (Llinás, 2001; Kepecs & Fishell, 2014).

LPFC exhibits unique properties pertinent for persistent activity such as increased connectivity between excitatory neurons – with many pyramidal neurons forming dense recurrent connections (Melchitzky et al., 1998). For example, the human and macaque PFC has more spines than neurons in primary sensory regions. One study found that pyramidal cells in macaque PFC were up to 16 times more spinous than those in V1 (Elston et al., 2001). Layer III pyramidal neurons in monkeys form significant bidirectional connections with other cells in layer III (Levitt et al., 1993; Kritzer & Goldman-Rakic, 1995; Pucak et al., 1996). Indeed, one experiment found that over 95% of layer III pyramidal neurons terminate onto other layer III pyramidal neurons (Melchitzky et al., 1998).

A basic local circuit model indicates that these extensive connections between pyramidal cells are essential for the generation of persistent activity. Recurrent excitatory activity between reciprocally connected layer III pyramidal cells with similar stimulus selectivity maintains neural firing over delay periods (Figure. 1.5a) (see for review: Durstewitz et al., 2000; Goldman-Rakic, 1995; Constantinidis & Wang 2004).

This recurrent activity is thought to rely on the activation of glutamatergic NMDA receptors based on several advantageous features of these receptors (Wang, 1999; Wang et al., 2013). NMDA receptors exhibit long-time constants (activation time can last several hundred milliseconds) compared to AMPA

receptors that display rapid activation and decay (Lester et al., 1990). This may help stabilize WM circuits as fast excitation and slow inhibition is modelled to destabilize local circuits (Wang, 1999; Wang, 2001; Wang et al., 2013). Experimentally, EPSCs in macaque LPFC do display slower kinetics than V1 (Medalla & Luebke, 2015). NMDA receptors, particularly, the GluN2B subunit fluxes high levels of calcium into the neuron which may be important for maintaining sustained activity by depolarizing the postsynaptic membrane for continued responsivity to excitatory inputs. The fact that NMDA receptors are voltage-dependent may increase the selectivity of excitation for a particular stimulus (e.g., a specific target location). A group of interconnected neurons with the same tuning may be more depolarized than other cells in the circuit with different tuning, allowing for a selective increase in neuron activation (Wang, 2001).

Experimental evidence does point to a reliance on NMDA receptor for WM. WM-related delay activity in LPFC is significantly more disrupted by NMDA Receptor antagonism using iontophoresis than AMPA receptor antagonism (Wang et al., 2013). Moreover, this same study demonstrates similar neural outcomes using systemic NMDA Receptor antagonism which decreases performance of an ODR task. These findings were also confirmed by an independent research group also using iontophoresis (van Vugt et al., 2020). This discovery contrasts findings in V1 where the neuronal response to visual stimuli depends on AMPA receptors (Yang et al., 2018).

Recurrent excitation requires balance by inhibition for circuit stability and signal specificity (Wang et al., 2004). Interneurons exert this important inhibitory control within these circuits. Considering accumulating evidence in rodents and computational modeling, one type of neuron, parvalbumin (PV) expressing interneurons, plays a key role in the functionality of prefrontal circuits (Wang et al., 2004; Homayoun & Moghaddam, 2007; Murray et al., 2015). PV interneurons are fast-spiking GABAergic neurons that strategically innervate the soma and proximal dendrites of excitatory pyramidal cells (Kawaguchi & Kubota, 1997). This allows

them to provide flexibility within cognitive circuits through dynamic inhibition of pyramidal neurons, which can serve to stabilize and refine circuit activity (Wang et al., 2004; Homayoun & Moghaddam, 2007; Murray et al., 2015).

One important role of interneurons may be to refine stimulus tuning during WM. One study reported similar saccadic direction tuning during an ODR task between spatially close pairs of pyramidal and putative interneurons, whereas neurons that were further away displayed opposite saccadic direction preferences (Rao et al., 1999). Local injection of bicuculline, a GABA receptor antagonist diminished saccadic directional tuning during an ODR task by increasing activity for non-preferred saccade directions, thus diminishing inhibitory control (Rao et al., 2000).

Since cortical interneurons display great diversity in morphology and function (Kepecs & Fishell, 2014), Wang and colleagues have elaborated on the basic circuit model by incorporating interneuron types with different properties within the LPFC circuitry including PV neurons, calretinin (CR) positive and calbindin (CB) positive neurons (Wang et al., 2004). CR cells receive inputs from pyramidal cells and inhibit CB cells. The CB cells inhibit inputs into the dendrites of pyramidal cells (Figure. 1.5a). Thus, an increase in the number or activation strength of CR neurons or their synapses onto CB cells would enhance the activation of the pyramidal cells (Figure. 1.5c). A decrease in CR numbers or synaptic strength on their targets may have the opposite effect (Figure. 1.5b). Therefore, a high ratio of CR cells in LPFC relative to sensory areas may favor the emergence of persistent firing encoding WM via the facilitation of recurrent excitatory dynamics amongst pyramidal cells (Torres-Gomez et al., 2020). Indeed, a larger proportion of CR cells relative to other interneurons has been identified in macaque LPFC compared to visual area MT (Torres-Gomez et al., 2020).

One issue that remains unclear is why areas such as MST, where neurons also display persistent firing during WM tasks, do not exhibit the same increase in the ratio of CR neurons observed in the LPFC. One possibility is that this increase

is not directly related to the ability to produce persistent firing, but to the ability of a local circuit to protect task relevant activity from incoming distracting sensory signals through flexible “gating” of inputs into a pyramidal cell network. Computational modeling shows that dendritic inhibition mediated by CB cells may be more efficient than soma-based inhibition mediated by PV cells in the filtering of task-irrelevant information. In favor of this explanation, inactivation or lesioning of the LPFC, where CR interneurons are abundant, increases distracter interference during WM tasks (Suzuki & Gottlieb, 2013; Malmo, 1942; Orbach & Fischer, 1959). Neural activity in LPFC is also less disrupted by incoming distracting signals than in other regions that generate delay-associated persistent activity such as LIP (Suzuki & Gottlieb, 2013).

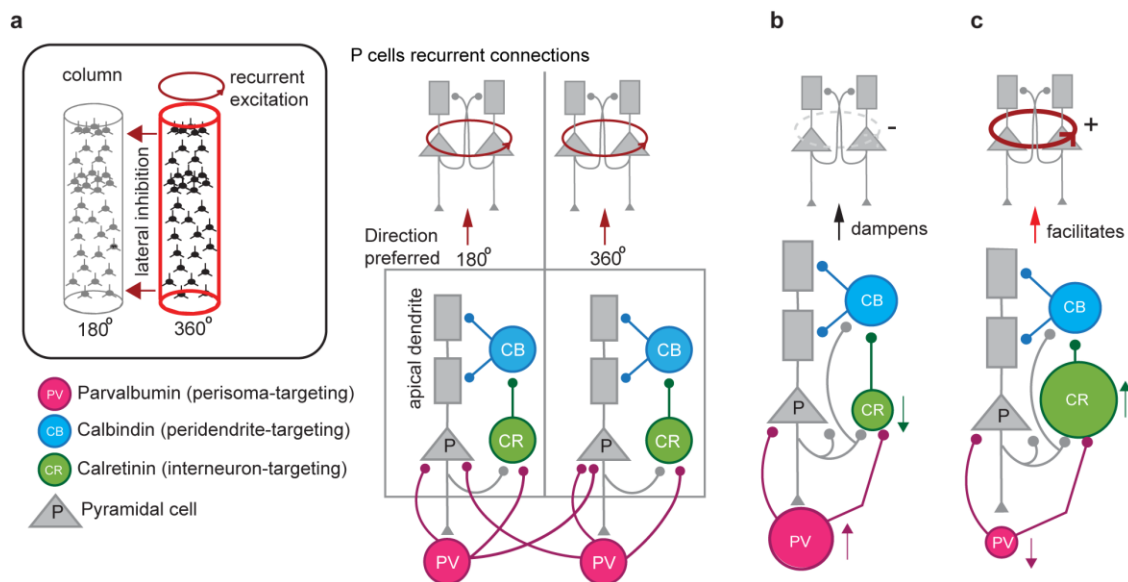


Figure. 1.5: Cellular circuits in the prefrontal cortex

a, Diagram showing the structure of two nearby cortical columns and the four main cell types. Observe pyramidal cells have at least two distinct compartments, the apical (distal) dendrites (gray rectangles) and the cell body. Left: pyramidal neurons with the same spatial selectivity (360°) are shown within a functional column. Neurons within this column generate recurrent excitation when their preferred location is presented, whereas neurons in a different column with a different preferred location (180°) are inhibited. Right: Soma-targeting PV interneurons inhibit pyramidal cells and CR interneurons. CR interneurons are excited by pyramidal cells and inhibit CB interneurons that target pyramidal cell dendrites. **b, c**, Different architectures based on the proportion of CR and PV interneurons and the ability to produce persistent firing. The architecture in 'c' occurs in cells tuned for the presented target location. Activation of pyramidal cells increases the activity of CR interneurons which inhibit CB cells. Reduced inhibition on pyramidal cells further increases activity, thus resulting in recurrent activity observed in PFC. Figure retrieved from Roussy et al., 2021

1.2.3 Alternative Theories of Working Memory Coding

Despite over 50 years of evidence, an amount of controversy has been accumulating around the concept of persistent firing. For example, whether WM coding is sustained during the entire delay period by single neurons or populations, or whether it has a more complex temporal structure has been debated (Sreenivasan et al., 2014; Lundqvist et al., 2016, 2018b; Constantinidis et al., 2018; Rainer & Miller, 2002). Recently, several research groups have suggested that persistent activity may be insufficient for coding of WM representations, especially when tasks increase in difficulty. This is based on observations that many neurons do not present with consistent firing during whole delay periods but instead display temporally diverse patterns of spiking within a trial (Batuev et al., 1979; Shafi et al., 2007). Some speculate that reported persistent activity is partially an artifact of trial averaging (Lundqvist et al., 2018b) and may not support the generation of observed dynamic neural states during WM (Spaak et al., 2017). Critics further point to the inefficiency of a code that relies on the continuous firing of high energy-consuming action potentials – making persistent activity a metabolically expensive mechanism (Lundqvist et al., 2018b; Lennie, 2003).

A logical extension of the single neuron persistent activity hypothesis is that the activity of subpopulations of neurons, or neural ensembles, encode WM representations through collective and co-varied activity (e.g., noise correlations) (Leavitt et al., 2017b; Harris, 2005). Indeed, even a small number of neurons functioning as an ensemble is capable of encoding WM representations of space to a greater extent than single neurons (Leavitt et al., 2017b). At the population level, even temporally fluctuating WM activity can be stably read out, thus forming a stable representation (Meyers et al., 2008; Spaak et al., 2017; Stokes et al., 2013; Druckmann & Chklovski, 2012). Within this dynamic activity, stable codes can be identified (Murray et al., 2017) in non-dynamic tasks. When distractors are presented, population codes may become more dynamic, evolving to address task dynamics while still representing mnemonic information (Parthasarathy et al., 2017; Parthasarathy et al., 2019).

Neural code refers to properties of neural activity and interactions that can process and transmit information. For example, neural information during WM must be remembered above all incoming sensory signals and outgoing motor signals. The previously mentioned proposed mechanisms of WM coding rely on a firing rate-based code in which WM-related information is amplified above background activity through increased neuron firing. This code however does not take into account the timing of action potentials or possible information during interspike intervals, thus firing rate averaged over periods of time may be too simplistic to describe the complexity of brain activity – especially during complex behavior and cognition.

A secondary code has been proposed that relies on the timing of spikes rather than the overall spike rate – this is generally referred to as temporal coding. Temporal coding assumes a meaningful temporal structure in the neural response. Evidence for precise temporal firing has often been identified in primary sensory areas including V1 (Butts et al., 2007; Havenith et al., 2011). Precise temporal firing in PFC neurons was also identified during WM - around the same time as persistent activity (Batuev et al., 1979). The main reasoning for the efficacy of a temporal code is that spikes arriving at a specific time may be more effective at depolarizing downstream neurons.

It should be noted that temporal codes likely do not exist without some influence of rate-coding. One clear example of parallel codes exists in the gustatory system in which rate coding is used to determine tastant type (i.e., chemical sensed as flavor – sweet, salty, bitter) and a temporal code is used for specific differentiation (consider a craft IPA beer that temporally evolves in flavor) (Carleton et al., 2010). Co-functioning parallel codes may be the case for WM as well.

Sequential population activity codes, composed of tiled activity from transiently active single neurons further propose that the relative order of firing of single neurons in a population carries information. Early studies have

acknowledged that patterns of neural ensemble firing may carry information in PFC and have demonstrated techniques to attempt to uncover these spatiotemporal patterns in a limited number of simultaneously recorded neurons (Abeles & Gerstein, 1988). Since the development of high-density neural recording, sequential activity has been identified during complex movement, navigation, and tasks in rodents requiring short-term memory (Chi & Margoliash, 2001; Tang et al., 2014; Srivastava et al., 2017; Okubo et al., 2015; Daliparthi et al., 2019; Itskov et al., 2011; Eichenbaum, 2014; Zhou et al., 2020; Harvey et al., 2012; Akhlaghpour et al., 2016). One may consider that sequential neural bursting may be related to WM coding in PFC in which temporally adjacent action potentials may trigger a heightened response in downstream neurons.

Another mechanism which has recently generated extensive attention is referred to as phase-of-firing coding. This proposes that neurons encode information based on spike rate with spike timing modulated by precise phases in network fluctuations (i.e., oscillations). Essentially, neuron firing is modulated by oscillatory phase, causing neurons to fire with greater synchrony. This mechanism is often reported in the visual cortex. For example, in one experiment, LFP phase was recorded from V1 as it was modulated by naturalistic visual stimuli (i.e., a movie). The phase of low-frequency LFP added more information about the stimuli than spike count alone (Montemurro et al., 2008).

LFP activity separated into different frequencies has also been reported to represent aspects of WM in NHPs in which magnitude, frequency, and oscillatory phase have been connected to remembered stimuli (Siegel et al., 2009; Lundqvist et al., 2016; Lundqvist et al., 2018a, 2018b). For example, the Miller lab identified that bursts of narrow-band gamma oscillations were related to neural spiking and were associated with WM maintenance (Lundqvist et al., 2016; Lundqvist et al., 2018a). Activity in the alpha and beta frequencies have been proposed to play inhibitory functions during WM as occurs in movement in which elevated beta activity is associated with movement inhibition (Lundqvist et al., 2018a; Zhang et al., 2008; Schmidt et al., 2019). Low-frequency theta has been proposed to

modulate gamma oscillations (Canolty et al., 2006) and may also be modulated by items held in WM (Jensen & Tesche, 2002).

1.3 « Disorders of Working Memory »

1.3.1 Schizophrenia

The expansion of the PFC has increased cognitive capacity and expanded the mental world of primates, with the greatest expansion occurring in humans. However, this expansion has also made the PFC more vulnerable, prompting the development of certain psychiatric disorders (Passingham & Wise, 2012). One such human-specific disorder is schizophrenia. Schizophrenia is a debilitating and chronic mental disorder that affects approximately 20 million people worldwide (Charlson et al., 2018). Symptoms are most often classified into three categories: positive, negative, and cognitive (NIMH, 2016). Positive symptoms include hallucinations and delusions, negative symptoms are the absence of typical emotion or behavior such as asociality and flattened affect, and cognitive symptoms include deficits in attention, WM, and executive functioning (NIMH, 2016).

Cognitive dysfunction has recently gained recognition as a core symptom of schizophrenia and closely predicts functional disease outcomes since these deficits contribute to impaired social and vocational functioning (Bowie & Harvey, 2006; Lepage et al., 2014). Many of the cognitive tasks in which patients perform poorly have some reliance on WM, specifically the ability to retain mnemonic information to perform an appropriate response. Accordingly, WM dysfunction is prevalent in schizophrenia (Forbes et al., 2009; Starc et al., 2017) and the PFC, which I have outlined earlier as an essential region for WM, has been identified as a central site of dysfunction in schizophrenia. More precisely, patients display abnormal LPFC activity during cognition (Smucny et al., 2022) and impairments in tasks associated with LPFC function like the Wisconsin Card Sorting Task (Weinberger et al., 1986) and the ODR task (Park & Holzman, 1992).

Unfortunately, cognitive symptoms are challenging to treat using currently available therapies including treatment with typical and atypical antipsychotic medication (Gold, 2004). This is exacerbated by our limited understanding of the cause of cognitive dysfunction in patients. We do know that schizophrenia is likely caused by a myriad of genetic and environmental influences in which increasing genetic similarities increase the risk of developing schizophrenia (monozygotic twins show a 50% concordance rate) (Henriksen et al., 2017). Symptoms are associated with abnormalities in brain structure such as increased ventricle size (Kempton et al., 2010; van Erp et al., 2016), abnormal cortical folding (Palaniyappan & Liddle, 2012; Matsuda & Ohi, 2018), and small pyramidal neurons with lower dendritic spine density in PFC layer 3 (Pierri et al., 2001; Kolluri et al., 2005). Additionally, studies have identified abnormalities in select neurotransmitter systems.

The dopamine hypothesis of schizophrenia was popularized after the discovery of first-generation antipsychotic drugs like haloperidol which treated positive symptoms through action on the dopaminergic system. Moreover, substances that increase dopamine levels, like amphetamines, are known to trigger psychosis (Bramness et al, 2012). In support of this theory, postmortem studies have found altered cortical dopamine innervation and increased concentrations of dopamine D2 receptors in the brains of patients with schizophrenia (Seeman et al., 1990; Akil et al., 1999). However, typical antipsychotics that function on dopaminergic receptors do not treat negative or cognitive symptoms of schizophrenia, suggesting that other systems are involved.

An imbalance of excitation and inhibition has been proposed to contribute to the development of schizophrenia which may occur through dysfunction of inhibitory GABAergic and/or excitatory Glutaminergic systems. GABAergic PV interneurons in the PFC are largely vulnerable across many psychiatric diseases, including schizophrenia (Lewis et al., 2012). For example, a meta-analysis of postmortem concentrations of PV interneurons concluded that the density of PV interneurons is reduced in the frontal cortex of patients with schizophrenia (Kaar

et al., 2019). PV interneuron dysfunction is also evidenced to play a large role in symptom formation through abnormalities in the enzyme glutamate decarboxylase (GAD67) (responsible for the conversion of glutamate into GABA) (Erlander & Tobin, 1991). GAD67 mRNA is downregulated in the dlPFC of patients with schizophrenia (Akbarian et al., 1995; Mirnics et al., 2000; Volk et al., 2000). Moreover, this downregulation was primarily found in PV-positive neurons with low levels of PV expression (Hashimoto et al., 2003).

Complex cognitive functioning relies on the neural circuits within the PFC consisting of diverse cell types. GABAergic PV-expressing interneurons maintain normal circuit functioning by providing inhibition that both stabilizes and refines circuit activity, leading to balanced excitation and inhibition. Aberrant PV-positive neurons may then inefficiently inhibit pyramidal cells leading to hyperexcitation through decreased lateral inhibition and/or decreased dendritic inhibition through interactions with CR and CB interneurons (Lewis et al., 2012).

Abnormalities in glutamatergic systems may also contribute to the pathophysiology of schizophrenia. Glutamatergic receptors are downregulated in PFC (Konradi & Heckers, 2003) and dysfunction of specific NMDA receptor subunits in schizophrenia has been identified including the gene for the 2B subunit (GRIN2B) (Li & He, 2007; Akbarian et al., 1996). PV interneurons receive reduced excitatory input (Nakazawa et al., 2012), evidenced by the reduced density of excitatory synapses on PV expressing interneurons in patients with schizophrenia (Chung et al., 2016). There is also evidence that symptom treatment through antipsychotic drugs facilitates excitatory transmission, particularly, NMDA receptor neurotransmission after acute and prolonged exposure (Arvanov & Wang, 1999; Gemperle et al., 2003).

Diseases that specifically target NMDA receptors like anti-NMDA receptor encephalitis, caused by an antibody-mediated reduction of NMDA receptors, display symptoms that are remarkably akin to those of schizophrenia, so much so that this rare autoimmune disease is often first diagnosed as schizophrenia (Luo

et al., 2022). Patients with both conditions also experience similar WM deficits (Lynch et al., 2018; Stein et al., 2020).

1.3.2 Ketamine as a Model of Schizophrenia

Several drugs can be used to mimic symptoms of schizophrenia, including amphetamines based on their aforementioned effect on dopaminergic systems and psychedelic drugs like LSD with hallucinogenic effects. In experimental settings, glutamatergic NMDA receptor antagonists like ketamine, phencyclidine (PCP), and dizocilpine (MK-801) are used to transiently produce multiple symptoms characteristic of schizophrenia including hallucinations, disassociation, and cognitive deficits (Javitt, 1987; Coyle, 1996; Ma et al., 2018; Olney et al., 1999). Ketamine consistently elicits WM deficits in humans and animals (Frohlich & van Horn, 2014; Morgan et al., 2004; Malhotra et al., 1997; Wang et al., 2013) and exacerbates cognitive impairment in patients with schizophrenia (Malhotra et al., 1997). Ketamine administration can also trigger increased symptoms of psychosis in patients with schizophrenia (Krystal et al., 1994).

Ketamine primarily acts on NMDA receptors as a non-competitive antagonist. NMDA receptors are voltage gated calcium channels with a Mg^{2+} ion 'plug' positioned inside the channel pore during its inactive state, preventing the inward flow of Ca^{2+} . Upon depolarization and attachment of several essential ligands including glycine, the Mg^{2+} ion is dislodged, opening the ion channel, and allowing for an influx of Ca^{2+} (Kroemer et al., 1998). Ketamine binds to the PCP binding site within the ion channel, thus Ca^{2+} remains blocked even when the Mg^{2+} plug is dislodged (Figure. 1.6).

Despite ketamine acting as a glutaminergic receptor blocker, it is documented to increase overall neural excitation. For example, in vitro ketamine administration often leads to the production of spontaneous action potentials without EPSP input, suggested to result from increased NMDA receptor currents for sodium, thus causing neurons to be more excitable (Benoit et al., 1986). Increased excitation is further evidenced by reports of excitotoxicity of ketamine

and PCP (Plitman et al., 2014) as well as evidence of increased metabolic activity and increased neural excitation in the human PFC after ketamine administration (Breier et al., 1997; Vollenweider et al., 1997).

Ketamine has differential effects on cell types that may contribute to increased excitation and symptom formation. Ketamine reduces the activity of interneurons and increases the activity of pyramidal cells in rodents (Homayoun & Moghaddam, 2007). NMDA receptor antagonists decrease the expression of PV in the rodent PFC, relating NMDA receptor hypoactivity to PV interneuron dysfunction (Cochran et al., 2003). Moreover, administering a GABA agonist shortly after ketamine can reduce the behavioral effects of ketamine (Castner et al., 2010).

Increased excitation related to abnormal activity of interneurons, caused by ketamine administration, may disrupt local circuits for WM as previously described in schizophrenia. This provides a clear pathological mechanism for WM dysfunction consistent between schizophrenia and subanesthetic ketamine use. This evidence and the similarity in symptom formation support ketamine as a model of cognitive deficits in schizophrenia.

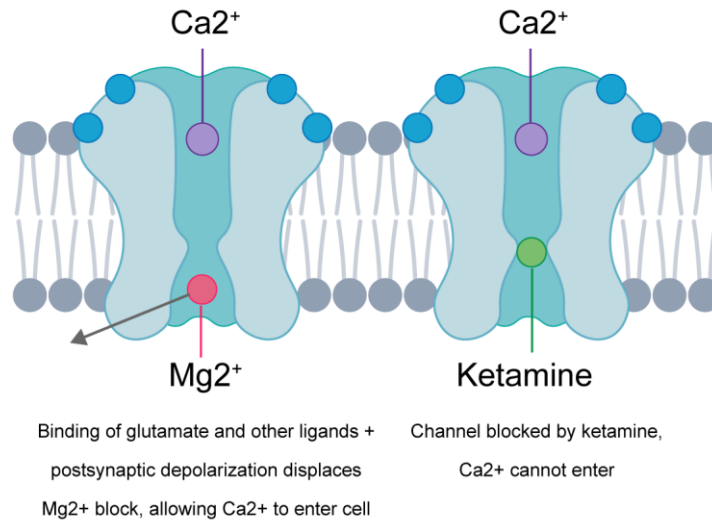


Figure. 1.6: Ketamine blockage of NMDA receptors

NMDA receptor in an inactivated state (left), during which, a Mg^{2+} plug blocks the ion channel. Depolarization and binding of specific ligands remove this block. Ketamine acts as a receptor antagonist by binding to the PCP binding site within the ion channel (right). Even upon channel activation, ketamine continues to block the ion channel.

1.4 « Dissertation Overview »

The work presented in this dissertation uses high-density single neuron recording in rhesus macaque monkeys performing a novel task to examine how visuospatial WM is coded in LPFC in naturalistic conditions. This novel WM task is set in a visually complex virtual environment. Unlike previous experiments, animals are permitted free visual exploration and utilize 3D navigation using a joystick to perform the task. Since LPFC activity has not been recorded in this type of environment before, it is important to first explore animal behavior and basic neural coding during this task. Therefore, in chapter 2, I explore how rhesus macaques perform WM and visual perception tasks in this virtual environment. I explore navigation and eye movement behaviors as well as neural signals related to eye movement and gaze position. Furthermore, I explore how WM and perceptual neural coding remain robust and differentiable in this complex environment.

Part of my motivation for creating this novel task was to explore cognitive dysfunction associated with mental disorders in more naturalistic settings. Patients with ADHD, dementia, schizophrenia, and other conditions that decrease WM function must use WM in complex situations and contexts that occur in day-to-day life. Therefore, I wanted to examine how WM deficits that resemble those in schizophrenia occur in more natural settings - akin to how patients use WM in real life. In chapter 3, I use ketamine, an NMDA receptor antagonist that mimics many of the symptoms of schizophrenia including WM deficits. I explore how ketamine distorts WM representations in the naturalistic WM task caused by distinctive effects of ketamine on different cell types.

The naturalistic task that I developed includes complex spatiotemporal elements; therefore, the task is more dynamic than traditional WM tasks. Elements of the environment change based on task timing. For example, when the navigation period begins, visual scenery changes as animals move in the arena. During the delay period, items in the environment may also serve as distractors – requiring the utilization of a robust yet flexible code to maintain WM

representations. We hypothesized that an additional neural code, parallel to persistent activity, may be involved in supporting these WM representations during a complex task. Therefore, in chapter 4, I explore how temporal coding may support WM maintenance during a naturalistic WM task. Specifically, I examine precise patterns of neural population activity in which single neurons sequentially fire forming a continuous ‘tiling’ of activity that represents target locations as well as abstract target trajectories. Finally, in chapter 5, I reiterate the questions driving my dissertation and present limitations of my studies, commentary connected to the field at large, and future directions to explore.

1.5 « References »

- Abeles, M., & Gerstein, G. L. (1988). Detecting spatiotemporal firing patterns among simultaneously recorded single neurons. *Journal of Neurophysiology*, *60*(3), 909–924. doi:10.1152/jn.1988.60.3.909
- Akhlaghpour, H., Wiskerke, J., Choi, J. Y., Taliaferro, J. P., Au, J., & Witten, I. B. (2016). Dissociated sequential activity and stimulus encoding in the dorsomedial striatum during spatial working memory. *eLife*, *5*, e19507. doi:10.7554/eLife.19507
- Akil, M., Pierri, J. N., Whitehead, R. E., Edgar, C. L., Mohila, C., Sampson, A. R., & Lewis, D. A. (1999). Lamina-specific alterations in the dopamine innervation of the PFC in schizophrenic subjects. *The American Journal of Psychiatry*, *156*(10), 580–1589. doi:10.1176/ajp.156.10.1580
- Akbarian, S., Kim, J. J., Potkin, S. G., Hagman, J. O., Tafazzoli, A., Bunney, W. E., Jr, & Jones, E. G. (1995). Gene expression for glutamic acid decarboxylase is reduced without loss of neurons in PFC of schizophrenics. *Archives of General Psychiatry*, *52*(4), 258–266. doi:10.1001/archpsyc.1995.03950160008002
- Akbarian, S., Sucher, N. J., Bradley, D., Tafazzoli, A., Trinh, D., Hetrick, W. P., Potkin, S. G., Sandman, C. A., Bunney, W. E., Jr, & Jones, E. G. (1996). Selective alterations in gene expression for NMDA receptor subunits in PFC of schizophrenics. *The Journal of Neuroscience*, *16*(1), 19–30. doi:10.1523/JNEUROSCI.16-01-00019.1996
- Arnsten, A. F. T. (2013). The neurobiology of thought: The groundbreaking discoveries of Patricia Goldman-Rakic 1937-2003. *Cerebral Cortex*, *23*(10), 2269–2281. doi:10.1093/cercor/bht195
- Arvanov, V. L., & Wang, R. Y. (1999). Clozapine, but not haloperidol, prevents the functional hyperactivity of N-methyl-D-aspartate receptors in rat cortical neurons induced by subchronic administration of phencyclidine. *The Journal of Pharmacology and Experimental Therapeutics*, *289*(2), 1000–1006.
- Baddeley, A. (2010). Working memory. *Current Biology*, *20*(4), 136–140. doi:10.1016/j.cub.2009.12.014
- Bachevalier, J., & Mishkin, M. (1986). Visual recognition impairment follows ventromedial but not dorsolateral prefrontal lesions in monkeys. *Behavioural Brain Research*, *20*, 249–261. doi:10.1016/0166-4328(86)90225-1
- Batuev, A. S., Pirogov, A. A., & Orlov, A. A. (1979). Unit activity of the PFC during delayed alternation performance in monkey. *Acta Physiologica Academiae Scientiarum Hungaricae*, *53*(3), 345–353.

- Behrmann, M., Winocur, G., & Moscovitch, M. (1992). Dissociation between mental imagery and object recognition in a brain-damaged patient. *Nature*, *359*, 636–637. doi:10.1038/359636a0
- Benoit, E., Carratù, M. R., Dubois, J. M., & Mitolo-Chieppa, D. (1986). Mechanism of action of ketamine in the current and voltage clamped myelinated nerve fibre of the frog. *British Journal of Pharmacology*, *87*(2), 291–297. doi:10.1111/j.1476-5381.1986.tb10817.x
- Bowie, C. R., & Harvey, P. D. (2006). Cognitive deficits and functional outcome in schizophrenia. *Neuropsychiatric Disease and Treatment*, *2*(4), 531–536. doi:10.2147/nedt.2006.2.4.531
- Bramness, J. G., Gundersen, Ø. H., Guterstam, J. *et al.* (2012). Amphetamine-induced psychosis - a separate diagnostic entity or primary psychosis triggered in the vulnerable? *BMC Psychiatry*, *12*, 221 doi:10.1186/1471-244X-12-221
- Breier, A., Malhotra, A. K., Pinals, D. A., Weisenfeld, N. I., & Pickar, D. (1997). Association of ketamine-induced psychosis with focal activation of the PFC in healthy volunteers. *The American Journal of Psychiatry*, *154*(6), 805–811. doi:10.1176/ajp.154.6.805
- Brodmann, K. (1905). Beitrage zur histologischen Lokalisation der Grosshirnrinde. III. Mitteilung. Die Rindenfelder der niederen Affen. *J. Psychol. Neurol*, *4*, 177–226.
- Butters, N., & Pandya, D. (1969). Retention of delayed-alternation: Effect of selective lesions of sulcus principalis. *Science*, *165*(3899), 1271–1273. doi:10.1126/science.165.3899.1271
- Butts, D. A., Weng, C., Jin, J., Yeh, C. I., Lesica, N. A., Alonso, J. M., & Stanley, G. B. (2007). Temporal precision in the neural code and the timescales of natural vision. *Nature*, *449*(7158), 92–95. doi:10.1038/nature06105
- Canolty, R. T., Edwards, E., Dalal, S. S., Soltani, M., Nagarajan, S. S., Kirsch, H. E., Berger, M. S., Barbaro, N. M., & Knight, R. T. (2006). High gamma power is phase-locked to theta oscillations in human neocortex. *Science*, *313*(5793), 1626–1628. doi:10.1126/science.1128115
- Carleton, A., Accolla, R., & Simon, S. A. (2010). Coding in the mammalian gustatory system. *Trends in Neurosciences*, *33*(7), 326–334. doi:10.1016/j.tins.2010.04.002
- Castner, S. A., Arriza, J. L., Roberts, J. C., Mrzljak, L., Christian, E. P., & Williams, G. V. (2010). Reversal of ketamine-induced working memory impairments by the GABA α 2/3 agonist TPA023. *Biological Psychiatry*, *67*(10), 998–1001. doi:10.1016/j.biopsych.2010.01.001

- Chung, D. W., Fish, K. N., & Lewis, D. A. (2016). Pathological basis for deficient excitatory drive to cortical parvalbumin interneurons in schizophrenia. *The American Journal of Psychiatry*, *173*(11), 1131–1139. doi:10.1176/appi.ajp.2016.16010025
- Charcot, M., & Bernard, D. (1883). Un cas de suppression brusque et isolée de la vision mentale des signes et des objets (formes et couleurs). *Progrès Médicale*, *11*, 568–571
- Chi, Z., & Margoliash, D. (2001). Temporal precision and temporal drift in brain and behavior of zebra finch song. *Neuron*, *32*(5), 899–910. doi:10.1016/S0896-6273(01)00524-4
- Charlson, F. J., Ferrari, A. J., Santomauro, D. F., Diminic, S., Stockings, E., Scott, J. G., McGrath, J. J., & Whiteford, H. A. (2018). Global epidemiology and burden of schizophrenia: Findings from the global burden of disease study 2016. *Schizophrenia Bulletin*, *44*(6), 1195–1203. doi:10.1093/schbul/sby058
- Chow, K. L., Blum, J. S., & Blum, R. A. (1951). Effects of combined destruction of frontal and posterior associative areas in monkeys. *Journal of Neurophysiology*, *14*(1), 59–71. doi:10.1152/jn.1951.14.1.59
- Collins, C. E., Airey, D. C., Young, N. A., Leitch, D. B., & Kaas, J. H. (2010). Neuron densities vary across and within cortical areas in primates. *Proceedings of the National Academy of Sciences of the United States of America*, *107*(36), 15927–15932. doi:10.1073/pnas.1010356107
- Cochran, S. M., Kennedy, M., McKerchar, C. E., Steward, L. J., Pratt, J. A., & Morris, B. J. (2003). Induction of metabolic hypofunction and neurochemical deficits after chronic intermittent exposure to phencyclidine: Differential modulation by antipsychotic drugs. *Neuropsychopharmacology*, *28*, 265–275. doi:10.1038/sj.npp.1300031
- Constantinidis, C., Funahashi, S., Lee, D., Murray, J. D., Qi, X. L., Wang, M., & Arnsten, A. (2018). Persistent spiking activity underlies working memory. *The Journal of Neuroscience*, *38*(32), 7020–7028. doi:10.1523/JNEUROSCI.2486-17.2018
- Constantinidis, C., & Wang, X.-J. (2004). A neural circuit basis for spatial working memory. *The Neuroscientist*, *10*(6), 553–565. doi:10.1177/1073858404268742
- Coyle J. T. (1996). The glutamatergic dysfunction hypothesis for schizophrenia. *Harvard Review of Psychiatry*, *3*(5), 241–253. doi:10.3109/10673229609017192
- Daliparthi, V. K., Tachibana, R. O., Cooper, B. G., Hahnloser, R. H. R., Kojima,

S., Sober, S. J., & Roberts, T. F. (2019). Transitioning between preparatory and precisely sequenced neuronal activity in production of a skilled behavior. *eLife*, *8*. doi:10.7554/ELIFE.43732

Dang, W., Li, S., Pu, S., Qi, X. L., & Constantinidis, C. (2022). More prominent nonlinear mixed selectivity in the dorsolateral prefrontal than posterior parietal cortex. *eNeuro*, *9*(2), ENEURO.0517-21.2022. doi:10.1523/ENEURO.0517-21.2022

Dombrowski, S. M., Hilgetag, C. C., & Barbas, H. (2001). Quantitative architecture distinguishes prefrontal cortical systems in the rhesus monkey. *Cerebral Cortex*, *11*(10), 975–988. doi:10.1093/cercor/11.10.975

Druckmann, S., & Chklovskii, D. B. (2012). Neuronal circuits underlying persistent representations despite time varying activity. *Current Biology*, *22*, 2095–2103. doi:10.1016/j.cub.2012.08.058

Durstewitz, D., Seamans, J., & Sejnowski, T. (2000). Neurocomputational models of working memory. *Nature Neuroscience*, *3*, 1184–1191. doi:10.1038/81460

Elston, G. N., Benavides-Piccione, R., & DeFelipe, J. (2001). The pyramidal cell in cognition: A comparative study in human and monkey. *The Journal of Neuroscience*, *21*, RC163 - RC163. doi:10.1523/JNEUROSCI.21-17-j0002.2001

Forbes, N. F., Carrick, L. A., McIntosh, A. M., & Lawrie, S. M. (2009). Working memory in schizophrenia: A meta-analysis. *Psychological Medicine*, *39*(6), 889–905. doi:10.1017/S0033291708004558

Frohlich, J., & van Horn, J. D. (2014). Reviewing the ketamine model for schizophrenia. *Journal of Psychopharmacology*, *28*(4), 287–302. doi:10.1177/0269881113512909

Funahashi, S., Bruce, C. J., & Goldman-Rakic, P. S. (1989). Mnemonic coding of visual space in the monkey's dorsolateral PFC. *Journal of Neurophysiology*, *61*(2), 331-349. doi:10.1152/jn.1989.61.2.331

Funahashi, S., Bruce, C. J., & Goldman-Rakic, P. S. (1993). Dorsolateral prefrontal lesions and oculomotor delayed-response performance: Evidence for mnemonic "scotomas". *The Journal of Neuroscience*, *13*(4), 1479–1497. doi:10.1523/JNEUROSCI.13-04-01479.1993

Fuster, J. M., & Alexander, G. E. (1970). Delayed response deficit by cryogenic depression of frontal cortex. *Brain Research*, *20*(1), 85–90. doi:10.1016/0006-8993(70)90156-3

Fuster, J. M., & Alexander, G. E. (1971). Neuron activity related to short-term memory. *Science*, *173*(3997), 652–654. doi:10.1126/science.173.3997.652

- Fuster, J. M. (1973). Unit activity in PFC during delayed-response performance: Neuronal correlates of transient memory. *Journal of Neurophysiology*, *36*(1), 61–78. doi:10.1152/jn.1973.36.1.61
- Fuster, J. M., Bodner, M., & Kroger, J. K. (2000). Cross-modal and cross-temporal association in neurons of frontal cortex. *Nature*, *405*(6784), 347–351. doi:10.1038/35012613
- Eichenbaum, H. (2014). Time cells in the hippocampus: A new dimension for mapping memories. *Nature Reviews Neuroscience*, *15*, 732–744. doi:10.1038/nrn3827
- Elston G. N., Benavides-Piccione R., & DeFelipe J. (2001). The pyramidal cell in cognition: A comparative study in human and monkey. *Journal of Neuroscience*, *21*, 163. doi:10.1523/JNEUROSCI.21-17-j0002.2001
- Erlander, M. G., & Tobin, A. J. (1991). The structural and functional heterogeneity of glutamic acid decarboxylase: a review. *Neurochemical Research*, *16*(3), 215–226. doi:10.1007/BF00966084
- Gemperle, A. Y., Enz, A., Pozza, M. F., Lüthi, A., & Olpe, H. R. (2003). Effects of clozapine, haloperidol and iloperidone on neurotransmission and synaptic plasticity in PFC and their accumulation in brain tissue: An in vitro study. *Neuroscience*, *117*(3), 681–695. doi:10.1016/s0306-4522(02)00769-8
- Goldman-Rakic, P. S. (1995). Cellular basis of working memory. *Neuron*, *14*(3), 477–485. doi:10.1016/0896-6273(95)90304-6
- Gold, J. M. (2004). Cognitive deficits as treatment targets in schizophrenia. *Schizophrenia Research*, *72*(1), 21–28. doi:10.1016/j.schres.2004.09.008
- Harlow, H. F., & Bromer, J. A. (1938). A test apparatus for monkeys. *The Psychological Record*, *2*, 434–436.
- Harris, K. (2005). Neural signatures of cell assembly organization. *Nature Review Neuroscience*, *6*, 399–407. doi:10.1038/nrn1669
- Hashimoto, T., Volk, D. W., Eggan, S. M., Mirnics, K., Pierri, J. N., Sun, Z., Sampson, A. R., & Lewis, D. A. (2003). Gene expression deficits in a subclass of GABA neurons in the PFC of subjects with schizophrenia. *The Journal of Neuroscience*, *23*(15), 6315–6326. doi:10.1523/JNEUROSCI.23-15-06315.2003
- Harvey, C. D., Coen, P., & Tank, D. W. (2012). Choice-specific sequences in parietal cortex during a virtual-navigation decision task. *Nature*, *484*, 62–68. doi:10.1038/nature10918

- Havenith, M. N., Yu, S., Biederlack, J., Chen, N. H., Singer, W., & Nikolić, D. (2011). Synchrony makes neurons fire in sequence, and stimulus properties determine who is ahead. *The Journal of Neuroscience*, *31*(23), 8570–8584. doi:10.1523/JNEUROSCI.2817-10.2011
- Henriksen, M. G., Nordgaard, J., & Jansson, L. B. (2017). Genetics of schizophrenia: Overview of methods, findings and limitations. *Frontiers in Human Neuroscience*, *11*, 322. doi:10.3389/fnhum.2017.00322
- Homayoun, H., & Moghaddam, B. (2007). NMDA receptor hypofunction produces opposite effects on PFC interneurons and pyramidal neurons. *The Journal of Neuroscience*, *27*(43), 11496–11500. doi:10.1523/JNEUROSCI.2213-07.2007
- Hubel, D. H. (1957). Tungsten microelectrode for recording from single units. *Science*, *125*, 549–550. doi:10.1126/science.125.3247.549
- Hunter, W. S. (1913). The delayed reaction in animals and children. *Animal Behavior Monographs*, *2*, 86.
- Iba, M., & Sawaguchi, T. (2003). Involvement of the dorsolateral PFC of monkeys in visuospatial target selection. *Journal of Neurophysiology*, *89*(1), 587–599. doi:10.1152/jn.00148.2002
- Itskov, V., Curto, C., Pastalkova, E., & Buzsáki, G. (2011). Cell assembly sequences arising from spike threshold adaptation keep track of time in the hippocampus. *Journal of Neuroscience*, *31*(8), 2828–2834. doi:10.1523/JNEUROSCI.3773-10.2011
- Jacobsen, C. F. (1936). Studies of cerebral function in primates. I. The functions of the frontal association areas in monkeys. *Comparative Psychology Monographs*, *13*, 1–60.
- Javitt, D. C. (1987). Negative schizophrenic symptomatology and the PCP (phencyclidine) model of schizophrenia. *The Hillside Journal of Clinical Psychiatry*, *9*(1), 12–35.
- Jensen, O., & Tesche, C. D. (2002). Frontal theta activity in humans increases with memory load in a working memory task. *The European Journal of Neuroscience*, *15*(8), 1395–1399. doi:10.1046/j.1460-9568.2002.01975.x
- Kaar, S. J., Angelescu, I., Marques, T. R., & Howes, O. D. (2019). Pre-frontal parvalbumin interneurons in schizophrenia: A meta-analysis of post-mortem studies. *Journal of Neural Transmission*, *126*(12), 1637–1651. doi:10.1007/s00702-019-02080-2
- Kawaguchi, Y., & Kubota, Y. (1997). GABAergic cell subtypes and their synaptic connections in rat frontal cortex. *Cerebral Cortex*, *7*(6), 476–486.

doi:10.1093/cercor/7.6.476

Kempton, M. J., Stahl, D., Williams, S. C., & DeLisi, L. E. (2010). Progressive lateral ventricular enlargement in schizophrenia: A meta-analysis of longitudinal MRI studies. *Schizophrenia Research*, *120*(1-3), 54–62. doi:10.1016/j.schres.2010.03.036

Kepecs, A., & Fishell, G. (2014). Interneuron cell types are fit to function. *Nature*, *505*(7483), 318–326. doi:10.1038/nature12983

Kojima, S., & Goldman-Rakic, P. S. (1982). Delay-related activity of prefrontal neurons in rhesus monkeys performing delayed response. *Brain Research*, *248*(1), 43–50. doi:10.1016/0006-8993(82)91145-3

Kolk, S. M., & Rakic, P. (2022). Development of PFC. *Neuropsychopharmacology*, *47*, 41–57. doi:10.1038/s41386-021-01137-9

Kolluri, N., Sun, Z., Sampson, A. R., & Lewis, D. A. (2005). Lamina-specific reductions in dendritic spine density in the PFC of subjects with schizophrenia. *The American Journal of Psychiatry*, *162*(6), 1200–1202. doi:10.1176/appi.ajp.162.6.1200

Konradi, C., & Heckers, S. (2003). Molecular aspects of glutamate dysregulation: Implications for schizophrenia and its treatment. *Pharmacology & Therapeutics*, *97*(2), 153–179. doi:10.1016/s0163-7258(02)00328-5

Kroemer, R. T., Koutsilieri, E., Hecht, P., Liedl, K. R., Riederer, P., & Kornhuber, J. (1998). Quantitative analysis of the structural requirements for blockade of the N-methyl-D-aspartate receptor at the phencyclidine binding site. *Journal of Medicinal Chemistry*, *41*(3), 393–400. doi:10.1021/jm9704412

Kritzer, M. F., & Goldman-Rakic, P. S. (1995). Intrinsic circuit organization of the major layers and sublayers of the dorsolateral PFC in the rhesus monkey. *The Journal of Comparative Neurology*, *359*(1), 131–143. doi:10.1002/cne.903590109

Krystal, J. H., Karper, L. P., Seibyl, J. P., Freeman, G. K., Delaney, R., Bremner, J. D., Heninger, G. R., Bowers, M. B., Jr., & Charney, D. S. (1994). Subanesthetic effects of the noncompetitive NMDA antagonist, ketamine, in humans. Psychotomimetic, perceptual, cognitive, and neuroendocrine responses. *Archives of General Psychiatry*, *51*(3), 199–214. doi:10.1001/archpsyc.1994.03950030035004

Kubota, K., & Niki, H. (1971). Prefrontal cortical unit activity and delayed alternation performance in monkeys. *Journal of Neurophysiology*, *34*(3), 337–347. doi:10.1152/jn.1971.34.3.337

- Laubach, M., Amarante, L. M., Swanson, K., & White, S. R. (2018). What, if anything, is rodent PFC?. *eNeuro*, *5*(5), ENEURO.0315-18.2018. doi:10.1523/ENEURO.0315-18.2018
- Li, D., & He, L. (2007). Association study between the NMDA receptor 2B subunit gene (GRIN2B) and schizophrenia: A HuGE review and meta-analysis. *Genetics in Medicine*, *9*(1), 4–8. doi:10.1097/01.gim.0000250507.96760.4b
- Levitt, J. B., Lewis, D. A., Yoshioka, T., & Lund, J. S. (1993). Topography of pyramidal neuron intrinsic connections in macaque monkey PFC (areas 9 and 46). *The Journal of Comparative Neurology*, *338*, 360-376. doi:10.1002/cne.903380304
- Leavitt, M. L., Mendoza-Halliday, D., & Martinez-Trujillo, J. C. (2017a). Sustained activity encoding working memories: Not fully distributed. *Trends in Neurosciences*, *40*(6), 328–346. doi:10.1016/j.tins.2017.04.004
- Leavitt, M. L., Pieper, F., Sachs, A. J., & Martinez-Trujillo, J. C. (2017b). Correlated variability modifies working memory fidelity in primate prefrontal neuronal ensembles. *Proceedings of the National Academy of Sciences of the United States of America*, *114*(12), 2494–E2503. doi:10.1073/pnas.1619949114
- Lennie, P. (2003). The cost of cortical computation. *Current Biology*, *13*(6), 493–497. doi:10.1016/s0960-9822(03)00135-0
- Lester, R., Clements, J., Westbrook, G., & Jahr, C. E. (1990). Channel kinetics determine the time course of NMDA receptor-mediated synaptic currents. *Nature* *346*, 565–567. doi:10.1038/346565a0
- Lewis, D. A., Curley, A. A., Glausier, J. R., & Volk, D. W. (2012). Cortical parvalbumin interneurons and cognitive dysfunction in schizophrenia. *Trends in Neurosciences*, *35*(1), 57–67. doi:10.1016/j.tins.2011.10.004
- Lepage, M., Bodnar, M., & Bowie, C. R. (2014). Neurocognition: Clinical and functional outcomes in schizophrenia. *Canadian Journal of Psychiatry*, *59*(1), 5–12. doi:10.1177/070674371405900103
- Llinás, R. R. (2001). *I of the vortex: From neurons to self*. The MIT Press.
- Luo, Y., Li, J., Jiang, F., Tan, A., Qin, X., Xiao, X., Wang, Z., Wang, P., Yi, Y., Li, J., Yuan, S., Liu, L., & Xiao, J. (2022). Autoimmune encephalitis with psychotic manifestations and cognitive impairment presenting as schizophrenia: Case report and literature review. *Frontiers in Psychiatry*, *13*, 827138. doi:10.3389/fpsy.2022.827138
- Lundqvist, M., Rose, J., Herman, P., Brincat, S. L., Buschman, T. J., & Miller, E.

- K. (2016). Gamma and beta bursts underlie working memory. *Neuron*, *90*(1), 152–164. doi:10.1016/j.neuron.2016.02.028
- Lundqvist, M., Herman, P., Warden, M. R., Brincat, S. L., & Miller, E. K. (2018a). Gamma and beta bursts during working memory readout suggest roles in its volitional control. *Nature Communications*, *9*(1), 394. doi:10.1038/s41467-017-02791-8
- Lundqvist, M., Herman, P., & Miller, E. K. (2018b). Working memory: Delay activity, yes! Persistent activity? Maybe not. *The Journal of Neuroscience*, *38*(32), 7013–7019. doi:10.1523/JNEUROSCI.2485-17.2018
- Lynch, D. R., Rattelle, A., Dong, Y. N., Roslin, K., Gleichman, A. J., & Panzer, J. A. (2018). Anti-NMDA receptor encephalitis: Clinical features and basic mechanisms. *Advances in Pharmacology*, *82*, 235–260. doi:10.1016/bs.apha.2017.08.005
- Malmö, R. B. (1942). Interference factors in delayed response in monkeys after removal of frontal lobes. *Journal of Neurophysiology*, *5*, 295–308.
- Ma, L., Skoblenick, K., Johnston, K., & Everling, S. (2018). Ketamine alters lateral prefrontal oscillations in a rule-based working memory task. *The Journal of Neuroscience*, *38*(10), 2482–2494. doi:10.1523/JNEUROSCI.2659-17.2018
- Malhotra, A. K., Pinals, D. A., Adler, C. M., Elman, I., Clifton, A., Pickar, D., & Breier, A. (1997). Ketamine-induced exacerbation of psychotic symptoms and cognitive impairment in neuroleptic-free schizophrenics. *Neuropsychopharmacology*, *17*(3), 141–150. doi:10.1016/S0893-133X(97)00036-5
- Matsuda, Y., & Ohi, K. (2018). Cortical gyrification in schizophrenia: Current perspectives. *Neuropsychiatric Disease and Treatment*, *14*, 1861–1869. doi:10.2147/NDT.S145273
- Mendoza-Halliday, D., & Martinez-Trujillo, J. (2017). Neuronal population coding of perceived and memorized visual features in the lateral PFC. *Nature Communications*, *8*, 15471. doi:10.1038/ncomms15471
- Melchitzky, D. S., Sesack, S. R., Pucak, M. L., & Lewis, D. A. (1998). Synaptic targets of pyramidal neurons providing intrinsic horizontal connections in monkey PFC. *The Journal of Comparative Neurology*, *390*, 211–224. doi:10.1002/(SICI)1096-9861(19980112)390:2<211::AID-CNE4>3.0.CO;2-4
- Medalla, M., & Luebke, J. I. (2015). Diversity of glutamatergic synaptic strength in lateral prefrontal versus primary visual cortices in the rhesus monkey. *The*

Journal of Neuroscience, 35(1), 112–127. doi:10.1523/JNEUROSCI.3426-14.2015

Meyers, E. M., Freedman, D. J., Kreiman, G., Miller, E. K., & Poggio, T. A. (2008). Dynamic population coding of category information in inferior temporal and PFC. *Journal of Neurophysiology*, 100(3), 1407–19. doi:10.1152/jn.90248.2008

Miller, E. K., Erickson, C. A., & Desimone, R. (1996). Neural mechanisms of visual working memory in PFC of the macaque. *Journal of Neuroscience*, 16, 5154–5167. doi:10.1523/JNEUROSCI.16-16-05154.1996

Mirnics, K., Middleton, F. A., Marquez, A., Lewis, D. A., & Levitt, P. (2000). Molecular characterization of schizophrenia viewed by microarray analysis of gene expression in PFC. *Neuron*, 28(1), 53–67. doi:10.1016/s0896-6273(00)00085-4

Montemurro, M. A., Rasch, M. J., Murayama, Y., Logothetis, N. K., & Panzeri, S. (2008). Phase-of-firing coding of natural visual stimuli in primary visual cortex. *Current Biology*, 18(5), 375–380. doi:10.1016/j.cub.2008.02.023

Morgan, C. J., Mofeez, A., Brandner, B., Bromley, L., & Curran, H. V. (2004). Acute effects of ketamine on memory systems and psychotic symptoms in healthy volunteers. *Neuropsychopharmacology*, 29(1), 208–218. doi:10.1038/sj.npp.1300342

Murray, A. J., Woloszynowska-Fraser, M. U., Ansel-Bollepalli, L., Cole, K. L., Foggetti, A., Crouch, B., Riedel, G., & Wulff, P. (2015). Parvalbumin-positive interneurons of the PFC support working memory and cognitive flexibility. *Scientific Reports*, 5, 16778. doi:10.1038/srep16778

Murray, J. D., Bernacchia, A., Roy, N. A., Constantinidis, C., Romo, R., & Wang, X. J. (2017). Stable population coding for working memory coexists with heterogeneous neural dynamics in PFC. *Proceedings of the National Academy of Sciences of the United States of America*, 114(2), 394–399. doi:10.1073/pnas.1619449114

Nakazawa, K., Zsiros, V., Jiang, Z., Nakao, K., Kolata, S., Zhang, S., & Belforte, J. E. (2012). GABAergic interneuron origin of schizophrenia pathophysiology. *Neuropharmacology*, 62(3), 1574–1583. doi:10.1016/j.neuropharm.2011.01.022

Orbach, J., & Fischer, G. J. (1959). Bilateral resections of frontal granular cortex. Factors influencing delayed response and discrimination performance in monkeys. *Archives of Neurology*, 1, 78–86. doi:10.1001/archneur.1959.03840010080010

Okubo, T. S., Mackevicius, E. L., Payne, H. L., Lynch, G. F., & Fee, M. S. (2015). Growth and splitting of neural sequences in songbird vocal development. *Nature*, *528*, 352. doi:10.1038/NATURE15741

Olney, J. W., Newcomer, J. W., & Farber, N. B. (1999). NMDA receptor hypofunction model of schizophrenia. *Journal of Psychiatric Research*, *33*(6), 523–533. doi:10.1016/s0022-3956(99)00029-1

Palaniyappan, L., & Liddle, P. F. (2012). Aberrant cortical gyrification in schizophrenia: A surface-based morphometry study. *Journal of Psychiatry & Neuroscience*, *37*(6), 399–406. doi:10.1503/jpn.110119

Passingham, R. E., & Wise, S. P. (2012). *The Neurobiology of the PFC: Anatomy, Evolution, and the Origin of Insight*. Oxford University Press. London. doi:10.1093/acprof:osobl/9780199552917.001.0001

Parthasarathy, A., Tang, C., Herikstad, R., Cheong, L-F., Yen, S-C., & Libedinsky, C. (2019). Time-invariant working memory representations in the presence of code-morphing in the lateral PFC. *Nature Communications*, *10*, 4995. doi:10.1038/s41467-019-12841-y

Parthasarathy, A., Herikstad, R., Bong, J. H., Medina, F. S., Libedinsky, C., & Yen, S. C. (2017). Mixed selectivity morphs population codes in PFC. *Nature Neuroscience*, *20*(12), 1770–1779. doi:10.1038/s41593-017-0003-2

Park, S., & Holzman, P. S. (1992). Schizophrenics show spatial working memory deficits. *Archives of General Psychiatry*, *49*(12), 975–982. doi:10.1001/archpsyc.1992.01820120063009

Pierri, J. N., Volk, C. L., Auh, S., Sampson, A., & Lewis, D. A. (2001). Decreased somal size of deep layer 3 pyramidal neurons in the PFC of subjects with schizophrenia. *Archives of General Psychiatry*, *58*(5), 466–473. doi:10.1001/archpsyc.58.5.466

Petrides, M., & Pandya, D. N. (1999). Dorsolateral PFC: Comparative cytoarchitectonic analysis in the human and the macaque brain and corticocortical connection patterns. *European Journal of Neuroscience*, *11*, 1011-1036. doi:10.1046/j.1460-9568.1999.00518.x

Petrides, M. (2005). Lateral PFC: Architectonic and functional organization. *Philosophical transactions of the Royal Society of London*, *360*(1456), 781–795. doi:10.1098/rstb.2005.1631

Plitman, E., Nakajima, S., de la Fuente-Sandoval, C., Gerretsen, P., Chakravarty, M. M., Kobylanski, J., Chung, J. K., Caravaggio, F., Iwata, Y., Remington, G., & Graff-Guerrero, A. (2014). Glutamate-mediated excitotoxicity in schizophrenia: A

review. *European Neuropsychopharmacology*, 24(10), 1591–1605.
doi:10.1016/j.euroneuro.2014.07.015

Preuss, T. M., Wise, S. P. (2022). Evolution of PFC. *Neuropsychopharmacology*, 47, 3–19. doi:10.1038/s41386-021-01076-5

Pucak, M. L., Levitt, J. B., Lund, J. S., & Lewis, D. A. (1996). Patterns of intrinsic and associational circuitry in monkey PFC. *The Journal of Comparative Neurology*, 376, 614–630. doi:10.1002/(SICI)1096-9861(19961223)376:4<614::AID-CNE9>3.0.CO;2-4

Rainer, G., & Miller, E. K. (2002). Time course of object-related neural activity in the primate PFC during a short-term memory task. *The European Journal of Neuroscience*, 15(7), 1244–1254. doi:10.1046/j.1460-9568.2002.01958.x

Rao, S. G., Williams, G. V., & Goldman-Rakic, P. S. (1999). Isodirectional tuning of adjacent interneurons and pyramidal cells during working memory: Evidence for microcolumnar organization in PFC. *Journal of Neurophysiology*, 81(4), 1903–1916. doi:10.1152/jn.1999.81.4.1903

Rao, S. G., Williams, G. V., & Goldman-Rakic, P. S. (2000). Destruction and creation of spatial tuning by disinhibition: GABA(A) blockade of prefrontal cortical neurons engaged by working memory. *The Journal of Neuroscience*, 20(1), 485–494. doi:10.1523/JNEUROSCI.20-01-00485.2000

Romo, R., Brody, C., Hernández, A., & Lemus, L. (1999). Neuronal correlates of parametric working memory in the PFC. *Nature*, 399, 470–473. doi:10.1038/20939

Roussy, M., Mendoza-Halliday, D., & Martinez-Trujillo, J. C. (2021). Neural substrates of visual perception and working memory: Two sides of the same coin or two different coins? *Frontiers Neural Circuits*, 15, 764177. doi:10.3389/fncir.2021.764177

Sawaguchi, T., & Goldman-Rakic, P. S. (1991). D1 dopamine receptors in PFC: Involvement in working memory. *Science*, 251(4996), 947–950.

Seeman, P., Niznik, H. B., & Guan, H.-C. (1990). Elevation of dopamine D₂ receptors in schizophrenia is underestimated by radioactive raclopride. *Archives of General Psychiatry*, 47(12), 1170–1172. doi:10.1001/archpsyc.1990.01810240090014

Schizophrenia, (2016). NIMH. Retrieved from:
<https://www.nimh.nih.gov/health/statistics/schizophrenia>

Schmidt, R., Herrojo Ruiz, M., Kilavik, B. E., Lundqvist, M., Starr, P. A., & Aron, A. R. (2019). Beta oscillations in working memory, executive control of movement

and thought, and sensorimotor function. *The Journal of Neuroscience*, 39 (42), 8231-8238. doi: 10.1523/JNEUROSCI.1163-19.2019

Shafi, M., Zhou, Y., Quintana, J., Chow, C., Fuster, J., & Bodner, M. (2007). Variability in neuronal activity in primate cortex during working memory tasks. *Neuroscience*, 146(3), 1082–1108. doi:10.1016/j.neuroscience.2006.12.072

Siegel, M., Warden, M. R., & Miller, E. K. (2009). Phase-dependent neuronal coding of objects in short-term Memory. *Proceedings of the National Academy of Sciences of the United States of America*, 106(50), 21341–21346. doi:10.1073/pnas.090819310

Smucny, J., Dienel, S. J., Lewis, D. A., & Carter, C. S. (2022). Mechanisms underlying dorsolateral prefrontal cortex contributions to cognitive dysfunction in schizophrenia. *Neuropsychopharmacology*, 47, 292–308. doi:10.1038/s41386-021-01089-0

Spaak, E., Watanabe, K., Funahashi, S., & Stokes, M. G. (2017). Stable and dynamic coding for working memory in primate PFC. *The Journal of Neuroscience*, 37(27), 6503–6516. doi:10.1523/JNEUROSCI.3364-16.2017

Starc, M., Murray, J. D., Santamauro, N., Savic, A., Diehl, C., Cho, Y. T., Srihari, V., Morgan, P. T., Krystal, J. H., Wang, X. J., Repovs, G., & Anticevic, A. (2017). Schizophrenia is associated with a pattern of spatial working memory deficits consistent with cortical disinhibition. *Schizophrenia Research*, 181, 107–116. doi:10.1016/j.schres.2016.10.011

Stein, H., Barbosa, J., Rosa-Justicia, M., Prades, L., Morato, A., Galan-Gadea, A., Arino, H., Martinez-Hernandez., Castro-Fornieles, J., Dalmau, J., & Compte, A. (2020). Reduced serial dependence suggests deficits in synaptic potentiation in anti-NMDAR encephalitis and schizophrenia. *Nature Communications*, 11, 4250. doi:10.1038/s41467-020-18033-3

Stokes, M. G., Kusunoki, M., Sigala, N., Nili, H., Gaffan, D., & Duncan, J. (2013). Dynamic coding for cognitive control in PFC. *Neuron*, 78(2), 364–375. doi:10.1016/j.neuron.2013.01.039

Sreenivasan, K. K., Vytlačil, J., & D'Esposito, M. (2014). Distributed and dynamic storage of working memory stimulus information in extrastriate cortex. *Journal of Cognitive Neuroscience*, 26(5), 1141–1153. doi:10.1162/jocn_a_00556

Srivastava, K. H., Holmes, C. M., Vellema, M., Pack, A. R., Elemans, C. P. H., Nemenman, I., & Sober, S. J. (2017). Motor control by precisely timed spike patterns. *Proceedings of the National Academy of Sciences*, 114(5), 1171–1176. doi:10.1073/PNAS.1611734114/-/DCSUPPLEMENTAL

Suzuki, M., & Gottlieb, J. (2013). Distinct neural mechanisms of distractor suppression in the frontal and parietal lobe. *Nature Neuroscience*, *16*(1), 98–104. doi:10.1038/nn.3282

Tang, C., Chehayeb, D., Srivastava, K., Nemenman, I., & Sober, S. J. (2014). Millisecond-scale motor encoding in a cortical vocal area. *PLOS Biology*, *12*(12), e1002018. doi:10.1371/JOURNAL.PBIO.1002018

Takeda, K., & Funahashi, S. (2002). Prefrontal task-related activity representing visual cue location or saccade direction in spatial working memory tasks. *Journal of Neurophysiology*, *87*(1), 567–588. doi:10.1152/jn.00249.2001

Tobias, T. J. (1975). Afferents to PFC from the thalamic mediodorsal nucleus in the rhesus monkey. *Brain Research*, *83*(2), 191–212. doi:10.1016/0006-8993(75)90930-0

Torres-Gomez, S., Blonde, J. B., Mendoza-Halliday, D., Kuebler, E., Everest, M., Wang, X-J., Inoue, W., Poulter, M. O., Martinez-Trujillo, J. (2020). Changes in the proportion of inhibitory interneuron types from sensory to executive areas of the primate neocortex: Implications for the origins of working memory representations. *Cerebral Cortex*, *30*(8), 4544–4562. doi:10.1093/cercor/bhaa056

Upright, N. A., Brookshire, S. W., Schnebelen, W., Damatac, C. G., Hof, P. R., Browning, P., Croxson, P. L., Rudebeck, P. H., & Baxter, M. G. (2018). Behavioral effect of chemogenetic inhibition is directly related to receptor transduction levels in rhesus monkeys. *The Journal of Neuroscience*, *38*(37), 7969–7975. doi:10.1523/JNEUROSCI.1422-18.2018

van Vugt, B., van Kerkoerle, T., Vartak, D., & Roelfsema, P. R. (2020). The contribution of AMPA and NMDA receptors to persistent firing in the dorsolateral PFC in working memory. *The Journal of Neuroscience*, *40*, 2458–2470. doi:10.1523/JNEUROSCI.2121-19.2020

van Erp, T. G., Hibar, D. P., Rasmussen, J. M., Glahn, D. C., Pearlson, G. D., Andreassen, O. A., Agartz, I., Westlye, L. T., Haukvik, U. K., Dale, A. M., Melle, I., Hartberg, C. B., Gruber, O., Kraemer, B., Zilles, D., Donohoe, G., Kelly, S., McDonald, C., Morris, D. W., Cannon, D. M., ... Turner, J. A. (2016). Subcortical brain volume abnormalities in 2028 individuals with schizophrenia and 2540 healthy controls via the ENIGMA consortium. *Molecular Psychiatry*, *21*(4), 547–553. doi:10.1038/mp.2015.63

Volk, D. W., Austin, M. C., Pierri, J. N., Sampson, A. R., & Lewis, D. A. (2000). Decreased glutamic acid decarboxylase67 messenger RNA expression in a subset of prefrontal cortical gamma-aminobutyric acid neurons in subjects with schizophrenia. *Archives of General Psychiatry*, *57*(3), 237–245. doi:10.1001/archpsyc.57.3.237

Vollenweider, F. X., Leenders, K. L., Scharfetter, C., Antonini, A., Maguire, P., Missimer, J., & Angst, J. (1997). Metabolic hyperfrontality and psychopathology in the ketamine model of psychosis using positron emission tomography (PET) and [18F]fluorodeoxyglucose (FDG). *European Neuropsychopharmacology*, *7*(1), 9–24. doi:10.1016/s0924-977x(96)00039-9

Walker, A. E. (1940). A cytoarchitectural study of the prefrontal area of the macaque monkey. *The Journal of Comparative Neurology*, *73*, 59-86. doi:10.1002/cne.900730106

Wang, X. J. (1999). Synaptic basis of cortical persistent activity: The importance of NMDA receptors to working memory. *The Journal of Neuroscience*, *19*(21), 9587–9603. doi:10.1523/JNEUROSCI.19-21-09587.1999

Wang, M., Yang, Y., Wang, C. J., Gamo, N. J., Jin, L. E., Mazer, J. A., Morrison, J. H., Wang, X. J., & Arnsten, A. F. (2013). NMDA receptors subserve persistent neuronal firing during working memory in dorsolateral PFC. *Neuron*, *77*(4), 736–749. doi:10.1016/j.neuron.2012.12.032

Wang, X. (2001). Synaptic reverberation underlying mnemonic persistent activity. *Trends in Neurosciences*, *24*, 455-463. doi: 10.1016/s0166-2236(00)01868-3

Wang, X. J., Tegnér, J., Constantinidis, C., & Goldman-Rakic, P. S. (2004). Division of labor among distinct subtypes of inhibitory neurons in a cortical microcircuit of working memory. *Proceedings of the National Academy of Sciences of the United States of America*, *101*(5), 1368–1373. doi:10.1073/pnas.0305337101

Weinberger, D. R., Berman, K. F., & Zec, R. F. (1986). Physiologic dysfunction of dorsolateral PFC in schizophrenia. I. Regional cerebral blood flow evidence. *Archives of General Psychiatry*, *43*(2), 114–124. doi:10.1001/archpsyc.1986.01800020020004

Xie, Y., Hu, P., Li, J., Chen, J., Song, W., Wang, X. J., Yang, T., Dehaene, S., Tang, S., Min, B., & Wang, L. (2022). Geometry of sequence working memory in macaque PFC. *Science*, *375*(6581), 632–639. doi:10.1126/science.abm0204

Yang, S-T., Wang, M., Paspalas, C. D., Crimins, J. L., Altman, M. T., Mazer, J. A., & Arnsten, A. F. T. (2018). Core differences in synaptic signaling between primary visual and dorsolateral PFC. *Cerebral Cortex*, *28*(4), 1458–1471. doi: 10.1093/cercor/bhx357

Zhou, S., Masmanidis, S. C., & Buonomano, D. V. (2020). Neural sequences as an optimal dynamical regime for the readout of time. *Neuron*, *108*(4), 651–658.e5. doi:10.1016/J.NEURON.2020.08.020

Zhang, Y., Chen, Y., Bressler, S. L., & Ding, M. (2008). Response preparation and inhibition: The role of the cortical sensorimotor beta rhythm. *Neuroscience*, *156*(1), 238–246. doi:10.1016/j.neuroscience.2008.06.061

Chapter 2

2 « Stable Working Memory and Perceptual Representations in Macaque Lateral Prefrontal Cortex During Naturalistic Vision »

We have developed a novel perception and working memory task that takes place in a complex virtual environment. This task allowed us to explore how the primate prefrontal cortex represents the location of items held in working memory in realistic conditions. We show that despite eye movement and complex visual input, neurons maintain robust working memory representations of space which are distinct from neuronal representations for perception. We provide evidence for separate processing of working memory, perception, and eye movement in virtual reality. We further provide novel insight on the use of virtual environments to construct behavioral tasks for electrophysiological experiments.

2.1 « Abstract »

Primates use perceptual and mnemonic visuospatial representations to perform everyday functions. Neurons in the lateral prefrontal cortex (LPFC) have been shown to encode both of these representations during tasks where eye movements are strictly controlled and visual stimuli are reduced in complexity. This raises the question of whether perceptual and mnemonic representations encoded by LPFC neurons remain robust during naturalistic vision — in the presence of a rich visual scenery and during eye movements. Here we investigate this issue by training macaque monkeys to perform working memory and perception tasks in a visually complex virtual environment that requires navigation using a joystick and allows for free visual exploration of the scene. We recorded the activity of 3950 neurons in the LPFC (areas 8a and 9/46) of two rhesus macaques using multi-electrode arrays, and measured eye movements using video tracking. We found that navigation trajectories to target locations and eye movement behavior differed

between the perception and working memory tasks suggesting that animals employed different behavioral strategies. Single neurons were tuned to target location during cue encoding and working memory delay and neural ensemble activity was predictive of the animals' behavior. Neural decoding of the target location was stable throughout the working memory delay epoch. However, neural representations of similar target locations differed between the working memory and perception tasks. These findings indicate that during naturalistic vision, LPFC neurons maintain robust and distinct neural codes for mnemonic and perceptual visuospatial representations.

2.2 « Introduction »

Seminal lesion studies in the early 20th century demonstrated that the primate lateral prefrontal cortex (LPFC) plays a pivotal role during delayed response tasks involving the maintenance of information in working memory (WM) (Baddeley, 1986; see Roussy, Mendoza-Halliday, & Martinez-Trujillo, 2021a for review). Neurons in the LPFC maintain WM representations of space (Funahashi, Bruce, & Goldman-Rakic, 1989; Goldman-Rakic, 1994; Leavitt, Mendoza-Halliday, & Martinez-Trujillo, 2017a; Constantinidis et al., 2018; Suzuki & Gottlieb, 2013; Miller, Erickson, & Desimone, 1996), as well as perceptual representations (Mendoza-Halliday, & Martinez-Trujillo, 2017; Roussy et al., 2021a). However, neurons in the LPFC are also thought to encode signals related to eye position (Bullock, et al., 2017; Hasegawa, Sawaguchi, Kubota, & Fuster, 1998; Boulay, Pieper, Leavitt, Martinez-Trujillo, & Sachs, 2016). Many of the previous studies of visual WM and perception in the LPFC that sampled neuronal activity have been conducted in conditions where gaze is constrained, and stimuli are shown on a homogenous computer screen. However, during natural vision, primates sample complex information via gaze shifts in visual scenes that contain multiple items and variable layouts. It is unclear whether perceptual and WM representations in LPFC neurons remain invariable or deteriorate under these naturalistic conditions.

One of the most universally recognized spatial WM tasks is the oculomotor delayed response (ODR) task in which animals are required to saccade to a remembered cued location (Funahashi, Bruce, & Goldman-Rakic, 1989; Leavitt, Pieper, Sachs, & Martinez-Trujillo, 2018). During the cue presentation and delay epoch of the task, animals must maintain gaze on a fixation point. Breaking fixation results in an 'error trial' meaning that correct performance of the task is contingent on maintaining proper eye position during the delay epoch. This intentional and task pertinent eye fixation limits the possible effect of gaze shifts and eye position on the measured neuronal activity. However, this strict control of eye position during memory maintenance deviates from how WM is used in naturalistic conditions. In day-to-day life, we move our eyes while using WM, yet we can maintain robust WM representations of locations despite those changes in eye position. It is currently unclear how unrestrained eye position in a visually complex environment may affect the ability of neurons and neuronal ensembles in the LPFC to represent perceptual and mnemonic information.

Here, we measure firing rates of neurons in the LPFC of two macaques during virtual WM and perceptual tasks while allowing the animals to freely view a rich visual environment. We recorded the activity of 3950 neurons in the LPFC (areas 8a and 9/46) (Petrides, 2005) of both animals while measuring eye position. Neuronal activity was predictive of target location during WM and perception despite changes in eye position. Eye position poorly predicted target location when compared to neuronal activity. Additionally, using linear classifiers, we found that coding of remembered and perceived targets does not generalize in LPFC neuronal populations.

2.3 « Results »

2.3.1 Naturalistic Working Memory and Perception Tasks

We developed a naturalistic spatial WM task using a virtual reality engine (Unreal Engine 3, UDK). The task took place in a virtual arena that allowed for free navigation using a joystick. Importantly, to simulate natural behavior, animals were permitted free visual exploration (unconstrained eye movements) during the entire trial duration. On each trial, a target was presented for 3 seconds during the cue epoch at 1 of 9 locations in the virtual arena (Figure. 2.1a, b). In the WM task, the target then disappeared during a 2-second delay epoch. Navigation was disabled (i.e., joystick movements did not trigger any movement in the virtual arena) during the cue and delay epochs. Subsequently, navigation was enabled, and animals were required to virtually navigate to the target location within a 10-second response epoch to obtain a juice reward (Figure. 2.1c). We also developed a perceptual version of this task in which the target remains on screen for the trial duration (Figure. 2.1c). We trained two rhesus monkeys (*Macaca mulatta*) on both virtual tasks and recorded neuronal activity during task performance using two 96-channel micro-electrode arrays (Utah Arrays) in each animal. Arrays were implanted in the left LPFC (area 8a and 9/46; one on each side of the principal sulcus, anterior to the arcuate sulcus) (Figure. 2.1d, e) (Petrides, 2005).

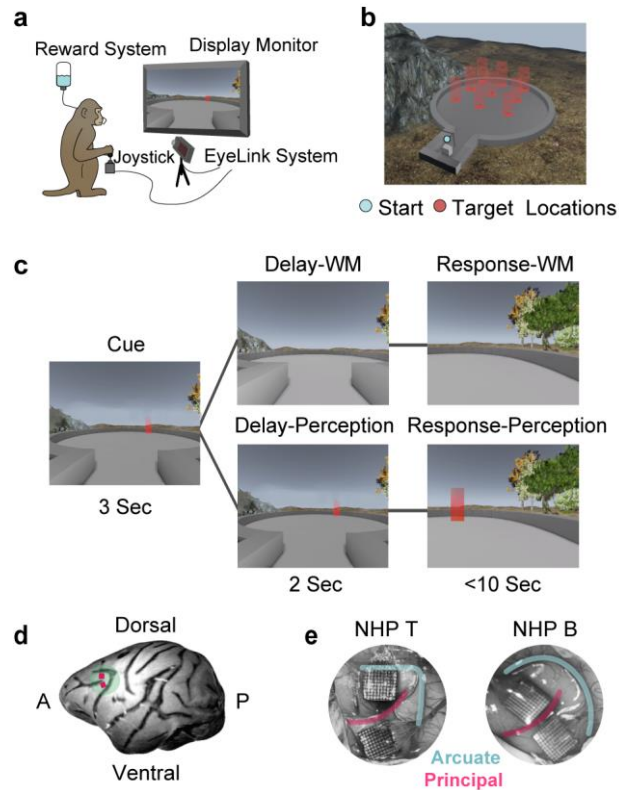


Figure. 2.1: Experimental setup

a. Animal in task setup with joystick, reward system, eye recording system, and monitor displayed. **b.** Overhead view of the virtual environment indicating the start location and the nine target locations. **c.** Task timeline displaying the cue, delay, and response epochs for the working memory and perception tasks. The target remains on screen throughout the delay and response epochs during the perception task. **d.** 3D modeled brain image from an MRI of NHP B with Utah array locations in the left hemisphere indicated by pink squares. **e.** Surgical images showing implanted Utah arrays in both animals.

2.3.2 Task Performance and Animal Behavior

We analyzed behavior from 20 WM sessions (12 from NHP B, 8 from NHP T) and 19 perception sessions (14 from NHP B, 5 from NHP T). Both animals performed the tasks above chance (theoretical chance ~11%). Both animals performed significantly better on the perception (NHP B: *Mean* = 98%, NHP T: *Mean* = 95%) than the WM memory task (NHP B: *Mean* = 87%; NHP T: *Mean* = 57%), reflecting the increased difficulty of including a memory delay epoch (Figure. 2.2a). Response times for correct trials were consistent between animals and tasks (Figure. 2.2b).

We plotted animal trajectories to two example target locations to understand how animals were navigating in the virtual space (Figure. 2.2c). We divided the environment into a 16-cell grid and calculated the number of times that animals entered each cell as part of their navigation trajectory. Two example target locations averaged over all sessions are shown in Figure. 2.2d. We next calculated the trajectory of animals in the environment in each correct trial from their starting location to the location of the target to determine how precise animals navigated towards targets. This real trajectory length was divided by the optimal trajectory length (i.e., Euclidean distance from start to target location), resulting in a measure of deviation from optimal trajectory where a value of 1 indicates that animals took the shortest possible trajectory to a target. Trajectory lengths were similar between animals during perception (NHP B: *Median* = 1.0; NHP T: *Median* = 1.1) and during WM (NHP B: *Median* = 1.8; NHP T: *Median* = 1.9). However, trajectories were more optimal during the perception task than during the WM task, indicating less precise navigation to targets during WM, when the target was not visible (Figure. 2.2e). Overall, these results indicate that both animals used similar behavioral strategies to perform the tasks based on similar response times and trajectories.

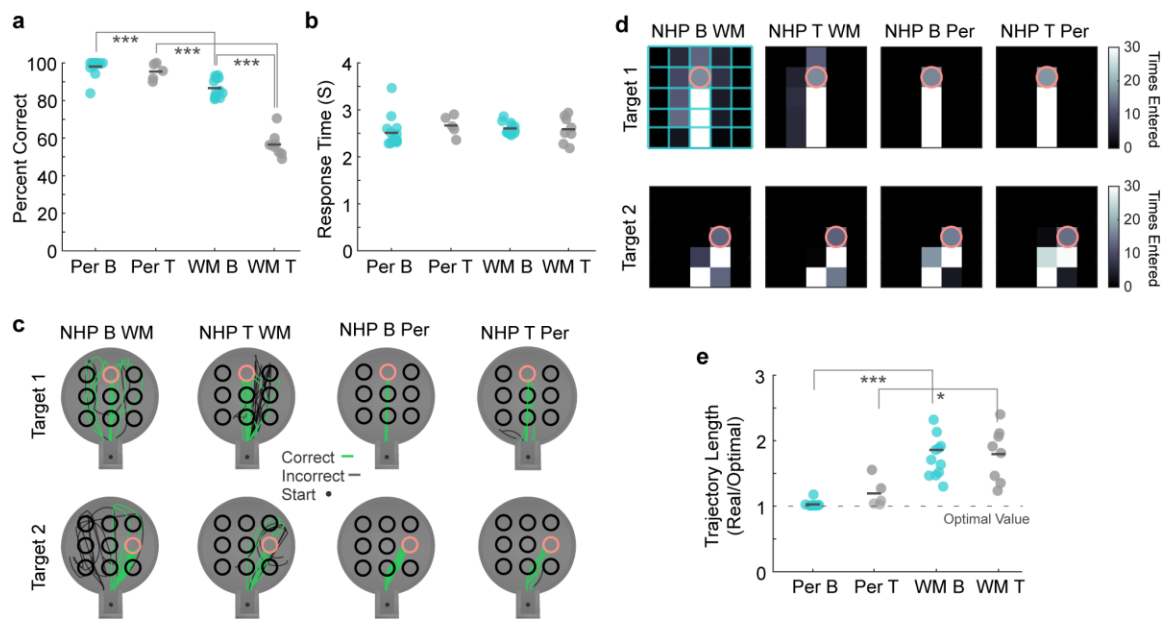


Figure. 2.2: Task behavior

a. Percent of correct trials for the working memory and perception tasks for each session.

b. Response time for correct trials for the working memory and perception tasks for each animal. Dark gray lines represent mean values and each data point represents a session.

c. Animal trajectories plotted for an example session and two example target locations (in pink) in which green trajectories indicate correct trials and black trajectories indicate incorrect trials. Example sessions are included for working memory and perception tasks as well as both animals.

d. The virtual arena divided into 16 regional cells. The number of times each cell is entered (i.e. the number of trajectory points within each cell) is shown averaged over sessions for two example locations (in pink). Examples are included for working memory and perception tasks as well as both animals.

e. Optimal trajectory measures how optimal the trajectory to correct target locations is based on path length in which a value of one, marked by the gray dashed line, reflects the shortest possible path. The optimal trajectory is plotted for the working memory and perception tasks for each animal. Dark gray lines represent median values and each data point represents a session. $p < 0.01 = *$, $p < 0.001 = **$, $p < 0.0001 = ***$.

2.3.3 Eye Behavior During Naturalistic Working Memory and Perception

Our virtual reality setup allowed for precise tracking of eye movement and gaze position; therefore, we measured eye movement behavior during both tasks. First, we calculated the proportion of eye position data points falling within the presentation screen. 'Eyes off screen' occurs when the animals close their eyes or most often, when they look away from the screen. The proportion of eye data points falling within screen boundaries differed between task epochs and between the WM and perception tasks. During WM, animals maintained eye position on the screen less during the delay epoch (*Mean* = 86.0%) than during the cue (*Mean* = 92.9%) or response epochs (*Mean* = 95.0%). During perception, animals maintained their eyes on the screen less during the response epoch (*Mean* = 81.0%) than during the delay (*Mean* = 89.9%) or cue epochs (*Mean* = 92.6%). Unlike during WM, the percentage of eye position on-screen during perception cue and delay epochs showed no significant difference (Figure. 2.3a).

We categorized eye movement into fixations, saccades, and smooth pursuits (Corrigan, Gulli, Doucet, & Martinez-Trujillo, 2017). Example traces displaying the categorization can be found in Figure. 2.3b, c. We compared the proportion of eye movements that fall within each category between task epochs during perception and WM. The proportion of eye movements classified as fixations significantly differed between trial epochs and between WM and perception tasks (Figure. 2.3d). During WM, animals made the most fixations during the cue epoch with fewer made during the delay and response epochs (Cue: *Mean* = 46.2%; Delay: *Mean* = 44.3%; Response: *Mean* = 33.3%). During perception, animals also fixated the least during the response epoch with more fixations made during the cue and delay epochs (Cue: *Mean* = 47.3%; Delay: *Mean* = 46.2%; Response: *Mean* = 35.9%).

The proportion of eye movements classified as saccades significantly differed between trial epochs and between WM and perception tasks. During WM,

the proportion of saccades was highest in the response epoch with fewer occurring in the cue epoch and fewest during the delay epoch (Cue: *Mean* = 37.2%; Delay: *Mean* = 36.9%; Response: *Mean* = 41.8%) (Figure. 2.3d, left panel). During perception, animals also made the highest proportion of saccades during the response epoch (*Mean* = 36.7%) with fewer occurring during the cue (*Mean* = 33.5%) and delay epochs (*Mean* = 27.6%) (Figure. 2.3d, right panel). Between WM and perception response epochs, there was a larger proportion of smooth pursuits during perception (*Mean* = 30.4%) than during WM (*Mean* = 28.1%). The latter may be linked to the presence of the target during perception but not during WM.

During the WM task delay epoch, there was a larger proportion of eye movements classified as saccades than during the corresponding epoch of the perception task (Figure. 2.3d). There was also a larger percentage of eye movements onscreen during the response epoch of the WM task than during the corresponding epoch of the perception task (Figure. 2.3a). During the WM task response epoch, there was also a larger proportion of eye movements classified as saccades than during the corresponding epoch of the perception task (Figure. 2.3d).

To further explore saccadic activity, we calculated the main sequence, reflecting the relationship between saccade peak velocity and amplitude (see methods) (Figure. 2.3e). Saccade velocity was significantly different (higher peak velocities as a function of saccade amplitude) in the response epoch compared to the cue and delay epochs during perception for all amplitude bins (t-test, $p < 0.05$, effect size > 0.2). The increased velocity of saccades during perception response may reflect the use of saccades to track the target during navigation which does not occur during WM when the targets were no longer present (Figure. 2.3e). It may also signify an increase in arousal during navigation, which would be more demanding than the other task epochs. We also compared the main sequences between saccades that land on target and off-target during the delay epoch (Figure. 2.3f). We found that on-target saccades resulted in larger peak velocities; however, these differences were more pronounced and were only significant

during the perception task (WM: t-test, $p > 0.05$; Perception, t-test, 6 bins, $p < 0.05$). Therefore, saccades that land on target versus those that land off-target show a greater difference when the target was physically present compared to when it was removed during the WM delay.

These behavioral results indicate a difference in animal behavior during different task epochs and between WM and perception. In particular, less time spent looking onscreen during the delay epoch of the WM task combined with fewer fixations, and no significant differences in saccade amplitude to targets compared to off-targets suggests that animals were less focused on the target location - likely due to its removal. It is possible that animals searched for landmarks that could serve as references for the target location. Decreased fixation and increased number of saccades during the response epoch as well as an increase in saccade peak velocity may suggest a similar strategy as well as reflect the dynamic nature of the task's response epoch in which the visual environment changes as the animal changes position in the arena.

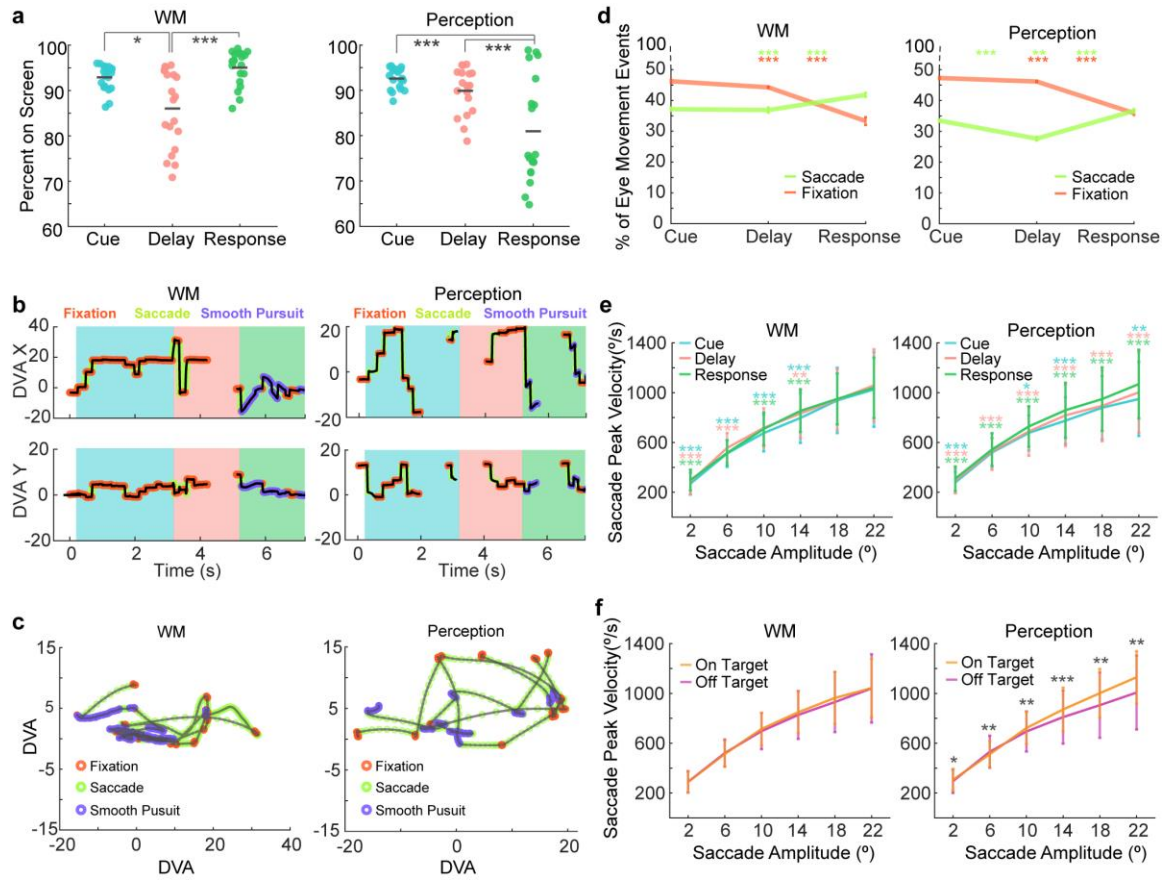


Figure. 2.3: Eye movement behavior

a. Left column: the percent of eye data points that fall within the boundaries of the screen during the cue, delay, and response epochs shown for working memory sessions. Each data point represents a session. Right column: the percent of eye data points that fall within the boundaries of the screen during the cue, delay, and response epochs shown for perception sessions. Each data point represents a session. **b.** Eye traces over trial time categorized into fixations (orange), saccades (green), and smooth pursuits (purple) for an example working memory trial and an example perception trial. **c.** All eye traces categorized into fixations (orange), saccades (green), and smooth pursuits (purple) in screen coordinates for an example working memory trial and an example perception trial. **d.** Percent of eye movement events classified as fixations or saccades during the different task epochs for working memory and perception sessions. Error bars represent the standard error of the mean. Asterisks on the left represent significance between the cue and delay epochs, asterisks in the middle represent significance between the cue and response epochs, and asterisks on the right represent significance between the delay and response epochs. Asterisk color corresponds to eye movement type. **e.** Main sequence for the working memory and perception task during different task epochs. Asterisks represent significance at each amplitude bin. Blue asterisks represent significance between the cue and delay epochs. Green asterisks represent significance between the cue and response epochs. Pink asterisks represent significance between the delay and response epochs. **f.** Main sequence for the working memory and perception tasks for saccades landing on and off of target location. Asterisks represent significance between on-target and off-target saccades at each amplitude bin. Error bars are SEM. $p < 0.01=*$, $p < 0.001=**$, $p < 0.0001=***$.

2.3.4 Neural Spatial Selectivity

We recorded the activity of 3950 units between the dorsally (1992 units) and ventrally (1958 units) placed multi-electrode arrays. Many units in this sample displayed delay activity. Figure. 2.4a, b shows activity patterns of two neurons that selectivity increased their activity during the delay epoch for preferred target locations. Tuning for target location was identified in the population for cue and delay epochs (Cue: Ventral: *Mean* = 22%, Dorsal: *Mean* = 16%; Delay: Ventral: *Mean* = 14%, Dorsal: *Mean* = 12%) and many neurons were tuned during both the cue and delay epochs (Ventral: *Mean* = 37%; Dorsal: *Mean* = 48%) (Figure. 2.4c, d).

At the population level, neurons with the same spatial tuning exhibited increased delay activity during single trials when their preferred target location was presented. Populations of neurons with different spatial tuning from the target presented displayed a lower magnitude of activity (Figure. 2.5).

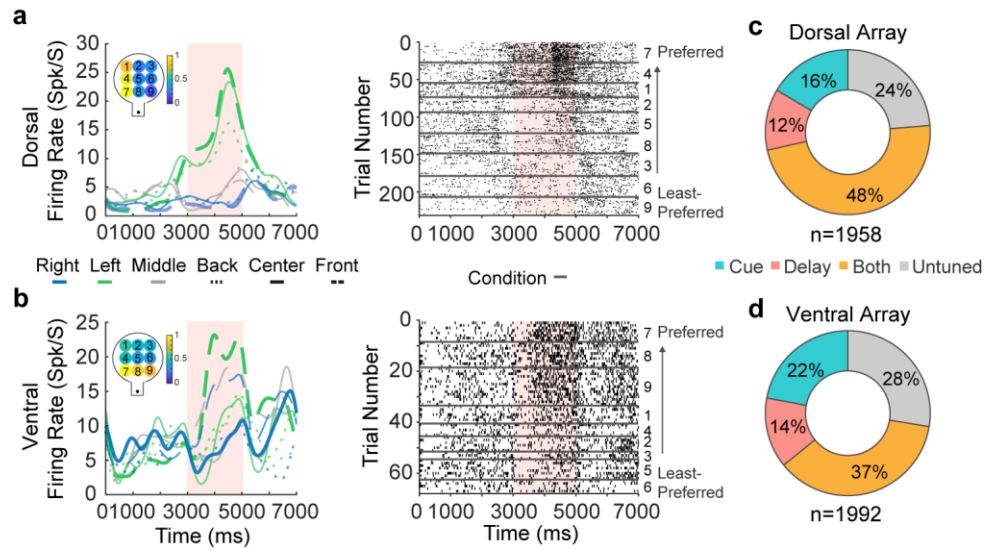


Figure. 2.4: Neural coding for remembered locations

a. Neural activity for an example neuron recorded by the dorsally located electrode array. The spike density function in the left panel displays the neuron's activity over trial time for the nine target locations. The inlet displays normalized firing rate for all target locations. The right panel displays a raster for the same neuron in which trials are sorted by preferred to least-preferred target locations. The delay period is indicated by the salmon-colored column. **b.** Neural activity for an example neuron recorded by the ventrally located electrode array. **c.** The proportion of tuned neurons during the cue (blue), delay (pink/salmon), and during both the cue and delay epochs (orange) recorded in the dorsally located array. **d.** The proportion of tuned neurons recorded in the ventrally located array.

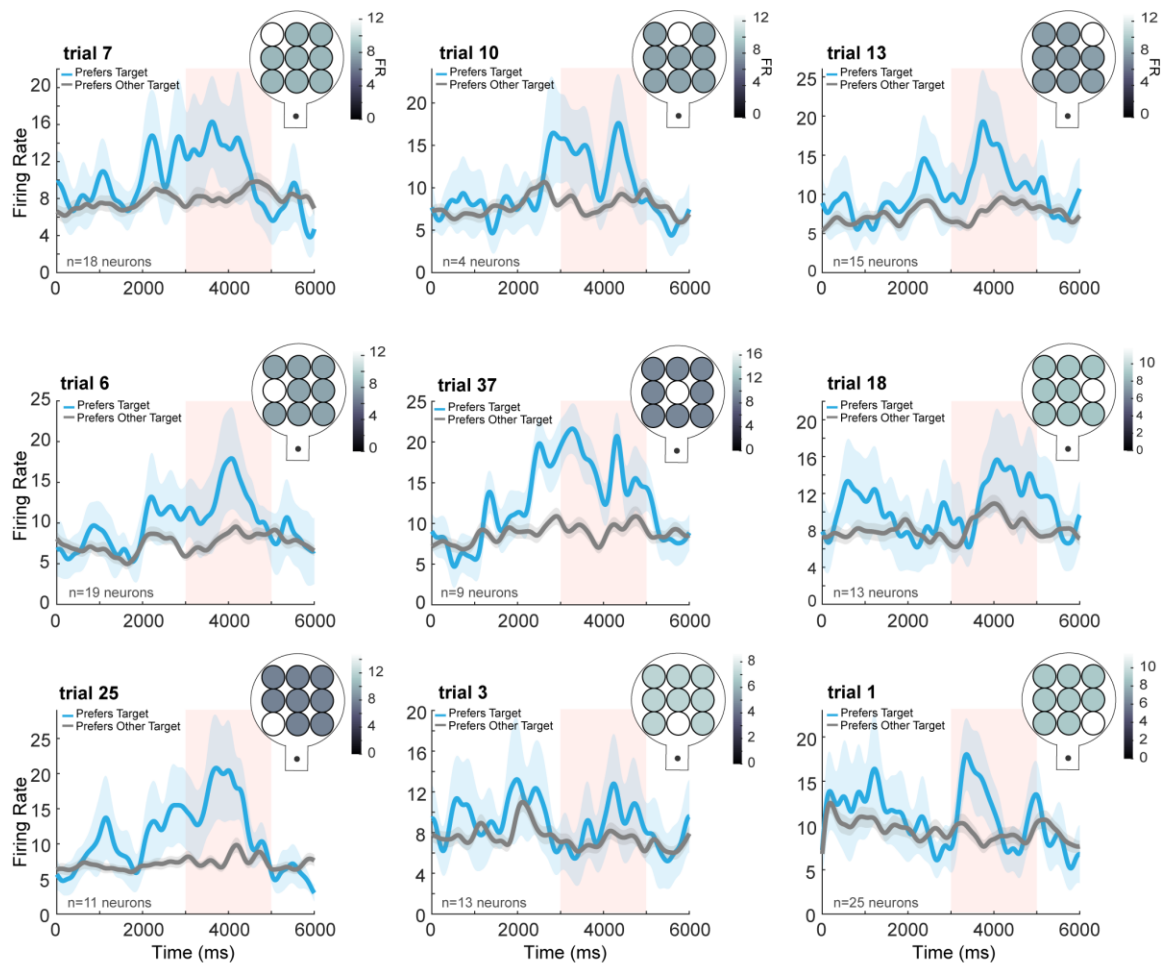


Figure 2.5: Single trial population activity

Delay neuron population activity plotted for single-trial examples for each target location during an example session. The delay period is indicated by the salmon-colored column. The target location for each trial is indicated by the arena inlet (white circle). Blue lines represent the population activity of delay neurons that prefer the target presented in the trial and gray lines represent the population activity of all other delay neurons tuned for other locations. The inlet displays the average delay activity for both populations. Error bars are SEM. n-values represent neurons in the blue population.

To determine how much information about the remembered target locations was contained in the population of neurons, we used a linear classifier (SVM - Support Vector Machine) to decode the target location from neuronal firing rates within 500 ms time bins. We used a best ensemble method in which the most informative unit was found and was paired with all other neurons in the population until the best pair was found. The best pair was grouped with all neurons in the population until the best trio was found. This process was continued until the ensemble contains 20 neurons (Leavitt, Pieper, Sachs, & Martinez-Trujillo, 2017b). To achieve a sample size required for training and testing the classifier for all sessions, we combined trials from all targets located on the right, left, and center of the environment so decoding was performed using three classes.

We were able to decode the target location in single trials from the neural activity during delay using linear classifiers. An example session in Figure. 2.6a shows decoding accuracy for different ensemble sizes during the delay epoch divided into four 500 ms time segments. Decoding accuracy over time was above chance (33.33%) for all time windows, ranging from 68% during the last 500 ms of the included response epoch to 87% towards the end of the cue epoch (Figure. 2.6b). The decoding accuracy was consistent over the delay epoch (Figure. 2.6b), indicating robust information content for remembered locations during our naturalistic task.

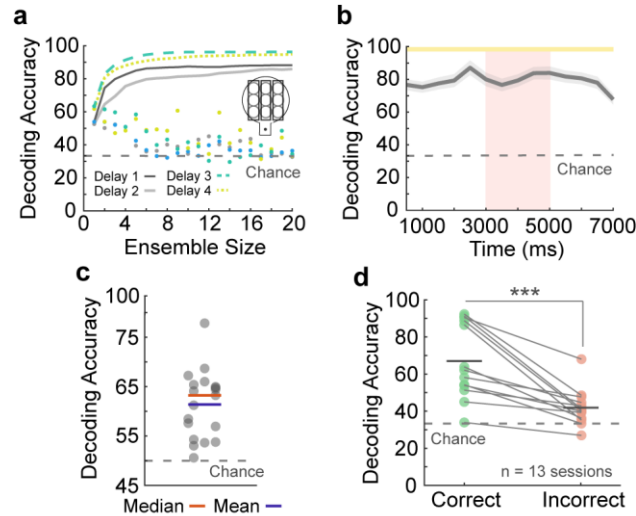


Figure. 2.6: Decoding of remembered locations

a. Decoding accuracy for one example session during the delay period divided into four 500 ms temporal segments using neural ensembles of different sizes. The inset illustrates the grouping of targets into three classes. The dashed gray line represents chance decoding performance. Dots represent the decoding accuracy of individual neurons. **b.** Median decoding accuracy over trial time. The salmon-colored column represents the delay period and the gray dashed line represents chance decoding. The yellow bars on top of the figure represent significance from chance performance for each time window (t-test, $p < 0.05$). Error bars are SEM. **c.** Decoding trial outcome. Dots represent data per session and the gray dashed line indicates chance performance (50%). **d.** Decoding accuracy using correct or incorrect trials. Dots represent data from different sessions and gray solid lines connect data from the session. The gray dashed line represents chance decoding.

We tested whether the firing rate of the recorded neuronal population during the delay period provided enough information to distinguish between correct and incorrect trials. Using linear SVM classification, we were able to predict trial outcome above chance (50%) based on delay epoch population activity (*Mean* = 61.4%, *Median* = 63.2%; t-test, $p = 9.19e-07$) (Figure. 2.6c). To determine whether decoding performance of remembered target location relates to task performance, we used linear SVM classification to predict target location (left, center right) using either all correct or all incorrect trials. We balanced the number of correct and incorrect trial samples in order to make a comparison between the two trial types. Decoding accuracy was significantly higher for correct trials compared to incorrect trials (correct trials: *Mean* = 67.05%; incorrect trials: *Median* = 41.86%; t-test, $p = 4.71e-04$) (Figure. 2.6d). This indicates that population activity during delay was more predictive of target location in correct trials than in incorrect trials.

2.3.5 Fixation on the Target Location

One potential issue in allowing for natural eye movements is that animals could maintain their gaze on the empty cued location during the delay or visually 'rehearse' their movement plan. We explored this possibility by analyzing gaze behavior on the targets. We plotted all fixation points on the screen for one session for two example target locations (Figure. 2.7a). Fixation points span the horizontal extent of the screen (constitutes the task-relevant area). Figure. 2.7b shows heat maps of fixation locations averaged over all sessions for two example target locations during the delay epoch. Gaze was not limited to the location in which the target was presented. It was also directed to non-target stimuli in the environment such as the tree, as would occur in naturalistic contexts.

To examine if increased fixation on the cued target location was used as a behavioral strategy to improve performance, we calculated the percent of fixations falling within the bounds of the target's location. Overall, the percentage of fixations on the target location was very low during the delay epoch (*Median* = 3%). There was no significant difference between correct and incorrect trials suggesting that

increased fixation on cued target locations during the delay epoch may not be an effective strategy in correctly performed trials. (Correct: *Median* = 3.5%; Incorrect: *Median* = 2.6%; Wilcoxon Rank-Sum, $p > 0.05$) (Figure. 2.7c).

To determine how predictive fixation location was of the target location, we divided the screen into 16 cells and calculated the number of fixation points that fell within each cell during the cue and delay epochs. We trained an SVM classifier with a linear kernel to predict which of the nine target locations was presented based on where on screen the animal was fixating. The classifier performed above chance (11.11%) during both epochs but performed significantly better during the cue epoch (*Median* Decoding Accuracy = 31.4%) compared to the delay epoch (*Median* Decoding Accuracy = 20.8%), suggesting reduced patterns of target-specific fixation during the delay (Figure. 2.7d).

To determine whether eye fixation was similar between cue and delay epochs of the WM task, we trained classifiers using eye fixation positions during the cue epoch and tested the classifiers using eye fixation positions from the delay epoch. We similarly trained classifiers on delay data and tested them on cue data. Decoding accuracy was close to chance level (11.11%) when classifiers were cross-trained between epochs of the WM task and it was significantly lower than training and testing on congruent epochs (Figure. 2.7d). This shows that the position of fixations (i.e., gaze position) were different between the cue and delay epochs during the WM task.

Previous studies have shown that LPFC neurons encode information related to eye movements and gaze position (Bullock, Pieper, Sachs, & Martinez-Trujillo, 2017). To corroborate these findings, we examined whether neuronal activity in our sample of LPFC neurons contained information about the animals' gaze position and planned saccade direction. We designed multiple linear regression models to predict firing rate for each neuron during delay epoch eye fixation periods from saccade direction, amplitude, and fixation position (Figure. 2.7e).

After fitting the model to a neuron, we obtained the residual values. These values represent the residual firing rates that are not accounted for by the model. We repeat the procedure for neurons within the same population (i.e., same recording session). We then trained linear SVM classifiers to predict target location using either the firing rate residual values or the raw firing rates from the same population of neurons during the same fixation periods. Decoding accuracy was similar using either type of data (residual: *Mean* = 21.39; real firing rate: *Mean* = 24.95; t-test, $p = 0.26$) (Figure. 2.7f) and both were significantly higher than chance (11.11%) (real firing rate: t-test, $p = 8.6e-06$; residual: t-test, $p = 1.7e-04$), indicating that saccade amplitude, direction, and eye position information were not the main contributors to the decoding of the remembered target location.

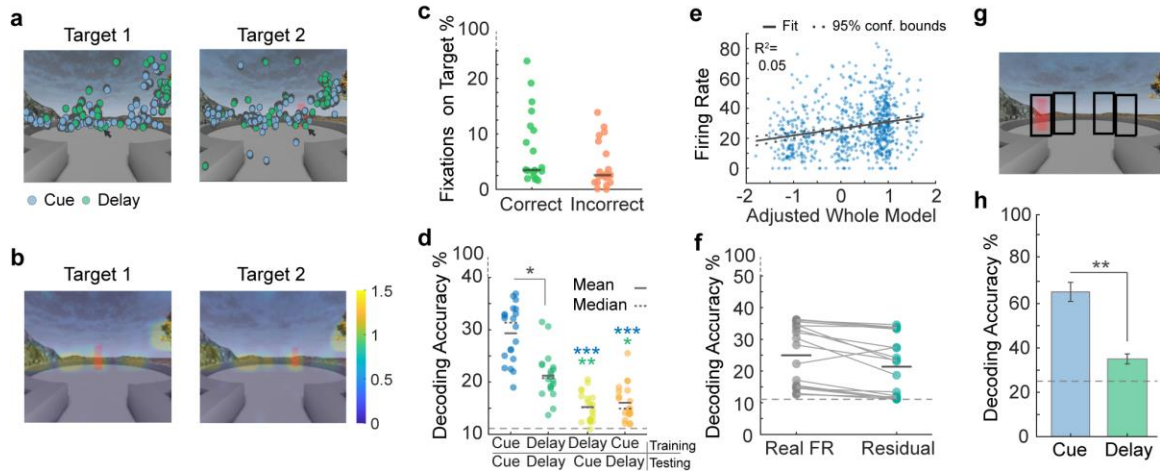


Figure. 2.7: Fixations on screen and target locations

a. All fixations for an example session plotted on screen for the cue period (blue) and delay period (green) for two example target locations. **b.** Heat maps averaged over working memory sessions showing fixation locations on-screen during the delay period for two example target locations. **c.** The percentage of total fixations that fall within the target location during the delay period for correct and incorrect trials. Dark gray lines represent median values, and each data point represents a session. **d.** Decoding accuracy for predicting target location from the location of eye fixations on-screen during the cue and delay epochs. Classifiers are trained on the first epoch listed in the x-axis label and tested on the second epoch. The dashed line represents chance decoding accuracy. **e.** Added variable plot for a linear regression model predicting firing rate during periods of eye fixation during delay epochs from eye position and saccade direction and amplitude for an example neuron. The solid black line represents the model fit and the dashed lines represent 95% confidence bounds of the fit. **f.** Decoding accuracy for predicting target location from real population firing rates during fixation periods and for predicting target location from residual values after fitting the model exemplified in 'e' to each neuron in a population. Dots represent data per session, dark gray lines represent mean values, and the dashed line represents chance decoding performance (11%). **g.** Outlined regions of the screen encompassing four target locations that are separable onscreen. **h.** Median decoding accuracy predicting eye position within the outlined regions shown in panel 'g' using neural population data during fixation periods during the cue and delay epochs. The gray dashed line represents chance decoding accuracy. Error bars are SEM. $p < 0.01=*$, $p < 0.001=**$, $p < 0.0001=***$.

2.3.6 Decoding of Gaze Position from Neural Activity in Prefrontal Neurons

To further examine neural activity related to gaze; particularly, fixation on task-relevant stimuli, we next examined neural activity during fixation on target locations. We selected four targets shown in Figure. 2.7g that were non-overlapping on the screen and measured neuronal firing rates while animals fixated on each one of the target locations. We used SVM classification and found that we could decode the gaze position from neural activity. The decoding accuracy was significantly higher during the cue epoch (*Median* Decoding Accuracy = 65.4%) of the WM task compared to the delay epoch (*Median* Decoding Accuracy = 35.0%) (Figure. 2.7h), suggesting that more information was available to the neuronal population when animals fixate on a target that was present on screen compared to when the target was no longer present. Indeed, the decoding accuracy during the delay epoch was close to chance (25%) suggesting that firing rates during fixation in the delay period carried little information about the remembered target location. One possible explanation for this finding is that decoding during the cue epoch may have been dominated by visual responses to the target. During the delay epoch, when no visual cue was present, eye position contributes poorly to decoding. These findings suggest that eye position signals do not necessarily contribute to the ability of many LPFC neurons to encode WM representations in complex and dynamic environments.

2.3.7 Separation Between Coding for Working Memory and Perception

Unlike the WM task, during the perception task, the target was accessible throughout the trial. Thus, it is possible that some neurons respond to the target only when it was present in the perception task (perceptual neurons) and some neurons are only active during the delay period of the WM task (mnemonic neurons) (Mendoza-Halliday et al., 2017; Roussy et al., 2021a). Therefore, we hypothesized that neural population activity profiles differ during the perception

and WM tasks. To test this hypothesis, we collected neuronal data from 13 sessions in which animals performed both the WM and perception tasks. The same population of simultaneously active neurons were recorded during both tasks during these sessions. This allowed us to use SVM classification to cross-train neural data between WM and perception to predict the 9 target locations. We specifically tested the prediction that SVM classifiers trained in one task will not generalize the performance to the other task.

Decoding performance was similar between WM and perception when classifiers were trained and tested on congruent tasks (i.e., trained on WM and tested on WM) (Figure. 2.8a, b). The same population of neurons can maintain similar amounts of information about the target location whether targets remain on screen (perception) or disappear (WM) (Perception: *Median* Decoding Accuracy = 71.5%; WM: *Median* Decoding Accuracy = 68.1%). Although the same neurons were recorded during each task, decoding performance dropped close to chance level (11.11%) when the classifiers were trained on perception trials and tested on WM trials or when the classifiers were trained on WM trials and tested on perception trials (Figure. 2.8a, b). In comparison, classifiers trained on one-half of the WM trials and tested on the other half resulted in performance well above chance levels (*Median* Decoding Accuracy = 51.3%) (Figure. 2.8c). The latter indicates that our results were not an artifact of using different sets of trials for testing and training the classifiers but were an effect of task type (perception vs WM).

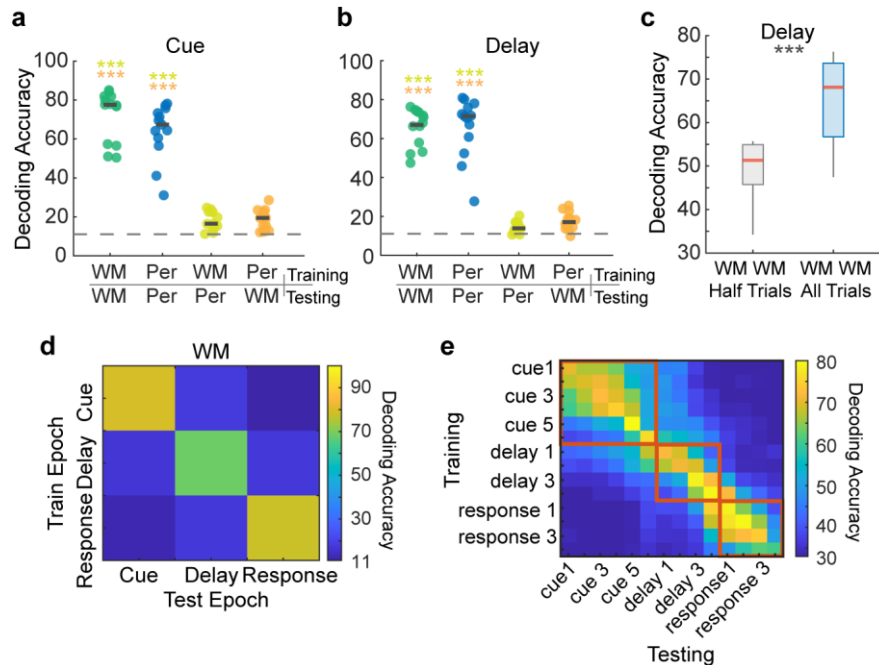


Figure 2.8: Neural coding for working memory and perception

a. Decoding accuracy for predicting target location for the perception and working memory tasks during the cue epoch. Classifiers are trained on the task that appears first in the x-axis label and tested on the task that appears second. Asterisk color represents significant differences with the condition of that color. Dark gray lines represent median values. The dashed gray line represents chance decoding. **b.** Decoding accuracy for predicting target location for the perception and working memory tasks during the delay epoch. **c.** Decoding accuracy for the working memory task during the delay epoch using all trials for classifier training and testing or training on half of the trials and testing on half of the trials. The red lines represent median values and the bottom and top edges of the box indicate the 25th and 75th percentiles. The whiskers extend to non-outlier data points (within 1.5 std). **d.** Cross-epoch median decoding accuracy for the working memory task. **e.** Decoding accuracy when classifiers are cross-trained between 500 ms time windows. $p < 0.01=*$, $p < 0.001=**$, $p < 0.0001=***$.

We also conducted cross-epoch decoding for WM in which we trained and tested on combinations of cue, delay, and response epochs. Decoding performance was greatest when the classifiers were trained and tested with data from the same epoch and lowest when it was trained and tested on data from response and cue epochs (Train on cue - test on response: *Median* Decoding Accuracy = 11.0%; Train on response - test on cue: *Median* Decoding Accuracy = 12.3%) and when data was trained on the delay epoch and tested on the cue epoch (*Median* Decoding Accuracy = 17.0%) (Figure. 2.8d). We also conducted cross-temporal decoding in which we trained and tested classifiers between congruent and incongruent time windows of 500 ms. These results indicate higher decoding accuracy when classifiers were trained and tested between temporally-near time windows within the same trial epoch (Figure. 2.8e). This data suggests that different neural activity profiles support LPFC neural codes for WM and perception.

2.4 « Discussion »

By using complex virtual reality tasks, we were able to explore visuospatial WM and perception in naturalistic settings - incorporating natural eye movements and virtual navigation. We found that animals were able to accurately perform both tasks and identified distinct navigation strategies and eye movement behavior that occur during WM and perception. Whereas animals used a visually guided strategy in the perception task, they necessarily switched their strategy during WM. We also demonstrate the suitability of naturalistic WM tasks for neuronal recording in the LPFC, particularly those that allow for natural eye movements. We found that neurons in the primate LPFC are strongly tuned for target location during cue and delay epochs and that the amount of information during delay about target location remains consistent within the population of neurons on the single-trial level. We also found that neuronal activity during fixation on target location is less predictive of target location during the delay epoch compared to the cue epoch indicating that eye position information does not necessarily contribute to decoding of target location during WM tasks. Information about target location encoded by the same neuronal population during the perception delay was not predictive of target

location during the memory delay, indicating different patterns of population activity during perception and WM. Different population dynamics also exist between target encoding and memory epochs in the WM task.

2.4.1 Influence of Naturalistic Task Elements

One unique element of our task is the complex virtual environment in which it takes place since it contains non-relevant task stimuli. Based on the robust WM signals we describe, the LPFC may allow for the encoding of representations that are uniquely dissociated from distracting stimuli. Indeed, previous studies demonstrate that LPFC differs from areas such as the posterior parietal cortex where WM representations are perturbed by visual distractors (Suzuki, & Gottlieb, 2013; Jacob & Nieder, 2014). Evidence collected decades earlier from Malmö (1942) and Orbach and Fischer (1959) also report the importance of the PFC in maintaining WM representations in the presence of irrelevant incoming visual signals. However, we must be cautious when defining non-relevant stimuli, particularly in our virtual WM task where some of the elements of the environment (e.g., tree) may potentially be used as landmarks to estimate the target location during navigation.

Importantly, despite unconstrained eye movements, animals perform well on our WM task and the neuronal population maintains target selectivity and information about remembered location throughout the delay epoch. These findings may seem to contradict some previous literature showing that forced saccadic eye movements during memory delay reduces WM performance in human subjects (Postle, Idzikowski, Sala, Della, Logie, & Baddeley, 1999) and differentiates the LPFC from regions like the frontal eye fields where shifts in gaze disrupt WM signals (Balan, Ferrera, 2003). However, a distinction between our task and previous research is the production of forced versus naturally occurring saccades. Because the latter may be spontaneously and voluntarily triggered by the subjects, they may not interfere with performance in the same manner as task-dependent saccades. Indeed, before the widespread use of the ODR and other

oculomotor dependent tasks, simple delayed response tasks were used that displayed two targets and relied on an arm motor response through the use of the Wisconsin General Test Apparatus or button pressing. Although eye movements were not controlled in these classic experiments, studies reported neurons in the PFC that displayed clear delay activity and spatial selectivity (Fuster, & Alexander, 1971; Kojima, & Goldman-Rakic, 1982).

2.4.2 Natural Eye Behavior and Visuospatial Working Memory

Although our experimental paradigms aimed to approach natural behavior, potential concerns may arise surrounding the decision to not control eye position. For example, one may argue that animals would simply visually rehearse the target location by maintaining gaze fixation on the target of interest. We found substantial evidence against this behavioral strategy. Eye behavior differed between periods when the target was available compared to times when the target was unavailable like during the WM delay and response epochs. During WM delay, animals spent significantly less time looking onscreen, suggesting eye movement behavior that is less focused on specific elements in the environment such as target location. The number of fixations to target locations during WM delay only comprised 3% of fixations and there was no significant difference between the number of fixations on target between correct and incorrect trials, suggesting that fixation on target location during delay was not used as a successful behavioral strategy. From these results, one may infer the LPFC maintains an allocentric representation of the remembered location that is independent from gaze or fixation position. This issue, however, needs further exploration.

Using linear classifiers, we also identified that eye position on-screen was significantly more predictive of target location during the cue epoch compared to the delay epoch. Classifiers that were trained on eye position data from the cue epoch and tested on eye position data from the delay epoch resulted in decoding accuracy below chance level suggesting different eye movement patterns between target encoding and memory maintenance.

Saccade characteristics are influenced by external motivations like task reward (Takikawa, Kawagoe, Itoh, Nakahara, & Hikosaka, 2002). Increases in peak velocities have been observed for task-related saccades - when fixating on a target is needed for information processing - compared to saccades without a task-related motivation (Bieg, Bresciani, Bühlhoff, & Chuang, 2012). This increased saccadic speed may be used to gather task-related information quicker. Saccades to target locations may be considered task-relevant compared to non-target saccades, thus supporting correct task completion and reward. We found that saccades that land on targets versus those that land off-target show a greater difference in velocity when the target is physically present during the cue epoch or perception task compared to when it is removed during the WM delay. In fact, there were no significant differences in saccade speed to targets compared to non-targets during the WM delay. This may suggest that saccades to target locations during memory delay were influenced less by task-relevant motivation and information seeking than those made during the cue encoding period. Alternatively, it may reflect the fact that visually guided saccades to a target show higher peak velocities than to an 'empty' location in space (Edelman, Valenzuela, Barton, 2006).

Another potential issue is contamination of WM signals by signals related to eye movement. We explored the amount of information contained by neural activity about target location during fixation on target locations during the cue and delay epochs. We found significantly lower decoding accuracy during the delay epoch compared to the cue epoch, suggesting that more information was available to the neuronal population when animals fixate on a target that is present compared to when the target is absent. Indeed, the decoding accuracy during the delay epoch was close to chance (25%), suggesting that animals did not receive substantial spatial information about the target location during periods of target location fixation during delay. These results may be due to the activation of visual neurons by the presence of a visual target during the cue epoch.

Although saccadic responses are seen in the PFC, the task and type of motor response required by the task have been shown to alter neuronal responses (Quintana, Yajeya, & Fuster, 1988; Sakagami, & Niki, 1994; Yajeya, Quintana, & Fuster, 1988; Johnston & Everling, 2006; Warden & Miller, 2010). Neuronal responses to eye movements like saccades in the PFC are often identified during trials of tasks that are contingent on an oculomotor response. Neuronal responses to saccades are however notably absent when saccades are spontaneous and task-independent such as during inter-trial intervals (Funahashi, 2014).

2.4.3 Perception and Working Memory in Areas 8a and 9/46

The separation of perception and WM has been recognized since 1883 when neurological conditions were described in which patients exclusively lost either the ability to perceive objects or picture them in mind (Bernard, 1883; Behrmann, Moscovitch, & Winocur, 1994). Early lesion studies also point to a separation of these functions in LPFC in which large lesions consistently produced WM deficits while retaining perceptual discrimination functions (Reviewed in Roussy et al., 2021a). Moreover, pharmacological manipulations using muscimol produce WM deficits without altering perceptual performance (Sawaguchi, & Iba, 2001).

Here, we found that population codes for perception and WM representations of target location are not interchangeable. This finding is supported by previous work from Mendoza-Halliday et al, who found separate populations of LPFC neurons that code for either perception or WM for visual motion direction (Mendoza-Halliday et al., 2017). After combining neurons into a pseudo-population, they further demonstrated that a decoder using population activity patterns could discriminate whether neuronal representations were perceptual or mnemonic, suggesting different patterns of neuronal activity corresponding to each function. That study, however, used pseudo populations of neurons rather than simultaneously recorded neurons to examine WM for motion direction and did not use naturalistic virtual tasks in which gaze is unconstrained.

Our results expand on and validate the results of that study for naturalistic visuospatial WM.

How is it possible for the LPFC to represent perceived visual features without confounding WM representations? One possibility is that patterns of activity remain separate through the activation of perceptual, mnemonic, and mixed neurons. Activity patterns of perception and WM cells may help the brain monitor and discriminate between the internal (WM) and external (perception) representations. Abnormal patterns of activation may cause disruptions in internal and externally driven representations triggering hallucinations for example if perceptual neurons are activated without visual input.

2.4.4 Conclusion

Our findings provide evidence of robust perceptual and WM representations in the macaque monkey LPFC during naturalistic tasks in virtual environments in which eye movements are unconstrained and the visual scene contains complex stimuli. We find minimal impact of natural eye movement on WM performance or neuronal coding for WM. Finally, we provide evidence for different neural codes for perceptual and mnemonic representations in the LPFC.

2.5 « Supplemental Results »

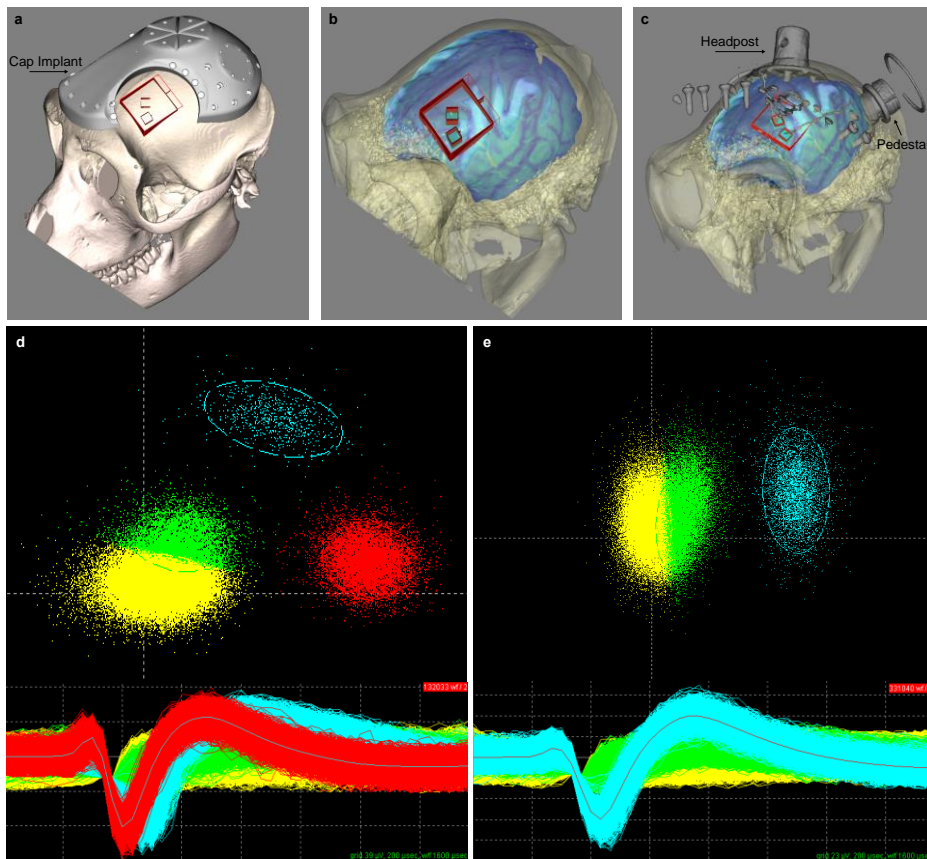


Figure. S2.9: Neural recording setup

a, Graphic of presurgical planning procedure showing 3D reconstructed skull and brain based on CT and MRI scans. Electrode array positioning is illustrated in blue with a red outline. The craniotomy is outlined by the larger red box. **b,c**, 3D modeled brain with electrode array placement in pink. **d**, Example of spike sorting for one electrode channel. Upper panel represents PCA space and the lower panel represents individual threshold crossing event waveforms. The blue and red clusters represent what we would classify as a single unit. The green cluster would be classified as a multiunit. **e**, Example of spike sorting for one electrode channel. The blue cluster would represent a single unit. The green cluster would represent multiunit activity.

2.6 « Methods »

Additional statistical information is outlined in appendix 1.

The same two male rhesus macaques (*Macaca mulatta*) were used in both tasks (age: 10, 9; weight: 12, 10 kg).

2.6.1 Ethics Statement

Animal care and handling including basic care, animal training, surgical procedures, and experimental injections were pre-approved by the University of Western Ontario Animal Care Committee. This approval ensures that federal (Canadian Council on Animal Care), provincial (Ontario Animals in Research Act), and other national CALAM standards for the ethical use of animals are followed. Regular assessments for physical and psychological well-being of the animals were conducted by researchers, registered veterinary technicians, and veterinarians.

2.6.2 Task

The current task takes place in a virtual environment that was created using Unreal Engine 3 development kit (UDK, May 2012 release; Epic Games). The nine targets were arranged in a 3 × 3 grid spaced approximately 0.5 seconds apart (movement speed during navigation was fixed). For the working memory task, the target is present only during the cue epoch. For the perception task, the target is present in the cue, delay, and response epochs. Detailed descriptions of this platform and the recording setup can be found in Doucet, Gulli, and Martinez-Trujillo, 2016.

2.6.3 Experimental Setup

During the task training period, animals were implanted with custom fit, PEEK cranial implants which housed the head posts and recording equipment (Neuronitek). See Blonde et al, 2018 for more information (Figure. S2.9a-c).

Subjects performed all experiments while seated in a standard primate chair (Neuronitek) located in an isolated radiofrequency (RF) shielded room with the only illumination originating from the computer monitor. Animals were head posted during experiments and were delivered juice reward through an electronic reward integration system (Crist Instruments). The task was presented on a computer LDC monitor positioned 80 cm from the animals' eyes (27" ASUS, VG278H monitor, 1024 × 768 pixel resolution, 75 Hz refresh rate, screen height equals 33.5 cm, screen width equals 45 cm). Eye position was tracked using a video-oculography system with sampling at 500 Hz (EyeLink 1000, SR Research).

2.6.4 Microelectrode Array Implant

We chronically implanted two 10×10 microelectrode Utah arrays (96 channel, 1.5 mm in length, separated by at least 0.4 mm) (Blackrock Microsystems) in each animal located in the left LPFC (area 8a dorsal and ventral, anterior to the arcuate sulcus and on either side of the principal sulcus) (Petrides, 2005). Electrode arrays were placed and impacted approximately 1.5 mm into the cortex. Reference wires were placed beneath the dura and a grounding wire was attached between screws in contact with the pedestal and the border of the craniotomy.

2.6.5 Processing of Neuronal Data

Neuronal data was recorded using a Cerebus Neuronal Signal Processor (Blackrock Microsystems) via a Cereport adapter. The neuronal signal was digitized (16 bit) at a sample rate of 30 kHz. Spike waveforms were detected online by thresholding at 3.4 standard deviations of the signal. The extracted spikes were semi-automatically resorted with techniques utilizing Plexon Offline Sorter (Plexon Inc.) (see Figure. S2.9d, e). Sorting results were then manually refined. We collected behavioral data across 20 WM sessions (12 in NHP B, 8 in NHP T) and neuronal data from 19 WM sessions. Behavior was recorded from 19 perception

sessions (14 in NHP B, 5 in NHP T). Neuronal data was analyzed from 13 sessions in which the WM and perception tasks were performed during the same session.

2.6.6 Task Performance

Percent of correct trials was calculated for both the WM and perception tasks. Response time was calculated for correct trials as the duration between the start of navigation and the time in which animals reach the correct target location. The task arena was divided into a 4 x 4 grid forming 16 area cells. The trajectory of the animal was calculated for each trial consisting of x and y coordinates sampled every 0.002 seconds. We calculated the number of samples that fell within each cell – this determined which cells the animals entered during navigation as well as how much of the total trajectory fell within each cell (related to time spent in cells). Our optimal trajectory measure is calculated by dividing the real length of the trajectory (the Euclidean distance from each x, y positional data point) by the true optimal distance (determined by the Euclidean distance from the start location to the target location for a particular trial). A value of 1 indicates the shortest possible (i.e., most optimal) trajectory length.

2.6.7 Characterizing Eye Movement

The percent of eye data points on-screen is calculated as the number of data points that fall within the screen limits divided by the total number of eye data points during a given epoch. Off-screen data points occur when the animal looks outside of the defined screen limits or when the animal closes its eyes (i.e., during blinking).

We characterized eye movements as saccades, fixations, or smooth pursuits based on methods outlined in Corrigan et al. (2017). Eye movement data were first cleaned by removing blinks, periods of lost signal, or corneal-loss spikes (occurs when corneal reflection is lost and regained). The clean eye signal was smoothed with a second-order Savitzky-Golay filter with a window of 11 samples. Saccades were identified by periods of high angular acceleration of the eye of at

least 10 ms. Individual saccades were determined by intersaccadic intervals of at least 40 ms. Saccade start and endpoints were determined by consistent direction and velocity considering a threshold of continuous change of $> 20^\circ$ for at least three samples, or an acute change of $> 60^\circ$ at one sample. Foveations were classified as fixations or smooth pursuits based on sample direction and ratios of distances. Dispersion of samples, consistency of direction, total path displacement, and the total spatial range were considered.

We calculated the percentage of total eye movement events classified as fixations or saccades for each epoch during WM and perception and the percentage of smooth pursuits for the response epoch.

2.6.8 Main Sequence Calculation

The main sequence reflects the relationship between the amplitude of the saccade and the peak velocity of the eye rotation towards the saccade's endpoint. Saccade amplitude and velocity can change based on the value of the saccade target (Bendiksby & Platt, 2006) or the alertness of the subject (Di Stasi, Catena, Cañas, Macknik, & Martinez-Conde, 2013). To calculate the main sequence, we separated saccades into bins of 3° of amplitude, starting at 2° , and computed the average peak velocity for each bin. Saccades within the same amplitude bins were matched between tasks to account for the influence of saccade start location and direction (direction with a tolerance of $\pm 13^\circ$, and the starting location within 7°).

2.6.9 Spatial Tuning

Tuning for spatial location was computed in all units (3950, 3092 in NHP B, 858 in NHP T) in 19 WM sessions using Kruskal–Wallis one-way analysis of variance on epoch-averaged firing rates with target location as the independent variable. A neuron was defined as tuned if the test resulted in $p < 0.05$.

2.6.10 Decoding Target Location from Neuronal Ensembles

We used a linear classifier (SVM) (Libsvm 3.14) (Fan, Chang, Hsieh, Wang, & Lin 2008) with 5-fold cross-validation to decode target position from z-score normalized population-level responses using both single units and multiunits on a single trial basis. We grouped targets based on location in the virtual arena into three groups: right targets, center targets, and left targets leaving us with 3 classes (33.33% chance level). We used the best ensemble method detailed in Leavitt et al. (2017b), in which we determined the highest performing neuron, paired this neuron with all others in the population to achieve the best pair and combined the best pair iteratively with all other neurons to form the best trio. This was repeated until we reached a best ensemble of 20 neurons. The classifiers used firing rates calculated over 500 ms time windows. Decoding accuracy at each time window was compared to chance performance using t-tests.

We used 13 sessions for the comparison between decoding of target column (left, right, center) using either correct or incorrect trials. These sessions were used because they contained samples from each target condition for incorrect trials. The number of trial observations was balanced between correct and incorrect trials for each session using data sampling. Results were averaged over 10 iterations of random sampling without replacement.

2.6.11 Gaze Analysis

We calculated the total fixation time during the delay epoch as well as the fixation time on the trial-specific target location for correct trials and incorrect trials. We compared the proportion of fixation time on the target location related to all fixation time during delay (target location fixation duration / total fixation duration) between correct and incorrect trials.

2.6.12 Decoding Target Location Using Eye Position

The screen was divided into 16 cells of equal dimensions. The number of foveations classified as fixations was calculated within each cell during the cue and delay epochs. We used a linear classifier (SVM) with 5-fold cross-validation to determine whether the target location could be predicted by the number of fixations within each area of the screen under the assumption that animals gather information from the virtual environment during such fixation periods (Corrigan et al., 2017).

2.6.13 Decoding Eye Position from Neuronal Data

To examine the influence of saccade direction, amplitude, and fixation (gaze) position, we calculated the firing rate, fixation location, saccade direction and amplitude during fixation periods in the delay epoch. We designed a linear regression for each neuron using firing rate during the fixation as the response (dependent variable) and binned saccade direction (binned into 8 bins spanning 45 degrees of a 360 degrees direction circular space), saccade amplitude in degrees of visual angle, and fixation position (x, y coordinates) as predictors (independent variables).

$$y = \beta_0 + \beta_1 x_1 + \beta_2 x_2 + \beta_3 x_3 + \beta_4 x_4 + \epsilon$$

In which y = single neuron firing rate during all fixations over a session, β_1 = saccade direction (categorical predictor derived by dividing the visual field into 8 sections - binning saccade direction by degrees), β_2 = saccade amplitude (in degrees of visual angle), β_3 = fixation position (x-screen coordinate), and β_4 = fixation position (y-screen coordinate).

We then used the residual firing rates from this model for each neuron as input into an SVM linear classifier with 5-fold cross-validation to predict the target condition. We used a SVM classifier with the same parameters to also predict the target location from the raw firing rates during the same fixation periods.

We used a linear classifier (SVM) with 5-fold cross-validation to decode eye position on screen based on neuronal firing rates during periods of eye fixation. Four target locations were selected as part of this analysis since their locations were non-overlapping on screen. Fixation periods occurring in either the cue or delay epoch that fell within these regions were used. Short fixation periods were removed (amplitude < 6 ms). The firing rate was calculated for each neuron during each fixation period and were z-score normalized. Neuronal populations included single units and multiunits.

2.6.14 Decoding Target Location for Working Memory and Perception

We used a linear classifier (SVM) with 5-fold cross-validation to decode target location (9 targets) based on population neuronal activity. We used 13 sessions in which animals performed both the WM and perception tasks so that we could use the same population of neurons. We altered training and testing conditions so that classifiers were either trained on population activity during congruent tasks or incongruent tasks (e.g., trained on WM and tested on perception).

We divided WM trials into two random and separate datasets and tested/trained classifiers on one-half of the trials and trained on the other half. For the WM task, we trained classifiers on either congruent or incongruent task epochs (e.g., train during cue and test during delay).

2.7 « References »

Baddeley, A. D. (1986). *Working Memory*. Clarendon Press/ Oxford University Press. Oxford, New York.

Balan, P. F., & Ferrera, V. P. (2003). Effects of gaze shifts on maintenance of spatial memory in macaque frontal eye field. *The Journal of Neuroscience*, 23(13), 5446–5454. doi:10.1523/JNEUROSCI.23-13-05446.2003

Behrmann, M., Moscovitch, M., & Winocur, G. (1994). Intact visual imagery and impaired visual perception in a patient with visual agnosia. *Journal of Experimental Psychology: Human Perception and Performance*, 20(5), 1068–1087. doi:10.1037/0096-1523.20.5.1068

Bendiksby, M. S., & Platt, M. L. (2006). Neural correlates of reward and attention in macaque area LIP. *Neuropsychologia*, 44(12), 2411–2420. doi:10.1016/J.NEUROPSYCHOLOGIA.2006.04.011

Bernard, D. A. F. (1883). *Clinique des maladies nerveuses : un cas de suppression brusque et isolée de la vision mentale des signes et des objets : Formes et couleurs*. Retrieved from <https://gallica.bnf.fr/ark:/12148/bpt6k5463028m>

Bieg, H. J., Bresciani, J. P., Bühlhoff, H. H., & Chuang, L. L. (2012). Looking for discriminating is different from looking for looking's sake. *PLoS ONE*, 7(9). doi:10.1371/JOURNAL.PONE.0045445

Blonde, J. D., Roussy, M., Luna, R., Mahmoudian, B., Gulli, R. A., Barker, K. C., ... Martinez-Trujillo, J. C. (2018). Customizable cap implants for neurophysiological experimentation. *Journal of Neuroscience Methods*, 304, 103–117. doi:10.1016/J.JNEUMETH.2018.04.016

Boulay, C. B., Pieper, F., Leavitt, M., Martinez-Trujillo, J., & Sachs, A. J. (2016). Single-trial decoding of intended eye movement goals from lateral prefrontal cortex neural ensembles. *Journal of Neurophysiology*, 115, 486–499. doi:10.1152/jn.00788.2015

Bullock, K. R., Pieper, F., Sachs, A. J., & Martinez-Trujillo, J. C. (2017). Visual and presaccadic activity in area 8Ar of the macaque monkey lateral prefrontal cortex. *Journal of Neurophysiology*, 118(1), 15–28. doi:10.1152/JN.00278.2016/ASSET/IMAGES/LARGE/Z9K0061741290010.JPEG

Constantinidis, C., Funahashi, S., Lee, D., Murray, J. D., Qi, X. L., Wang, M., & Arnsten, A. F. T. (2018). Persistent spiking activity underlies working memory. *The Journal of Neuroscience*, 38(32), 7020–7028. doi:10.1523/JNEUROSCI.2486-17.2018

- Corrigan, B. W., Gulli, R. A., Doucet, G., & Martinez-Trujillo, J. C. (2017). Characterizing eye movement behaviors and kinematics of non-human primates during virtual navigation tasks. *Journal of Vision*, 17(12). doi:10.1167/17.12.15
- Di Stasi, L. L., Mccamy, M. B., Catena, A., Macknik, S. L., Cañas, J. J., & Martinez-Conde, S. (2013). Microsaccade and drift dynamics reflect mental fatigue. *European Journal of Neuroscience*, 38(3), 2389–2398. doi:10.1111/EJN.12248
- Doucet, G., Gulli, R. A., & Martinez-Trujillo, J. C. (2016). Cross-species 3D virtual reality toolbox for visual and cognitive experiments. *Journal of Neuroscience Methods*, 266, 84–93. doi:10.1016/J.JNEUMETH.2016.03.009
- Edelman, J. A., Valenzuela, N., & Barton, J. J. (2006). Antisaccade velocity, but not latency, results from a lack of saccade visual guidance. *Vision Research*, 46(8-9), 1411–1421. doi:10.1016/j.visres.2005.09.013
- Fan, R.-E., Chang, K.-W., Hsieh, C.-J., Wang, X.-R., & Lin, C.-J. (2008). LIBLINEAR: A Library for Large Linear Classification. *Journal of Machine Learning Research*, 9, 1871–1874. doi:10.1145/1390681.1442794
- Funahashi, S., Bruce, C. J., & Goldman-Rakic, P. S. (1989). Mnemonic coding of visual space in the monkey's dorsolateral prefrontal cortex. *Journal of Neurophysiology*, 61(2), 331–349. doi:10.1152/JN.1989.61.2.331
- Funahashi, S. (2014). Saccade-related activity in the prefrontal cortex: Its role in eye movement control and cognitive functions. *Frontiers in Integrative Neuroscience*, 8. doi:10.3389/FNINT.2014.00054
- Fuster, J. M., & Alexander, G. E. (1971). Neuron activity related to short-term memory. *Science*, 173(3997), 652–654. doi:10.1126/SCIENCE.173.3997.652
- Goldman-Rakic, P. S. (1994). Cellular basis of working memory. *Neuron*, 14(3), 477-485. doi:10.1016/0896-6273(95)90304-6.
- Hasegawa, R., Sawaguchi, T., Kubota, K., & Fuster, K. (1998). Monkey prefrontal neuronal activity coding the forthcoming saccade in an oculomotor delayed matching-to-sample task. doi:10.1152/jn.1998.79.1.322
- Jacob, S. N., & Nieder, A. (2014). Complementary roles for primate frontal and parietal cortex in guarding working memory from distractor stimuli. *Neuron*, 83(1), 226–237. doi:10.1016/j.neuron.2014.05.009
- Johnston, K., & Everling, S. (2006). Neural activity in monkey prefrontal cortex is modulated by task context and behavioral instruction during delayed-match-to-sample and conditional prosaccade-antisaccade tasks. *Journal of Cognitive Neuroscience*, 18(5), 749–765. doi:10.1162/jocn.2006.18.5.749

- Kojima, S., & Goldman-Rakic, P. S. (1982). Delay-related activity of prefrontal neurons in rhesus monkeys performing delayed response. *Brain Research*, 248(1), 43–50. doi:10.1016/0006-8993(82)91145-3
- Leavitt, M. L., Mendoza-Halliday, D., & Martinez-Trujillo, J. C. (2017a). Sustained activity encoding working memories: Not fully distributed. *Trends in Neurosciences*, 40(6), 328–346. doi:10.1016/J.TINS.2017.04.004
- Leavitt, M. L., Pieper, F., Sachs, A. J., & Martinez-Trujillo, J. C. (2017b). Correlated variability modifies working memory fidelity in primate prefrontal neuronal ensembles. doi:10.1073/pnas.1619949114
- Leavitt, M. L., Pieper, F., Sachs, A. J., & Martinez-Trujillo, J. C. (2018). A quadratic bias in prefrontal representation of visual-mnemonic space. *Cerebral Cortex*, 28(7), 2405–2421. doi:10.1093/cercor/bhx142
- Malmö, R. B. (1942). Interference factors in delayed response in monkeys after removal of frontal lobes. *Journal of Neurophysiology*, 5, 295–308. doi:10.1152/jn.1942.5.4.295
- Mendoza-Halliday, D., & Martinez-Trujillo, J. C. (2017). Neuronal population coding of perceived and memorized visual features in the lateral prefrontal cortex. *Nature Communications*, 8(1), 1–13. doi:10.1038/ncomms15471
- Miller, E. K., Erickson, C. A., & Desimone, R. (1996). Neural mechanisms of visual working memory in prefrontal cortex of the macaque. *Journal of Neuroscience*, 16, 5154–67. doi:10.1523/JNEUROSCI.16-16-05154.1996
- Orbach J., & Fischer G. J. (1959). Bilateral resections of frontal granular cortex: Factors influencing delayed response and discrimination performance in monkeys. *JAMA Neurology*, 1(1), 78–86. doi:10.1001/archneur.1959.03840010080010
- Petrides M. (2005). Lateral prefrontal cortex: Architectonic and functional organization. *Philosophical transactions of the Royal Society of London. Series B, Biological sciences*, 360(1456), 781–795. doi:10.1098/rstb.2005.1631
- Postle, B. R., Idzikowski, C., Sala, S. Della, Logie, R. H., & Baddeley, A. D. (1999). *Quarterly Journal of Experimental Psychology*, 59(1), 100–120. doi:10.1080/17470210500151410
- Roussy, M., Mendoza-Halliday, D., & Martinez-Trujillo, J. C. (2021a). Neural substrates of visual perception and working memory: Two sides of the same coin or two different coins? *Frontiers in Neural Circuits*, 15, 131. doi:10.3389/FNCIR.2021.764177/BIBTEX
- Roussy, M., Luna, R., Duong, L., Corrigan, B., Gulli, R. A., Nogueira, R., ... Martinez-Trujillo, J. C. (2021b). Ketamine disrupts naturalistic coding of working

memory in primate lateral prefrontal cortex networks. *Molecular Psychiatry* 2021, 1–16. doi:10.1038/s41380-021-01082-5

Sawaguchi, T., & Iba, M. (2001). Prefrontal cortical representation of visuospatial working memory in monkeys examined by local inactivation with muscimol. *Journal of Neurophysiology*, 86(4), 2041–2053. doi:10.1152/jn.2001.86.4.2041

Sakagami, M., & Niki, H. (1994). Encoding of behavioral significance of visual stimuli by primate prefrontal neurons: Relation to relevant task conditions. *Experimental Brain Research*, 97(3), 423-436. doi:10.1007/BF00241536

Suzuki, M., & Gottlieb, J. (2013). Distinct neural mechanisms of distractor suppression in the frontal and parietal lobe. *Nature Neuroscience*, 16(1), 98–104. doi:10.1038/nn.3282

Takikawa, Y., Kawagoe, R., Itoh, H., Nakahara, H., & Hikosaka, O. (2002). Modulation of saccadic eye movements by predicted reward outcome. *Experimental Brain Research*, 142(2), 284–291. doi:10.1007/s00221-001-0928-1

Quintana, J., Yajeya, J., Fuster, J. M. (1988). Prefrontal representation of stimulus attributes during delay tasks. I. Unit activity in cross-temporal integration of sensory and sensory-motor information. *Brain Research*, 474(2), 211-221. doi:10.1016/0006-8993(88)90436-2

Warden, M. R., & Miller, E. K. (2010) Task-dependent changes in short-term memory in the prefrontal cortex. *Journal of Neuroscience*, 30(47):15801-15810. doi: 10.1523/JNEUROSCI.1569-10.2010

Yajeya, J., Quintana, J., & Fuster, J. M. (1988). Prefrontal representation of stimulus attributes during delay tasks. II. The role of behavioral significance. *Brain Research*, 474(2), 222–230. doi:10.1016/0006-8993(88)90437-4

Chapter 3

3 « Ketamine Disrupts Naturalistic Coding of Working Memory in Primate Lateral Prefrontal Cortex Networks »

3.1 « Abstract »

Ketamine is a dissociative anesthetic drug, which has more recently emerged as a rapid-acting antidepressant. When acutely administered at subanesthetic doses, ketamine causes cognitive deficits like those observed in patients with schizophrenia, including impaired working memory. Although these effects have been linked to ketamine's action as an N-methyl-D-aspartate receptor antagonist, it is unclear how synaptic alterations translate into changes in brain microcircuit function that ultimately influence cognition. Here, we administered ketamine to rhesus monkeys during a spatial working memory task set in a naturalistic virtual environment. Ketamine induced transient working memory deficits while sparing perceptual and motor skills. Working memory deficits were accompanied by decreased responses of fast spiking inhibitory interneurons and increased responses of broad spiking excitatory neurons in the lateral prefrontal cortex. This translated into a decrease in neuronal tuning and information encoded by neuronal populations about remembered locations. Our results demonstrate that ketamine differentially affects neuronal types in the neocortex; thus, it perturbs the excitation inhibition balance within prefrontal microcircuits and ultimately leads to selective working memory deficits.

3.2 « Introduction »

Ketamine was developed as a dissociative anesthetic but more recently, at subanesthetic doses, it is used in medical practice as a rapid action antidepressant. It is additionally used as a recreational drug (Pribish, Wood, & Kalava, 2020; Gerhard et al., 2020; Wei, Chang, & Hashimoto, 2020; Sassano-Higgins, Baron, Juarez, Esmaili, & Gold, 2016; Domino, 2010). Through its action

as an N-methyl-D-aspartate receptor (NMDAR) antagonist, it has been long known to induce a trance-like state providing pain relief, sedation, and memory loss (Pribish, Wood, & Kalava, 2020; Domino, 2010; Frohlich, & Van Horn, 2014). Ketamine is also observed to induce negative, positive, and cognitive symptoms of schizophrenia (Frohlich, & Van Horn, 2014; Morgan, Mofeez, Brandner, Bromley, & Curran, 2004; Breier, Malhotra, Pinals, Weisenfeld, & Pickar, 1997; Malhotra et al., 1997). Despite its widely observed effects, how ketamine induced blockage of NMDARs in individual synapses translate to cognitive and behavioral changes is still unclear.

For the particular case of ketamine induced cognitive deficits, some studies have hypothesized that ketamine decreases the stability of mental representations maintained by the primate lateral prefrontal cortex (LPFC) (Wang et al., 2013; Murray et al., 2014). Neuronal populations in the LPFC are thought to encode mental representations that are dissociable from sensory and motor signals and are therefore essential to processes like working memory (WM). However, because this part of the brain appears *de novo* in anthropoid primates and has a unique architecture relative to other phylogenetically older areas such as the medial prefrontal cortex, this hypothesis has been difficult to test in commonly used animal models, including rodents (Passingham & Wise, 2012). Illuminating how ketamine affects the function of primate lateral prefrontal microcircuits could explain its effects on human cognition as well as provide cautionary guidelines for its use in medical practice or as a recreational drug.

One prominent cognitive function that is impaired by ketamine is WM: the ability to temporarily hold and manipulate information relevant to a task (Baddeley, 1986) This function is widely supported to depend on the activity of PFC neurons (Funahashi, Chafee, & Goldman-Rakic, 1993; Suzuki & Gottlieb, 2013; Miller, Erickson, & Desimone, 1996; Mendoza-Halliday & Martinez-Trujillo, 2017; Jacobsen & Nissen, 1937; Funahashi, Bruce, & Goldman-Rakic, 1989, Leavitt, Mendoza-Halliday, & Martinez-Trujillo, 2017). Previous studies have reported that NMDAR blockade by ketamine modulates single neuron activity within the LPFC

during WM, leading to reduced neuronal tuning (Wang et al., 2013; Ma, Skoblenick, Seamans, & Everling, 2015). However, these studies have employed behavioral tasks involving simple visual displays relative to the complexity of natural environments and have strictly controlled for eye movements. This contrasts real-life settings, when WM representations must be held during dynamic viewing of natural scenes through saccades. Currently, it remains unknown whether neuronal population in LPFC can support WM function in ethologically valid settings and whether ketamine has any effect on WM function and brain microcircuit dynamics in these conditions. Here, we aimed to clarify this issue.

We used a virtual reality engine to build a virtual arena featuring a naturalistic visual scene. We trained two rhesus monkeys (*Macaca mulatta*) on a visuospatial WM task that took place in this arena (Figure. 3.1a, b). As during natural behavior, animals were permitted free visual exploration (unconstrained eye movements), as well as free spatial navigation using a joystick. During task trials, a target was presented for 3 s at 1 of 9 locations in the arena. The target then disappeared during a 2 s delay epoch. During the target and delay epoch, navigation was disabled. Subsequently, navigation was enabled, and animals were required to virtually approach the target location within 10 s to obtain a juice reward (Figure. 3.1c). We recorded neuronal activity during this task using 96-channel microelectrode arrays (Utah Arrays). Two arrays were implanted in each animal in the left LPFC, one on each side of the principal sulcus (Figure. 3.1d, e) (Petrides, 2005).

In order to block NMDARs, we administered ketamine intramuscularly. NMDARs are evidenced to be critically involved in balancing prefrontal circuit interactions between pyramidal cells and inhibitory interneurons that are crucial for WM processing (Wang et al., 2013; Wang, 1999; Wang, Tegnér, Constantinidis, Goldman-Rakic, 2004; Lisman, Fellous, & Wang, 1998). Ketamine is reported to impair WM performance through primarily blocking NMDARs, which are highly expressed in the human prefrontal cortex (Frohlich & Van Horn, 2014; Breier, Malhotra, Pinals, Weisenfeld, & Pickar, 1997; Wang et al., 2013; Lisman, Fellous,

& Wang, 1998; Uhlén et al., 2015). Local administration of NMDAR antagonists into the primate LPFC is also sufficient to perturb WM signals (Wang et al., 2013). Accordingly, it is reasonable to assume that low doses of systemically administered ketamine would produce the greatest effect on prefrontal neuronal activity (Breier, Malhotra, Pinals, Weisenfeld, & Pickar, 1997; Anticevic et al., 2015).

We recorded neuronal responses during the task in three blocks of trials, which were defined relative to the injection time. Blocks were chosen based on ketamine's intramuscular post-injection peak plasma point (5 min) and observed time of action (3–30 min) (Zanos et al., 2018). Trial blocks were therefore defined as: before subanesthetic ketamine (0.25–0.8 mg/kg) or saline injection (pre-injection period), 30 min post injection (early post-injection period), and 30 min post injection to 1 h post injection (late post-injection period) (Figure. 3.1f). In some sessions, we used a control task in which targets remained on screen for the duration of the trial (ketamine-perception variant). Here, the animals did not have to remember the target location; therefore, WM was not required to complete the trials. This control variant of the task allowed us to separate the effect of ketamine on WM function from potential effects on processes like perception and movement.

We hypothesized that neuronal populations in LPFC would robustly encode WM information in our naturalistic WM task. We further hypothesized that ketamine would selectively impair WM performance by disrupting the tuning of single neurons as well as the amount of information encoded by neuronal populations about remembered locations.

3.3 « Results »

3.3.1 Ketamine Impairs Behavioral Performance in a Naturalistic Working Memory Task

The following results are divided based on the three injection periods defined by their temporal relationship to the injection time: pre-injection (prior to

injection), early-post injection (up to 30 min post injection), and late-post injection (30 min post injection to 1 h post injection). Both animals performed significantly above chance (~11%, nine locations) on all task variants before ketamine injections (pre-injection period, $p < 0.001$), indicating proficiency in the task. Performance differed significantly between injection periods (Two-way ANOVA, $F(2,69) = 4.3$, $p = 0.017$) and between saline and ketamine sessions (Two-way ANOVA, $F(1,69) = 9.57$, $p = 0.003$). In ketamine-WM sessions, performance decreased significantly during the early post-injection period compared to the pre-injection period (Two-way ANOVA, post hoc, $p < 0.0001$), to subsequently recover during the late post-injection period compared to the early post-injection period (Two-way ANOVA, post hoc, $p = 0.002$). Performance did not significantly change between injection periods in saline-WM sessions (Two-way ANOVA, post hoc, pre-injection and early post-injection, $p = 0.999$). Importantly, ketamine injections did not significantly alter performance between injection periods in perception sessions (ANOVA, $F(2,6) = 0.25$, $p = 0.786$), indicating that the ketamine induced performance deficit was specific to the WM task (Figure. 3.1g).

Navigation time to the remembered target location also significantly varied between injection periods (ANOVA, $F(2,250) = 16.81$, $p < 0.0001$). Navigation time increased significantly after ketamine injection compared to the pre-injection period (ANOVA, post hoc, $p < 0.0001$) and decreased in the late post-injection period compared to the early post-injection period (ANOVA, post hoc, $p < 0.0001$). No significant changes were found between injection periods in saline-WM (ANOVA, $F(2,108) = 1.71$, $p = 0.186$) or ketamine-perception sessions (ANOVA, $F(2,60) = 0.22$, $p = 0.800$) (Figure. 3.1h).

Trajectories to remembered targets also became more dispersed after ketamine injections in the early post-injection period compared to the pre-injection period (Figure. 3.1i). To quantify this observation, we divided the task environment into a 5×5 grid creating 25 regional cells (see Figure. 3.1j) and calculated the percent of trials in which each cell was entered during navigation to a target location (Figure. 3.1k). The difference in the percent of trials in which cells were

entered between pre and post-injection periods in ketamine-WM and saline-WM sessions was then calculated. In ketamine-WM sessions, more cells were visited in more trials in the early post-injection compared to the pre-injection period relative to saline-WM sessions (Two-way ANOVA, post hoc, animal T, $p = 0.002$; animal B, $p = 0.004$). Fewer cells were visited in the late post-injection period compared to the early post-injection period in ketamine-WM sessions compared to saline-WM sessions (Two-way ANOVA, post hoc, animal T, $p = 0.001$; animal B, $p = 0.044$) (Figure. 3.1l). We observed less dispersion of the trajectories in the post-injection period relative to the pre-injection period during ketamine perception sessions compared to ketamine WM sessions (Figure. 3.1k last row, Two-way ANOVA, post hoc, $p < 0.0001$). These results indicate that ketamine selectively impaired the animals' ability to maintain the location of the target in WM.

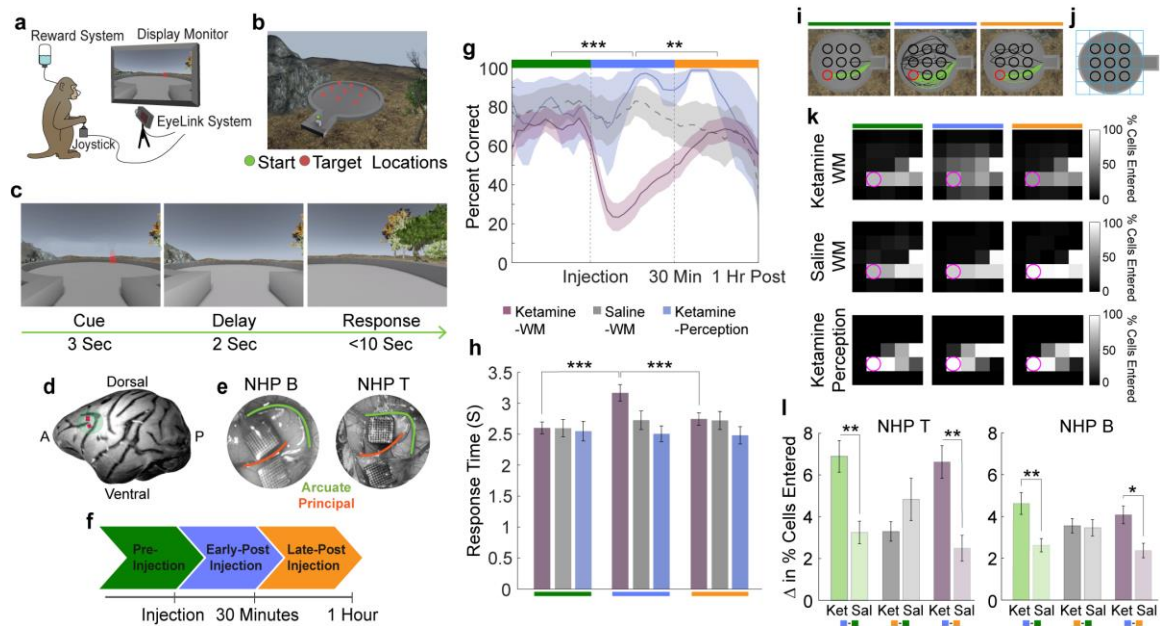


Figure. 3.1: Virtual working memory task and behavioral performance

a, Illustration of experimental setup. **b**, Overhead view of task arena in virtual environment. **c**, Trial epoch timeline. **d**, Depiction of Utah array locations. **e**, Surgical images of Utah arrays in LPFC. **f**, Injection period timeline in which the pre-injection period refers to trials occurring before the time of injection, early post-injection period refers to injection time to 30 min post injection, and late post-injection period refers to 30 min post to 1 h post-injection time. Data from pre-injection period represented by green, early post-injection period by blue, and late post-injection period by orange. **g**, Average percent of correct trials for ketamine-WM sessions (pink), saline-WM sessions (gray), and ketamine-perception sessions (blue). **h**, Average response time for correct trials for all session types. **i**, Trajectories to example target location (red) in one ketamine-WM session for correct (green) and incorrect (black) trials. **j**, Task arena divided into 5×5 grid. **k**, Percent of trials in which each cell of the arena is entered for example target location (pink) averaged over sessions. **l**, Average difference (increase) in percent of trials in which cells are entered between injection periods (green = early post-injection – pre-injection; gray = late post-injection – pre-injection; purple = early post-injection – late post-injection) compared between ketamine-WM and saline-WM sessions. All error bars are SEM. * <0.05 , ** <0.01 , *** <0.001 .

3.3.2 Ketamine Decreases Tuning of Single Neurons for Remembered Locations

To investigate the neuronal correlates of the behaviors illustrated in Figure 3.1, we recorded the activity of 2906 units (1814 single neurons and 1092 multiunits) during 17 ketamine-WM sessions (8 in animal T, 9 in animal B). We recorded an additional 1117 units (674 single units and 443 multiunits) during seven saline-WM sessions (3 in animal T, 4 in animal B). Single neurons exhibited spatial tuning for cued locations during the delay epoch in the pre-injection period (example neurons in Figure 3.2a, b). We compared the proportion of tuned units between injection periods during ketamine-WM and saline-WM sessions. In ketamine sessions, the proportion of spatially tuned neurons significantly decreased in the early post-injection period compared to the pre-injection period (Chi-Square, $X^2 = 128.67$, $p < 0.0001$) and significantly increased in the late post-injection period compared to the early-post injection period (Chi-Square, $X^2 = 126.52$, $p < 0.0001$) (Figure 3.2c). There were no significant differences in the proportion of tuned single neurons between pre-injection and early post-injection periods during saline-WM sessions (Chi-Square, $X^2 = 1.44$, $p = 0.231$) (Figure 3.2d).

We additionally analyzed tuning functions of single neurons by ranking their responses per target location during the delay epoch in the three injection periods. We computed the slope of a straight line fitted to the responses (Figure 3.2e shows data pooled across neurons from one example session). Slope magnitude changed significantly between injection periods (Kruskal–Wallis, $H(2,48) = 13.48$, $p = 0.001$). The slopes significantly decreased in magnitude during the early post-injection period compared to the pre-injection period (Kruskal–Wallis, post hoc, $p = 0.001$) (Figure 3.2f, g). This was not the case for the saline control sessions (Kruskal–Wallis, $H(2,18) = 5.7$, $p = 0.058$). These results demonstrate that single neurons in LPFC encode spatial WM signals in naturalistic conditions and that low doses of ketamine significantly impair single neuron tuning.

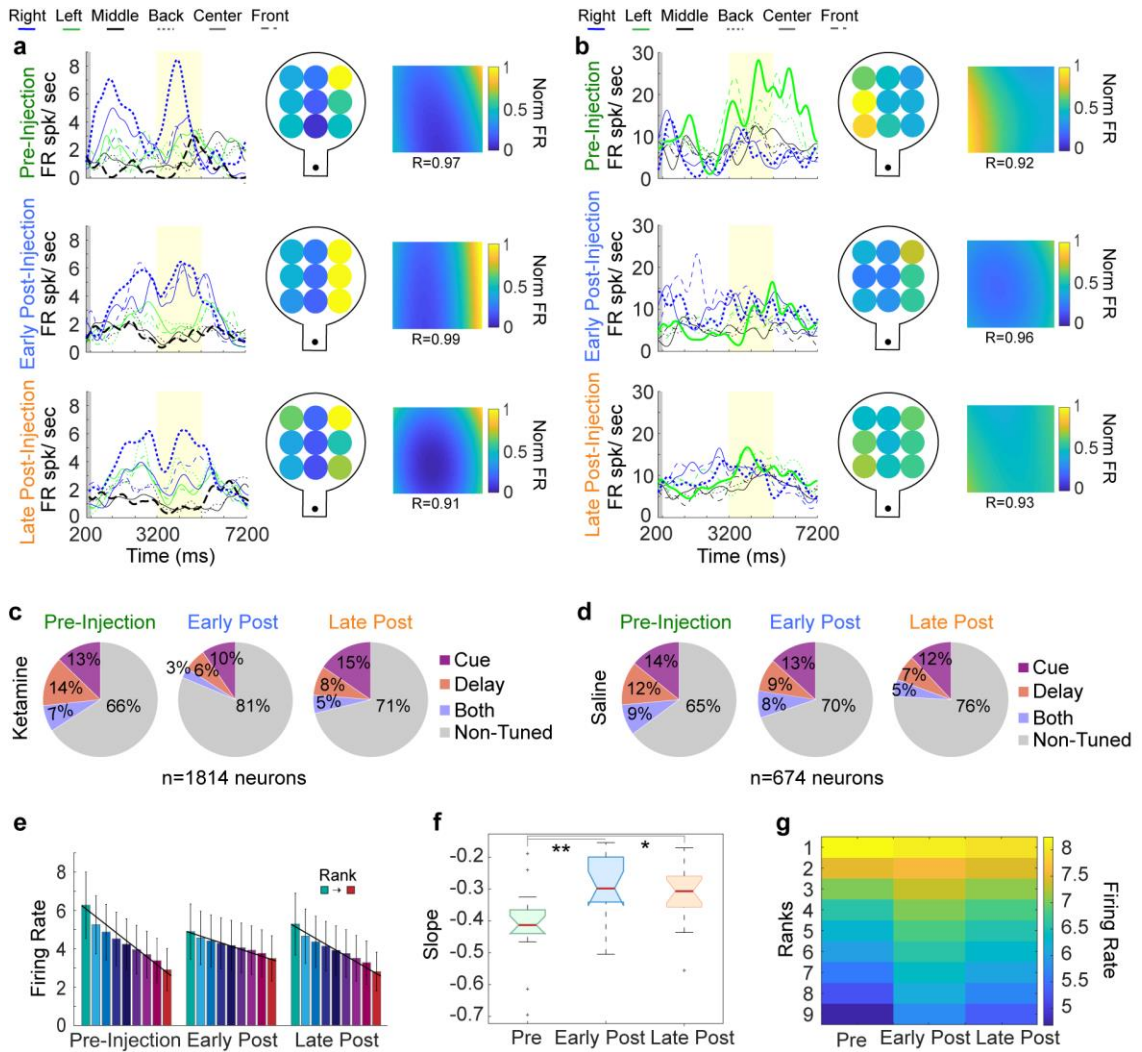


Figure. 3.2: Ketamine decreases tuning of single neurons for remembered locations

a, Firing rate of an example neuron for a ketamine-WM session. On the left, spike density functions (SDFs) over the pre-cue interval (gray column), cue, delay (yellow), and response epochs. Preferred locations and least-preferred locations are bolded. Center, firing rates during the delay epoch for all target locations. Right, firing rates fitted to a polynomial plane. **b**, Firing rate of a second example neuron during a ketamine-WM session. **c**, Average proportion of tuned single units during the cue epoch (pink), delay epoch (orange), or during both (purple) for each injection period for ketamine-WM sessions. **d**, Average proportion of tuned single units during each epoch for saline-WM sessions. **e**, Example session indicating firing rate averaged over neurons for target locations ranked from preferred to least-preferred locations. Black lines represent slope. **f**, Fitted slope for each injection period averaged over sessions. **g**, Firing rate for each target location ranked and averaged over sessions for each injection period. All error bars are SEM. * <0.05 , ** <0.01 , *** <0.001 . Red center lines indicate median, the bottom and top edges of the box indicate the 25th and 75th percentiles. The whiskers extend to non-outlier data points (approximately within 2.7 std) and the outliers are plotted using '+'.

3.3.3 Ketamine Disrupts Population Decoding of Remembered Locations

Single neuron tuning is essential for information coding. However, the information encoded by a neuronal population also depends on the correlated activity of neurons and can only be accurately estimated by examining the activity of simultaneously recorded neurons (Leavitt, Mendoza-Halliday, & Martinez-Trujillo, 2017; Nogueira, Peltier, Anzai, DeAngelis, Martinez-Trujillo, & Moreno-Bote, 2020). We used a linear classifier (Support Vector Machine, SVM) to predict from neuronal ensemble activity whether targets were presented on the left, right, or center of the virtual arena on a single trial basis. We pooled locations in order to reach a sufficient sample size (trials) to use cross-validation procedures. Decoding accuracy for different ensemble sizes was higher than chance (33%) in all analyzed experimental sessions (Figure. 3.3a, b). Decoding accuracy decreased after ketamine injection between pre-injection and early post-injection periods (Figure. 3.3a), predominantly during the delay and response epochs (16 neuron ensemble, Kruskal–Wallis, post hoc: delay; $p = 0.015$, response; $p = 0.023$). The classifier made systematically more errors after ketamine injection. Similar results were observed when using only correct trials or decoding 9 target locations in sessions with sufficient sample sizes (Figure. S3.6). On the other hand, decoding accuracy remained stable between injection periods in saline-WM sessions (16 neuron ensemble, Kruskal–Wallis: delay; $H(2,18) = 1.12$, $p = 0.571$, response; $H(2,18) = 1.36$, $p = 0.507$) (Figure. 3.3b). These results indicate that LPFC neuronal ensembles encode spatial WM in naturalistic settings and that ketamine disrupts these ensemble codes.

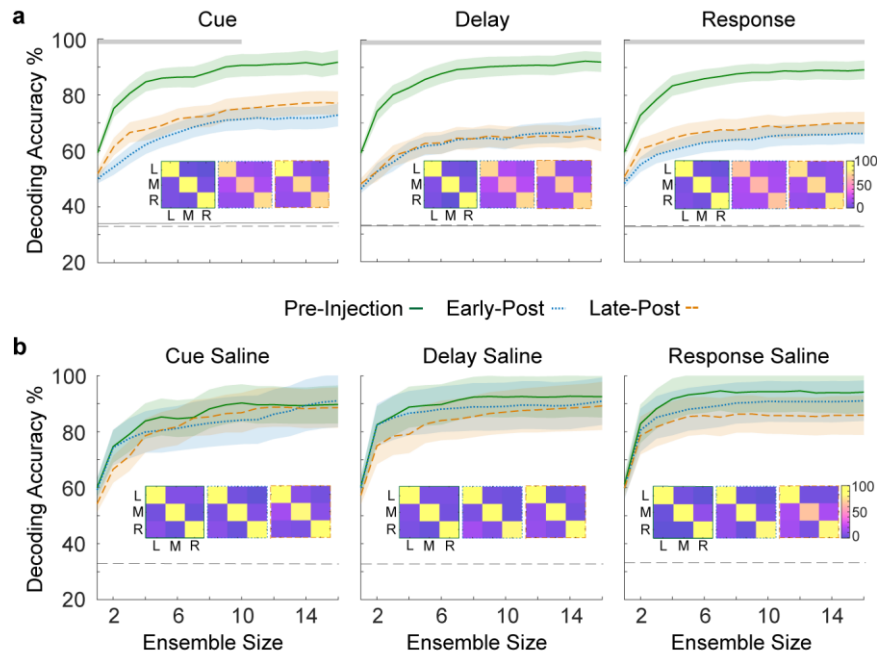


Figure. 3.3: Neuronal population decoding of target locations

a, Median decoding accuracy for ketamine-WM sessions for pre-injection (green), early post-injection (blue), and late post-injection periods (orange) for trial epochs. Chance performance is indicated by dashed gray line and shuffled results are indicated by solid gray line. Confusion matrices for each injection period indicate classifier performance for each target location. Gray bars near the top of the plot indicate ensemble sizes showing a significant reduction in decoding accuracy from pre-injection to early post-injection periods (Kruskal–Wallis, $p < 0.05$). **b**, Same as (a), for saline-WM sessions. All error bars are SEM.

3.3.4 Ketamine Has Differential Effects on Excitatory and Inhibitory Cell Types

Ketamine induces a variety of effects on individual neurons (Wang et al., 2013; Homayoun & Moghaddam, 2007). A loss of neuronal tuning may result from neurons increasing their response to least-preferred locations (see example neuron Figure. 3.2a) or decreasing their response to preferred locations (see example neuron Figure. 3.2b). One possible explanation for this heterogeneity is that different cell types (e.g., excitatory pyramidal cells and inhibitory interneurons) may be differentially affected by ketamine. To test this hypothesis, we divided neurons that were tuned during the delay epoch into narrow and broad spiking (BS) based on waveform peak-to-trough duration (width) (Figure. 3.4a, b). In mouse neocortex, BS neurons are largely putative pyramidal cells or in a smaller proportion, vasoactive intestinal peptide expressing (VIP) neurons. On the other hand, narrow spiking neurons are largely parvalbumin (PV) expressing, or in a smaller proportion, somatostatin expressing inhibitory interneurons (Torres-Gomez et al., 2020).

We then calculated the firing rates for each neuron's preferred and least-preferred target locations during the pre-injection and post-injection periods. After ketamine injection (early post-injection), narrow spiking neurons showed a loss of tuning during the delay epoch due to a decrease in firing for their preferred locations compared to the pre-injection period (Wilcoxon Rank-sum, $p = 0.049$) with no significant change for their least-preferred locations (Wilcoxon Rank-sum, $p = 0.546$) (Figure. 3.4c, d). In contrast, BS neurons showed a loss of tuning due to a significant increase in firing for their least-preferred locations compared to the pre-injection period (Wilcoxon Rank-sum, $p = 0.006$) with no significant change for their preferred locations (Wilcoxon Rank-sum, $p = 0.649$) (Figure. 4e, f; see change in firing rate per condition in Figure. S3.7c, d). Such changes were not observed during saline-WM sessions (Figure. S3.7a, b).

Considering that our populations of NS and BS neurons are dominated by PV and pyramidal cells respectively, our findings align with a proposed pathophysiological mechanism for WM dysfunction: reduced NMDAR conductance on inhibitory PV interneurons, amounting to generalized disinhibition of pyramidal cells and resultant loss of tuning (Murray et al., 2014; Homayoun & Moghaddam, 2007). Indeed, ketamine has high affinity for GluN2B NMDAR subunits which are expressed in PV interneurons (Gerhard et al., 2020; Kelsch et al., 2014). Loss of pyramidal cell tuning reduces the spatial specificity of WM representations, the PS, and encoded information by a population of neurons regarding remembered target location.

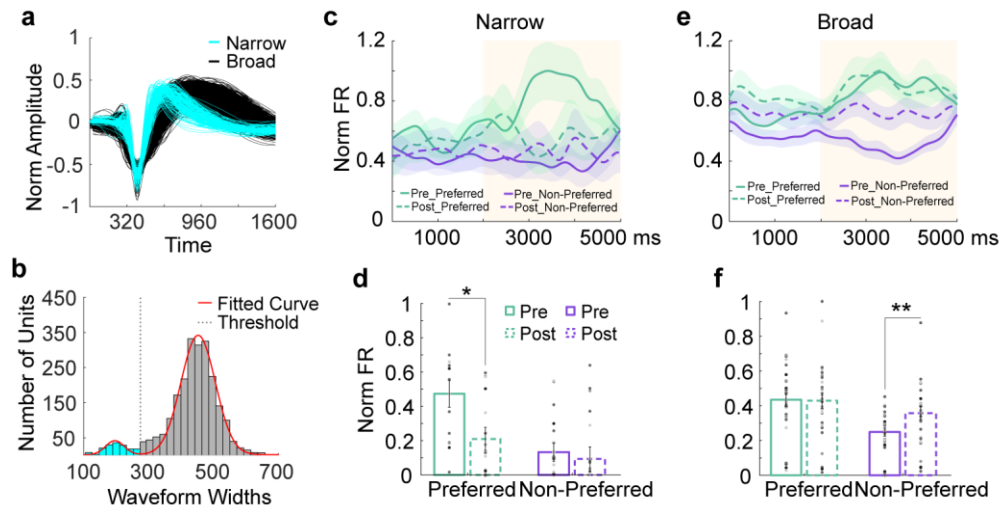


Figure. 3.4: Cell type specific effects of ketamine on working memory signals

a, Waveforms of narrow and broad spiking neurons. **b**, Distribution of waveform widths (microseconds) fitted with a 2-Gaussian model. Boundary line between narrow and broad spiking neurons is at the intersection point between Gaussians (275, dotted line). Gaussian at the lower width boundary indicates narrow spiking neurons (blue) and the upper boundary indicates broad spiking neurons (dark gray). **c**, Normalized average population SDFs for cue and delay (yellow) epochs for delay tuned narrow spiking neurons. **d**, Median population SDF for narrow spiking neurons over the delay epoch. Data points represent value per electrode array for each session. **e**, Normalized average population SDF for cue and delay epochs (yellow) for delay tuned broad spiking neurons. **f**, Median population SDF for broad spiking neurons over the delay epoch. All error bars are SEM. * <0.05 , ** <0.01 , *** <0.001 .

3.3.5 Ketamine Did Not Affect Gaze Behavior

A proportion of neurons in the LPFC encode signals related to gaze (Bullock, Pieper, Sachs, & Martinez-Trujillo, 2017). Since gaze was unconstrained in our task, it is possible that the coding of remembered locations predominantly reflect systematic biases in eye position signals. To explore this possibility, we first determined whether animals showed biases in eye position toward the target location (see example target locations in Figure. 3.5a). We calculated the duration in which the position of eye fixation was directed to the target location during the delay epoch divided by total time in which animals were fixating during the delay. We found that only 3.6% of fixation time during the delay epoch was spent looking at the target location in the pre-injection period. There were no significant differences between injection periods or between saline and ketamine sessions (Two-way ANOVA, drug, $F(1,69) = 1.73$, $p = 0.193$, injection period, $F(2,69) = 1.42$, $p = 0.248$, interaction, $F(2,69) = 1.35$, $p = 0.267$ (Figure. 3.5b).

As an additional measure, we used a linear classifier to predict target location from the position of eye fixations on the screen. We divided the screen into 16 cells and calculated the number of fixations falling within each cell. During the pre-injection period, the accuracy for decoding remembered locations from fixations was significantly higher than chance, indicating a target specific gaze bias (cue: t-test, $T(15) = 8.38$, $p < 0.0001$, delay: $T(15) = 8.53$, $p < 0.0001$; Figure. 3.5c, d). Such a bias was less pronounced during the delay relative to the cue epoch (Wilcoxon Rank-sum, $p = 0.002$; Figure. 3.5c). However, decoding accuracy for remembered locations from eye position was significantly lower than decoding accuracy of a classifier that uses neuronal firing rate and the same number of features ($n = 16$) (Kruskal–Wallis, cue: $H(1,30) = 14.78$, $p = 0.0001$; delay: $H(1,30) = 22.91$, $p < 0.0001$; Figure. 3.5d). Together, this data suggests that biases in eye position signals are not sufficient to account for the amount of information encoded by the population activity regarding target location.

After ketamine injections (early post-injection), decoding accuracy for remembered locations from eye position remained stable compared to the pre-injection period, Kruskal–Wallis; cue, $H(2,45) = 4.01$, $p = 0.135$, delay, $H(2,45) = 4.59$, $p = 0.101$; Figure. 3.5c). On the other hand, decoding accuracy for remembered locations from neuronal activity significantly decreased after ketamine injection (delay: Kruskal–Wallis, $H(2,45) = 11.26$, $p = 0.004$, post hoc, $p = 0.015$) (Figure. 3.3a). These results indicate that biases in eye position cannot account for the effects of ketamine on decoding of target locations from neuronal activity and suggest a dissociation between eye position and WM signals within LPFC microcircuits.

Finally, we calculated the proportion of single units tuned for eye position in both retinocentric and spatiocentric reference frames using Kruskal–Wallis analysis of variance. Using the retinocentric reference frame, saccade landing position was determined relative to the starting point of the saccade, independent from the landing location on the screen. In a spatiocentric reference frame, saccades were characterized according to their landing position on the screen, independent from the saccade starting position (Martinez-Trujillo, Medendorp, Wang, & Crawford, 2004). During the delay epoch, 9% of the neurons showed tuning for saccades in a retinocentric reference frame and 11% in a spatiocentric frame. However, only 2% of single units were tuned for both target location and saccades in the retinocentric frame and 3% of single units were tuned both for target location and saccades in spatiocentric frame (Figure. 3.5e). These results indicate that only a small number of neurons were tuned for eye position, and from those, only a small fraction were tuned for WM representations of target location. These results further argue against eye position related activity as the explanation for the coding of target position during the delay epoch.

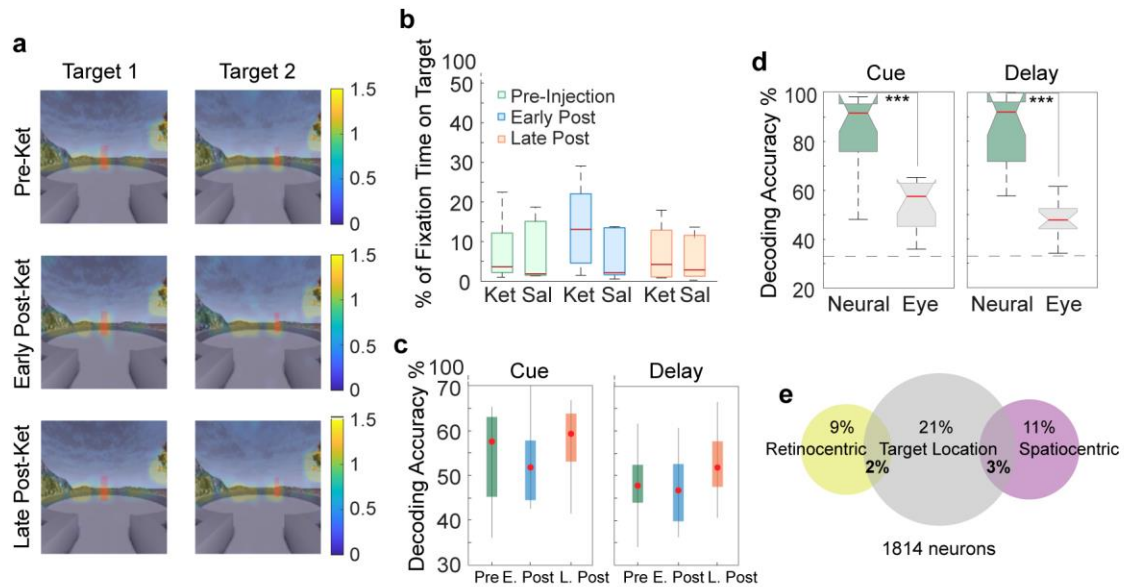


Figure. 3.5: Effect of ketamine on gaze behavior

a, Heat maps indicating eye fixation locations for two example target locations during the different injection periods. **b**, Proportion of fixation time falling on the target location compared to all fixation time during the delay epoch for ketamine and saline sessions. **c**, Comparison of decoding accuracy for target locations using eye fixation position between pre, early, and late- post ketamine-injection periods for the cue and delay epochs. **d**, Comparison between decoding target location accuracy using neuronal ensemble activity (green) and eye fixation position on screen (gray) during the ketamine pre-injection period for the cue and delay epochs. **e**, Proportion of single units tuned for target location during the delay epoch and tuned for saccade position in retinocentric or spatiocentric reference frames. Red center lines indicate median, the bottom and top edges of the box indicate the 25th and 75th percentiles. The whiskers extend to non-outlier data points (approximately within 2.7 std) and the outliers are plotted using '+'. * <0.05 , ** <0.01 , *** <0.001 .

3.4 « Discussion »

We used multielectrode arrays to simultaneously record the responses of single units in the macaque LPFC (pre/periarcuate areas 8 A/46) (Petrides, 2005) before and after administering subanesthetic doses of ketamine. We report three major findings: (1) ketamine selectively perturbs WM representations of targets in a naturalistic spatial WM task, (2) this effect is mediated by reduced spatial tuning of individual neurons leading to a loss of encoded information regarding target location at a neuronal population level, (3) ketamine induced changes in neuronal tuning were due to different effects on narrow and BS neurons; response decrease in the former and response increase in the latter.

Our study shows that macaque LPFC neurons encode WM representations during naturalistic tasks, regardless of potential interference by sensory and motor signals generated during natural behavior. Thus, the LPFC differs from areas such as the posterior parietal cortex where WM representations are perturbed by visual distractors (Suzuki & Gottlieb, 2013) and the frontal eye fields where shifts in gaze disrupt WM signals (Balan & Ferrera, 2003). Indeed, previous studies exploring the effects of ketamine on prefrontal neuronal activity while maintaining strict control of eye position show similar results to ours. Using the traditional spatial WM oculomotor delayed response task, which controls for eye position, Wang et al. (Wang et al., 2013) found that persistent activity in a small sample of delay cells was abolished and that spatial tuning was reduced after administration of specific NMDAR antagonists as well as systemic ketamine. In a rule-based WM task that restricted eye position, systemic ketamine decreased the rule signal during the delay epoch (i.e., differences in neuronal responses to prosaccade and anti-saccade trials) (Ma et al., 2015).

The granular LPFC, an anthropoid primate specialization, may allow for the encoding of representations that are uniquely dissociated from distraction and action. This seems to differ from the rodent prefrontal cortex, where neurons primarily encode prospective information about movement plans (Tsutsui, Oyama,

Nakamura, & Iijima, 2016). Thus, the granular LPFC may have allowed expanding the mental world of primates; consequently, enhancing their adaptability to changing environments (Passingham & Wise, 2012; Miller & Cohen, 2001). However, it may have also brought about new vulnerabilities upon which particular types of mental diseases develop as well as susceptibility to certain drugs.

One may argue that a limitation of our study was that ketamine was administered systemically, and since we recorded from LPFC, we may have not been able to observe effects in other brain regions. This is possible; however, the observed effects of ketamine were specific to WM and resembled those of early lesion studies in the same region (Jacobsen & Nissen, 1937). Moreover, local iontophoresis of NMDAR blocker, MK-801, produces similar changes in single neuron tuning and firing rate in the macaque prefrontal cortex during spatial WM tasks as systemically administered ketamine (Wang et al., 2013). In addition, ketamine shows the greatest effects on prefrontal activity in imaging studies (Breier et al., 1997; Anticevic et al., 2015). One possibility is that changes in the architecture of LPFC circuits, such as expansion of layers 2/3 and increase in the size and number of spines on pyramidal cells with an abundance of NMDARs, makes the LPFC more vulnerable to the effects of ketamine relative to other areas. Indeed, the density of dendritic spines in pyramidal cells is higher in LPFC relative to LIP (González-Burgos et al., 2019). Although systemic administration of a drug may produce similar concentrations across brain vascular networks, idiosyncrasies in receptor distribution and their molecular regulation may allow heterogeneity of dose dependent local effects (Datta & Arnsten, 2018).

The effects of ketamine reported here resemble results of previous studies using NMDAR blockers that have examined changes in neuronal activity during cognitive tasks. For example, using MK-801, a specific NMDAR blocker, Wang et al. (Wang et al., 2013) reported reduced neuronal tuning during a spatial WM task. Homayoun and Moghaddam (Homayoun & Moghaddam, 2007) also demonstrated differential effects of NMDAR blockage using MK-801 on narrow and BS cells in rodents, which are similar to what we report here using ketamine. Finally, Zick et

al. (Zick et al., 2018) showed that phencyclidine reduced cognitive performance in macaque monkeys when administered systemically. The latter was accompanied by reduction in synchronous firing between neurons and reduced effective connectivity within prefrontal microcircuits.

We show that ketamine impaired the animals' performance in the WM task. However, it did not do so in the perceptual task when animals had continuous visual access to the target. Moreover, ketamine neither impaired the ability of the animals to make saccades or navigate the virtual environment. These results suggest that in low doses, similar to the ones used in medical practice to treat depression (Fava et al., 2018), ketamine mainly affects mental representations. The latter corresponds with the common use of ketamine to mimic symptoms of schizophrenia (Frohlich & Van Horn, 2014; Morgan et al., 2004; Malhotra et al., 1997; Wang et al., 2013; Ma et al., 2015). Interestingly, WM deficits are one of the most prevalent symptoms of schizophrenia and are also hypothesized to result from NMDAR hypofunction, which may explain how ketamine so closely replicates symptoms of the disorder (Frohlich & Van Horn, 2014; Malhotra et al., 1997; Lee & Park, 2005).

In our study, spatial tuning of pyramidal cells was diminished by an increase in responses to the least-preferred locations, so one could speculate that mental representations were not abolished by ketamine, but they became less precise or distorted. Indeed, our decoding analysis indicated less reliable neuronal population codes for discriminating between remembered locations (see confusion matrices in Figure. 3.3a). This may explain the documented cases of ketamine causing perceptual distortions and hallucinations, especially in cases with decreased feedforward input from sensory cortices and enhanced top-down feedback signaling emanating from prefrontal mental representations (Domino, 2010; Powers, Gancsos, Finn, Morgan, & Corlett, 2015). Higher reliance on distorted representations may cause perceptual aberrations, explaining early descriptions of ketamine's dissociative properties (Sassano-Higgins et al., 2016).

Ketamine continues to gain popularity for the treatment of conditions like depression (Pribish et al., 2020; Wei et al., 2020). Patients with depression also suffer from WM deficits (Shiroma, Albott, Johns, Thuras, Wels, & Lim, 2014). So how could ketamine improve WM in patients with depression but cause WM deficits in healthy subjects? One explanation is that the mechanism of WM deficits during depression are associated with a decrease in the overall activity of LPFC microcircuits mediated by a decrease in excitatory neurotransmission or an imbalance of inhibition/excitation (Lener et al., 2017). We show that ketamine increases the level of activity of certain neuron types (e.g., BS excitatory cells). This increased activity may cause deficits in healthy subjects but ‘restore’ activity levels in patients with depression; however, this explanation requires specific testing. Nonetheless, our findings call for a careful evaluation on the impact of therapeutically administered ketamine on prefrontal cortex mediated cognition.

Finally, our results suggest that population codes for mental representations in LPFC rely on a delicate balance between the activation of excitatory and inhibitory neuron types mediated by NMDARs. A break-down of this balance may explain cognitive symptoms found in schizophrenia and other brain diseases exhibiting LPFC abnormalities and NMDAR hypoactivity (Frohlich & Van Horn, 2014; Malhotra et al., 1997; Wang et al., 2013; Lee & Park, 2005), as well as the disparate actions of ketamine on cognition and behavior.

3.5 « Supplementary Data »

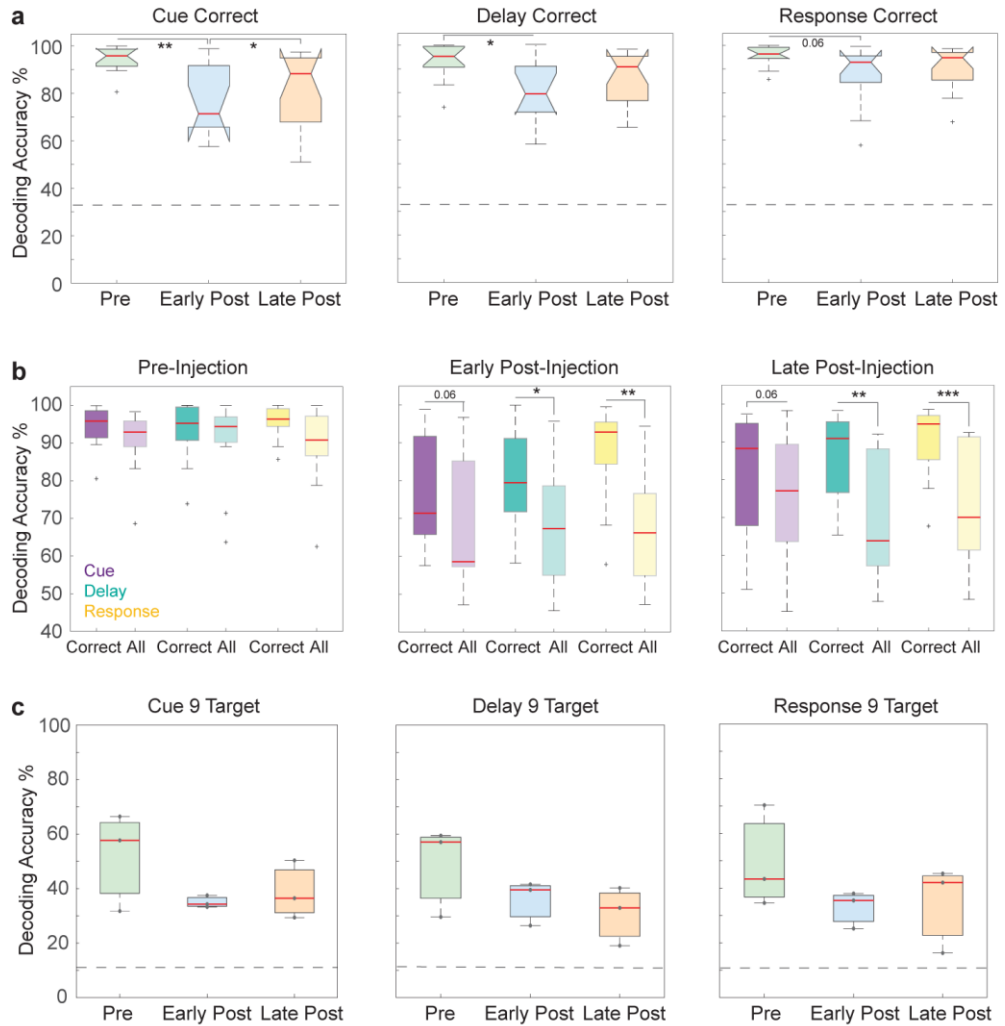


Figure. S3.6: Ensemble decoding for correct trials and nine target locations

a, Decoding target location from neuronal ensembles using correct trials. Decoding accuracy for ketamine-WM sessions for pre-injection (green), early post-injection (blue), and late post injection periods(orange) for trial epochs. Chance performance is indicated by dashed grey line. **b**, Comparison between decoding accuracy using correct trials and using all trials for trial epochs and injection periods. **c**, Decoding nine target locations from neuronal ensembles. Decoding accuracy for ketamine-WM sessions for pre-injection (green), early post-injection (blue), and late post-injection periods (orange) ($n = 3$ sessions) for trial epochs. Data points represent decoding accuracy per session. Chance performance is indicated by dashed grey line. Red center lines indicate median, the bottom and top edges of the box indicate the 25th and 75th percentiles. The whiskers extend to non-outlier data points (approximately within 2.7 std) and the outliers are plotted using '+'. * <0.05 , ** <0.01 , *** <0.001 .

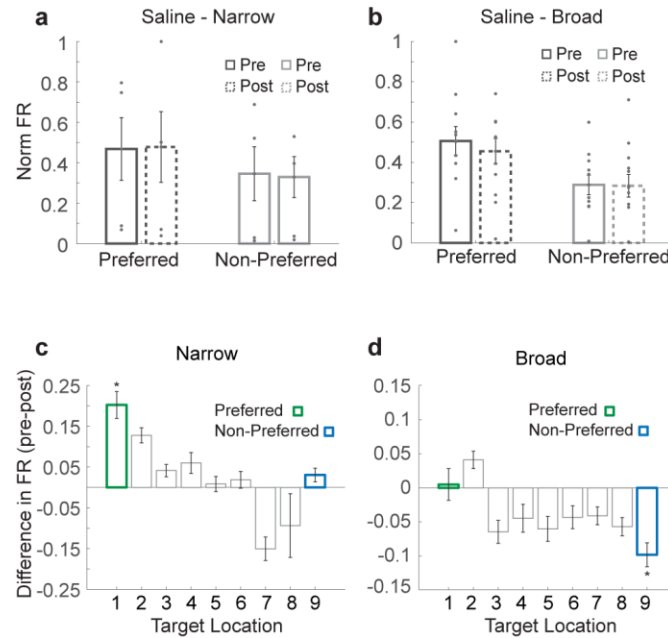


Figure. S3.7: Changes in narrow and broad neuron firing rates per subject

a, Firing rates for saline-WM sessions for narrow spiking neurons averaged over the delay epoch for preferred and least-preferred locations. **b**, Firing rates for saline-WM sessions for broad spiking neurons averaged over the delay epoch for preferred locations and least-preferred locations. Data points represent values per electrode array for each session. **c**, Difference in firing rate (pre-post injection) for delay tuned narrow spiking neurons for target locations ranked from preferred to least-preferred. **d**, Difference in firing rate (pre post injection) for delay tuned broad spiking neurons for target locations ranked from preferred to least- preferred.

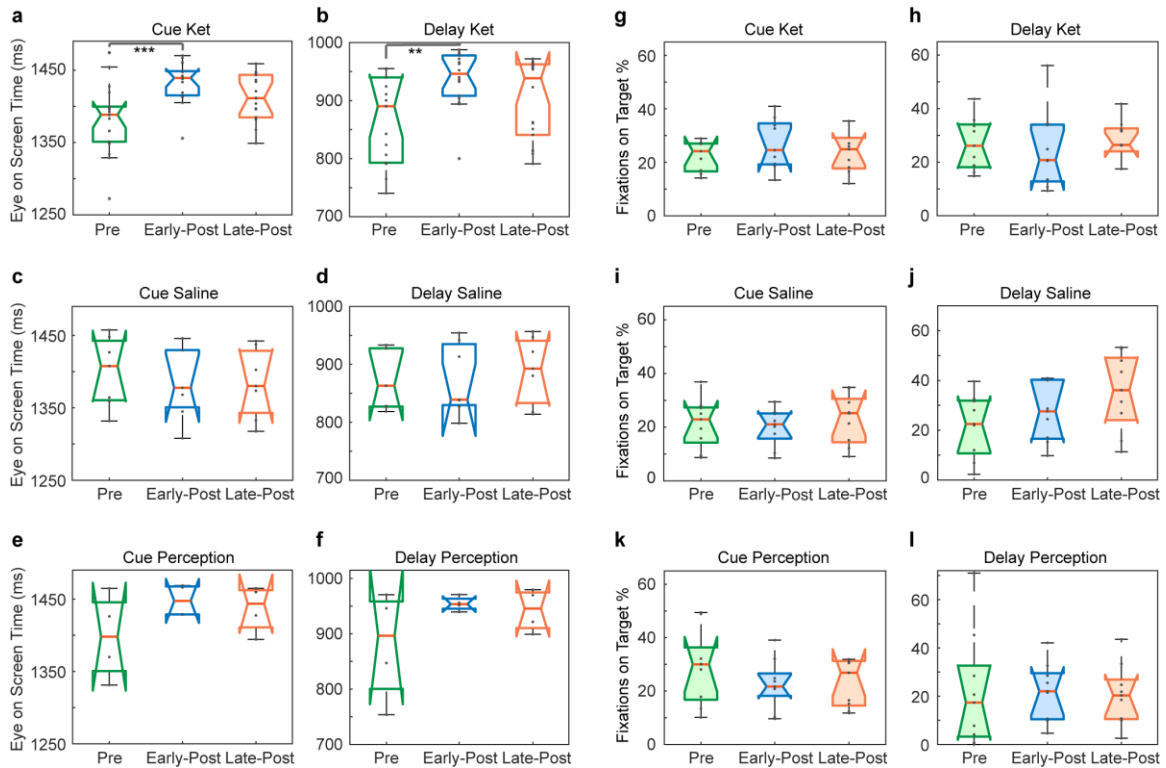


Figure. S3.8: Gaze behavior

a, Duration of eyes on screen during the cue epoch for ketamine-WM. **b**, Eyes on screen during the delay epoch for ketamine-WM. **c**, Eyes on screen during the cue epoch for saline-WM. **d**, Eyes on screen during the delay epoch for saline-WM. **e**, Eyes on screen during the cue epoch for ketamine-perception. **f**, Eyes on screen during the delay epoch for ketamine-perception. Data points represent values per session. **g**, Percentage of fixations on target location during the cue epoch for ketamine-WM. **h**, Percentage of fixations on target location during the delay epoch for ketamine-WM. **i**, Percentage of fixations on target location during the cue epoch for saline-WM. **j**, Percentage of fixations on target location during the delay epoch for saline-WM. **k**, Percentage of fixations on target location during the cue epoch for ketamine-perception. **l**, Percentage of fixations on target location during the delay epoch for ketamine-perception. Red center lines indicate median, the bottom and top edges of the box indicate the 25th and 75th percentiles. The whiskers extend to non-outlier data points (approximately within 2.7 std) and the outliers are plotted using '+'. * <math>< 0.05</math>, ** <math>< 0.01</math>, *** <math>< 0.001</math>.

3.6 « Methods »

Two adult male rhesus macaques (*Macaca mulatta*) were used in this experiment (age: 10, 9; weight: 12, 10 kg). We chose to use two animals in order to minimize the number of non-human primates used in the experiment and to ensure reproducibility between at least two animals. The n value for each analysis was determined individually as the smallest unit of observation, which was most often session. Results shown in the main text and figures represent results across subjects unless otherwise specified.

3.6.1 Ethics Statement

Animal care and handling including basic care, animal training, surgical procedures, and experimental injections were pre-approved by the University of Western Ontario Animal Care Committee. This approval ensures that federal (Canadian Council on Animal Care), provincial (Ontario Animals in Research Act), regulatory bodies (e.g., CIHR/NSERC), and other national standards (CALAM) for the ethical use of animals are followed. Regular assessments for physical and psychological well-being of the animals were conducted by researchers, registered veterinary technicians, and veterinarians.

3.6.2 Task and Experimental Setup

The current task takes place in a virtual environment. This environment was developed using Unreal Engine 3 development kit, utilizing Kismet sequencing and UnrealScript (UDK, May 2012 release; Epic Games). More about this platform and the recording setup can be found in Doucet et al. (Doucet, Gulli, & Martinez-Trujillo, 2016) Within this virtual environment, target locations were arranged in a 3 × 3 grid and spaced 290 unreal units apart (time between adjacent targets is ~0.5 s). Movement speed was fixed throughout navigation.

The task was presented on a computer LDC monitor positioned 80 cm from the subjects' eyes (27" ASUS, VG278H monitor, 1024 × 768 pixel resolution, 75 Hz

refresh rate, screen height equals 33.5 cm, screen width equals 45 cm). Subjects performed the experiment in an isolated room with no illumination other than the monitor. The walls, doors, and ceiling of the room were RF shielded and contained no AC power lines. Cables providing power to the setup equipment entered the room through a small aperture in a wall and were shielded to minimize interference with the recordings. Eye positions were monitored using a video-oculography system with sampling at 500 Hz (EyeLink 1000, SR Research). A custom computer program-controlled the stimulus presentation (through Unreal Engine 3), reward dispensation, and recorded eye position signals and behavioral responses. Subjects performed the experiment while seated in a standard enclosed primate chair (Neuronitek) and were delivered juice reward through a tube attached to the chair and an electronic reward integration system (Crist Instruments). Prior to the experiments, subjects were implanted with custom fit, PEEK cranial implants which housed the head posts and recording equipment (Neuronitek). See Blonde et al. (Blonde, Roussy et al, 2018) for more information. The head posts were attached to a head holder to fix the monkeys' heads to the primate chair during training and experimental sessions.

3.6.3 Microelectrode Array Implant

Surgical procedures were conducted under general anesthesia induced by ketamine and maintained using isoflurane and propofol. Two 10×10 , microelectrode Utah arrays (96 channels, 1.5 mm in length and separated by at least 0.4 mm) (Blackrock Microsystems) were chronically implanted in each animal. They were located in the left LPFC (anterior to the arcuate sulcus and on either side of the posterior end of the principal sulcus) (Petrides, 2005) . Brain navigation for surgical planning was conducted using Brainsight (Rogue Research Inc.). Arrays were placed and impacted ~ 1.5 mm into the cortex. Reference wires were placed beneath the dura and a grounding wire was attached between screws in contact with the pedestal and the border of the craniotomy. Electrode placement was approximated using CT imaging post-operatively.

3.6.4 Neuronal Recordings and Spike Detection

Neuronal data was recorded using a Cerebus Neural Signal Processor (Blackrock Microsystems) via a Cereport adapter. The neural signal was digitized (16 bit) at a sample rate of 30 kHz. Spike waveforms were detected online by thresholding at 3.4 standard deviations of the signal. The extracted spikes were semi-automatically resorted with techniques utilizing Plexon Offline Sorter (Plexon Inc.). Sorting results were then manually supervised. Multiunits consisted of threshold-crossing events from multiple neurons with action potential-like morphology that were not isolated well enough to be classified as a well-defined single unit. We collected behavioral data across 18 ketamine-WM sessions (nine in animal T, nine in animal B) and neuronal data from 17 ketamine-WM sessions with one session from animal T removed due to incomplete synchronization of neuronal data during the recording. This yielded a total of 2906 units recorded during ketamine-WM sessions: 1814 single neurons (259 in animal T, 1555 in animal B) and 1092 multiunits (533 in animal T, 559 in animal B). Behavior and neuronal data was recorded from seven saline-WM sessions resulting in 1117 units in total: 674 single units (48 in animal T, 626 in animal B) 443 multiunits (126 in animal T, 317 in animal B). Behavioral data from four ketamine-perception sessions were analyzed (two in animal T, two in animal B).

3.6.5 Ketamine Injection

Both animals experienced all experimental conditions. The sessions in which either ketamine or saline was administered were randomized. Animals were trained to voluntarily receive injections in the primate chair while in the experimental setup. An intramuscular injection of either ketamine (0.25, 0.4, or 0.8 mg/kg) or saline (0.25 mg/kg) was administered in the hamstring muscles by a registered veterinary technician. The ketamine doses were titrated so they did not induce visible behavioral changes in the animals such as nystagmus or somnolence. Ketamine injections were spaced at least 2 days apart to allow for washout of the drug (Zanos et al., 2018).

3.6.6 Behavioral Analysis

Correct trials are trials in which subjects reach the correct target location within 10 s. The percent of correct trials was compared to chance (11%) for each session using binomial tests.

The percent of correct trials over time was calculated using 15 equally sized trial bins for each injection period. The resulting 45 data points per session were averaged over all ketamine-WM and saline-WM sessions for each animal and then combined across subjects. Statistical analysis was conducted by comparing the percent of correct trials binned over the three injection periods (pre, early post, and late post-injection periods) for ketamine-WM and saline-WM sessions. Response time was calculated for correct trials as the duration between navigation onset and end of trial for each experimental condition (target location) for each recording session.

Analyses of animals' trajectories within the navigation period are conducted on trials in which the animals cross a predetermined line that divides the start enclave from the main body of the task arena. The task environment was divided into a 5×5 grid containing 25 regional cells of equal dimensions. The grid was sized so that cells tightly enclose target locations. For each trial, we calculated whether the subject entered each cell during navigation resulting in either 1 (entered) or 0 (not entered) per cell. The number of trials in which each cell was entered was then divided by the total number of trials. This resulted in a percent value for each cell for each target location condition (25×9 conditions, $n = 225$ per session) that was then averaged over all ketamine-WM or saline-WM sessions. We then calculated increases in average percent values for each cell between injection periods (values above 0 included).

3.6.7 Spatial Selectivity

Single units (2488 from 17 ketamine-WM and seven saline-WM sessions) were tested for selectivity for target location during a given epoch for all trials by

computing a one-way analysis of variance on epoch-averaged firing rates with target location as the independent variable. A unit was defined as selective if the test resulted in $p < 0.05$. A neuron's preferred location was defined as the location that elicited the largest response during the epoch of interest. The least-preferred location was defined as the location that elicited the smallest response.

To ensure consistent sample size between injection periods, we subsampled trials without replacement to the minimal number of trials between the pre, early post and late post-injection periods. This was repeated 50 times and the median values from all iterations was calculated. The proportion of tuned single units for each task epoch (cue and delay) were compared between injection periods for ketamine-WM and saline-WM sessions using Chi-Square tests.

3.6.8 Ranked Target Selectivity

Neurons were ranked from their preferred to least-preferred location based on average firing rate. This was repeated for each injection period. We then calculated the slope of a linear regression model fitted to the ranked responses averaged across neurons in a session for each of the nine target locations. A higher negative slope indicates higher firing rate for preferred locations (higher ranked) compared to less preferred locations (lower ranked) which gives a proxy of tuning. This was calculated for each injection period in each session ($n = 17$).

3.6.9 Plane Fitting

In order to visualize neuronal responses to different target locations within the 2D space, we fit a second order polynomial surface to the mean normalized firing rate for the 9 target location conditions to the x- and y- coordinates of each target location. Firing rate was normalized by the maximum firing rate in the ketamine pre-injection period. This method was used for visualization, not for quantitative analysis.

$$f(x, y) = p_{0,0} + p_{1,0}x + p_{0,1}y + p_{2,0}x^2 + p_{0,2}y^2 + p_{1,1}xy$$

3.6.10 Neuronal Ensemble Decoding

We used a linear SVM (Libsvm 3.14) (Fan, Chang, Hsieh, Wang, & Lin, 2008) with fivefold cross-validation to extract task-related activity from z-score normalized population-level responses using both single units and multiunits on a single trial basis. The regularization parameter used was the optimal penalty parameter C (refer to Eq. 1 in Fan et al. (Fan et al., 2008)). The classifiers used firing rates calculated over epoch durations (cue, 3000 ms; delay, 2000 ms; response first 2000 ms) from ensembles of neurons simultaneously recorded within each session to predict target location for correct and incorrect trials within the virtual arena (left, center, right).

For each session, we calculated decoding performance for neuronal ensembles with a maximum of 16 neurons since decoding performance plateaued around this point. We began building ensembles by selecting the neuron with highest individual performance for decoding target location. This neuron was then paired with all remaining neurons to find the pair of neurons that maximized decoding performance. We then used this pair and combined it iteratively with all remaining neurons to find the best trio. This procedure was repeated until 16 neurons were reached.

We pooled target locations across depth in order to have a sufficient number of trials for training and testing the classifiers. We chose to combine trials based on target direction in the environment (left, center, right) based on observations that neurons tended to show more similar responses to targets located in the same direction compared to targets located at the same depth within the environment. Observations were balanced between classes using subsampling (without replacement) which was repeated 20 times.

We maintained the same neurons in ensembles (for ensembles of 16 neurons) and used the same procedure to calculate chance performance obtained by randomizing class labels (all other data features remained unaltered). We repeated this shuffling procedure 10 times for each session. Subsampling was

conducted 20 times in each iteration. Using this procedure, the shuffled decoding accuracy for one ketamine-WM session from animal T was higher than expected by chance; therefore, this session was removed from the analysis. Decoding accuracy between injection periods for ketamine-WM and saline-WM sessions was compared for each neuronal ensemble size. We ran the decoding procedure a second time restricting to correct trials only (in sessions with a sufficient number of samples for cross-validation). Finally, a third decoding analysis was conducted using all 9 target locations from neuronal data on a single trial basis using SVM with fourfold cross validation (in sessions with a sufficient number of samples: one session in animal T, two sessions in animal B).

3.6.11 Waveform Classification

Single units were classified as either narrow (NS) or BS based on action potential width measured as peak-to-trough interval duration (Torres-Gomez et al., 2020). Average waveforms for each unit were interpolated with a cubic spline fit to increase the resolution of the data ($\times 100$). The duration between waveform peak and trough was then calculated based on time stamps from the minimal and maximal voltage values. Waveform widths for all neurons were plotted in a histogram. After removing outlier widths (>675 microseconds), 2314 units remained and are included in the analysis. A bimodal distribution was visualized and then quantified by fitting the data with either a single (1-Gaussian) or sum of two Gaussian functions (2-Gaussian) to determine optimal fit. The goodness of fit for both functions was determined using Akaike Information Criterion (Akaike, 1974) with the lowest value determined for 2-Gaussians indicating bimodality.

The threshold dividing NS and BS (275 microseconds) was determined by setting a boundary at the inflection point of the two Gaussian fitted distributions (Torres-Gomez et al., 2020; McCormick, Connors, Lighthall, & Prince, 1985). Waveform amplitudes were normalized to the difference between the highest and lowest amplitudes for each unit waveform and waveforms were aligned at threshold crossing for visualization. Based on this threshold, 161 neurons were

classified as NS and 2153 neurons were classified as BS. 750 delay tuned BS neurons were included for further analysis for ketamine-WM sessions and 246 delay tuned units were included for saline-WM sessions. 41 delay tuned narrow spiking neurons were included for ketamine-WM sessions and 11 delay tuned neurons were included for saline-WM sessions.

3.6.12 Firing Rate for Preferred and Non-Preferred Locations

Spike density functions (SDFs) using Gaussian kernels (150 ms std) were calculated for NS and BS neurons that were significantly tuned for target locations during the delay epoch (ANOVA, $p < 0.1$). We specifically obtained the SDFs for these neurons for their preferred and least-preferred locations during the delay epochs before ketamine or saline injection. We then calculated SDFs for these same locations in the post-injection period. Population activity was calculated by averaging SDFs between simultaneously recorded single units within the same electrode array and responses were normalized by the maximum population response. These population responses for each electrode array were then averaged over all ketamine-WM or saline-WM sessions. Firing rates were averaged during the delay epoch and were statistically compared using 1-tailed Wilcoxon Rank-sum tests between pre and early post-injection periods for preferred and least-preferred locations.

In addition, we used the same procedure as the preferred and least-preferred analysis but included responses to all target locations ranked from preferred (1) to least-preferred (9). We compared the firing rates from the pre-injection and post-injection periods for each target condition using 1-tailed Wilcoxon Rank-sum tests.

3.6.13 Gaze Analysis

Gaze position was computed from eye tracking signals synchronized with the neuronal recordings and behavioral performance measurements (Corrigan, Gulli, Doucet, & Martinez-Trujillo, 2017). The amount of time that gaze fell within

the screen boundaries was calculated during the cue and delay epochs of the task and were statistically compared before and after ketamine or saline injection (Figure. S3.8a-f).

Eye movements were classified as saccades, fixations, or smooth pursuits based on previously published methods for eye movement classification in virtual environments in which periods of high acceleration approximate saccade epochs and movement patterns were used to determine precise saccade onset and offset. Foveations are classified as fixations or smooth pursuits based on measures of spatial range (see Corrigan et al. (Corrigan et al., 2017) for detailed method). The proportion of fixations falling within the trial specific target location compared to other potential target locations on the screen was calculated (Figure. S3.8g-l).

We calculated the total fixation time during the delay epoch as well as the fixation time on the trial specific target location for correct trials. We compared the proportion of fixation time on the target location related to all fixation time during delay (target location fixation duration / total fixation duration) between the three injection periods for ketamine and saline sessions using 2-way analysis of variance with injection period and drug (saline or ketamine) as factors.

To decode target location using eye position during the cue and delay epochs, the screen was divided into 16 cells of equal dimensions. The number of foveations classified as fixations were calculated within each cell under the assumption that animals gather information from the virtual environment during such fixation periods (Corrigan et al., 2017). We used a linear classifier (SVM) with fivefold cross-validation to determine whether target location could be predicted on a single trial basis by the number of fixations within each cell (i.e., the extent to which animals fixate in each part of the visual environment). This analysis was compared with a decoding analysis using neuronal ensembles utilizing the same number of features (16 neuron ensembles).

To calculate the proportion of single units tuned for eye position in both retinocentric and spatiocentric reference frames, we assessed saccade position in

both retinocentric and screen centered coordinates. We used a quadrant binning pattern for a $40^\circ \times 30^\circ$ field. To keep reference frames for a particular neuron consistent, we made sure that both reference frames had the same Fpower by ordering the bins from highest saccade count to lowest, then pairing them across reference frames, and then dropping saccades from the bin that had more out of the pair. A bin had to have at least ten saccades to be acceptable and sessions had at least three acceptable bins. Neurons with sufficient data were then analyzed using Kruskal–Wallis analysis of variance.

3.7 « References »

Pribish, A., Wood, N., & Kalava, A. A. (2020). Review of nonanesthetic uses of ketamine. *Anesthesiology Research and Practice*, 5798285. doi: 10.1155/2020/5798285

Gerhard, D. M., Pothula, S., Liu, R-J., Wu, M., Li, X-Y., Girgenti, M. J., et al. (2020). GABA interneurons are the cellular trigger for ketamine's rapid antidepressant actions. *The Journal of Clinical Investigation*, 130, 1336–49. doi: 10.1172/JCI130808

Wei, Y., Chang, L., & Hashimoto, K. (2020). A historical review of antidepressant effects of ketamine and its enantiomers. *Pharmacology Biochemistry and Behavior*, 190, 172870. doi: 10.1016/j.pbb.2020.172870

Sassano-Higgins, S., Baron, D., Juarez, G., Esmaili, N., & Gold, M. (2016). A review of ketamine abuse and diversion. *Depression and Anxiety*, 33, 718–27. doi: 10.1002/da.22536

Domino, E. F. (2010). Taming the ketamine tiger. *Anesthesiology*, 113, 678–86. doi: 10.1097/ALN.0b013e3181ed09a2

Frohlich, J., & Van Horn, J. D. (2014). Reviewing the ketamine model for schizophrenia. *Journal of Psychopharmacology*, 28, 287–302. doi: 10.1177/0269881113512909

Morgan, C. J. A., Mofeez, A., Brandner, B., Bromley, L., & Curran, H. V. (2004). Acute effects of ketamine on memory systems and psychotic symptoms in healthy volunteers. *Neuropsychopharmacology*, 29, 208–18. doi: 10.1038/sj.npp.1300342

Breier, A., Malhotra, A. K., Pinals, D. A., Weisenfeld, N. I., & Pickar, D. (1997). Association of ketamine-induced psychosis with focal activation of the prefrontal cortex in healthy volunteers. *The American Journal of Psychiatry*, 154, 805–11. doi: 10.1176/ajp.154.6.805

Malhotra, A. K., Pinals, D. A., Adler, C. M., Elman, I., Clifton, A., Pickar, D., et al. (1997). Ketamine-induced exacerbation of psychotic symptoms and cognitive impairment in neuroleptic-free schizophrenics. *Neuropsychopharmacology*, 17, 141–50. doi: 10.1016/S0893-133X(97)00036-5

Wang, M., Yang, Y., Wang, C-J., Gamo, N. J., Jin, L. E., Mazer, J. A., et al. (2013). NMDA receptors subserve persistent neuronal firing during working memory in dorsolateral prefrontal cortex. *Neuron*, 77, 736–49. doi: 10.1016/j.neuron.2012.12.032

- Murray, J. D., Anticevic, A., Gancsos, M., Ichinose, M., Corlett, P. R., Krystal J. H., et al. (2014). Linking microcircuit dysfunction to cognitive impairment: Effects of disinhibition associated with schizophrenia in a cortical working memory model. *Cerebral Cortex*, *24*, 859–72. doi: 10.1093/cercor/bhs370
- Passingham, R. E., & Wise, S. P. (2012). *The neurobiology of the prefrontal cortex: Anatomy, evolution, and the origin of insight*. New York: Oxford University Press.
- Baddeley, A. D. (1986). *Working memory*. New York: Oxford University Press.
- Funahashi, S., Chafee, M. V., & Goldman-Rakic, P. S. (1993). Prefrontal neuronal activity in rhesus monkeys performing a delayed anti-saccade task. *Nature*, *365*, 753–6. doi: 10.1038/365753a0
- Suzuki, M., & Gottlieb, J. (2013). Distinct neural mechanisms of distractor suppression in the frontal and parietal lobe. *Nature Neuroscience*, *16*, 98–104. doi:10.1038/nn.3282
- Miller, E. K., Erickson, C. A., & Desimone, R. (1996). Neural mechanisms of visual working memory in prefrontal cortex of the macaque. *The Journal of Neuroscience*, *16*, 5154–67. doi:10.1523/JNEUROSCI.16-16-05154.1996
- Mendoza-Halliday, D., & Martinez-Trujillo, J. C. (2017). Neuronal population coding of perceived and memorized visual features in the lateral prefrontal cortex. *Nature Communication*, *8*, 15471. doi:10.1038/ncomms15471
- Jacobsen, C. F., & Nissen, H. W. (1937). Studies of cerebral function in primates. IV. The effects of frontal lobe lesions on the delayed alternation habit in monkeys. *Journal of Comparative Psychology*, *23*, 101–12.
- Funahashi, S., Bruce, C. J., & Goldman-Rakic, P. S. (1989). Mnemonic coding of visual space in the monkey's dorsolateral prefrontal cortex. *Journal of Neurophysiology*, *61*, 331–49. doi: 10.1152/jn.1989.61.2.331
- Leavitt, M. L., Mendoza-Halliday, D., & Martinez-Trujillo, J. C. (2017). Sustained activity encoding working memories: Not fully distributed. *Trends in Neuroscience*, *40*, 328–46. doi: 10.1016/j.tins.2017.04.004
- Ma, L., Skoblenick, K., Seamans, J. K., & Everling, S. (2015). Ketamine-induced changes in the signal and noise of rule representation in working memory by lateral prefrontal neurons. *The Journal of Neuroscience*, *35*, 11612–22. doi: 10.1523/JNEUROSCI.1839-15.2015
- Petrides, M. (2005). Lateral prefrontal cortex: Architectonic and functional organization. *Philos Trans R Soc Lond B Biol Sci*, *360*, 781–95. doi: 10.1098/rstb.2005.1631

- Wang, X. J. (1999). Synaptic basis of cortical persistent activity: the importance of NMDA receptors to working memory. *The Journal of Neuroscience*, *19*, 9587–603. doi: 10.1523/JNEUROSCI.19-21-09587.1999
- Wang, X-J., Tegnér, J., Constantinidis, C., & Goldman-Rakic, P. S. (2004). Division of labor among distinct subtypes of inhibitory neurons in a cortical microcircuit of working memory. *PNAS*, *101*, 1368–73. doi:10.1073/pnas.0305337101
- Lisman, J. E., Fellous, J-M., & Wang, X-J. (1998). A role for NMDA-receptor channels in working memory. *Nature Neuroscience*, *1*, 273–75. doi:10.1038/1086
- Uhlén, M., Fagerberg, L., Hallström, B. M., Lindskog, C., Oksvold, P., Mardinoglu, A., et al. (2015). Tissue-based map of the human proteome. *Science*, *347*, 1260419. doi:10.1126/science.1260419
- Anticevic, A., Corlett, P. R., Cole, M. W., Savic, A., Gancsos, M., Tang, Y., et al. (2015). N-methyl-D-aspartate receptor antagonist effects on prefrontal cortical connectivity better model early than chronic schizophrenia. *Biological Psychiatry*, *77*, 569–80. doi:10.1016/j.biopsych.2014.07.022
- Zanos, P., Moaddel, R., Morris, P. J., Riggs, L. M., Highland, J. N., Georgiou, P., et al. (2018). Ketamine and ketamine metabolite pharmacology: Insights into therapeutic mechanisms. *Pharmacology Review*, *70*, 621–60. doi: 10.1124/pr.117.015198
- Nogueira, R., Peltier, N. E., Anzai, A., DeAngelis, G. C., Martinez-Trujillo, J., Moreno-Bote, R. (2020). The effects of population tuning and trial-by-trial variability on information encoding and behavior. *The Journal of Neuroscience*, *40*, 1066–83. doi:10.1523/JNEUROSCI.0859-19.2019
- Homayoun, H., Moghaddam, B. (2007). NMDA receptor hypofunction produces opposite effects on prefrontal cortex interneurons and pyramidal neurons. *The Journal of Neuroscience*, *27*, 11496–500. doi:10.1523/JNEUROSCI.2213-07.2007
- Torres-Gomez, S., Blonde, J. D., Mendoza-Halliday, D., Kuebler, E., Everest, M., Wang, X-J, et al. (2020). Changes in the proportion of inhibitory interneuron types from sensory to executive areas of the primate neocortex: Implications for the origins of working memory representations. *Cerebral Cortex*, *30*, 4544–62. doi:10.1093/cercor/bhaa056
- Kelsch, W., Li, Z., Wieland, S., Senkov, O., Herb, A., Göngrich, C., et al. (2014). GluN2B-Containing NMDA receptors promote glutamate synapse development in hippocampal interneurons. *The Journal of Neuroscience*, *34*, 16022–30. doi: 10.1523/JNEUROSCI.1210-14.2014

- Bullock, K. R., Pieper, F., Sachs, A. J., & Martinez-Trujillo, J. C. (2017). Visual and presaccadic activity in area 8Ar of the macaque monkey lateral prefrontal cortex. *Journal of Neurophysiology*, *118*, 15–28. doi:10.1152/jn.00278.2016
- Martinez-Trujillo, J. C., Medendorp, W. P., Wang, H., & Crawford, J. D. (2004). Frames of reference for eye-head gaze commands in primate supplementary eye fields. *Neuron*, *44*, 1057–66. doi:10.1016/j.neuron.2004.12.004
- Balan, P. F., Ferrera, V. P. (2003). Effects of gaze shifts on maintenance of spatial memory in macaque frontal eye field. *The Journal of Neuroscience*, *23*, 5446–54. doi:10.1523/JNEUROSCI.23-13-05446.2003
- Tsutsui, K-I., Oyama, K., Nakamura, S., & Iijima, T. (2016). Comparative overview of visuospatial working memory in monkeys and rats. *Frontier in Systems Neuroscience*, *10*, 99. doi:10.3389/fnsys.2016.00099
- Miller, E. K., & Cohen, J. D. (2001). An integrative theory of prefrontal cortex function. *Annual Review of Neuroscience*, *24*, 167–202. doi:10.1146/annurev.neuro.24.1.167
- González-Burgos, G., Miyamae, T., Krimer, Y., Gulchina, Y., Pafundo, D. E., Krimer, O., et al. (2019). Distinct properties of layer 3 pyramidal neurons from prefrontal and parietal areas of the monkey neocortex. *The Journal of Neuroscience*, *39*, 7277–90. doi:10.1523/JNEUROSCI.1210-19.2019
- Datta, D., & Arnsten, A. F.T. (2018). Unique molecular regulation of higher-order prefrontal cortical circuits: Insights into the neurobiology of schizophrenia. *ACS Chemical Neuroscience*, *9*, 2127–45. doi:10.1021/acschemneuro.7b00505
- Zick, J. L., Blackman, R. K., Crowe, D. A., Amirikian, B., DeNicola, A. L., Netoff, T. I., et al. (2018). Blocking NMDAR disrupts spike timing and decouples monkey prefrontal circuits: Implications for activity-dependent disconnection in schizophrenia. *Neuron*, *98*, 1243–55. doi:10.1016/j.neuron.2018.05.010
- Fava, M., Freeman, M. P., Flynn, M., Judge, H., Hoepfner, B. B., Cusin, C., et al. (2018). Double-blind, placebo-controlled, dose-ranging trial of intravenous ketamine as adjunctive therapy in treatment-resistant depression (TRD). *Molecular Psychiatry*, *25*, 1592–603. doi:10.1038/s41380-018-0256-5
- Lee, J., & Park, S. (2005). Working memory impairments in schizophrenia: A meta-analysis. *Journal of Abnormal Psychology*, *114*, 599–611. doi:10.1037/0021-843X.114.4.599
- Powers, A. R., Gancsos, M. G., Finn, E. S., Morgan, P. T., Corlett, P. R. (2015). Ketamine-induced hallucinations. *Psychopathology*, *48*, 376–85. doi:10.1159/000438675

- Shiroma, P. R., Albott, C. S., Johns, B., Thuras, P., Wels, J., & Lim, K. O. (2014). Neurocognitive performance and serial intravenous subanesthetic ketamine in treatment-resistant depression. *The International Journal of Neuropsychopharmacology*, *11*, 1805–13. doi:10.1017/S1461145714001011
- Lener, M. S., Niciu, M. J., Ballard, E. D., Park, M., Park, L. T., Nugent, A. C., et al. (2017). Glutamate and gamma-aminobutyric acid systems in the pathophysiology of major depression and antidepressant response to ketamine. *Biological Psychiatry*, *81*, 886–97. doi:10.1016/j.biopsych.2016.05.005
- Doucet, G., Gulli, R. A., & Martinez-Trujillo, J. C. (2016). Cross-species 3D virtual reality toolbox for visual and cognitive experiments. *Journal of Neuroscience Methods*, *266*, 84–93. doi:10.1016/j.jneumeth.2016.03.009
- Blonde, J. D., Roussy, M., Luna, R., Mahmoudian, B., Gulli, R. A., Barker, K. C., et al. (2018). Customizable cap implants for neurophysiological experimentation. *Journal of Neuroscience Methods*, *304*, 103–17. doi:10.1016/j.jneumeth.2018.04.016
- Fan, R-E., Chang, K-W., Hsieh, C-J., Wang, X-R., & Lin, C-J. (2008). LIBLINEAR: A library for large/linear classification. *The Journal of Machine Learning Research*, *9*, 1871–4.
- Akaike, H. (1974). A new look at the statistical model identification. *IEEE Transactions on Automatic Control*, *19*, 716–23. doi:10.1109/TAC.1974.1100705
- McCormick, D. A., Connors, B. W., Lighthall, J. W., & Prince, D. A. (1985). Comparative electrophysiology of pyramidal and sparsely spiny stellate neurons of the neocortex. *Journal of Neurophysiology*, *54*, 782–806. doi:10.1152/jn.1985.54.4.782
- Corrigan, B. W., Gulli, R. A., Doucet, G., & Martinez-Trujillo, J. C. (2017). Characterizing eye movement behaviors and kinematics of non-human primates during virtual navigation tasks. *Journal of Vision*, *17*, 1–22. doi:10.1167/17.12.15

Chapter 4

4 « Neural Sequences in Primate Prefrontal Cortex Encode Working Memory in Naturalistic Environments »

4.1 « Abstract »

Working memory is the ability to remember and manipulate information ‘in mind’ for short time periods. Candidate brain mechanisms for encoding working memory include persistent firing of neurons selective for memorized items, oscillations, and synaptic storage. Here we demonstrate a mechanism for working memory coding in which populations of prefrontal neurons dynamically represent memory content in a naturalistic environment through sequential activation of single neurons. We simultaneously recorded the activity of hundreds of neurons in the lateral prefrontal cortex of macaque monkeys during a naturalistic visuospatial working memory task in a virtual environment. We found that the sequential activation of single neurons encoded trajectories to target locations held in working memory. Neural sequences were not a mere activation of cells with memory fields at spatial locations, but an abstract representation of the subject’s trajectory to the target. Sequences were not found during working memory tasks lacking the spatiotemporal structure of the naturalistic task. Finally, ketamine administration distorted neural sequences, selectively decreasing working memory performance. Our results indicate that neurons in the lateral prefrontal cortex causally encode working memory in naturalistic conditions via complex and temporally precise activation patterns.

4.2 « Introduction »

Working memory (WM) is the ability to briefly maintain and manipulate information ‘in mind’ to achieve a current goal (Baddeley, 1986). Brain circuits supporting WM differ from those for sensory processing in that they must represent precise information in naturalistic contexts in the absence of sensory inputs (see

Roussy et al., 2021 for review). They also differ from long-term memory circuits in that the information is only maintained for short time intervals - just long enough to complete a specific task. Despite five decades of study, the neural mechanisms underlying WM remain controversial.

The primate lateral prefrontal cortex (LPFC) has been widely implicated in WM function as evidenced by previous lesion and electrophysiological studies in macaque monkeys (Leavitt et al., 2017a; Roussy et al., 2021). A long-supported mechanism for coding of WM representations in LPFC of primates during delayed response tasks is persistent firing in single neurons selective for the memorized information (Fuster & Alexander, 1971; Constantinidis et al., 2018). During such tasks, subjects must remember the location or features of a sample item for a few seconds after its disappearance, and then produce a behavioral response, e.g., a saccade to a remembered location. However, most delayed response tasks used to explore the neural mechanisms of WM lack the spatiotemporal structure of naturalistic behavior (i.e., they use simple stationary displays and constrain eye movements during memory maintenance). During many natural behaviors involving WM the visual scenery is rich, dynamic, and eye gaze is unconstrained.

Studies using delayed response tasks with increased spatiotemporal complexity report few single neurons with persistent firing during the entire delay period. Instead, many neurons fire transiently, during brief time intervals (Batuev et al., 1979; Lundqvist et al., 2016). Thus, researchers have proposed alternative mechanisms to persistent firing, such as short-term synaptic storage (Stokes et al., 2015; Pals et al., 2020), or oscillatory dynamics (Lundqvist et al., 2016). However, evidence in favor of such mechanisms is highly debated (Wang, 2021).

Here, we hypothesize that coding of WM during natural behavior, in the presence of eye movements and rich visual displays, relies on sequential activation of neurons in primate LPFC. Neuronal sequences, consisting of temporally precise patterns of neural activity, have been reported to encode the varying spatiotemporal structure of motor signals in the high vocal center (HVC) of

songbirds (Chi et al., 2001; Tang et al., 2014; Srivastava et al., 2017; Okubo et al., 2015; Daliparthi et al., 2019), and of spatial trajectories to remembered locations during navigation in the parietal cortex (Harvey et al., 2012) and the hippocampus of rodents (Itskov et al., 2011; Eichenbaum et al., 2014; Zhou et al., 2020). Early investigations in macaque monkeys suggested that the spiking activity of a few single neurons in LPFC could have a precise spatiotemporal structure (Abeles, 1993). However, sequences of single unit spiking activity have not been directly observed or causally linked to WM during naturalistic behavior in primates (Wang, 2021).

We tested this using high-density microelectrode arrays to record neuronal activity in LPFC of macaque monkeys during a naturalistic WM task set in a 3D virtual environment. We find that temporally precise sequential patterns of neural activity, extending over behaviorally relevant timescales of several seconds, in LPFC represent important task variables for the successful maintenance of and navigation to remembered target locations in the 3D environment. These neural sequences are adept at robustly and flexibly representing trajectories to remembered locations during shifts in eye positions toward various elements of the environment. Sequences were not found during standard tasks used to explore WM in previous studies. Further, pharmacological blockade of NMDA receptors with sub-anesthetic doses of ketamine demonstrates a causal link between sequences and WM.

4.3 « Results »

We trained two rhesus macaque monkeys on a visuospatial working memory task that took place in a virtual circular arena containing naturalistic elements (see Figure. 4.1a, b). We recorded neuronal activity using two 96-channel microelectrode Utah Arrays (Blackrock Neurotech, UT, USA) implanted in the left LPFC of both animals (Brodmann area 8a, 9/46 (Petrides, 2005)) (see Figure. 4.1c). The task began with a three-second presentation of a target in one of nine possible locations in the arena (cue epoch). The target then disappeared

and after a two-second delay period, the animal was required to navigate towards the cued target location using a joystick (see Figure. 4.1d). Virtual navigation within the environment was exclusively available during the navigation epoch. Animals were able to successfully perform this naturalistic WM task (average correct trial rates across sessions were: NHP B: *Mean* = 87%, NHP T: *Mean* = 57%; chance = ~11%) (Figure. 4.1e).

4.3.1 Neural Sequences in Prefrontal Neurons

Although precise patterns of neural activity appear to be a fundamental mechanism for representing complex processes (Buzsáki, 2010), such patterns have not been identified during visuospatial WM tasks in primates. We hypothesize that WM representations during our naturalistic task are maintained by temporally precise neural sequences (Figure. 4.1f). We observed that LPFC neurons exhibited consistent brief elevations of spike rate at specific points during the task. To identify potentially relevant patterns in these elevations of spike rate, we sorted neurons by their normalized peak firing times (Figure. 4.1g, h).

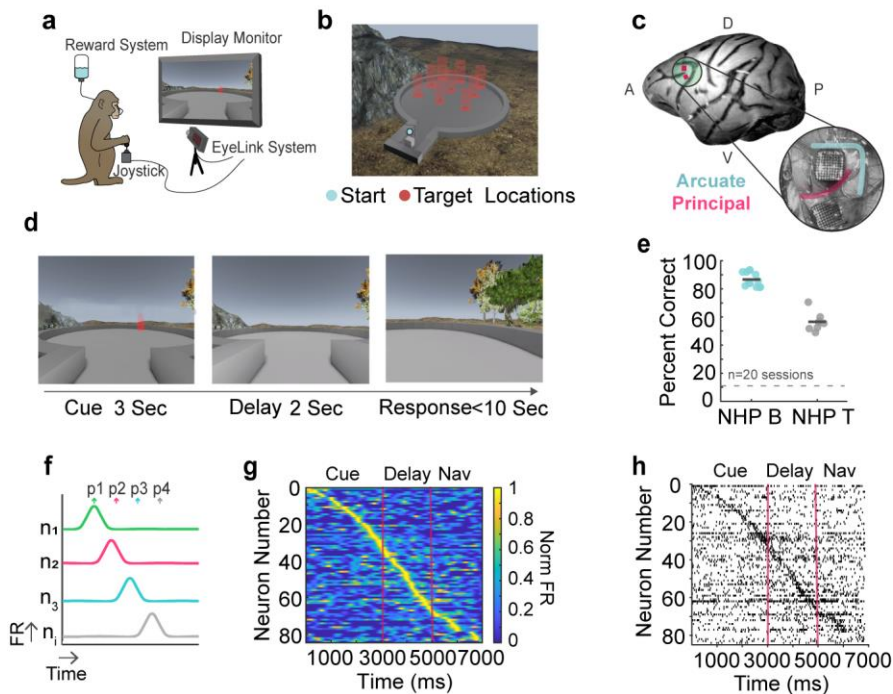


Figure. 4.1: Experimental design

a, An animal depicted in the virtual reality experimental setup. **b**, Overhead view of the nine target locations in the virtual environment. **c**, Locational representation and surgical image of the two Utah arrays implanted in the left LPFC of NHP T. **d**, Working memory trial timeline. **e**, Percent of correct trials for NHP B and NHP T. The dark gray lines represent mean values per animal and the gray dashed line represents chance behavioral performance. Data points represent data from individual sessions. **f**, Illustration of temporally tiled activation of individual neurons which may generate sequential patterns of activity at the population level. **g**, Normalized firing rates for simultaneously recorded neurons over trial time in one trial. **h**, Raster plot for the same example trial as 'g' in which each small vertical line represents an action potential.

A code that relies on neural sequences implies precise temporal activation of single neurons within subpopulations (see Figure. 4.2a for schematic) (Buzsáki, 2010; van der Meij & Voytek, 2018). We examined the firing properties of 3543 neurons in 17 recording sessions (*Mean* of 208, *Median* of 229 simultaneously recorded neurons per session). Many neurons transiently fired during the same time in different trials of the same target condition (Figure. 4.2b, c, d, more examples in Figure. S4.8). To quantify this regularity, we calculated the standard deviation (time consistency) of peak firing time between trials of the same condition for each neuron (Figure. S4.9a). 20% of neurons (699 neurons) demonstrated a standard deviation (std) below 1000 ms and 65% (2297 neurons) demonstrated a std below 1500 ms.

We additionally shuffled the peak firing times for each neuron across trials to generate random firing time estimates within each trial. The distributions of stds for correct trials were shifted to lower values relative to the corresponding shuffled distributions (example session in Figure. 4.2e, f). The area of non-overlapping between the lower tails of the real and shuffled distributions represents the neurons with peak firing times occurring more regularly than expected by chance. On the other hand, the real and shuffled distributions overlapped considerably for incorrect trials (example session in Figure. 4.2e), suggesting that neurons' peak firing occurred at less consistent times during single trials of the same condition when animals made mistakes. Indeed, the difference between means of the real and shuffled distributions (Figure. 4.2f) was lower for incorrect trials than correct trials (correct: *Median* = 270.9, incorrect: *Median* = 71.4. Wilcoxon Signed-Rank Test, $p = 0.001$) (Figure. 4.2g; Figure. S4.9b, c).

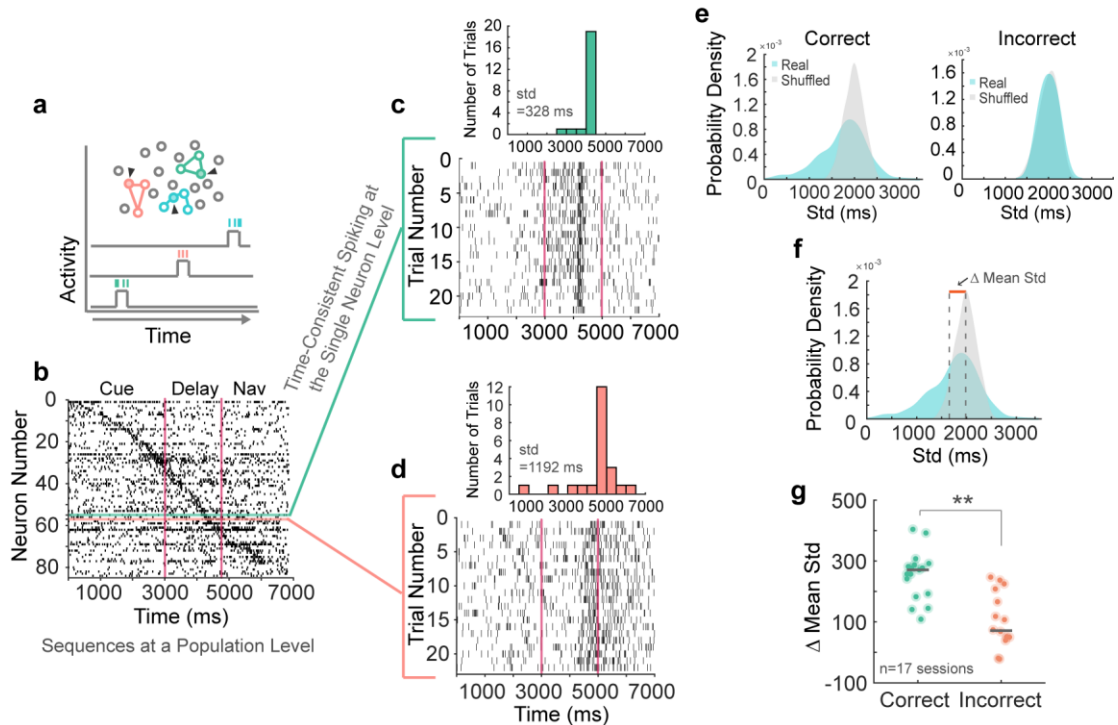


Figure 4.2: Time consistent neurons underlie sequence formation

a, Depiction of neural ensembles that are activated at different time points throughout a trial. Activity of a single neuron within the ensemble is represented by a bump in activity at a precise time point. Black arrows represent recording electrodes. **b**, Single trial raster showing the activity of all simultaneously recorded neurons. The green and pink horizontal lines highlight two example neurons. **c**, Example neuron one. The raster plot displays action potentials over trial time for this neuron over all trials in a certain condition. The inlet histogram shows the number of trials in which the max firing time falls within a certain trial time. **d**, Represents the same information as 'c' for a second example neuron. **e**, Real and shuffled distributions of correct and incorrect trial-trial standard deviations of max firing time for all neurons in an example session. **f**, same as 'e' for correct trials. Dashed gray lines represent distribution means and the orange line indicates the difference in distribution means. **g**, Difference in real and shuffled distribution means for correct and incorrect trials. Dark gray lines represent median values per group and each dot represents data from a different session. * $p < 0.05$, ** $p < 0.01$, *** $p < 0.001$.

Using 11 sessions in which there are sufficient correct and incorrect trials in all nine conditions, we show that the std of neurons ($n = 2051$) during correct trials is significantly lower than incorrect trials (1-way ANOVA, post hoc, $p = 3.8E-09$; Figure. S4.9a). This suggests that consistent temporal firing in single neurons is needed for correct task performance.

4.3.2 Neural Sequences are Predictive of Trajectory to Remembered Targets

We have demonstrated a pattern of sequential activity that spans the trial duration and is driven by temporally consistent firing of single neurons. Next, we examined whether these identified sequences are related to WM; more precisely, whether sequences can encode the contents of WM during memory delay. Therefore, we developed a computational method to analyze spike sequences in single trials, allowing for efficient unsupervised discovery of neural sequences that are consistent within the same target condition. We represented individual sequences of peak firing during the delay epoch in each trial across the population of recorded neurons as complex-valued vectors. We performed dimensionality reduction on the resulting correlation matrix (Figure. 4.3a). The resulting component values are projected into a 3-dimensional space where each colored circle represents a cluster centroid for a different target condition (Figure. 4.3b, c).

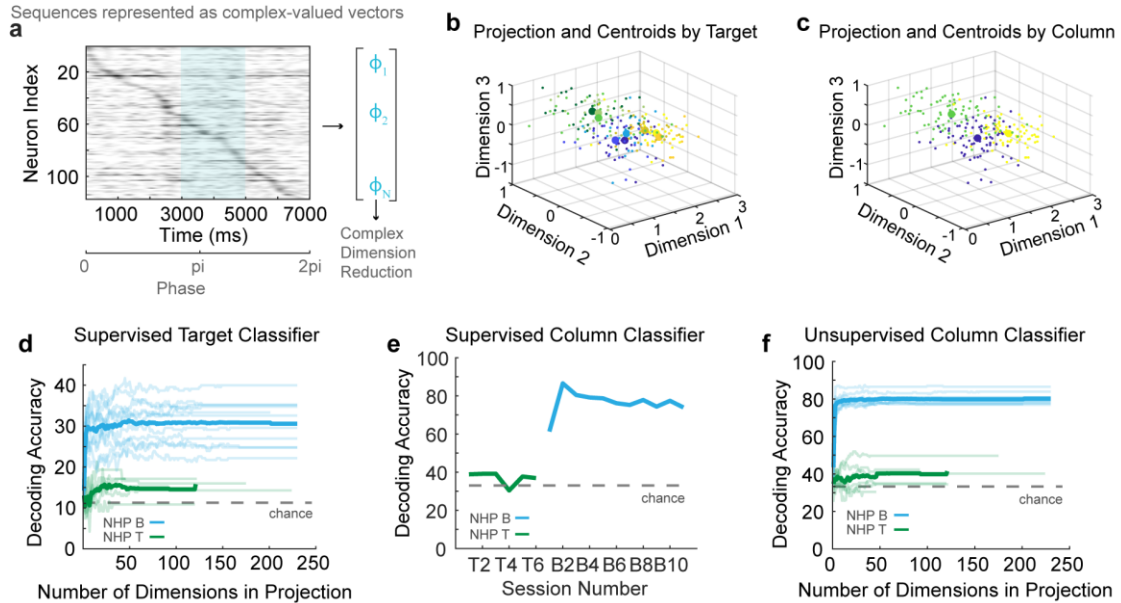


Figure. 4.3: Classification using sequential coding

a, Representation of max firing times per neuron during delay being converted to complex phase values and used in our complex vector dimensionality reduction method. **b**, 3D projection of neural sequence data. Large dots represent projected target centroids in 3D space. Smaller dots represent individual trials. **c**, 3D projection of neural sequence data. Large dots represent projected column centroids in 3D space. Columns contain pooled trials between right, left, and center targets. Smaller dots represent individual trials. **d**, Supervised classification of target location using centroid distances. Each line represents decoding accuracy over number of dimensions considered for one session. Bold lines represent median values over sessions. **e**, Supervised classification performance for predicting target column averaged over sessions per NHP using three dimensions. Gray dashed line is theoretical chance performance. **f**, Unsupervised classification of target column (left, right center) using centroid distances. Each line represents decoding accuracy over number of dimensions considered for one session. Bold lines represent median values over sessions

Using a supervised distance-based classifier on a single trial level, we demonstrated that centroids can correctly predict target condition (9 locations: median = 15% above chance; see Methods – Projection Classification Analysis) (Figure. 4.3d). We then observed that the condition centroids reliably clustered into three groups based on the three general trajectory directions to targets (left, center, right) (Figure. 4.3c). Based on this observation, we then hypothesized that this clustering may relate to task behavior. A supervised classifier based on this hypothesis can correctly predict target condition column (left, center, right) based on delay-epoch sequence activity on single trials (*Median* = 41% above chance) (Figure. 4.3e). Further, an unsupervised classifier developed from our analysis could predict target column in a single trial based on the emergent clustering of projected data into column-based clusters - without any training required (*Median* = 33% above chance) (Figure. 4.3f). Taken together, these results demonstrate that these patterns of spiking activity contain a unique temporal structure for different trial conditions that may be related to remembered target locations.

To explore the direct relationship between sequences and task-relevant behavior during WM, we compare distance between centroids during the memory delay epoch to distances between target trajectories (i.e., representing the trajectories navigated towards the remembered target location). We calculated the Spearman correlation between matrices containing the Euclidean distance between condition centroids (Figure. 4.4b), and the Frechet distance between average traveled trajectories to targets in the virtual arena (see Figure. 4.4c, d; Figure. 4.4e, f) (see Figure. S4.10a-c for alternative methods). The Frechet distance between two trajectories is a measure of similarity between them that takes into account the location and ordering of the points along the trajectories (Alt & Godau, 1995). The distance matrices were more positively correlated compared to those obtained when shuffling the target locations, suggesting that the separation between neural sequences in multidimensional space parallels the discriminability between trajectories to targets held in WM (observed: *Median* = 0.50, shuffle: *Median* = 0.34, Wilcoxon Signed-Rank Test: $p = 0.02$). Moreover, the relationship between sequences and target location relates to whether information

is successfully maintained during WM delay, with higher positive correlations for correct than incorrect trials (correct: *Mean* = 0.45, incorrect: *Mean* = 0.30. t-test, $p = 0.0005$) (Figure. 4.4g).

We also compared the correlations during the WM delay period with that during a temporally equivalent period of a perceptual task, where the target did not disappear, thus the animals did not need to represent the trajectory in WM. The correlation is higher during the WM delay epoch than during the perceptual control delay epoch (Figure. 4.4h; WM: *Mean* = 0.51 perception: *Mean* = 0.33, t-test, $p = 1.4E-05$), indicating that sequences were more correlated to behavior during WM.

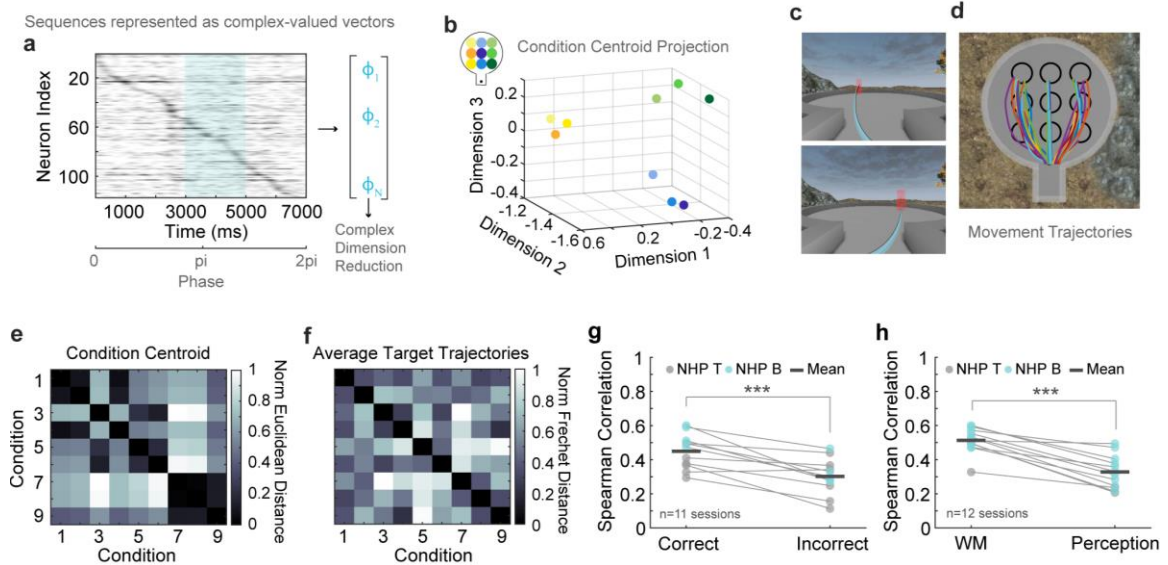


Figure. 4.4: Neural sequences represent working memory content

a, Representation of max firing times per neuron during delay being converted to complex phase values and used in our complex vector dimensionality reduction method. **b**, Condition cluster centroids projected in 3D space. Centroid colors correspond with their position in the virtual environment (see inset). **c**, Depiction of trajectories to two target locations. **d**, Example trajectories to the 9 target locations. Each line represents a trial. **e**, Coefficient matrix of Euclidean distances between condition centroids. **f**, Coefficient matrix of Fréchet distances between average target trajectories for each target location. **g**, Correlation values for all sessions for correct and incorrect trials colored by animal. Dots represent individual sessions and matching sessions are connected by lines. **h**, Correlation values for all WM and perception sessions colored by animal. Dots represent individual sessions and matching sessions are connected by lines. * $p < 0.05$, ** $p < 0.01$, *** $p < 0.001$.

Furthermore, sequences during WM were unique from those that occur during the cue and navigation epochs (Figure. 4.5 a-c) and they were most predictive of target column condition (cue: *Median* decoding performance = 52%, delay: *Median* decoding performance = 66%, navigation: *Median* decoding performance = 52%; 1-way ANOVA, $p = 0.03$) (Figure. 4.5d). Sequences are also more correlated to target trajectories when we limit a neuron's contribution to a sequence to one epoch (i.e., one neuron is only allowed to participate in a single epoch sequence – considering a single max firing time) compared to contributing to multiple epoch sequences (i.e., allows for multiple peak firing times) (single: *Mean* = 0.48, multiple: *Mean* = 0.37; t-test, $p = 0.006$) (Figure. S4.10c). This latter result indicates sequences are most informative when different neurons contribute to different epochs, suggesting unique contributions of neurons over trial states.

4.3.3 Neural Sequences are Specific to Naturalistic Working Memory

Neural sequences may operate when information held in WM has a spatiotemporal structure. To test this prediction, we conducted the same set of analyses exploring macaque LPFC single neuron temporal precision and population sequences in an oculomotor delayed response task (ODR) (Figure. S4.11a, b). In this task, animals must remember a spatial location during a delay period and make a saccade when a central fixation point disappears (Leavitt, 2017b, Leavitt, 2018). The task we used included 16 possible target locations. Saccades are ballistic movements and there is no path 'traveled' towards the location during the saccade execution. As opposed to the VR navigation task, when neurons during the ODR task were ordered by peak firing time, the patterns of activation were often disrupted or incomplete (Figure. S4.11c), suggesting that the organization of spiking activity may be different from the VR task. This may be related to neurons during the ODR delay epoch exhibiting less temporally consistent peak firing times from trial to trial. For many instances, real and shuffled distributions of standard deviations were overlapping (Figure. S4.11d). Indeed, the difference in means between real and shuffled distributions was significantly smaller in the ODR task compared to our naturalistic VR task (ODR1: *Median* =

93.22. ODR2: *Median* = 31.57, VR: *Median* = 270.93; Kruskal Wallis, $p = 1.2e-06$) (Figure. S4.11e).

To further explore this issue, we applied the complex-valued dimensionality reduction analysis described above to the ODR task data. Condition centroids were interestingly clustered in quadrants based on position of target location as reported previously using spike rate-based analysis (Leavitt, 2018) (Figure. 4.5e). We calculated the correlation between the matrices of centroid distances and target location Euclidean distances. The correlation was significantly smaller in the ODR than in the naturalistic VR task (ODR: *Median* = 0.21, VR: *Median* = 0.43. Wilcoxon Rank Sum, $p = 0.004$) (Figure. 4.5f).

These results indicate that sequences are more correlated to behavior during the naturalistic VR task than during the classic ODR task. The naturalistic VR task is different in several ways. First, it measures visuospatial WM in a dynamic and more spatiotemporally complex environment. Second, it allows for free visual exploration via saccades. Third, it requires 3D navigation to a target location. Neural sequences may be best utilized in the dynamic spatiotemporal context of our WM task.

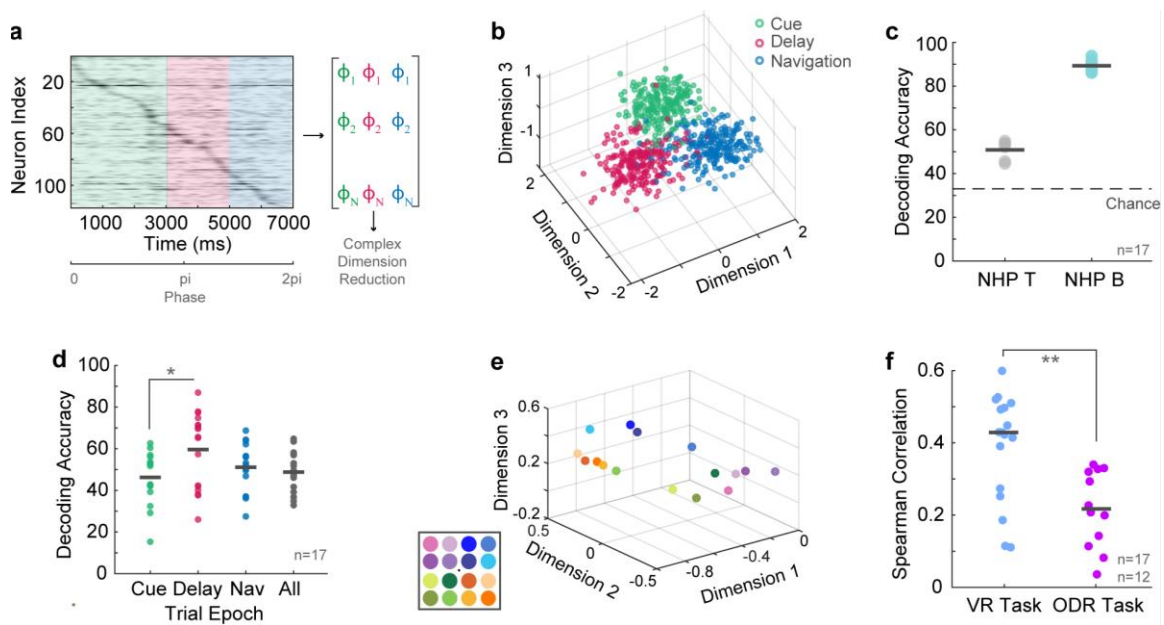


Figure 4.5: Working memory sequences are unique to naturalistic behavior

a, Representation of max firing times per neuron during the three task epochs being converted to complex phase values and used in our complex vector dimensionality reduction method. **b**, Epoch specific sequences projected in 3D space. Colored dots correspond to epochs and represent a single trial. **c**, Decoding accuracy using unsupervised classifiers for predicting task epoch. Dots represent data from different sessions. **d**, Decoding accuracy using unsupervised classifiers for predicting target column (left, middle, right) for sequences during task epochs. **e**, Condition cluster centroids for an ODR task projected in 3D space. Centroid colors correspond with their position in the virtual environment (see inset). **f**, Correlation values for centroid distance and the distance between target locations for the virtual reality task and the ODR task. Dots represent data per session. * $p < 0.05$, ** $p < 0.01$, *** $p < 0.001$.

4.3.4 Neuronal Sequences Represent Abstract Trajectories

The previous analysis demonstrates that WM sequences contain information about the trajectories to remembered target locations, suggesting that sequences map into behavioral paths. Condition centroids were more highly correlated to the Frechet distance between the trajectories to target locations (*Median* = 0.50) than to the Euclidean distance between target locations (*Median* = 0.43); therefore, sequences more strongly represent trajectories to target locations than target location alone. Real trajectories are also more correlated to condition centroids than ideal trajectories to targets (calculated by Euclidean distance from the start location to the target location) (Figure. 4.6a) (*Median* = 0.42). Here one must consider that traveled trajectories are imperfect and can be distinct from ideal trajectories. Real trajectories reflect idiosyncrasies of remembered trajectories and the virtual environment which may reflect perceived curvature of the arena and obstacles in space (i.e., arena walls)(see Figure. 4.6b for example trajectories).

One may argue that the observed sequences represent activation of neurons with mnemonic ‘place fields’ similar to sequential activity of place cells in the hippocampus (Itskov, 2011; Eichenbaum, 2014; Zhou, 2020). Inconsistent with this idea, the sequences are differentiable between memory delay and navigation, evidenced through classification analysis (*Mean* decoding = 76%, *Median* decoding = 87%, compared to chance (33%): t-test, $p = 9.2e-08$) (Figure. 4.5b,c), suggesting that WM sequences are not a direct representation of space that is rehearsed and played-back during navigation.

We explored trajectories to different locations that contain overlapping spatial segments (primarily occurs for center targets). We wanted to test whether sequences corresponding to these overlapping trajectories contain similar neurons (Figure. 4.6b, c). During the delay epoch, the neural sequences corresponding to pairs of these similar trajectories had no more neurons in common than pairs of trajectories with any direction, depth, or curvature (delay epoch: *Means*: similar-center = 0.40, all = 0.37, $p = 0.7$) (Figure. 4.6d). The correlation between sequences for ideal overlapping trajectories was

similar to correlations between sequences for all trajectories when using all neurons, and even when considering only neurons shared between the trajectories (1-way ANOVA, post hoc; all neurons: ideal - all trajectories, $p = 1$; shared neurons ideal - all trajectories, $p = 0.15$) (Figure. 4.6e). This shows that sequences likely do not represent a direct spatial path as occurs in hippocampal place cells. Instead, sequences may reflect a task condition-specific abstract spatial representation of the environment in reference to the target location.

If sequences were caused primarily by motor planning during the delay period or neural replay of planned trajectories during the response period, we could expect neural sequences during the delay and response epochs from the same trial to be highly correlated, and this correlation would be higher than sequences from different trials. This was not the case. Delay and navigation epoch sequences were equally correlated between different trials as they were within the same trial (Figure. 4.6f, g). These results indicate that neural sequences in macaque LPFC represent remembered trajectories to target locations, and that such representations are different from those found in other brain areas.

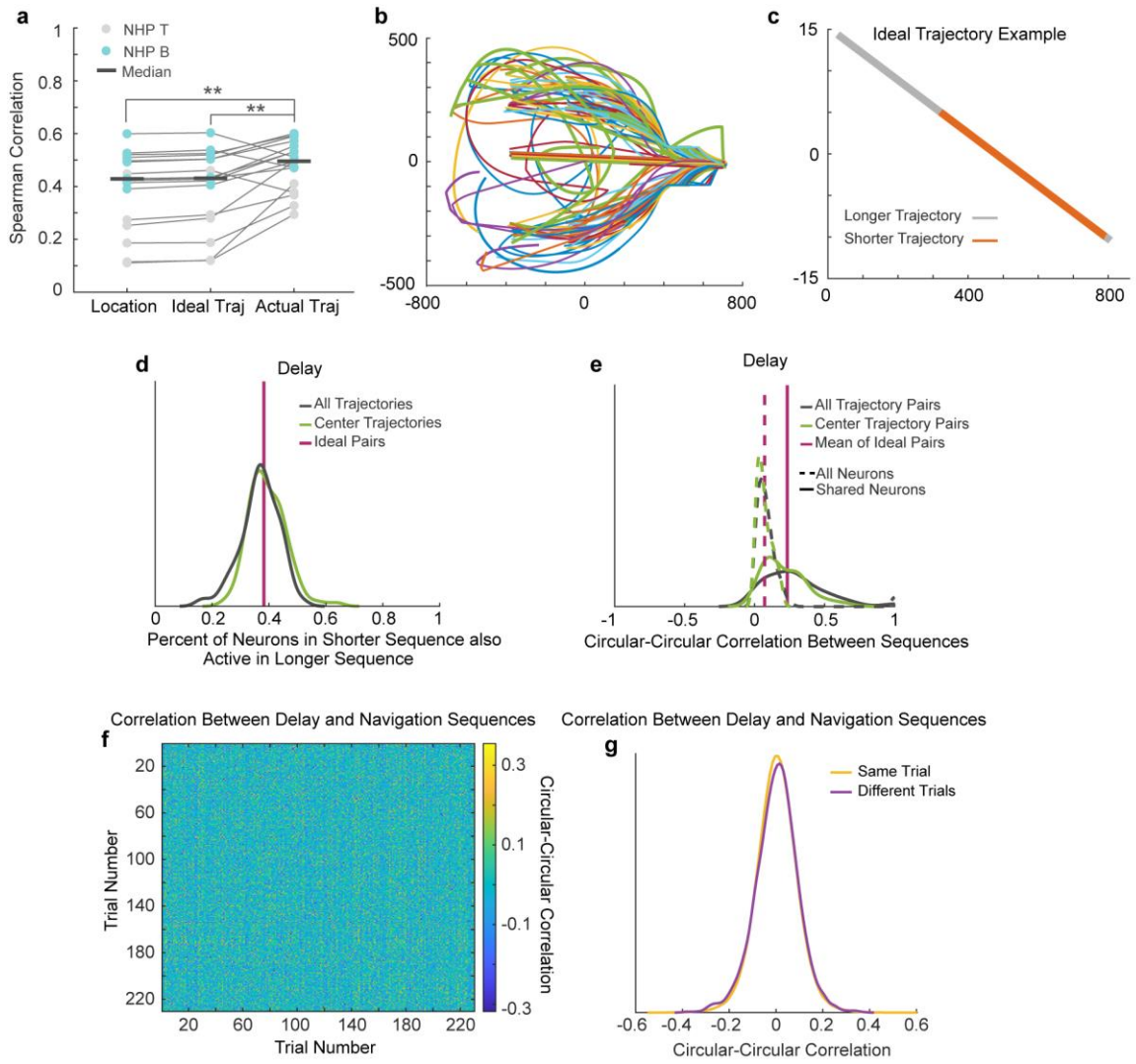


Figure. 4.6: Trajectory analysis

a, Correlation between condition centroids and target location, ideal trajectories (i.e., Euclidean distance from start location to targets), or actual trajectories to target locations. Dots represent data per session. **b**, Trajectory examples within a session to the nine possible locations. **c**, Ideal trajectory reflecting situations in which a shorter trajectory falls precisely within the same path as a longer trajectory. **d**, Percent of neurons during the delay epoch in shorter sequences that are also active in longer sequences for all trajectories, all center target trajectories, and all ideal trajectories. **e**, The correlation between shorter and longer sequences during the delay epoch for all trajectories, all center target trajectories, and all ideal trajectories. Presented for the full population of neurons and for neurons shared between shorter and longer sequences. **f**, The correlation between delay and navigation epoch neural sequences between trials for an example session. The diagonal represents sequence correlations within the same trial. If neural sequences repeated between delay and response epochs in the same trial, a clear diagonal of increased correlation values would be present. **g**, Correlation between delay and navigation neural sequences within the same trial and between different trials for all sessions. * $p < 0.05$, ** $p < 0.01$, *** $p < 0.001$.

4.3.5 Ketamine Disrupts Neuronal Sequences and Impairs Working Memory Performance

In order to demonstrate a causal link between neuronal sequences and WM in our naturalistic task, one must conduct a causal manipulation. We used ketamine, a N-methyl-D-aspartate (NMDA) receptor non-competitive antagonist that induces selective WM deficits in humans and animals (Frohlich, 2014, Wang, 2013). We injected subanesthetic doses of ketamine (0.25 mg/kg - 0.8 mg/kg) intramuscularly while animals performed the task (see experimental timeline in Figure. 4.7a). Ketamine drastically reduced performance of our virtual WM task without affecting performance on a perception control task. WM performance recovered 30 minutes to 1-hour post-injection in the late post-injection period (Pre-Injection: *Median* = 77%, Early Post-Injection: *Median* = 28%, Late Post-Injection: *Median* = 66%; Kruskal Wallis, $p = 8.5e-05$) (Figure. 4.7b; Figure. S4.12a, b).

After ketamine injection, the differences in std distribution means for peak firing times between the real and shuffled data decreased suggesting that neurons fired with less temporal consistency after ketamine (Pre-Injection: *Median* = 171.6, Early Post-Injection: *Median* = 40.2, Late Post-Injection: *Median* = 100.4; Kruskal Wallis, post hoc, $p = 0.001$) (Figure. 4.7c; Figure. S4.12c, d). Behaviorally relevant groupings of condition centroids were similar between the non-injection data set and the pre-injection ketamine data set (Figure. 4.4b; Figure. 4.7d). This grouping was lost after ketamine injection but was regained 1 hour later as behavioral performance recovered (Figure. 4.7d).

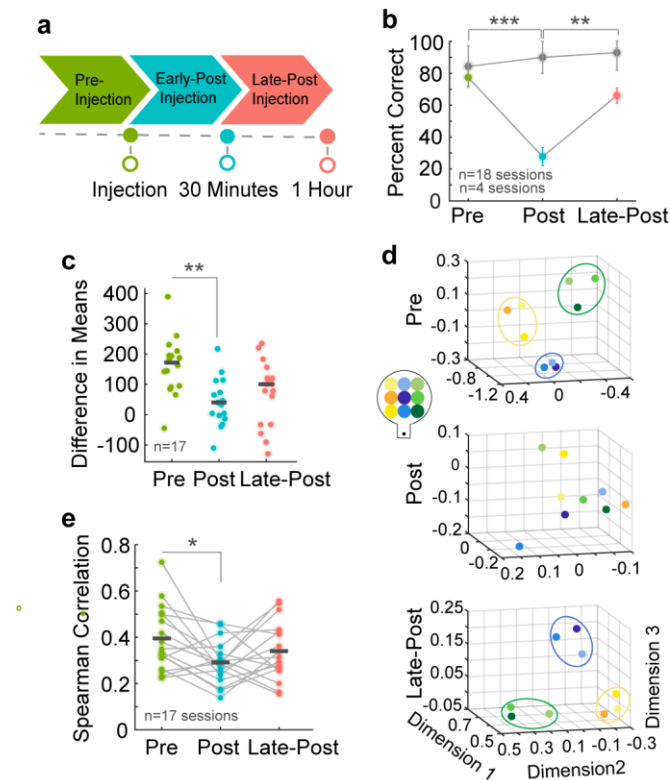


Figure. 4.7: Ketamine manipulation distorts neural sequences and working memory

a, Experimental timeline for ketamine injection. Pre-injection period is depicted in green, early-post injection in blue, and late-post injection (recovery) in pink. **b**, Task performance as percent of correct trials for each injection period. Color dots represent median values per injection period for WM data and gray dots represent median values per injection period for perception control data. Asterisks indicate significance between WM injection periods. **c**, Difference in real and shuffled distribution means between ketamine injection periods. **d**, Condition centroids projected in 3D space. Centroid colors correspond with their position in the virtual environment (see inlet). Ellipsoids are illustrated guides to indicate behaviorally relevant groupings of targets in the pre-injection and late post-injection periods. These groupings are notably absent in the post-injection period. **e**, Spearman correlation values for each ketamine injection period. Dots represent individual sessions and matching sessions are connected by lines. * $p < 0.05$, ** $p < 0.01$, *** $p < 0.001$.

We also saw that the correlation between condition centroid distances and target trajectory distances decreased after ketamine injection and then recovered when behavioral performance recovered. This indicates that sequences were less associated with remembered target location following ketamine injection (Pre-Injection: *Mean* = 0.39, Early Post-Injection: *Mean* = 0.29, Late Post-injection: *Mean* = 0.34. 1-way ANOVA, post hoc, $p = 0.04$) (Figure. 4.7e; Figure. S4.12e, f). There was no change in any of the described measures in a saline control condition (Figure. S4.12g, h). These results indicate a causal link between NMDA receptor dysfunction caused by ketamine and disruption of neuronal sequences leading to deficits in WM.

4.4 « Discussion »

We recorded the responses of hundreds of single neurons in the macaque LPFC during a complex visuospatial WM task set in a naturalistic virtual environment. We report three major findings: (1) sequences of population activity represented trajectories to remembered locations in the environment (2) neural sequences of single neurons spiking activity were predictive of behavioral performance (3) NMDA receptor antagonism by ketamine disrupted neuronal sequences, selectively impairing WM performance.

4.4.1 Neural Sequences and Working Memory Coding

Prefrontal neural activity during tasks that require holding a single item in WM during a delay response period have demonstrated persistent activity that represents the memoranda (Leavitt et al., 2017a). One major shortcoming of the persistent firing hypothesis is that it may not be able to support WM representations with rich spatiotemporal structure (Steveninck et al., 1997; Lestienne & Strehler, 1987; Lundqvist et al., 2016). Indeed, in tasks during which sequences of multiple items need to be held in WM, persistent firing is scarce (Lundqvist et al., 2016). A recent study reported that during a multi-item spatial WM task in which monkeys had to remember a series of spatial locations in sequential

order, temporally organized neuronal populations represented the order in which items were remembered (Xie et al., 2022). These studies demonstrate that additional mechanisms may be needed to support coding of WM representations when the memoranda have spatiotemporal structure.

Our paradigm differs from those used in previous studies. We did not use multiple memoranda, instead; our subjects remembered a single target location and the trajectory to the location in a 3D virtual naturalistic environment. Importantly, our study did not restrain eye position, allowing for naturalistic exploration of the scene while information is being held in WM. The rationale behind studies restraining eye position is to avoid the interference caused by eye position signals and changes in the retinal image and consequently, in visual inputs on the WM representations (Suzuki & Gottlieb, 2013). However, in naturalistic conditions WM coding must be robust to such changes. To our knowledge, WM coding has not been tested under these conditions.

Previous studies in macaques have tried to approach the idea of transiently active neurons maintaining WM through shared temporal relationships by exploring spike chain patterns of several neurons. However, due to methodological constraints, these studies were unable to record large numbers of simultaneously active neurons and thus, unable to demonstrate sequence coding (Prut et al., 1998). Our study has overcome this limitation by recording from hundreds of simultaneously active neurons, revealing precise sequences of single unit spiking activity that encode specific WM content.

Studies in mice that simultaneously record from many neurons have reported neuronal activation sequences during short-term memory tasks in the posterior parietal cortex and dorsomedial striatum (Harvey et al., 2012; Akhlaghpour et al., 2016). In the rodent hippocampus, sequences of place cell activation signal trajectories to remembered locations that are stored in long-term memory (Skaggs & McNaughton, 1996). Thus, sequential activation of neurons to

encode spatiotemporal episodes appears to be a general coding mechanism across species.

However, the sequences we report in this study are different from those previously described. First, they occur in the LPFC, a brain area that appears *de novo* in anthropoid primates (Passingham & Wise, 2012). More specifically, the sequences reported here occur within the expanded supragranular layers 2 and 3, where WM representations have been reported (Bastos et al., 2018; Finn et al., 2019). The abstract WM representations we have described here may allow primates to represent short-term spatiotemporal episodes ‘in the mind’. Such episodes can be dissociated from sensory and motor signals and may be key to the enhanced cognitive control and planning observed in primates (Passingham & Wise, 2012).

4.4.2 Ketamine Selectively Decreases Working Memory Performance and Disrupts Sequences

Through pharmaceutical manipulation, we identify that sequence generation relies on NMDA receptor function. The interactions between inhibitory interneurons and excitatory pyramidal cells plays an important role in LPFC prefrontal circuits during WM tasks (Wang, 2004). Therefore, the precise activation of pyramidal cells may be dependent on a temporally coordinated ‘release of inhibition’ by interneurons (Cannon, 2015; Kosche, 2015). We have demonstrated in past research that NMDA receptor antagonism decreases the firing of narrow spiking neurons and decreases the selectivity of firing for putative pyramidal cells resulting in decreased neuronal tuning (see Chapter 3).

Here, we show that NMDA receptor antagonism also decreases the consistency of single neuron timing and makes sequences less differentiable between target conditions. Similar to how neuronal tuning is broadened, population sequences become less precise. Thus, it is likely that failures of inhibitory control by interneurons in individuals with NMDA receptor dysfunction like patients with

schizophrenia and NMDA-receptor encephalitis causes the reported WM deficits in these populations. However, this issue requires further investigation.

Sequential activity does not discredit persistent activity as a mechanism for WM maintenance. Temporal variations in delay period activity can still result in stable working memory representation as seen in Chapter 2 in which decoding accuracy for target location using firing rate over time remains stable throughout the delay epoch. In fact, we believe that these two forms of coding coexist. There is evidence that neurons display temporally precise firing during WM in which individual neurons are consistently spatially tuned during a small temporal window during the delay epoch (Papadimitriou, 2021). The potential relationship between spike rate-based selectivity and spike timing should be explored in future research.

Sequential population activity patterns serve to benefit WM coding. For example, a temporally based code would be more energy efficient than one that relies solely on continuous spiking activity. A code that does not rely solely on continuous activity may also be robust to distraction as would occur in a naturalistic environment or to neuronal injury. The robust nature of sequential activity is exemplified by removing a percentage of neurons from the population. The correlation between neural sequences and target location during correct trials remains stable even after removing 70% of neurons from the population. 80 - 90% of neurons must be removed for this correlation to significantly change, at which point, the correct trial correlation becomes equal to the incorrect trial correlation (Figure. S4.10d, e). Temporal specificity may also add complexity to prefrontal networks, allowing for higher dimensional representations and flexible cognition.

4.4.3 Conclusions

These results reveal a mechanism in which neural populations encode WM representations in the primate LPFC via neuronal activation sequences. We demonstrate robust and behaviorally relevant temporal organization of spiking activity. Our task requires filtering of distractors, internal manipulation of spatial representations due to dynamic visual scenes, and online rerouting of trajectories

to remembered target locations. Indeed, under these naturalistic conditions, requiring complex spatiotemporal elements, population sequential activity underlies WM maintenance.

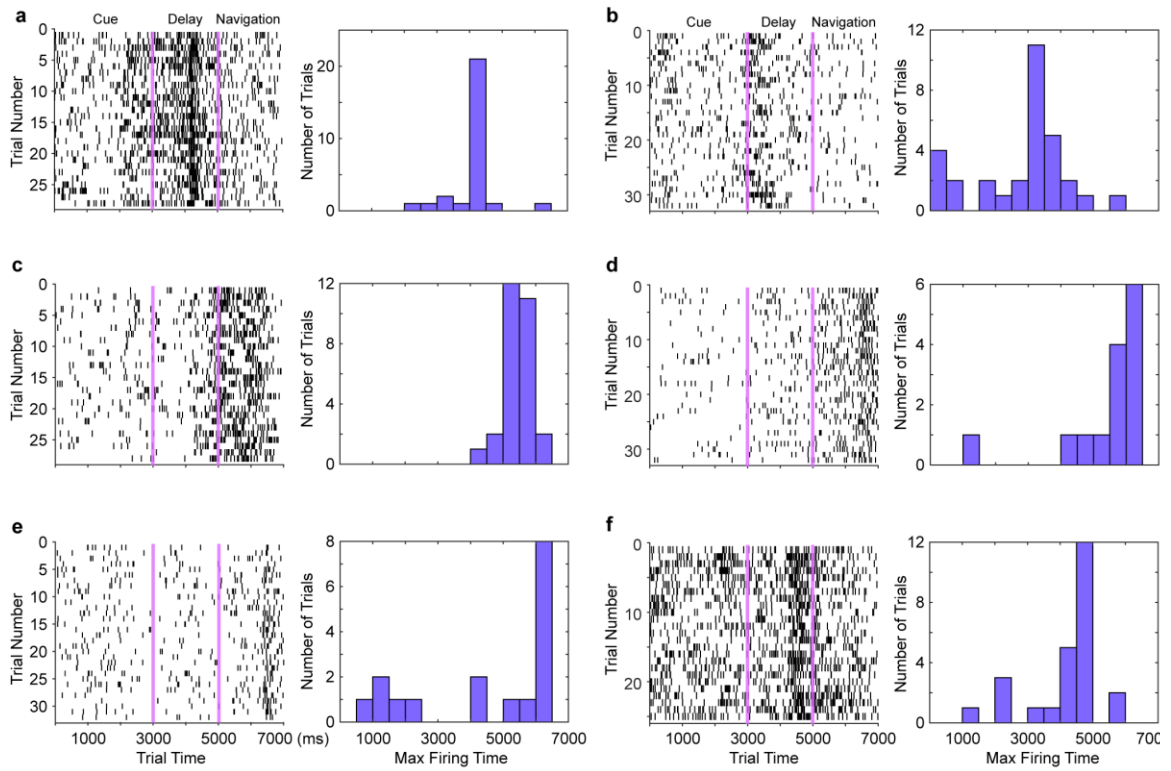


Figure. S4.8: Example time consistent neurons

a-f, Example single neurons. Left column represents the activity of a neuron over trial time over all trials of a certain condition. Pink lines separate task epochs. Right column shows a histogram of max firing times per trial.

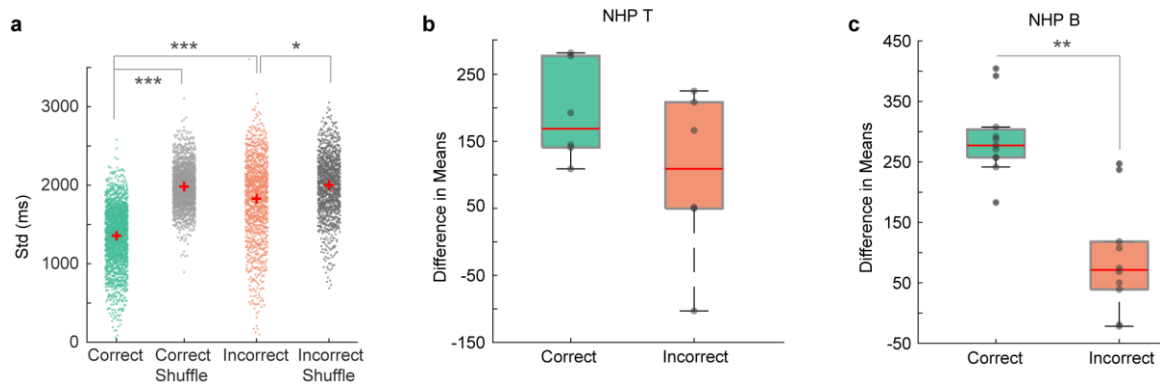


Figure. S4.9: Standard deviation of peak firing times

a, Trial-trial standard deviation in max firing time for each neuron across sessions during correct and incorrect trials. The Red crosses indicate group means. **b**, Difference in real and shuffled distribution of the deviation in neuron action potential timing between trials. Presented for correct and incorrect trials for NHP T. The red lines represent median values. Dots represent data for individual sessions. **c**, Difference in real and shuffled distribution of the deviation in neuron action potential timing between trials. Presented for correct and incorrect trials for NHP B. The red lines represent median values. Dots represent data for individual sessions. * $p < 0.05$, ** $p < 0.01$, *** $p < 0.001$.

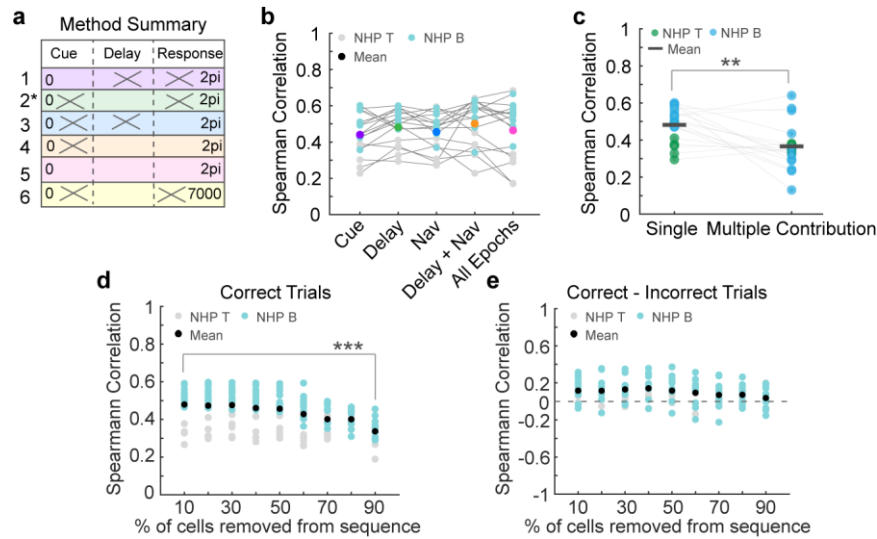


Figure. S4.10: Deviations of correlation method

a, Method summary outlining different ways to calculate sequences. Crossed-out epochs indicate epoch data that was not used as part of the complex vectors for a given method. The asterisk indicates the method used in the main figures and text. **b**, Correlation based on each method outlined in 'a'. Dots represent data per session. Colored dots represent mean and correspond to the table in 'a'. **c**, Correlation when neurons are only considered in one epoch sequence or when all neurons participate in all sequences. This reflects the possibility of one instance of peak activity versus multiple occurrences of increased firing. Dots represent data per session. **d**, Spearman correlations for correct trials between delay neural sequences and target trajectories after removing 10 - 90% of neurons from the sequence. **e**, The difference between spearman correlations for correct and incorrect trials after removing 10 - 90% of neurons from delay sequences. The dashed gray line represents 0 difference. * $p < 0.05$, ** $p < 0.01$, *** $p < 0.001$.

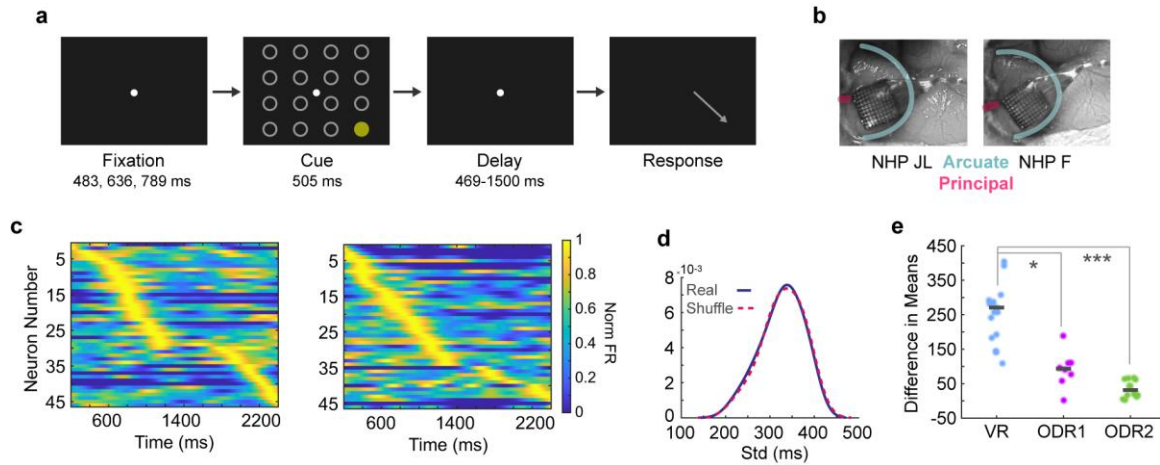


Figure. S4.11: Temporal organization of neural activity during oculomotor delayed response task

a, Depiction of ODR task with 16 targets. **b**, Surgical images showing location of Utah arrays implanted in left LPFC of NHP JL and NHP F. **c**, Two trial examples of simultaneously recorded population activity. Normalized firing rate for each neuron is arranged by max firing time. **d**, Real and shuffled distributions of max firing time trial-to-trial deviation for an example session. **e**, Difference in the means between real and shuffled distributions for the virtual reality task and the ODR task. Gray lines indicate median values and dots represent data per session. * $p < 0.05$, ** $p < 0.01$, *** $p < 0.001$.

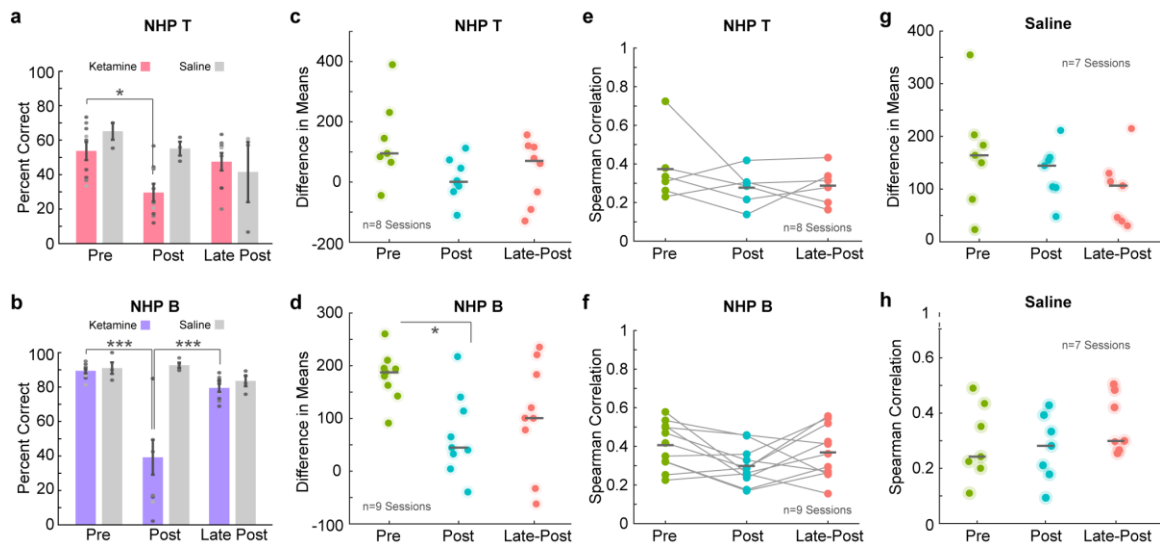


Figure. S4.12: Ketamine and saline control analysis

a, Percent of correct trials for ketamine and saline sessions over injection periods for NHP T. Dots represent data for individual sessions and error bars are SEM. **b**, Percent of correct trials for ketamine and saline sessions over injection periods for NHP B. Dots represent data for individual sessions and error bars are SEM. **c**, Difference in the means between real and shuffled distributions of standard deviation values for neuron max firing time between trials. Presented for each ketamine injection period for NHP T. Dots represent data for each session. **d**, Difference in means between real and shuffled distributions for each ketamine injection period for NHP B. Dots represent data for each session. **e**, Correlation between the distance between condition cluster centroids and distance between target trajectories. Correlation values are presented for ketamine injection periods for NHP T. Dots represent data per session. **f**, Correlation values for ketamine injection periods for NHP B. Dots represent data per session. **g**, Difference in mean values between real and shuffled distributions for saline injection periods. Dots represent data for each session (NHP T and NHP B combined). **h**, Correlation between the distance between condition cluster centroids and distance between target trajectories. Correlation values are presented for saline injection periods for both animals combined. * $p < 0.05$, ** $p < 0.01$, *** $p < 0.001$.

4.5 « Methods »

We used the same two adult male rhesus macaques (*Macaca mulatta*) in the main experiment as well as the ketamine and saline experiments (age: 10, 9; weight: 12, 10 kg). The oculomotor delayed response task was recorded from two different male macaques using one multielectrode Utah array implanted in each animal (Leavitt, 2017b, Leavitt, 2018).

4.5.1 Ethics Statement

Animal care and handling (i.e., basic care, animal training, surgical procedures, and experimental injections) were pre-approved by the University of Western Ontario Animal Care Committee. This approval ensures that federal (Canadian Council on Animal Care), provincial (Ontario Animals in Research Act), regulatory bodies (e.g., CIHR/NSERC), and other national standards (CALAM) for the ethical use of animals are followed. The oculomotor delayed response task experiment was in agreement with Canadian policies and regulations and was preapproved by the McGill University Animal Care Committee (Leavitt, 2017b, Leavitt, 2018). Regular assessments for physical and psychological well-being of the animals were conducted by researchers, registered veterinary technicians, and veterinarians.

4.5.2 Experimental Setup

Animals performed the task in an isolated room with no illumination other than the monitor. The room contained no AC power lines and was RF shielded. The task was presented on a computer LDC monitor positioned 80 cm from the subjects' eyes (27" ASUS, VG278H monitor, 1024 × 768 pixel resolution, 75 Hz refresh rate, screen height equals 33.5 cm, screen width equals 45 cm). Eye positions were monitored using a video-oculography system with sampling at 500 Hz (EyeLink 1000, SR Research). Stimulus presentation was controlled through a custom computer program (through Unreal Engine 3). Subjects were seated in a standard enclosed primate chair (Neuronitek) during the experiment and were

delivered juice through an electronic reward integration system (Crist Instruments). Prior to the experiments, subjects were implanted with custom fit, PEEK cranial implants which housed the head posts and recording equipment (Neuronitek). See Blonde et al. for more information. The head posts were attached to the primate chair for head fixation.

The experimental setup for the oculomotor delayed response task is outlined in both Leavitt et al. 2017b and Leavitt et al., 2018.

4.5.3 Task

The virtual task environment was developed using Unreal Engine 3 development kit, utilizing Kismet sequencing and UnrealScript (UDK, May 2012 release; Epic Games). Details about this platform and the recording setup can be found in Doucet et al. 2016. Movement speed through the environment was fixed. Target locations within the virtual arena were arranged in a 3×3 grid and spaced 290 unreal units apart (time between adjacent targets is approximately 0.5 seconds). The perception control variation of the task was identical to the WM version except that the targets remained onscreen through the trial.

The oculomotor delayed response task was separated into four epochs: fixation, stimulus presentation, delay, and response. The animal began a trial by fixating on a fixation dot and by pressing a lever. The duration of the fixation period was either 482, 636, or 789 ms. A sine-wave grating target then appeared at 1 of 16 randomly selected locations positioned in a 4×4 grid for 505 ms. This was followed by a delay period ranging from 494–1500 ms. The fixation point was removed, cueing the animal to make a saccade to the location of the previously presented target and then to release the lever.

4.5.4 Surgical Procedure

Custom PEEK implants which housed recording hardware and a headpost were developed and implanted in each animal (Blonde, Roussy et al., 2018). Brain

navigation for surgical planning was conducted using Brainsight (Rogue Research Inc.). Two 10×10, microelectrode Utah arrays (96 channels, 1.5 mm in length and separated by at least 0.4 mm) (Blackrock Neurotech) were chronically implanted in each animal. Electrodes were implanted in the left LPFC (anterior to the arcuate sulcus and on either side of the posterior end of the principal sulcus). Arrays were impacted approximately 1.5 mm into the cortex. Reference wires were placed beneath the dura and a grounding wire was attached between screws in contact with the pedestal and the border of the craniotomy. Surgical procedures were conducted under general anesthesia induced by ketamine and maintained using isoflurane and propofol.

For the oculomotor delayed response task data, a 96-channel Utah array was implanted in each monkey's left LPFC in the same region that electrodes were implanted for recording during performance of the virtual WM task. Detailed surgical methods can be found in Leavitt et al. (2017b, 2018).

4.5.5 Task Performance

Correct trials are trials in which the animal reaches the correct target location within 10 seconds. An incorrect trial occurs if the animal does not reach the target location within 10 seconds. Percent of correct trials is calculated as the number of correct trials divided by the total number of trials.

4.5.6 Spike Processing

Neuronal data was recorded using a Cerebus neuronal Signal Processor (Blackrock Microsystems) via a Cereport adapter. The neuronal signal was digitized (16 bit) at a sample rate of 30 kHz. Spike waveforms were detected online by thresholding at 3.4 standard deviations of the signal. The extracted spikes were semi-automatically resorted with techniques utilizing Plexon Offline Sorter (Plexon Inc.). Sorting results were then manually supervised. Multiunits consisted of threshold-crossing events from multiple neurons with action potential-like

morphology that were not isolated well enough to be classified as a well-defined single unit.

4.5.7 Time Consistent Neurons

To quantify time consistent neurons, we created spike density functions (SDFs) combined between electrodes arrays over the entire trial time using neurons with firing rates above 0.5 Hz. SDFs were created for each condition that contained at least five trials. We calculated the peak firing time for each neuron in the population, calculated the standard deviation of the peak firing time for each neuron over all trials in a condition and created a probability distribution from the standard deviation values. We shuffled the peak firing times for each neuron from trial to trial so that the peak firing time no longer aligned for any one neuron. We created a shuffled probability distribution. We calculated the difference in mean values between the real and shuffled distributions to get the mean difference value.

To calculate the standard deviation values plotted in Figure. S4.9a, we calculated trial-trial standard deviation of peak spike time for the target condition in which each neuron fired the most consistently during correct trials (i.e., lowest trial-trial deviation). The same conditions were used for shuffled data and for incorrect trials.

To match the task structure of the VR task, we did not use data from the ODR fixation period. Since the ODR task had jittered delay epoch timing, we used trials with delay periods > 1000 ms and analyzed the first 1000 ms of the epoch.

4.5.8 Complex Vector Decomposition

In a related work, we introduce a complex valued dimensionality reduction technique focused on LFPs and spike trains. In brief, it is used to find repeated patterns in time series of phase variables. Here, we applied it to the spike trains to create a three-dimensional representation of the data. Each point in this three-dimensional projection represents a single trial, which corresponds to a target

location $l \in [1,9]$ and a task outcome, correct or incorrect, which are considered separately. The locations of the points in the 3D-space were determined by the relative similarity of the spike trains (More precisely, by the correlation between the complex-valued sequences of spikes, which were created by mapping the peak firing time of each neuron to a phase between $-\pi$ and π).

The points corresponding to a specific target location defined a cluster, and the centroids were computed, resulting in one coordinate triple, $c_l = (x_l, y_l, z_l) \in R^3$, corresponding to each target location. The matrix, D , of Euclidean distances between each pair of centroids was then computed, with

$$D_{i,j} = \text{dist}(c_i, c_j) = \sqrt{((x_j - x_i)^2 - (y_j - y_i)^2 + (z_j - z_i)^2)}$$

For each recording session, mean trajectories followed by the subject to each target location were obtained by averaging the group of correct trajectories to that target (excluding outlier trajectories with zscore > 1 of mean Frechet distance to other trajectories in the group). A 9x9 distance matrix was then created from the Frechet distances between each of the mean trajectories.

In this way, each recording session was described by two 9x9 normalized distance matrices, one representing the relationships between target centroids in 3D-space, and the other representing distances between behavioral trajectories to the target locations in the virtual environment. The correlation between the two distance matrices was then computed, which measures the similarity between the neuronal representations of the targets and the physical trajectories to them. Since centroids of targets in the same column tended to cluster together, a null model for comparison was created by shuffling the target columns while preserving the target rows, thereby destroying the correlation while preserving more of the structure of the data.

When repeating the analysis for the oculomotor delayed response task, 16 targets were included so the data was reduced to a 16x16 distance matrix describing the relationships between the neuronal representations of the target

locations. Furthermore, since the ODR task does not contain a navigation component, the distance matrix of the projection centroids was compared to the matrix of Euclidean distances between targets (rather than a Frechet distance matrix).

4.5.9 Projection Classification Analysis

We used a simple classifier based on our computational approach with 5-fold cross-validation to classify sequences on a single trial basis. The classifier assigns labels to points in the projected 3D-space, assigning each trial in the test set to the centroid of trials in the training set which has the minimum Euclidean distance to the trial in question. In the supervised version, the training set centroids are determined using the trial condition labels. The unsupervised version uses K-means clustering to determine the training set centroids. The same method is used to classify both trial condition and trial epoch (in which case each trial is split into three sequences, one for each epoch, prior to creating the projection).

4.5.10 Trajectory Analysis

We repeated the centroids analysis described above but replaced the distance matrix describing mean trajectories with two other task-relevant measures. First, we constructed geometrically 'ideal' trajectories straight from the start location to each target and repeated the analysis using Frechet distance between trajectories. Second, we used the matrix of Euclidean distances between target locations. Unlike the mean trajectory analysis, these measures only described the task set up and did not include behavioral data.

We then considered the subset of correct trials during one recording session which corresponded to the most direct trajectories to center targets. These trials defined a group of similar trajectories with no curvature, similar direction, and three lengths, so that many trajectories overlapped, and some longer trajectories contained shorter trajectories from other trials. For each pair of neural sequences corresponding to trials in this group, we computed three measures: 1) the fraction

of cells active in the shorter sequence that were also active in the longer sequence, 2) the circular-circular correlation between the sequences, 3) the circular-circular correlation between the sequences when only the shared neurons were considered. We then computed the same measures for all pairs of correct trials in the recording session (i.e., pairs in which the trajectories could have any direction, depth, or target location). We also computed the same measures for 12 pairs of overlapping trajectories, where the shorter trajectories were completely contained within longer trajectories

4.6 « References »

- Abeles, M., Bergman, H., Margalit, E., & Vaadia, E. (1993). Spatiotemporal firing patterns in the frontal cortex of behaving monkeys. *Journal of Neurophysiology*, *70*(4), 1629–1638. doi:10.1152/JN.1993.70.4.1629
- Akhlaghpour, H., Wiskerke, J., Choi, J. Y., Taliaferro, J. P., Au, J., & Witten, I. B. (2016). Dissociated sequential activity and stimulus encoding in the dorsomedial striatum during spatial working memory. *eLife*, *5*, e19507. doi:10.7554/eLife.19507
- Alt, H., & Godau, M. (1995). Computing the Fréchet distance between two polygonal curves. *International Journal of Computational Geometry & Applications*, *5*, 75-91. doi:10.1142/S0218195995000064.
- Baddeley, A. (1986). *Working Memory*. Clarendon Press/Oxford University Press.
- Batuev, A. S., Pirogov, A. A., & Orlov, A. A. (1979). Unit activity of the prefrontal cortex during delayed alternation performance in monkey. *Acta Physiologica Academiae Scientiarum Hungaricae*, *53*(3), 345–353. Retrieved from <https://europepmc.org/article/med/120674>
- Bastos, A. M., Loonis, R., Kornblith, S., Lundqvist, M., & Miller, E. K. (2018). Laminar recordings in frontal cortex suggest distinct layers for maintenance and control of working memory. *Proceedings of the National Academy of Sciences of the United States of America*, *115*(5), 1117–1122. doi:10.1073/pnas.1710323115
- Blonde, J. D., Roussy, M., Luna, R., Mahmoudian, B., Gulli, R. A., Barker, K., Lau, J. C., & Martinez-Trujillo, J. C. (2018). Customizable cap implants for neurophysiological experimentation. *Journal of Neuroscience Methods*, *304*, 103-117. doi:10.1016/j.jneumeth.2018.04.016
- Buzsáki, G. (2010). Neural syntax: Cell assemblies, synapsembles, and readers. *Neuron*, *68*(3), 362–385. doi:10.1016/j.neuron.2010.09.023
- Cannon, J., Kopell, N., Gardner, T., & Markowitz, J. (2015). Neural sequence generation using spatiotemporal patterns of inhibition. *PLOS Computational Biology*, *11*(11), e1004581. doi:10.1371/JOURNAL.PCBI.1004581
- Chi, Z., & Margoliash, D. (2001). Temporal precision and temporal drift in brain and behavior of zebra finch song. *Neuron*, *32*(5), 899–910. doi:10.1016/S0896-6273(01)00524-4
- Constantinidis, C., Funahashi, S., Lee, D., Murray, J. D., Qi, X. L., Wang, M., & Arnsten, A. F. T. (2018). Persistent spiking activity underlies working memory.

The Journal of Neuroscience, 38(32), 7020. doi:10.1523/JNEUROSCI.2486-17.2018

Daliparthi, V. K., Tachibana, R. O., Cooper, B. G., Hahnloser, R. H. R., Kojima, S., Sober, S. J., & Roberts, T. F. (2019). Transitioning between preparatory and precisely sequenced neuronal activity in production of a skilled behavior. *ELife*, 8. doi:10.7554/ELIFE.43732

Doucet, G., Gulli, R. A., & Martinez-Trujillo, J. C. (2016). Cross-species 3D virtual reality toolbox for visual and cognitive experiments. *Journal of Neuroscience Methods*, 266, 84–93. doi:10.1016/j.jneumeth.2016.03.009

Eichenbaum, H. (2014). Time cells in the hippocampus: A new dimension for mapping memories. doi:10.1038/nrn3827

Finn, E. S., Huber, L., Jangraw, D. C., Molfese, P. J., & Bandettini, P. A. (2019). Layer-dependent activity in human prefrontal cortex during working memory. *Nature Neuroscience*, 22, 1687–1695. doi:10.1038/s41593-019-0487-z

Frohlich, J., & Van Horn, J. D. (2014). Reviewing the ketamine model for schizophrenia. *Journal of Psychopharmacology*, 28(4), 287–302. doi:10.1177/0269881113512909

Fuster, J. M., & Alexander, G. E. (1971). Neuron activity related to short-term memory. *Science*, 173(3997), 652–654. doi:10.1126/SCIENCE.173.3997.652

Harvey, C. D., Coen, P., & Tank, D. W. (2012). Choice-specific sequences in parietal cortex during a virtual-navigation decision task. *Nature*, 484, 62–68. doi:10.1038/nature10918

Itskov, V., Curto, C., Pastalkova, E., & Buzsáki, G. (2011). Cell assembly sequences arising from spike threshold adaptation keep track of time in the hippocampus. *Journal of Neuroscience*, 31(8), 2828–2834. doi:10.1523/JNEUROSCI.3773-10.2011

Kosche, G., Vallentin, D., & Long, M. A. (2015). Interplay of inhibition and excitation shapes a premotor neural sequence. doi:10.1523/JNEUROSCI.4346-14.2015

Leavitt, M. L., Mendoza-Halliday, D., & Martinez-Trujillo, J. C. (2017a). Sustained activity encoding working memories: Not fully distributed. *Trends in Neurosciences*, 40(6), 328–346. doi:10.1016/j.tins.2017.04.004

Leavitt, M. L., Pieper, F., Sachs, A. J., & Martinez-Trujillo, J. C. (2017b). Correlated variability modifies working memory fidelity in primate prefrontal neuronal ensembles. *Proceedings of the National Academy of Sciences*, 114 (12). doi:10.1073/pnas.1619949114

- Leavitt, M. L., Pieper, F., Sachs, A. J., & Martinez-Trujillo, J. C. (2018). A quadrant bias in prefrontal representation of visual-mnemonic space. *Cerebral Cortex*, *28*(7), 2405–2421. doi:10.1093/cercor/bhx142
- Lestienne, R., & Strehler, B. L. (1987). Time structure and stimulus dependence of precisely replicating patterns present in monkey cortical neuronal spike trains. *Brain Research*, *437*(2), 214–238. doi:10.1016/0006-8993(87)91638-6
- Lundqvist, M., Rose, J., Herman, P., Brincat, S. L. L., Buschman, T. J. J., & Miller, E. K. K. (2016). Gamma and beta bursts underlie working memory. *Neuron*, *90*(1), 152–164. doi:10.1016/J.NEURON.2016.02.028
- Okubo, T. S., Mackevicius, E. L., Payne, H. L., Lynch, G. F., & Fee, M. S. (2015). Growth and splitting of neural sequences in songbird vocal development. *Nature*, *528*, 352. doi:10.1038/NATURE15741
- Pals, M., Stewart, T. C., Akyürek, E. G., & Borst, J. P. (2020). A functional spiking-neuron model of activity-silent working memory in humans based on calcium-mediated short-term synaptic plasticity. *PLOS Computational Biology*, *16*(6), e1007936. doi:10.1371/JOURNAL.PCBI.1007936
- Passingham, R. E., & Wise, S. P. (2012). *The Neurobiology of the PFC: Anatomy, Evolution, and the Origin of Insight*. Oxford University Press. London. doi:10.1093/acprof:osobl/9780199552917.001.0001
- Papadimitriou, C., Holmes, C. D., & Snyder, L. H. (2021). Primate spatial memory cells become tuned early and lose tuning at cell-specific times. *Cerebral Cortex*, *31*(9), 4206–4219. doi:10.1093/CERCOR/BHAB079
- Prut, Y., Vaadia, E., Bergman, H., Haalman, I., Slovin, H., & Abeles, M. (1998). Spatiotemporal structure of cortical activity: Properties and behavioral relevance. *Journal of Neurophysiology*, *79*(6), 2857–2874. doi:10.1152/jn.1998.79.6.2857
- Roussy, M., Mendoza-Halliday, D., & Martinez-Trujillo, J. C. (2021). Neural substrates of visual perception and working memory: Two sides of the same coin or two different coins? *Frontiers in Neural Circuits*, *15*, 131. doi:10.3389/FNCIR.2021.764177/BIBTEX
- Skaggs, W. E., & McNaughton, B. L. (1996). Replay of neuronal firing sequences in rat hippocampus during sleep following spatial experience. *Science*, *271*(5257), 1870–1873. doi:10.1126/science.271.5257.1870
- Stokes, M. G. (2015). ‘Activity-silent’ working memory in prefrontal cortex: A dynamic coding framework. *Trends in Cognitive Sciences*, *19*(7), 394–405. doi:10.1016/J.TICS.2015.05.004
- Srivastava, K. H., Holmes, C. M., Vellema, M., Pack, A. R., Elemans, C. P. H., Nemenman, I., & Sober, S. J. (2017). Motor control by precisely timed spike

patterns. *Proceedings of the National Academy of Sciences*, 114(5), 1171–1176. doi:10.1073/PNAS.1611734114/-/DCSUPPLEMENTAL

Steveninck, R. R., Lewen, G. D., Strong, S. P., Koberle, R., & Bialek, W. (1997). Reproducibility and variability in neural spike trains. *Science*, 275(5307), 1805–1808. doi:10.1126/science.275.5307.1805

Tang, C., Chehayeb, D., Srivastava, K., Nemenman, I., & Sober, S. J. (2014). Millisecond-scale motor encoding in a cortical vocal area. *PLOS Biology*, 12(12), e1002018. doi:10.1371/JOURNAL.PBIO.1002018

van der Meij, R., & Voytek, B. (2018). Uncovering neuronal networks defined by consistent between-neuron spike timing from neuronal spike recordings. *eNeuro*, 5(3), ENEURO.0379-17.2018. doi:10.1523/ENEURO.0379-17.2018

Wang, M., Yang, Y., Wang, C. J., Gamo, N. J., Jin, L. E., Mazer, J. A., ... Arnsten, A. F. T. (2013). NMDA receptors subserve persistent neuronal firing during working memory in dorsolateral prefrontal cortex. *Neuron*, 77(4), 736–749. doi:10.1016/J.NEURON.2012.12.032

Wang, X-J., Tegnér, J., Constantinidis, C., & Goldman-Rakic, P. S. (2004). Division of labor among distinct subtypes of inhibitory neurons in a cortical microcircuit of working memory. *Proceedings of the National Academy of Sciences*, 101(5), 1368–1373. doi:10.1073/PNAS.0305337101

Wang, X-J. (2021). 50 years of mnemonic persistent activity: quo vadis? *Trends in Neurosciences*, 44(11), 888-902. doi:10.1016/j.tins.2021.09.001

Xie, Y., Hu, P., Li, J., Chen, J., Song, W., Wang, X. J., Yang, T., Dehaene, S., Tang, S., Min, B., & Wang, L. (2022). Geometry of sequence working memory in macaque prefrontal cortex. *Science*, 375(6581), 632–639. doi:10.1126/science.abm0204

Zhou, S., Masmanidis, S. C., & Buonomano, D. V. (2020). Neural sequences as an optimal dynamical regime for the readout of time. *Neuron*, 108(4), 651–658.e5. doi:10.1016/J.NEURON.2020.08.020

5 General Discussion

5.1 « Overview »

Everyday functions like cooking a recipe, having a conversation, or calculating a tip at a restaurant use working memory (WM). You may easily envision a situation in which you manage to read and remember multiple steps of a recipe while kids are running around the house, a dog is barking, or you take breaks to clean the kitchen as you cook. During this time, you are maintaining a functional mental representation of those instructions while faced with a multitude of incoming sensory signals. How do we manage this?

The lateral prefrontal cortex (LPFC) evolved to process information and guide behavior in a world with complex and interacting elements. However, WM research in macaques traditionally aims to isolate single task features using simple visual stimuli and responses. Previous experiments have maintained a high level of control to elucidate specific elements of WM but deviate from the naturalistic use of WM. Therefore, it is unclear how LPFC neurons encode WM representations in naturalistic contexts - in the presence of incoming visual stimuli, distractors, eye movement, and 3D navigation.

In this dissertation, I explored how the primate PFC processes WM in such complex, naturalistic conditions. Naturalistic conditions were achieved through the development of a novel visuospatial WM task and matching perceptual control task that takes place in a complex virtual environment. There are several naturalistic elements to this task: 1) The virtual environment is visually complex, containing 3D stimuli and cues for depth perception, 2) animals are permitted free visual exploration of the environment, and 3) The task response requires 3D navigation. I was able to provide a level of experimental control through control of task timing and by maintaining a constant environment trial-to-trial. Elements that were not controlled such as animal movement in the environment and eye movement were continuously recorded.

In Chapter 2, I first explored animal behavior during the naturalistic task. Animals were able to perform both the perception and WM variants of the task. Task performance was lower during WM than perception, and trajectories to targets were less optimal, reflecting the increased difficulty of the WM task. Eye movement and gaze behavior differed between perception and WM, implying a visually guided strategy during perception that was not utilized when the targets were during WM.

I demonstrate robust coding of WM in prefrontal neurons during the naturalistic task. Single neurons displayed selective firing for specific target locations, similar to activity observed during traditional tasks like the ODR task (Levitt et al 2017). Populations of neurons encoded stable mnemonic representations of target location on a single trial level in the presence of potential distractors, changing visual scenery, and changes in eye position.

Representations for target location were unaffected by removing neural signals associated with saccade direction and amplitude and gaze location. Additionally, the population of neurons tuned for saccade landing position and neurons tuned for remembered target location do not overlap (presented in chapter 3). These findings suggest distinct processing for visuospatial WM and eye-related signals in LPFC. At the population level, neural activity also differentiates between mnemonic and perceptual representations of target location. As demonstrated in chapter 3, ketamine also distorts WM representations and decreases WM task performance without significantly impacting eye movement behavior or decreasing performance of the perceptual task variant.

In chapter 3, I use ketamine, an NMDA receptor antagonist, to produce selective WM deficits. Ketamine caused WM deficits by decreasing neuron firing selectivity (i.e., distorted neural tuning). This resulted in weakened population-level representations of target location evidenced by decreased decoding performance. Different effects of ketamine on putative interneurons and pyramidal cells indicate a potential mechanism in which reduced firing of interneurons results in

disinhibition of excitatory cells thus, broadening spatial selectivity and distorting representations of space.

Finally, in chapter 4, I investigate a parallel code for WM coding that may support WM in complex, dynamic environments. I show that neurons fire transiently during the task and that this firing is temporally consistent between trials of the same target location condition. Together, the firing of these neurons created neural sequences - patterns of tiled population activity that spanned the duration of a trial. Using a novel computational method, I demonstrate that these sequences of neural activity robustly represent target location and target trajectory selectively during WM. Moreover, causal manipulation using ketamine distorts these sequences, leading to WM deficits.

5.2 « What Unique Role does the Prefrontal Cortex Play in Naturalistic Working Memory? »

In the visual system, there exists a hierarchical flow of visual information between regions of the cortex. These regions successively elaborate on representations derived by processing in earlier visual areas and begins to integrate this information to generate recognizable perceptual representations. For example, neurons in V1 evaluate edges which are used by specialized cells to detect corners and then used by neurons in association regions to represent visual perceptions of shapes and objects (Grill-Spector & Malach, 2004). Perceptions of our visual world can also be maintained after stimuli are removed, as occurs in WM.

Along this path of visual information processing, mnemonic representations of visual stimuli develop. Leavitt, et al, 2017 conducted a thorough investigation into regional specification of delay activity, the findings of which suggest a gradient within the primate visual system in which properties that support WM emerge in the brain from sensory regions to the PFC. The appearance of WM-related persistent activity in the brain is first observed in association areas like the medial

superior temporal region (MST) or parietal region LIP/ 7a and are most prevalent in PFC. Functional boundaries appear to exist along both the dorsal and ventral visual pathways in which persistent activity and WM representations emerge (Mendoza-Halliday et al., 2014; Leavitt et al., 2017). See Figure. 5.1 for an illustration of visual information flow through the cortex.

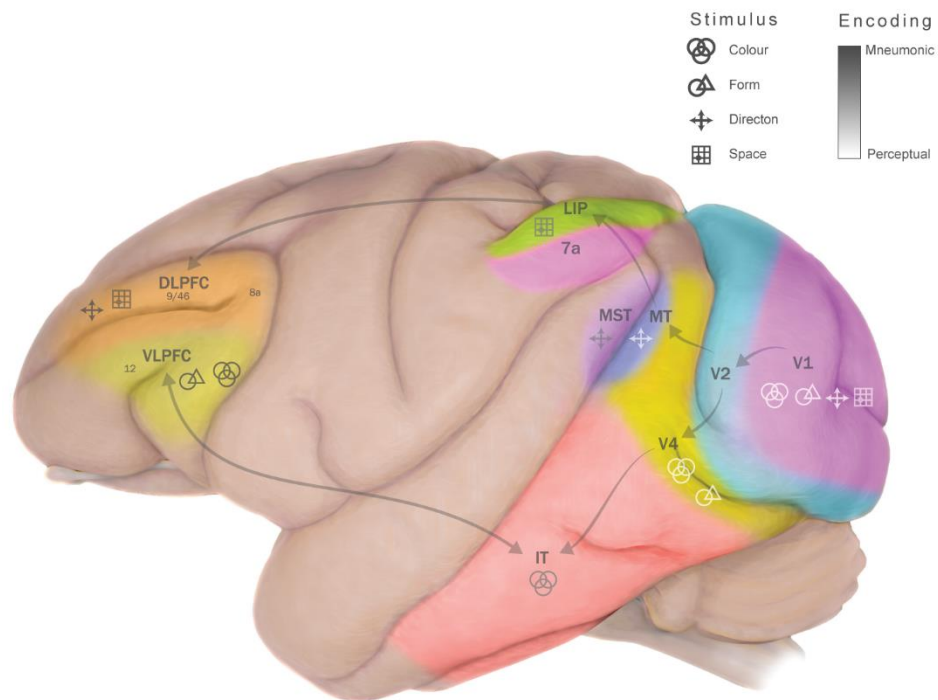


Figure. 5.1: Flow of visual information in the brain

This figure illustrates the flow of visual and mnemonic information in the macaque cortex. Shapes represent the type of visual information primarily stored in each region and the color denotes the ratio of mnemonic to perceptual encoding. Representation of mnemonic information begins to appear in MST and IT, with the greatest mnemonic representation occurring in PFC.

Although other regions exhibit delay-related activity, the PFC presents functional differences from other association areas (Katsuki et al., 2014). For example, the relative proportion of neurons showing selectivity for perceptual and mnemonic visual attributes changes along the hierarchy of visual processing. For representations of motion direction, the proportion of cells encoding mnemonic relative to perceptual representations is lowest in MT with 100% of cells representing perception and lower in MST (93% of cells represent perception, 36% of cells represent WM) than LPFC (70% of cells represent perception, 55% of cells represent WM). The same trend is also evident during the performance of an ODR task in which LPFC contains a higher proportion of exclusively delay selective neurons and parietal area 7ip contains a higher proportion of exclusively cue selective neurons (Chafee, & Goldman-Rakic, 1998).

The LPFC also contains neurons that exclusively encode motion direction during a perceptual delayed match-to-sample task as well as neurons that exclusively encode memory representations of the same motion direction (Mendoza-Halliday and Martinez-Trujillo, 2017). A study found that about 1/3 of the neurons encoded perceptual representations of motion direction but not mnemonic representations, another 1/3 encoded mnemonic representations but not perceptual representations, and another 1/3 encoded a mix of both perceptual and mnemonic representations (Mendoza-Halliday & Martinez-Trujillo, 2017). I present similar findings for visuospatial WM in chapter 2 in which separate populations of single neurons are tuned for either mnemonic or perceptual representations of space or display a mix of selectivity for both types of representation.

The existence of subpopulations of perceptual and mnemonic neurons within the LPFC circuitry provide evidence for a system unique to LPFC in which separate substrates for perception and WM are “concentrated” within a single brain area microcircuit. Unlike observations in sensory areas such as MT where neurons are topographically organized according to their RF location and motion direction they encode (Born & Bradley, 2005), perceptual and mnemonic cells are

distributed within area 9/46 without any apparent clustering by the type of representation (perceptual or mnemonic), suggesting a spatial integration of mnemonic and perceptual neurons. Functional clustering also could not be found in my electrode arrays based on spatial tuning or representation type. Instead, cells with different response properties created a speckled salt-and-pepper pattern within the spatial resolution of the recording electrodes (electrodes are 400 micrometers apart), consistent with previous findings in my lab using Utah arrays in LPFC (Backen et al., 2017).

Despite the spatial integration, the functional segregation of the different populations (perceptual and mnemonic) within LPFC still allows a linear decoder to use single neuron activity to estimate whether a direction of motion is held in WM or is visually presented (perception-memory decoder) as well as which direction is perceived or memorized (direction decoder) (Mendoza-Halliday & Martinez-Trujillo, 2017). I present a similar result in chapter 2 in which cross-training of perception and WM results in poor decoding accuracy, signifying a distinct population code. In chapter 4, I also demonstrate that neural sequences differ between cue presentation and WM delay. This indicates that perceptual and mnemonic signals as well as the features they encode can be discriminated, with reasonable accuracy, from the activity of neurons within the LPFC circuitry.

One potential benefit of a local system capable of representing both WM and perception while maintaining functional segregation is that a “read-out” of the population activity in the LPFC can provide a substrate for rapidly “identifying” the nature of the representation (perceptual or mnemonic). This may be important for protecting mnemonic representations from incoming sensory signals and the ability to differentiate between internally and externally generated representations. The importance of which is highlighted in patients with schizophrenia that lose the ability to differentiate between perceptual and mental representations (e.g., during hallucinations and delusions). WM deficits are also common in patients with schizophrenia and abnormal LPFC activity is consistently reported (Glahn et al., 2005; Forbes et al., 2009; Callicott et al., 2000; Callicott et al., 2000). As reported

in chapter 3, ketamine causes WM deficits by distorting mental representations. A similar distortion of mental representations may occur in schizophrenia.

Another unique function of PFC is protection from distraction which is essential in a naturalistic task. LPFC activity for task-relevant information remains robust during WM in the presence of incoming sensory signals and task-irrelevant information (Constantinidis & Steinmetz, 1996; Qi et al., 2010; Suzuki & Gottlieb, 2013). Since my task allows for free visual exploration, every eye movement may result in new incoming sensory signals which could act as distractors - potentially eroding WM representations. However, in chapter 2, I demonstrate robust population encoding of remembered target locations. Decoding accuracy for predicting target location remains stable throughout the delay period when using neural ensembles or the full population of recorded neurons. This may occur by populations maintaining a stable subspace that we did not examine (Murray et al., 2017; Parthasarathy et al., 2019) or that a stable representation is maintained through an additional temporal code that binds spatial representations over trial time.

5.3 « Utility of Sequential Activity »

In chapter 4, I present evidence for an additional neural code that appears to support WM in naturalistic environments. I propose that precise patterns of population activity may, along with persistent activity, support WM in complex spatiotemporal conditions. As outlined in the introduction, types of sequential activity are well known to support complex behaviors in other animals and brain regions. Here, I demonstrate for the first time that they can represent WM in the primate LPFC as well (expressed by Wang, 2021).

Sequential population activity patterns potentially serve to benefit WM coding in several ways: 1) An element of temporal coding may increase the amount of information that can be conveyed within a circuit since information could be transmitted through spike rate (firing over time) as well as alterations in spike

timing or spatiotemporal firing patterns of a group of neurons, thus potentially allowing for more complex computations. 2) A code that does not rely on continuous activity may be robust to distraction as would occur in a naturalistic environment. If an individual neuron changes its firing pattern in response to a distractor, thus losing its tuning for a target location, the population can still maintain a similar temporal pattern. Indeed, in chapter 4 I detail a neural ablation experiment in which temporal patterns of population activity can still represent target trajectory when 70% of neurons are removed from the population. 3) This code is robust to trial-trial differences in firing rate. Using this code, the magnitude of firing matters less than the relative timing of peak firing in relation to the population. 4) This code may maintain the temporal relationship and timing consistency in the population despite changes in environment (e.g., changes in visual scene after eye movements). A temporal code may propagate task related information over trial time creating temporal consistency, through which delay information could be integrated over the delay period for a stable and uniform representation in spite of complex task dynamics. This may also result in the tracking of temporal order – an overall representation of task structure or states over time (cue, delay, navigation). In chapter 4, neural sequences do appear to represent task state in which epoch can be predicted with high accuracy.

5.4 « Mechanisms of Sequential Activation »

Neuronal sequences have been reported to underlie temporally precise behaviors in other species such as song production in songbirds (Long et al., 2010). One proposed mechanism is a feedforward network in which activity linearly propagates from one group of neurons to the next, resembling synfire chain circuit models (Abeles, 2009). However, this mechanism does not consider complex interactions between cell types (e.g., excitatory and inhibitory interneurons). Previous studies point to the importance of interneurons in WM circuits (Wang, 2004); Therefore, it is important to consider the complexity of neuronal circuits that contain multiple neuronal types. A second mechanism proposes that excitation is controlled by temporally structured inhibition. The temporally precise activation of

pyramidal cells is dependent on a 'release of inhibition' by interneurons (Cannon et al., 2015; Kosche et al., 2015). Therefore, neural sequences may form through an interaction between recurrent excitation and precise inhibition within a local circuit.

I demonstrate in chapter 3 that NMDA receptor antagonism decreases the firing of narrow spiking neurons, resulting in reduced spatial tuning of putative pyramidal cells. In chapter 4 I show that NMDA receptor antagonism by ketamine also decreases the consistency of single neuron timing and makes sequences less differentiable between target conditions. Similar to how neuronal tuning is broadened, population sequences become less precise. This evidence supports NMDA-dependent inhibitory control of precise neural timing during WM. This mechanism may also relate to WM deficits in individuals with NMDA receptor dysfunction like patients with schizophrenia and NMDA-receptor encephalitis. Curiously, other symptoms of schizophrenia, like disorganized behavior, have also been associated with disturbances in the temporal processing of information, resulting in distorted timing of perceptual and cognitive processes (Carroll et al., 2008).

Are local circuits capable of producing sequential activity? Using a network model consisting of a population of oscillators (each oscillator could reflect a single neuron spike train), my research team has shown that complex spatiotemporal patterns of activity emerge when a stimulus input is modeled. Specific patterns of activity evolve based on a specific input and these activity patterns are robust to perturbation (what may be related to distractor input). With appropriate input, these modeled networks produce sequential activity similar to the neural sequences I present in chapter 4. This may reflect how neurons in a local circuit with asynchronous activity could generate informative neural sequences based on precise input (i.e., target location).

A final mechanism may rely on temporally precise phase-locked neuron firing driven by oscillatory activity that modulates the excitability of neurons.

According to some fields of thought, gamma oscillations are related to bursts of neural activity (Lundqvist, 2018). My research team briefly explored this possibility in my dataset, but we found little evidence of gamma frequency modulation. We did find some gamma modulated single neurons; however, after despiking the LFP signal (i.e., removing spike correlated signals) (Zanos et al., 2011), zero neurons in our population of recorded cells were gamma modulated. This suggests that gamma oscillations or bursts in gamma power do not contribute to sequence formation during my WM task.

Sequence generation through theta oscillations is another candidate mechanism. My team used a spike-triggered average approach to average the oscillatory power around each neuron's peak firing time. We found evidence of increased theta power corresponding to peak firing times. However, it is currently unclear if this theta activity constitutes sustained oscillatory activity. It is also unclear whether the theta we recorded is generated from a local or distant source. A potential way to determine whether peak firing bursts results from theta oscillations and to dissociate local contributions from distant contributions is to consider the relevant timing of the events. If theta increases before the peak firing time, this may indicate a distant source of this activity. The relationship between neurons and LFP activity is an avenue we wish to explore in future studies.

5.5 « Limitations in Modeling Schizophrenia using Ketamine»

It is truly amazing that the brain can represent and manipulate complex representations of locations, objects, and even rules that no longer exist to our senses. It is capable of building robust and expansive mental worlds. Humans may take the complexities of our mental worlds for granted – the importance of which may only be understood when these processes go awry as occurs in some psychiatric conditions.

Although ketamine does appear to represent similar symptoms and pathophysiology of schizophrenia, no model can fully represent the complexities of the disorder. There are several limitations to consider. The first is the difference between the PFC in macaques and humans. Although the PFC is expanded in macaques, the surface area of human PFC is 10-fold larger than macaque PFC and the grey matter occupying human PFC is 1.9 times greater than that of macaque PFC. With this expansion came further expansion in cognitive function (Donahue et al., 2018) and increased vulnerability to diseases like schizophrenia that do not occur naturally in other primates, including my animal model (Passingham & Wise, 2012).

The second limitation is that I administer ketamine systemically which may reflect systemic dysfunction in the brain that occurs in schizophrenia and results in clear behavioral effects that can be correlated with neural activity; however, it becomes less clear whether changes in neural activity are caused solely by ketamine's effect on PFC. In this dissertation, I discuss WM from the perspective of local circuit processing within LPFC. Significant modeling and experimental evidence support the importance of local circuit function for WM maintenance (Wang et al., 2004; Constantinidis et al., 2018; Roussy et al., 2021); however, the PFC does not exist in a vacuum. By only recording from LPFC, we only see part of the picture. It is unlikely that the LPFC alone is responsible for the complex cognition and behavior that is represented in my task, thus it would be insufficient to only consider local connections when considering systemic drug effects.

The PFC plays an important executive role, incorporating sensory signals with mental representations, and planned motor response. To fulfill this role, the PFC must be interconnected with various cortical and subcortical regions. Of particular interest to WM, the lateral PFC is largely bidirectionally connected to temporal and posterior parietal cortices (Goldman-Rakic & Schwartz, 1982; Leichnetz, 1980; Schwartz & Goldman-Rakic, 1984; Yeterian et al., 2012; Arnsten, 2013).

WM may be partially maintained through cortical-cortical or cortical-subcortical loops (Floresco et al., 1999; Christophel et al., 2017). One cortical-cortical connection that is particularly relevant for visuospatial WM and may be affected by ketamine (Muthukumaraswamy et al., 2015) is that between LPFC and the posterior parietal cortex. In 1998, Chafee and Goldman-Rakic observed that patterns of neuronal activity in the dlPFC and parietal area LIP/7a were remarkably similar including their spatial tuning and ability to generate persistent activity (Chafee & Goldman-Rakic, 1998). They later demonstrated, using cortical cooling, that WM-related activity in both regions were dependent on shared reciprocal activity (Chafee & Goldman-Rakic, 2000). Synchronized activity between PFC and PPC underlying WM has since been substantiated (Salazar et al., 2012). The prefrontal and parietal cortices thus represent two regions in which persistent activity is frequently observed but the role of their reciprocal connections is still debated (Christophel et al., 2017; Constantinidis et al., 2018).

To explore the function of these prefrontal-parietal connections, Murray et al., (2017) developed a computational model of two bidirectionally connected modules that biophysically represented local networks of PFC and PPC. This model shows that PPC functions in a weak attractor state and transiently encodes the stimulus and propagates this sensory signal to PFC. Although both maintain the WM representation after stimulus offset, the attractor state is stronger in the PFC module, allowing for robustness against distractors. Feedback projections from PFC can additionally switch PPC neurons back to encoding target stimuli after distractor presentation. Therefore, in this model, persistent activity was supported by both local and long-range network connections, highlighting the importance of recognizing multiple levels of processing when considering systemic pharmaceutical manipulation.

It is easy to imagine that changes in PFC activity may also result from ketamine's action on these interconnected regions. Local manipulation of PFC through local micro drug injection or iontophoresis would need to be conducted to separate these effects. A study by Wang, Arnsten, and colleagues does

convincingly alter PFC activity using NMDA receptor antagonists during WM using local iontophoresis and systemic ketamine injection (Wang et al., 2013). Neural activity in dlPFC was comparably altered using both methods.

The third limitation is that ketamine may not exclusively alter NMDAR systems. Although ketamine is thought to exert its effects as an NMDA receptor antagonist, it appears to have varying levels of influence on other neurotransmitter systems. Ketamine appears to have some influence on the dopaminergic system due to its rewarding properties evidenced by recreational abuse and proclivity for self-administration in macaques (Moreton et al., 1977). Indeed, one meta-analysis shows that acute ketamine administration in rodents results in increased dopamine in the cortex (Kokkinou et al., 2018). One study reports that ketamine acts as a direct agonist for D2 dopamine receptors (Kapur & Seeman, 2002); although this finding has not been clearly replicated to my knowledge.

More likely, ketamine disinhibits dopaminergic neurons, thus increasing the level of dopamine released. Ketamine increases the release of dopamine in the frontal cortex and ventral striatum (Moghaddam., et al. 1997). During an amphetamine challenge, pre-treatment with MK-801, PCP, or ketamine increases the amount of dopamine released compared to amphetamine administration alone (Miller & Abercrombie, 1996; Kegeles., et al. 2000). This resembles the increased amphetamine-triggered dopamine release in patients with schizophrenia (Laruelle et al., 1996; Breier et al., 1997). Chronic use of NMDA antagonists like ketamine can also result in abnormal dopaminergic signaling resembling that in schizophrenia (Jentsch & Roth, 1999).

Dopamine is essential for WM function (Brozoski et al., 1979; Williams & Goldman-Rakic, 1995) and it has been associated with the ability to filter distracter stimuli (Jacob et al., 2016). It may be of little surprise then that association regions most involved in WM function have unequal distribution of D1 receptors in the macaque cerebral cortex (Froudust-Walsh et al., 2021). The concentration of D1 receptors increases along the hierarchy of visual processing reaching their

maximal concentration in the parietal and prefrontal cortices. Froudish-Walsh and coworkers elaborated on a computational model in which release of dopamine favors persistent firing and resilience to distracters in association areas via its action on D1 receptors. Insufficient or excessive dopamine release on the other hand, makes persistent firing less robust to distracter interference (Froudish-Walsh et al., 2021).

Together, ketamine-induced alterations in glutaminergic and dopaminergic systems may explain the formation of positive and cognitive symptoms including WM dysfunction. Could interactions between these two systems trigger symptoms in schizophrenia as well? I believe this is an important research field to explore. To separate the effects of both systems, more precise NMDA antagonists like MK-801 could be used.

5.6 « Future Studies »

5.6.1 Exploration of Cortical-Cortical and Subcortical Connections

The results of chapter 4 draw an interesting parallel between the function of the PFC and the hippocampus. Since this thesis focuses on a WM task that includes memory-guided navigation, I feel it important to consider potential LPFC-hippocampal interactions.

Hippocampal-prefrontal interactions are commonly demonstrated to underlie short-term memory for spatial locations in rodents (Jones & Wilson, 2005; Liu et al., 2018; Tang et al., 2021). Rodent studies demonstrate functional connectivity between these regions. Coordination between mPFC and hippocampus during complex spatial WM appears to occur through theta oscillations in which theta oscillations facilitate hippocampal inputs to the medial prefrontal cortex during memory tasks (Jones & Wilson, 2005; Liu et al., 2018; Tang et al., 2021).

Could this occur in macaques as well? To my knowledge, neural correlates of spatial WM have not been simultaneously recorded from primate LPFC and hippocampus. Early studies of patients with hippocampus lesions often reported unobstructed spatial WM function, suggesting that primates may differ from rodents in this relationship; however, more recent studies have refuted this claim, proposing that the medial temporal lobe (MTL) and hippocampus may have a greater role in spatial WM and even visual perception than previously assumed (Jeneson et al., 2012). Future research is needed to establish the role of the primate hippocampus during spatial WM.

As surgical techniques and electrode development continue to advance, future studies will be able to simultaneously record from many single units from macaque PFC and PPC or hippocampus with relative ease. Chronically implanted high-density microelectrodes can be used in PFC and PPC such as the Utah array or more modern acute multi-shank, high-density electrodes that allow for optical stimulation and drug delivery for causal experiments (Shin et al., 2021). There are also many current options for electrodes with multiple recording sites for high-yield recording in deep brain regions like the hippocampus such as multisite planar probes with the ability to electrically stimulate, and interface with optical stimulation and drug delivery systems (Pemba & Tang, 2013).

A virtual task like mine is ideal for studying the interaction between spatial navigation and WM in large animals as one can maintain a high level of experimental control. Alternatives to virtual tasks may be freely moving macaques with wireless signal transmission (Mao et al., 2021). Although this approach benefits ecological validity, there are logistical challenges to designing freely moving tasks in large animals with the most prominent being the space required for navigation. It also becomes more difficult to record eye position, a signal that is important to consider when measuring visuospatial WM in PFC.

5.6.2 Towards Naturalistic Research

There is an obvious benefit to testing specific elements of a cognitive process or behavior. Much of what we understand of the brain and behavior results from the careful isolation of specific variables. However, this careful manipulation of individual elements may not amount to a comprehensive or holistic understanding of naturalistic brain function. For this reason, there has been a movement towards increasing task complexity in neuroscience to test the ecological validity of our experimental findings – to make the connection between brain function in highly controlled experiments and real-world contexts.

In human research, subjects are now often presented with rich stimuli and contexts like video sequences or movies. Moreover, immersive virtual reality now allows participants to directly interact with experiments (Bohil et al., 2011). With the development of sophisticated behavior tracking software like DeepLabCut (Lauer et al., 2022), we can now effectively track precise behavior in humans or animals in complex environments. The development of virtual reality (demonstrated in this dissertation and Gulli et al., 2020), and the development of large recording chambers for experiments on freely moving subjects, allow for more immersive experimentation in animal research. Hardware breakthroughs allow for high-quality wireless and high-density neural recording during such experiments (Schwarz et al., 2014; Mao et al., 2021).

Despite the benefits of increasing task complexity, issues can arise when introducing multiple variables at once. Here, I chose to develop a task with as many natural elements as possible while still maintaining experimental control (i.e., the surrounding environment is consistent from trial-to-trial and task structure and timing is precisely controlled). Since we do add multiple elements to our task, it is difficult to know which element drives new research findings. I believe this is a limitation in chapter 4 with the discovery of neural sequences during WM. Sequences were correlated to task behavior during my naturalistic task but not during an ODR task. There are several differences between the tasks that could

drive this distinction. Sequence generation could be required based on any task with complex spatiotemporal elements which may create short-term episodes. It could result in any task with memory-guided navigation, or it could occur in tasks requiring a complex behavioral response without a navigation requirement.

Intermediate steps are also required in which a small number of highly controlled variables may be studied in conjunction. Experiments that present multiple items for encoding, ones that include sequential presentation of items, ones that introduce different types of distractors in a highly controlled environment, and those that require complex responses are still essential to bridge the information between reductionist experiments (in which the complex behavior is reduced to a single isolated variable) and fully naturalistic approaches.

5.7 « Concluding Remarks »

Methodology for neural recording is developing rapidly due to academic and private investments (Neuralink, CA, USA) with the development of high-density electrodes that can record hundreds of isolated units (Neuropixels, Cambridge NeuroTech) while offering highly controlled causal manipulation, new experiments are becoming possible every day with thrilling potential – it is truly an exciting time to be a neurophysiologist. Increased recording capability, along with developments in the analysis of high-dimensional datasets, will undoubtedly increase our understanding of complex behavior. I believe that the work of this dissertation begins to pave a way for us to understand complex cognition in naturalistic settings. My hope is that continued research on this trajectory will not only help us understand the complexities of PFC in primates as well as the development of our vast mental worlds as humans, but also the vulnerabilities to disease that accompany it.

5.8 « References »

- Abeles, M. *Synfire Chains*. (2009). Encyclopedia of Neuroscience. 829-832. Academic Press, MA, USA. doi:10.1016/B978-008045046-9.01437-6
- Arnsten, A. F. T. (2013). The neurobiology of thought: The groundbreaking discoveries of Patricia Goldman-Rakic 1937–2003. *Cerebral Cortex*, 23(10), 2269–2281. doi:10.1093/cercor/bht195
- Backen, T., Treue, S., & Martinez-Trujillo, J. C. (2018). Encoding of spatial attention by primate prefrontal cortex neuronal ensembles. *eNeuro*, 5(1), ENEURO.0372-16.2017. doi:10.1523/ENEURO.0372-16.2017
- Born, R. T., & Bradley, D. C. (2005). Structure and function of visual area MT. *Annual Review of Neuroscience*, 28(1), 157–189. doi:10.1146/annurev.neuro.26.041002.131052
- Bohil, C. J., Alicea, B., & Biocca, F. A. (2011). Virtual reality in neuroscience research and therapy. *Nature Reviews. Neuroscience*, 12(12), 752–762. doi:10.1038/nrn3122
- Breier, A., Su, T. P., Saunders, R., Carson, R. E., Kolachana, B. S., de Bartolomeis, A., Weinberger, D. R., Weisenfeld, N., Malhotra, A. K., Eckelman, W. C., & Pickar, D. (1997). Schizophrenia is associated with elevated amphetamine-induced synaptic dopamine concentrations: evidence from a novel positron emission tomography method. *Proceedings of the National Academy of Sciences of the United States of America*, 94(6), 2569–2574. doi:10.1073/pnas.94.6.2569
- Brozoski, T. J., Brown, R. M., Rosvold, H. E., & Goldman, P. S. (1979). Cognitive deficit caused by regional depletion of dopamine in prefrontal cortex of rhesus monkey. *Science*, 205(4409), 929–932. doi:10.1126/science.112679
- Cannon, J., Kopell, N., Gardner, T., & Markowitz, J. (2015). Neural sequence generation using spatiotemporal patterns of inhibition. *PLoS Computational Biology*, 11(11), e1004581. doi:10.1371/journal.pcbi.1004581
- Carroll, C. A., Boggs, J., O'Donnell, B. F., Shekhar, A., & Hetrick, W. P. (2008). Temporal processing dysfunction in schizophrenia. *Brain and Cognition*, 67(2), 150–161. doi:10.1016/j.bandc.2007.12.005
- Callicott, J. H., Bertolino, A., Mattay, V. S., Langheim, F. J., Duyn, J., Coppola, R., Goldberg, T. E., & Weinberger, D. R. (2000). Physiological dysfunction of the dorsolateral prefrontal cortex in schizophrenia revisited. *Cerebral Cortex*, 10(11), 1078–1092. doi:10.1093/cercor/10.11.1078

Chafee, M. V., & Goldman-Rakic, P. S. (1998). Matching patterns of activity in primate prefrontal area 8a and parietal area 7ip neurons during a spatial working memory task. *Journal of Neurophysiology*, *79*(6), 2919–2940. doi:10.1152/jn.1998.79.6.2919

Chafee, M. V., & Goldman-Rakic, P. S. (2000). Inactivation of parietal and prefrontal cortex reveals interdependence of neural activity during memory-guided saccades. *Journal of Neurophysiology*, *83*(3), 1550–1566. doi:10.1152/jn.2000.83.3.1550

Christophel, T. B., Klink, P. C., Spitzer, B., Roelfsema, P. R., & Haynes, J. D. (2017). The distributed nature of working memory. *Trends in Cognitive Sciences*, *21*(2), 111–124. doi:10.1016/j.tics.2016.12.007

Constantinidis, C., Funahashi, S., Lee, D., Murray, J. D., Qi, X. L., Wang, M., & Arnsten, A. (2018). Persistent spiking activity underlies working memory. *The Journal of Neuroscience*, *38*(32), 7020–7028. doi:10.1523/JNEUROSCI.2486-17.2018

Constantinidis, C., & Steinmetz, M. A. (1996). Neuronal activity in posterior parietal area 7a during the delay periods of a spatial memory task. *Journal of Neurophysiology*, *76*(2), 1352–1355. doi:10.1152/jn.1996.76.2.1352

Donahue, C. J., Glasser, M. F., Preuss, T. M., Rilling, J. K., & Van Essen, D. C. (2018). Quantitative assessment of prefrontal cortex in humans relative to nonhuman primates. *Proceedings of the National Academy of Sciences of the United States of America*, *115*(22), E5183–E5192. doi:10.1073/pnas.1721653115

Floresco, S. B., Braaksma, D. N., & Phillips, A. G. (1999). Thalamic-cortical-striatal circuitry subserves working memory during delayed responding on a radial arm maze. *The Journal of Neuroscience*, *19*(24), 11061–11071. doi:10.1523/JNEUROSCI.19-24-11061.1999

Forbes, N. F., Carrick, L. A., McIntosh, A. M., & Lawrie, S. M. (2009). Working memory in schizophrenia: A meta-analysis. *Psychological Medicine*, *39*(6), 889–905. doi:10.1017/S0033291708004558

Froudust-Walsh, S., Bliss, D. P., Ding, X., Rapan, L., Niu, M., Knoblauch, K., Zilles, K., Kennedy, H., Palomero-Gallagher, N., & Wang, X. J. (2021). A dopamine gradient controls access to distributed working memory in the large-scale monkey cortex. *Neuron*, *109*(21), 3500–3520.e13. doi:10.1016/j.neuron.2021.08.024

Goldman-Rakic, P. S., & Schwartz, M. L. (1982). Interdigitation of contralateral and ipsilateral columnar projections to frontal association cortex in primates. *Science*, *216*(4547), 755–757. doi:10.1126/science.6177037

- Glahn, D. C., Ragland, J. D., Abramoff, A., Barrett, J., Laird, A. R., Bearden, C. E., & Velligan, D. I. (2005). Beyond hypofrontality: A quantitative meta-analysis of functional neuroimaging studies of working memory in schizophrenia. *Human Brain Mapping, 25*(1), 60–69. doi:10.1002/hbm.20138
- Grill-Spector, K., & Malach, R. (2004). The human visual cortex. *Annual Review of Neuroscience, 27*, 649–677. doi:10.1146/annurev.neuro.27.070203.144220
- Gulli, R. A., Duong, L. R., Corrigan, B. W., Doucet, G., Williams, S., Fusi, S., & Martinez-Trujillo, J. C. (2020). Context-dependent representations of objects and space in the primate hippocampus during virtual navigation. *Nature Neuroscience, 23*(1), 103–112. doi:10.1038/s41593-019-0548-3
- Jacob, S., Stalter, M., & Nieder, A. (2016). Cell-type-specific modulation of targets and distractors by dopamine D1 receptors in primate prefrontal cortex. *Nature Communications, 7*, 13218. doi:10.1038/ncomms13218
- Jones, M. W., & Wilson, M. A. (2005). Theta rhythms coordinate hippocampal-prefrontal interactions in a spatial memory task. *PLoS Biology, 3*(12), e402. doi:10.1371/journal.pbio.0030402
- Jentsch, J. D., & Roth, R. H. (1999). The neuropsychopharmacology of phencyclidine: From NMDA receptor hypofunction to the dopamine hypothesis of schizophrenia. *Neuropsychopharmacology, 20*(3), 201–225. doi:10.1016/S0893-133X(98)00060-8
- Jeneson, A., Wixted, J. T., Hopkins, R. O., & Squire, L. R. (2012). Visual working memory capacity and the medial temporal lobe. *The Journal of Neuroscience, 32*(10), 3584–3589. doi:10.1523/JNEUROSCI.6444-11.2012
- Katsuki, F., Qi, X. L., Meyer, T., Kostelic, P. M., Salinas, E., & Constantinidis, C. (2014). Differences in intrinsic functional organization between dorsolateral prefrontal and posterior parietal cortex. *Cerebral Cortex, 24*(9), 2334–2349. doi:10.1093/cercor/bht087
- Kapur, S., & Seeman, P. (2002). NMDA receptor antagonists ketamine and PCP have direct effects on the dopamine D(2) and serotonin 5-HT(2)receptors-implications for models of schizophrenia. *Molecular Psychiatry, 7*(8), 837–844. doi:10.1038/sj.mp.4001093
- Kegeles, L. S., Abi-Dargham, A., Zea-Ponce, Y., Rodenhiser-Hill, J., Mann, J. J., Van Heertum, R. L., Cooper, T. B., Carlsson, A., & Laruelle, M. (2000). Modulation of amphetamine-induced striatal dopamine release by ketamine in humans: Implications for schizophrenia. *Biological Psychiatry, 48*(7), 627–640. doi:10.1016/s0006-3223(00)00976-8

- Kosche, G., Vallentin, D., & Long, M. A. (2015). Interplay of inhibition and excitation shapes a premotor neural sequence. *The Journal of Neuroscience*, *35*(3), 1217–1227. doi:10.1523/JNEUROSCI.4346-14.2015
- Kokkinou, M., Ashok, A. H., & Howes, O. D. (2018). The effects of ketamine on dopaminergic function: Meta-analysis and review of the implications for neuropsychiatric disorders. *Molecular Psychiatry*, *23*(1), 59–69. doi:10.1038/mp.2017.190
- Laruelle, M., Abi-Dargham, A., van Dyck, C. H., Gil, R., D'Souza, C. D., Erdos, J., McCance, E., Rosenblatt, W., Fingado, C., Zoghbi, S. S., Baldwin, R. M., Seibyl, J. P., Krystal, J. H., Charney, D. S., & Innis, R. B. (1996). Single photon emission computerized tomography imaging of amphetamine-induced dopamine release in drug-free schizophrenic subjects. *Proceedings of the National Academy of Sciences of the United States of America*, *93*(17), 9235–9240. doi:10.1073/pnas.93.17.9235
- Lauer, J., Zhou, M., Ye, S. *et al.* (2022). Multi-animal pose estimation, identification and tracking with DeepLabCut. *Nature Methods*, *19*, 496–504. doi:10.1038/s41592-022-01443-0
- Leichnetz, G. R. (1980). An intrahemispheric columnar projection between two cortical multisensory convergence areas (inferior parietal lobule and prefrontal cortex): An anterograde study in macaque using HRP gel. *Neuroscience Letters*, *18*(2), 119–124. doi:10.1016/0304-3940(80)90313-4
- Leavitt, M. L., Mendoza-Halliday, D., & Martinez-Trujillo, J. C. (2017). Sustained activity encoding working memories: Not fully distributed. *Trends in Neurosciences*, *40*(6), 328–346. doi:10.1016/j.tins.2017.04.004
- Long, M. A., Jin, D. Z., & Fee, M. S. (2010). Support for a synaptic chain model of neuronal sequence generation. *Nature*, *468*(7322), 394–399. doi:10.1038/nature09514
- Liu, T., Bai, W., Xia, M., & Tian, X. (2018). Directional hippocampal-prefrontal interactions during working memory. *Behavioural Brain Research*, *338*, 1–8. doi:10.1016/j.bbr.2017.10.003
- Lundqvist, M., Herman, P., Warden, M. R., Brincat, S. L., & Miller, E. K. (2018). Gamma and beta bursts during working memory readout suggest roles in its volitional control. *Nature Communications*, *9*, 394. doi:10.1038/s41467-017-02791-8
- Mao, D., Avila, E., Caziot, B., Laurens, J., Dickman, J. D., & Angelaki, D. E. (2020). Spatial modulation of hippocampal activity in freely moving macaques. *Neuron*, *109*, 3521–3534. doi:10.1016/j.neuron.2021.09.032

- Miller, D. W., & Abercrombie, E. D. (1996). Effects of MK-801 on spontaneous and amphetamine-stimulated dopamine release in striatum measured with in vivo microdialysis in awake rats. *Brain Research Bulletin*, *40*(1), 57–62. doi:10.1016/0361-9230(95)02144-2
- Mendoza-Halliday, D., Torres, S., & Martinez-Trujillo, J. C. (2014). Sharp emergence of feature-selective sustained activity along the dorsal visual pathway. *Nature Neuroscience*, *17*(9), 1255–1262. doi:10.1038/nn.3785
- Mendoza-Halliday, D., & Martinez-Trujillo, J. (2017). Neuronal population coding of perceived and memorized visual features in the lateral prefrontal cortex. *Nature Communications*, *8*, 15471. doi:10.1038/ncomms15471
- Moreton, J. E., Meisch, R. A., Stark, L., & Thompson, T. (1977). Ketamine self-administration by the rhesus monkey. *The Journal of Pharmacology and Experimental Therapeutics*, *203*(2), 303–309.
- Moghaddam, B., Adams, B., Verma, A., & Daly, D. (1997). Activation of glutamatergic neurotransmission by ketamine: A novel step in the pathway from NMDA receptor blockade to dopaminergic and cognitive disruptions associated with the prefrontal cortex. *The Journal of Neuroscience*, *17*(8), 2921–2927. doi:10.1523/JNEUROSCI.17-08-02921.1997
- Murray, J. D., Jaramillo, J., & Wang, X. (2017). Working memory and decision-making in a frontoparietal circuit model. *The Journal of Neuroscience*, *37*, 12167 - 12186. doi:10.1523/JNEUROSCI.0343-17.2017
- Muthukumaraswamy, S. D., Shaw, A. D., Jackson, L. E., Hall, J., Moran, R., & Saxena, N. (2015). Evidence that subanesthetic doses of ketamine cause sustained disruptions of NMDA and AMPA-mediated frontoparietal connectivity in humans. *The Journal of Neuroscience*, *35*(33), 11694-11706. doi:10.1523/JNEUROSCI.0903-15.2015
- Parthasarathy, A., Tang, C., Herikstad, R., Cheong, L. F., Yen, S-C, & Libedinsky, C. (2019). Time-invariant working memory representations in the presence of code-morphing in the lateral prefrontal cortex. *Nature Communications*, *10*, 4995. doi:10.1038/s41467-019-12841-y
- Passingham, R. E., & Wise, S. P. (2012). *The neurobiology of the prefrontal cortex: Anatomy, evolution, and the origin of insight*. Oxford University Press.
- Petrides M. (2005). Lateral PFC: Architectonic and functional organization. *Philosophical transactions of the Royal Society of London*, *360*(1456), 781–795. doi:10.1098/rstb.2005.1631
- Pemba, D., & Tang, W.C. (2013). A multisite neural probe with simultaneous neural recording and drug delivery capabilities. *2013 6th International IEEE/EMBS Conference on Neural Engineering (NER)*, 1493-1496.

- Qi, X. L., Katsuki, F., Meyer, T., Rawley, J. B., Zhou, X., Douglas, K. L., & Constantinidis, C. (2010). Comparison of neural activity related to working memory in primate dorsolateral prefrontal and posterior parietal cortex. *Frontiers in Systems Neuroscience*, 4, 12. doi:10.3389/fnsys.2010.00012
- Roussy, M., Mendoza-Halliday, D., & Martinez-Trujillo, J. C. (2021). Neural substrates of visual perception and working memory: Two sides of the same coin or two different coins? *Frontiers Neural Circuits*, 15, 764177. doi:10.3389/fncir.2021.764177
- Schwartz, M. L., & Goldman-Rakic, P. S. (1984). Callosal and intrahemispheric connectivity of the prefrontal association cortex in rhesus monkey: Relation between intraparietal and principal sulcal cortex. *The Journal of Comparative Neurology*, 226, 403-420. doi:10.1002/cne.902260309
- Schwarz, D. A., Lebedev, M. A., Hanson, T. L., Dimitrov, D. F., Lehew, G., Meloy, J., Rajangam, S., Subramanian, V., Ifft, P. J., Li, Z., Ramakrishnan, A., Tate, A., Zhuang, K. Z., & Nicolelis, M. A. (2014). Chronic, wireless recordings of large-scale brain activity in freely moving rhesus monkeys. *Nature Methods*, 11(6), 670–676. doi:10.1038/nmeth.2936
- Shin, H., Jeong, S., Lee, J. H., Sun, W., Choi, N., & Cho, I-J. (2021). 3D high-density microelectrode array with optical stimulation and drug delivery for investigating neural circuit dynamics. *Nature Communications*, 12, 492. doi:10.1038/s41467-020-20763-3
- Salazar, R. F., Dotson, N. M., Bressler, S. L., & Gray, C. M. (2012). Content-specific fronto-parietal synchronization during visual working memory. *Science*, 338(6110), 1097–1100. doi:10.1126/science.1224000
- Suzuki, M., & Gottlieb, J. (2013). Distinct neural mechanisms of distractor suppression in the frontal and parietal lobe. *Nature Neuroscience*, 16(1), 98–104. doi:10.1038/nn.3282
- Tang, W., Shin, J. D., & Jadhav, S. P. (2021). Multiple time-scales of decision-making in the hippocampus and prefrontal cortex. *eLife*, 10:e66227. doi:10.7554/eLife.66227
- Wang, X. J., Tegnér, J., Constantinidis, C., & Goldman-Rakic, P. S. (2004). Division of labor among distinct subtypes of inhibitory neurons in a cortical microcircuit of working memory. *Proceedings of the National Academy of Sciences of the United States of America*, 101(5), 1368–1373. doi:10.1073/pnas.0305337101
- Wang X. J. (2021). 50 years of mnemonic persistent activity: quo vadis? *Trends in Neurosciences*, 44(11), 888–902. doi:10.1016/j.tins.2021.09.001

Wang, M., Yang, Y., Wang, C. J., Gamo, N. J., Jin, L. E., Mazer, J. A., Morrison, J. H., Wang, X. J., & Arnsten, A. F. (2013). NMDA receptors subserve persistent neuronal firing during working memory in dorsolateral prefrontal cortex. *Neuron*, *77*(4), 736–749. doi:10.1016/j.neuron.2012.12.032

Wimmer, K., Nykamp, D. Q., Constantinidis, C., & Compte, A. (2014). Bump attractor dynamics in prefrontal cortex explains behavioral precision in spatial working memory. *Nature Neuroscience*, *17*(3), 431–439. doi:10.1038/nn.3645

Williams, G., & Goldman-Rakic, P. (1995). Modulation of memory fields by dopamine D1 receptors in prefrontal cortex. *Nature*, *376*, 572–575. doi:10.1038/376572a0

Yeterian, E. H., Pandya, D. N., Tomaiuolo, F., & Petrides, M. (2012). The cortical connectivity of the prefrontal cortex in the monkey brain. *Cortex*, *48*(1), 58–81. doi:10.1016/j.cortex.2011.03.004

Zanos, T. P., Mineault, P. J., & Pack, C. C. (2011). Removal of spurious correlations between spikes and local field potentials. *Journal of Neurophysiology*, *105*(1), 474–486. doi:10.1152/jn.00642.2010

« Appendices »

« Appendix A: Ethics Approval »



2019-084:5:

AUP Number: 2019-084

AUP Title: Neural Mechanisms of Cognition

Yearly Renewal Date: 08/01/2022

The **annual renewal** to Animal Use Protocol (AUP) 2019-084 has been approved by the Animal Care Committee (ACC), and will be approved through to the above review date.

Please at this time review your AUP with your research team to ensure full understanding by everyone listed within this AUP.

As per your declaration within this approved AUP, you are obligated to ensure that:

1. This Animal Use Protocol is in compliance with:
 - [Western's Senate MAPP 7.12 \[PDF\]](#); and
 - [Applicable Animal Care Committee policies and procedures](#).
2. Prior to initiating any study-related activities—[as per institutional OH&S policies](#)—all individuals listed within this AUP who will be using or potentially exposed to hazardous materials will have:
 - Completed the appropriate institutional OH&S training;
 - Completed the appropriate facility-level training; and
 - Reviewed related (M)SDS Sheets.

Submitted by: Cristancho, Martha on behalf of the Animal Care Committee

Dr. Timothy Regnault,
Animal Care Committee Chair

Animal Care Committee
The University of Western Ontario

Appendix A: Animal use protocol approval

« Appendix B: Article Reuse Permissions »

Neural Substrates of Visual Perception and Working Memory: Two Sides of the Same Coin or Two Different Coins?

[Megan Roussy](#), ¹ [Diego Mendoza-Halliday](#), ² and [Julio C. Martinez-Trujillo](#) ^{1,*}

► [Author information](#) ► [Article notes](#) ▼ [Copyright and License information](#) [Disclaimer](#)

[Copyright](#) © 2021 Roussy, Mendoza-Halliday and Martinez-Trujillo.

This is an open-access article distributed under the terms of the Creative Commons Attribution License (CC BY). The use, distribution or reproduction in other forums is permitted, provided the original author(s) and the copyright owner(s) are credited and that the original publication in this journal is cited, in accordance with accepted academic practice. No use, distribution or reproduction is permitted which does not comply with these terms.

Figure A1: Licensing information for Frontiers in Neural Circuits (Chapter 1)

Rights and permissions

Open Access This article is licensed under a Creative Commons Attribution 4.0 International License, which permits use, sharing, adaptation, distribution and reproduction in any medium or format, as long as you give appropriate credit to the original author(s) and the source, provide a link to the Creative Commons license, and indicate if changes were made. The images or other third party material in this article are included in the article's Creative Commons license, unless indicated otherwise in a credit line to the material. If material is not included in the article's Creative Commons license and your intended use is not permitted by statutory regulation or exceeds the permitted use, you will need to obtain permission directly from the copyright holder. To view a copy of this license, visit

Figure A2. Licensing information for Molecular Psychiatry (Chapter 2)

« Appendix C: Statistical Reporting Tables »

Table 1C: Statistics reporting table for chapter 2.

Figure	Subj.	Data Counts	Stat Test	Comparison	Stat.	P Value	
2.2a Percent of Correct Trials	NHP B, NHP T	20 WM sessions, 19 perception sessions	2-way ANOVA	Animal Task	$F(1,35) = 84.7$	$p < 0.0001$	
				Interaction	$F(1,35) = 199.6$	$p < 0.0001$	
					$F(1,35) = 58.9$	$p < 0.0001$	
				Tukey- Kramer Multiple Comparison	NHP B Per- NHP B WM		$p < 0.0001$
				NHP T Per- NHP T WM		$p < 0.0001$	
				NHP B WM- NHP T WM		$p < 0.0001$	
2.2b Response Time	NHP B, NHP T	20 WM sessions, 19 perception sessions	2-way ANOVA	Animal Task	$F(1,35) = 0.62$	$p = 0.44$	
				Interaction	$F(1,35) = 0.01$	$p = 0.94$	
					$F(1,35) = 0.98$	$p = 0.33$	
2.2e Optimal Trajectory	NHP B, NHP T	20 WM sessions, 19 perception sessions	Wilcoxon Rank-Sum Test	NHP B	$Rank = 234$	$p = 0.0002$	
				NHP T	$Rank = 72$	$p = 0.02$	
2.3a Percent on Screen	NHP B, NHP T	20 WM sessions, 19 perception sessions	2-way ANOVA	Epoch Task	$F(2,111) = 6.9$	$p = 0.002$	
				Interaction	$F(1,111) = 8.4$	$p = 0.005$	
					$F(2,111) = 20$	$p < 0.0001$	
				Tukey- Kramer Multiple Comparison	cueWM- delayWM		$p = 0.01$
					delayWM- responseWM		$p = 0.0004$
					cueWM- responseWM		$p = 0.9$
	cuePer- delayPer		$p = 0.8$				
	delayPer- responsePer		$p = 0.0007$				

				cuePer- responsePer		$p < 0.0001$
				cueWM- cuePer		$p = 1$
				delayWM- delayPer		$p = 0.44$
				responseWM- responsePer		$p < 0.0001$
2.3d Percent Eye Movement Events	NHP B, NHP T	20 WM sessions, 19 perception sessions	2-way ANOVA	<u>Fixation</u>		
				Epoch Task	$F(2,111) = 191.8$	$p < 0.0001$
				Interaction	$F(1,111) = 11.3$	$p = 0.001$
					$F(2,111) = 0.62$	$p = 0.54$
			Tukey- Kramer Multiple Comparison	cueWM- delayWM		$p = 0.3$
				cueWM- responseWM		$p < 0.0001$
				delayWM- responseWM		$p < 0.0001$
				cuePer- delayPer		$p = 0.85$
				cuePer- responsePer		$p < 0.0001$
				delayPer- responsePer		$p < 0.0001$
2-way ANOVA	<u>Saccade</u>					
	Epoch Task	$F(2,111) = 64$	$p < 0.0001$			
	Interaction	$F(1,111) = 142.2$	$p < 0.0001$			
		$F(2,111) = 10.9$	$p < 0.0001$			
Tukey- Kramer Multiple Comparison	cueWM- delayWM		$p = 0.99$			
	cueWM- responseWM		$p < 0.0001$			

				delayWM- responseWM		$p < 0.0001$
				cuePer- delayPer		$p < 0.0001$
				cuePer- responsePer		$p = 0.007$
				delayPer- responsePer		$p < 0.0001$
				cueWM- cuePer		$p = 0.0007$
				delayWM- delayPer		$p < 0.0001$
				responseWM- responsePer		$p < 0.0001$
2.3e Main Sequence Between Epochs	NHP B, NHP T	20 WM sessions, 19 perception sessions	1-way ANOVA Tukey- Kramer	<u>WM</u> Amplitude bin Delay-cue Cue- response Delay- response	 Cohen's d Cohen's d Cohen's d	4 bins, $p < 0.05$ 4 bins, $p < 0.05$ 2 bin > 0.2 3 bin, $p < 0.05$ 3 bin > 0.2 3 bin, $p < 0.05$ 1 bin > 0.2
			1-way ANOVA Tukey- Kramer	<u>Perception</u> Amplitude bin Delay-cue Cue- response	 Cohen's d Cohen's d	6 bins, $p < 0.05$ 4 bins, $p < 0.05$ 1 bin > 0.2 6 bins, $p < 0.05$ 6 bin > 0.2

				Delay-response	Cohen's d	6 bins, $p < 0.05$ 3 bin > 0.2
2.3f Main Sequence On and Off Target	NHP B, NHP T	20 WM sessions, 19 perception sessions	T-Test	<u>WM</u>	Cohen's d	0 bins, $p < 0.05$ 0 bin > 0.2
				<u>Perception</u>	Cohen's d	6 bins, $p < 0.05$ 3 bin > 0.2
2.6b Decoding Ensemble Over Time	NHP B, NHP T	19 WM sessions	Kruskal- Wallis	Time windows All trial time	$h(13,252) = 17.3$	$p = 0.19$
		14 time windows		Delay time	$h(3,72) = 4.9$	$p = 0.18$
2.6c Decoding Trial Outcome	NHP B, NHP T	19 WM sessions	T-Test	Compare decoding accuracy to chance (50%)		$p = 9.19e-07$
2.6d Decoding using Correct or Incorrect Trials	NHP B, NHP T	13 WM sessions	T-Test	Correct - Incorrect	$t(24) = 4.04$	$p = 4.71e-04$
2.7c Fixation on Target	NHP B, NHP T	20 WM sessions	Wilcoxon Rank-Sum Test	Correct - Incorrect	$Rank = 482$	$p = 0.053$

2.7d Eye Position Decoding	NHP B, NHP T	20 WM sessions	Kruskal- Wallis Tukey- Kramer Multiple Comparison	Epochs	$h(3,76) = 51.1$	$p < 0.0001$
				cueCue- delayDelay		$p = 0.04$
				cueCue- delayCue		$p < 0.0001$
				cueCue- cueDelay		$p < 0.0001$
				delayDelay- delayCue		$p < 0.0001$
				delayDelay- cueDelay		$p = 0.002$
				delayCue- cueDelay		$p = 0.01$
						$p = 0.96$
2.7f Decoding using firing rate or residuals	NHP B, NHP T	19 WM sessions	T-Test	Firing rate, residual values from linear model	$t(36) = 1.14$	$p = 0.26$
2.7h Decoding Neural Data Eye Position	NHP B, NHP T	19 WM sessions	Wilcoxon Rank-Sum Test	Cue - Delay	$Rank = 472$	$p = 0.003$
2.8a Cue - Cross Task Decoding	NHP B, NHP T	13 WM sessions, 13 perception sessions	Kruskal- Wallis Tukey- Kramer Multiple Comparison	Tasks	$h(3,48) = 39.2$	$p < 0.0001$
				WMWM- PerPer		$p = 0.77$
				WMWM- WMPer		$p < 0.0001$
				WMWM- PerWM		$p < 0.0001$
				PerPer - WMPer		$p = 0.0007$
				PerPer- PerWM		$p = 0.0005$
WMPer- PerWM	$p = 1$					

2.8b Delay - Cross Task Decoding	NHP B, NHP T	13 WM sessions, 13 perception sessions	Kruskal- Wallis Tukey- Kramer Multiple Comparison	Tasks	$h(3,48) =$ 39.2	$p <$ 0.0001
				WMWM- PerPer		$p = 0.99$
				WMWM- WMPer		$p <$ 0.0001
				WMWM- PerWM		$p =$ 0.0009
				PerPer - WMPer		$p <$ 0.0001
				PerPer- PerWM		$p =$ 0.0003
			WMPer- PerWM		$p = 0.79$	
2.8c WM Half- Trial Decoding	NHP B, NHP T	13 WM sessions	Kruskal- Wallis	Full and half WM trials	$h(1,24) =$ 11.6	$p =$ 0.0006
2.8e Cross Temporal Decoding	NHP B, NHP T	19 WM sessions	Kruskal- Wallis	Time windows		
				All trial time	$h(3,72) =$ 7.7	$p = 0.05$
				Delay time	$h(13,252) =$ 21.7	$p = 0.06$

Table 2C: Statistics reporting table for chapter 3.

Figure	Sample	Stat Test	Values																											
Task performance (percent correct) compared to chance (11%)	Ketamine-WM 18	Binomial test	<p>Pre-Injection: Ketamine-WM sessions $p < 0.001$ Saline-WM sessions $p < 0.001$ Ketamine-Perception sessions $p < 0.001$</p> <p>Early Post-Injection: Ketamine-WM sessions 13 sessions, $p < 0.05$ Saline-WM sessions $p < 0.0001$ Ketamine-Perception sessions $p < 0.0001$</p> <p>Late Post-Injection: Ketamine-WM sessions $p < 0.05$ Saline-WM sessions 6 sessions, $p < 0.05$ Ketamine-Perception sessions $p < 0.05$</p>																											
	Saline-WM 7																													
Fig. 3.1g Task performance (percent correct) compared between injection periods	Ketamine-WM 18	Two-way analysis of variance with post hoc pairwise comparisons	<p>Ketamine-WM: Pre-Injection, $mean=72$, $std=77$ Early Post-Injection, $mean=34$, $median=28$ Late Post-Injection, $mean=64$, $median=66$</p> <p>Saline-WM: Pre-Injection, $mean=80$, $median=84$ Early Post-Injection, $mean=77$, $median=90$ Late Post-Injection, $mean=66$, $median=76$</p> <p>Drug: $F=9.57$, $p=0.003$, $df=1,69$ Injection Period: $F=4.3$, $p=0.017$, $df=2,69$ Interaction: $F=4.85$, $p=0.011$, $df=2,69$</p> <table> <tr> <td>Ket pre-inject,</td> <td>Sal pre-inject,</td> <td>0.96</td> </tr> <tr> <td>Ket pre-inject,</td> <td>Ket early post-inject,</td> <td>0</td> </tr> <tr> <td>Ket pre-inject,</td> <td>Sal early post-inject,</td> <td>0.1</td> </tr> <tr> <td>Ket pre-inject,</td> <td>Ket late post-inject,</td> <td>0.88</td> </tr> <tr> <td>Ket pre-inject,</td> <td>Sal late post-inject,</td> <td>0.99</td> </tr> <tr> <td>Sal pre-inject,</td> <td>Ket early post-inject,</td> <td><0.01</td> </tr> <tr> <td>Sal pre-inject,</td> <td>Sal early post-inject,</td> <td>0.1</td> </tr> <tr> <td>Sal pre-inject,</td> <td>Ket late post-inject,</td> <td>0.55</td> </tr> <tr> <td>Sal pre-inject,</td> <td>Sal late post-inject,</td> <td>0.82</td> </tr> </table>	Ket pre-inject,	Sal pre-inject,	0.96	Ket pre-inject,	Ket early post-inject,	0	Ket pre-inject,	Sal early post-inject,	0.1	Ket pre-inject,	Ket late post-inject,	0.88	Ket pre-inject,	Sal late post-inject,	0.99	Sal pre-inject,	Ket early post-inject,	<0.01	Sal pre-inject,	Sal early post-inject,	0.1	Sal pre-inject,	Ket late post-inject,	0.55	Sal pre-inject,	Sal late post-inject,	0.82
	Ket pre-inject,			Sal pre-inject,	0.96																									
Ket pre-inject,	Ket early post-inject,	0																												
Ket pre-inject,	Sal early post-inject,	0.1																												
Ket pre-inject,	Ket late post-inject,	0.88																												
Ket pre-inject,	Sal late post-inject,	0.99																												
Sal pre-inject,	Ket early post-inject,	<0.01																												
Sal pre-inject,	Sal early post-inject,	0.1																												
Sal pre-inject,	Ket late post-inject,	0.55																												
Sal pre-inject,	Sal late post-inject,	0.82																												
Saline-WM 7																														

	Ketamine-Perception 4	Repeated measures analysis of variance	<p>Ket early post-inject, Sal early post-inject, <0.01</p> <p>Ket early post-inject, Ket late post-inject, 0.002</p> <p>Ket early post-inject, Sal late post-inject, 0.03</p> <p>Sal early post-inject, Ket late post-inject, 0.77</p> <p>Sal early post-inject, Sal late post-inject, 0.94</p> <p>Ket late post-inject, Sal late post-inject, 0.1</p> <p>Ketamine-Perception: Pre-Injection, <i>mean</i>=79, <i>median</i>=84 Early Post-Injection, <i>mean</i>=84, <i>median</i>=90 Late Post-Injection, <i>mean</i>=85, <i>median</i>=93</p> <p>$F=0.25, p=0.786, df=2,6$</p>
Fig. 3.1h Response time compared between injection periods	<p>Ketamine-WM 18 <i>n</i>=126 (values calculated per target location for conditions with trials in all injection periods)</p> <p>Saline-WM 7 <i>n</i>=55</p> <p>Ketamine-Perception 4 <i>n</i>=31</p>	Repeated measures analysis of variance with post hoc pairwise comparisons	<p>Ketamine-WM: Pre-Injection, <i>mean</i>=2.6, <i>median</i>=2.4 Early Post-Injection, <i>mean</i>=3.2, <i>median</i>=2.9 Late Post-Injection, <i>mean</i>=2.7, <i>median</i>=2.5</p> <p>$F=16.81, p<0.0001, df=2,250$</p> <p>Post Hoc Early Post-Injection, Pre-Injection $p<0.0001$ Late Post-Injection, Pre-Injection $p=0.330$ Early Post-Injection, Late Post-Injection $p<0.0001$</p> <p>Saline-WM: Pre-Injection, <i>mean</i>=2.6, <i>median</i>=2.4 Early Post-Injection, <i>mean</i>=2.7, <i>median</i>=2.5 Late Post-Injection, <i>mean</i>=2.7, <i>median</i>=2.4 $F=1.71, p=0.186, df=2,108$</p> <p>Ketamine-Perception: Pre-Injection, <i>mean</i>=2.5, <i>median</i>=2.3 Early Post-Injection, <i>mean</i>=2.5, <i>median</i>=2.5 Late Post-Injection, <i>mean</i>=2.5, <i>median</i>=2.5 $F=0.22, p=0.800, df=2,60$</p>
Fig. 3.1l Navigation in environment (difference in cells entered)	NHP T 8 Number of cells (25) * number of target locations with trials Early post injection – pre-injection	Two-way analysis of variance with interaction effect with post hoc comparisons	<p>NHP T: Ketamine Early Post-Injection – Pre-Injection, <i>mean</i>=6.9, <i>median</i>=4.2 Late Post-Injection – Pre-Injection, <i>mean</i>=3.3, <i>median</i>=0.9 Early Post-Injection – Late Post-Injection, <i>mean</i>=6.6, <i>median</i>=2.9</p> <p>Saline Early Post-Injection – Pre-Injection,</p>

<p>Ketamine, $n=154$ Saline, $n=161$ Late post-injection – pre-injection Ketamine, $n=124$ Saline, $n=125$ Early post-injection – late post-injection Ketamine, $n=159$ Saline, $n=115$</p> <p>NHP B 9 Number of cells (25) * number of target locations with trials Early post injection – pre-injection Ketamine, $n=162$ Saline, $n=158$ Late post-injection – pre-injection Ketamine, $n=163$ Saline, $n=157$ Early post-injection – late post-injection Ketamine, $n=134$ Saline, $n=145$</p> <p>Ketamine-Perception 4 Early post injection – pre-injection Perception, $n=197$ Late post-injection – pre-injection Perception, $n=194$</p>	<p>$mean=3.2$, $median=0$ Late Post-Injection – Pre-Injection, $mean=4.8$, $median=0$ Early Post-Injection – Late Post-Injection, $mean=2.5$, $median=0$</p> <p>Ketamine and Saline Comparison Epoch, $F=0.97$, $p=0.380$, $df=2,832$ Drug, $F=12.1$, $p=0.0005$, $df=1,832$ Interaction, $F=8.73$, $p=0.0002$, $df=2,832$</p> <p>Post Hoc Early Post-Injection, Pre-Injection $p=0.002$ Late Post-Injection, Pre-Injection $p=0.717$ Early Post-Injection, Late Post-Injection $p=0.001$</p> <p>NHP B: Ketamine Early Post-Injection – Pre-Injection, $mean=4.6$, $median=2.1$ Late Post-Injection – Pre-Injection, $mean=3.6$, $median=1.8$ Early Post-Injection – Late Post-Injection, $mean=4.1$, $median=2.3$</p> <p>Saline Early Post-Injection – Pre-Injection, $mean=2.6$, $median=1.2$ Late Post-Injection – Pre-Injection $mean=3.4$, $median=1.4$, Early Post-Injection – Late Post-Injection, $mean=2.4$, $median=0.8$</p> <p>Ketamine and Saline Comparison Epoch, $F=0.51$, $p=0.604$, $df=2,913$ Drug, $F=15.16$, $p=0.0001$, $df=1,913$ Interaction, $F=3.4$, $p=0.034$, $df=2,913$</p> <p>Post Hoc Early Post-Injection, Pre-Injection $p=0.004$ Late Post-Injection, Pre-Injection $p=1$ Early Post-Injection, Late Post-Injection $p=0.044$</p> <p>Perception Early Post-Injection – Pre-Injection, $mean=1.8$, $median=0$ Late Post-Injection – Pre-Injection</p>
--	---

	<p>Early post-injection – late post-injection Perception, $n=203$</p> <p>Ketamine-WM 17</p>		<p>$mean=2.2, median=0$ Early Post-Injection – Late Post-Injection, $mean=2.0, median=0$</p> <p>Ketamine-WM and Ketamine-Perception Comparison</p> <p>Epoch, $F=3.09, p=0.046, df=2,1022$ Drug, $F=25.6, p=0, df=1,1022$ Interaction, $F=5.26, p=0.005, df=2,1022$</p> <p>Post Hoc Early Post-Injection, Pre-Injection $p=0$ Late Post-Injection, Pre-Injection $p=0.999$ Early Post-Injection, Late Post-Injection $p=0.007$</p>
Fig. 3.2c Proportion of tuned units ketamine-WM sessions compared between injection periods	<p>17 $n=51$, selectivity proportions combined (17 per epoch)</p>	<p>Analysis of variance with post hoc testing</p> <p>Chi-Square Test</p>	<p>Pre-Injection, $mean=11.36, median=10.93$ Early Post-Injection, $mean=6.23, median=5.20$ Late Post-Injection, $mean=9.62, median=7.79$</p> <p>$F=8.73, p=0.0002, df=2,303$ Post Hoc Pre-Injection, Early Post-Injection $p=0.0001$ Pre-Injection, Late Post-Injection $p=0.342$ Early Post-Injection, Late Post-Injection $p=0.018$</p> <p>Pre-Injection- Early Post-Injection, $p=0, \chi^2=128.67$ Pre-Injection- Late Post-Injection, $p=0.97, \chi^2=0.002$ Early Post-Injection- Late Post-Injection, $p=0, \chi^2=126.52$</p>
Fig. 3.2d Proportion of tuned units saline-WM sessions compared between injection periods	<p>7 $n=21$, selectivity proportions combined (7 per epoch)</p>	<p>One-way analysis of variance</p> <p>Chi-Square Test</p>	<p>Pre-Injection, $mean=11.7, median=13.5$ Early Post-Injection, $mean=10.04, median=10.26$ Late Post-Injection, $mean=8.04, median=8.39$ $F=1.93, p=0.1498, df=2,123$</p> <p>Pre-Injection- Early Post-Injection, $p=0.231, \chi^2=1.44$ Pre-Injection- Late Post-Injection, $p=5.26e-07, \chi^2=25.17$ Early Post-Injection- Late Post-Injection, $p=1.3e-04, \chi^2=14.65$</p>
Fig. 3.2f Change in slope magnitude	<p>17</p>	<p>Kruskal-Wallis one-way analysis</p>	<p>Ketamine Pre-Injection, $mean=-0.411, median=-0.413$ Early Post-Injection, $mean=-0.286, median=-0.298$</p>

between injection periods		of variance with post hoc testing	<p>Late Post-Injection, <i>mean</i>=-0.315, <i>median</i>=-0.306 <i>H</i>=13.48, <i>p</i>=0.0012, <i>df</i>=2,48</p> <p>Post Hoc Pre-Injection, Early Post-Injection, <i>p</i>=0.001 Pre-Injection, Late Post-Injection, <i>p</i>=0.017 Early Post-Injection, Late Post-Injection, <i>p</i>=0.741</p> <p>Saline <i>H</i>=5.7, <i>p</i>= 0.058, <i>df</i>=2,18</p> <p>Post Hoc Pre-Injection, Early Post-Injection, <i>p</i>=0.097 Pre-Injection, Late Post-Injection, <i>p</i>=0.097 Early Post-Injection, Late Post-Injection, <i>p</i>=1</p>																																																																																																																				
Fig. 3.3a SVM decoding accuracy ketamine-WM compared between injection periods	16	Kruskal-Wallis one-way analysis of variance with post hoc testing	<p>Cue: <i>df</i>=2</p> <table border="1" data-bbox="813 682 1422 1207"> <thead> <tr> <th># of Neurons</th> <th><i>p</i></th> <th><i>H</i></th> <th>pre-post, <i>p</i></th> </tr> </thead> <tbody> <tr><td>1</td><td>0.013</td><td>8.76</td><td>0.012</td></tr> <tr><td>2</td><td>0.008</td><td>9.74</td><td>0.007</td></tr> <tr><td>3</td><td>0.008</td><td>9.61</td><td>0.008</td></tr> <tr><td>4</td><td>0.015</td><td>8.37</td><td>0.016</td></tr> <tr><td>5</td><td>0.016</td><td>8.25</td><td>0.018</td></tr> <tr><td>6</td><td>0.024</td><td>7.42</td><td>0.023</td></tr> <tr><td>7</td><td>0.046</td><td>6.15</td><td>0.039</td></tr> <tr><td>8</td><td>0.050</td><td>5.99</td><td>0.042</td></tr> <tr><td>9</td><td>0.052</td><td>5.91</td><td>0.046</td></tr> <tr><td>10</td><td>0.049</td><td>6.03</td><td>0.043</td></tr> <tr><td>11</td><td>0.069</td><td>5.36</td><td>0.062</td></tr> <tr><td>12</td><td>0.075</td><td>5.17</td><td>0.067</td></tr> <tr><td>13</td><td>0.069</td><td>5.36</td><td>0.062</td></tr> <tr><td>14</td><td>0.067</td><td>5.4</td><td>0.060</td></tr> <tr><td>15</td><td>0.108</td><td>4.45</td><td>0.099</td></tr> <tr><td>16</td><td>0.076</td><td>5.15</td><td>0.072</td></tr> </tbody> </table> <p>Delay: <i>df</i>=2</p> <table border="1" data-bbox="813 1249 1422 1845"> <thead> <tr> <th># of Neurons</th> <th><i>p</i></th> <th><i>H</i></th> <th>pre-post, <i>p</i></th> </tr> </thead> <tbody> <tr><td>1</td><td>0.002</td><td>12.78</td><td>0.002</td></tr> <tr><td>2</td><td>0.004</td><td>10.86</td><td>0.006</td></tr> <tr><td>3</td><td>0.008</td><td>9.79</td><td>0.011</td></tr> <tr><td>4</td><td>0.009</td><td>9.43</td><td>0.016</td></tr> <tr><td>5</td><td>0.013</td><td>8.63</td><td>0.023</td></tr> <tr><td>6</td><td>0.006</td><td>10.21</td><td>0.013</td></tr> <tr><td>7</td><td>0.004</td><td>10.91</td><td>0.012</td></tr> <tr><td>8</td><td>0.006</td><td>10.21</td><td>0.018</td></tr> <tr><td>9</td><td>0.006</td><td>10.34</td><td>0.017</td></tr> <tr><td>10</td><td>0.004</td><td>11.06</td><td>0.010</td></tr> <tr><td>11</td><td>0.002</td><td>12.71</td><td>0.006</td></tr> </tbody> </table>	# of Neurons	<i>p</i>	<i>H</i>	pre-post, <i>p</i>	1	0.013	8.76	0.012	2	0.008	9.74	0.007	3	0.008	9.61	0.008	4	0.015	8.37	0.016	5	0.016	8.25	0.018	6	0.024	7.42	0.023	7	0.046	6.15	0.039	8	0.050	5.99	0.042	9	0.052	5.91	0.046	10	0.049	6.03	0.043	11	0.069	5.36	0.062	12	0.075	5.17	0.067	13	0.069	5.36	0.062	14	0.067	5.4	0.060	15	0.108	4.45	0.099	16	0.076	5.15	0.072	# of Neurons	<i>p</i>	<i>H</i>	pre-post, <i>p</i>	1	0.002	12.78	0.002	2	0.004	10.86	0.006	3	0.008	9.79	0.011	4	0.009	9.43	0.016	5	0.013	8.63	0.023	6	0.006	10.21	0.013	7	0.004	10.91	0.012	8	0.006	10.21	0.018	9	0.006	10.34	0.017	10	0.004	11.06	0.010	11	0.002	12.71	0.006
# of Neurons	<i>p</i>	<i>H</i>	pre-post, <i>p</i>																																																																																																																				
1	0.013	8.76	0.012																																																																																																																				
2	0.008	9.74	0.007																																																																																																																				
3	0.008	9.61	0.008																																																																																																																				
4	0.015	8.37	0.016																																																																																																																				
5	0.016	8.25	0.018																																																																																																																				
6	0.024	7.42	0.023																																																																																																																				
7	0.046	6.15	0.039																																																																																																																				
8	0.050	5.99	0.042																																																																																																																				
9	0.052	5.91	0.046																																																																																																																				
10	0.049	6.03	0.043																																																																																																																				
11	0.069	5.36	0.062																																																																																																																				
12	0.075	5.17	0.067																																																																																																																				
13	0.069	5.36	0.062																																																																																																																				
14	0.067	5.4	0.060																																																																																																																				
15	0.108	4.45	0.099																																																																																																																				
16	0.076	5.15	0.072																																																																																																																				
# of Neurons	<i>p</i>	<i>H</i>	pre-post, <i>p</i>																																																																																																																				
1	0.002	12.78	0.002																																																																																																																				
2	0.004	10.86	0.006																																																																																																																				
3	0.008	9.79	0.011																																																																																																																				
4	0.009	9.43	0.016																																																																																																																				
5	0.013	8.63	0.023																																																																																																																				
6	0.006	10.21	0.013																																																																																																																				
7	0.004	10.91	0.012																																																																																																																				
8	0.006	10.21	0.018																																																																																																																				
9	0.006	10.34	0.017																																																																																																																				
10	0.004	11.06	0.010																																																																																																																				
11	0.002	12.71	0.006																																																																																																																				

			<table> <tbody> <tr><td>12</td><td>0.003</td><td>11.35</td><td>0.012</td></tr> <tr><td>13</td><td>0.004</td><td>11.08</td><td>0.015</td></tr> <tr><td>14</td><td>0.004</td><td>11.07</td><td>0.013</td></tr> <tr><td>15</td><td>0.004</td><td>11.07</td><td>0.014</td></tr> <tr><td>16</td><td>0.004</td><td>11.26</td><td>0.015</td></tr> </tbody> </table> <p>Response: $df=2$</p> <table> <thead> <tr> <th># of Neurons</th> <th>p</th> <th>H</th> <th>pre-post, p</th> </tr> </thead> <tbody> <tr><td>1</td><td>0.007</td><td>10.03</td><td>0.007</td></tr> <tr><td>2</td><td>0.014</td><td>8.48</td><td>0.010</td></tr> <tr><td>3</td><td>0.010</td><td>9.32</td><td>0.007</td></tr> <tr><td>4</td><td>0.007</td><td>9.94</td><td>0.005</td></tr> <tr><td>5</td><td>0.009</td><td>9.42</td><td>0.007</td></tr> <tr><td>6</td><td>0.009</td><td>9.46</td><td>0.007</td></tr> <tr><td>7</td><td>0.006</td><td>10.18</td><td>0.006</td></tr> <tr><td>8</td><td>0.011</td><td>9.08</td><td>0.013</td></tr> <tr><td>9</td><td>0.011</td><td>8.96</td><td>0.014</td></tr> <tr><td>10</td><td>0.010</td><td>9.15</td><td>0.014</td></tr> <tr><td>11</td><td>0.010</td><td>9.25</td><td>0.014</td></tr> <tr><td>12</td><td>0.010</td><td>9.3</td><td>0.016</td></tr> <tr><td>13</td><td>0.013</td><td>8.68</td><td>0.020</td></tr> <tr><td>14</td><td>0.014</td><td>8.54</td><td>0.018</td></tr> <tr><td>15</td><td>0.013</td><td>8.75</td><td>0.017</td></tr> <tr><td>16</td><td>0.018</td><td>8</td><td>0.023</td></tr> </tbody> </table>	12	0.003	11.35	0.012	13	0.004	11.08	0.015	14	0.004	11.07	0.013	15	0.004	11.07	0.014	16	0.004	11.26	0.015	# of Neurons	p	H	pre-post, p	1	0.007	10.03	0.007	2	0.014	8.48	0.010	3	0.010	9.32	0.007	4	0.007	9.94	0.005	5	0.009	9.42	0.007	6	0.009	9.46	0.007	7	0.006	10.18	0.006	8	0.011	9.08	0.013	9	0.011	8.96	0.014	10	0.010	9.15	0.014	11	0.010	9.25	0.014	12	0.010	9.3	0.016	13	0.013	8.68	0.020	14	0.014	8.54	0.018	15	0.013	8.75	0.017	16	0.018	8	0.023
12	0.003	11.35	0.012																																																																																								
13	0.004	11.08	0.015																																																																																								
14	0.004	11.07	0.013																																																																																								
15	0.004	11.07	0.014																																																																																								
16	0.004	11.26	0.015																																																																																								
# of Neurons	p	H	pre-post, p																																																																																								
1	0.007	10.03	0.007																																																																																								
2	0.014	8.48	0.010																																																																																								
3	0.010	9.32	0.007																																																																																								
4	0.007	9.94	0.005																																																																																								
5	0.009	9.42	0.007																																																																																								
6	0.009	9.46	0.007																																																																																								
7	0.006	10.18	0.006																																																																																								
8	0.011	9.08	0.013																																																																																								
9	0.011	8.96	0.014																																																																																								
10	0.010	9.15	0.014																																																																																								
11	0.010	9.25	0.014																																																																																								
12	0.010	9.3	0.016																																																																																								
13	0.013	8.68	0.020																																																																																								
14	0.014	8.54	0.018																																																																																								
15	0.013	8.75	0.017																																																																																								
16	0.018	8	0.023																																																																																								
Fig. 3.3b SVM decoding accuracy saline-WM compared between injection periods	7	Kruskal-Wallis one-way analysis of variance	<p>Ensemble of 16 neurons:</p> <p>Cue: Pre-Injection, $mean=82.6$, $median=89.7$ Early Post-Injection, $mean=74.4$, $median=91.0$ Late Post-Injection, $mean=76.0$, $median=88.6$ $H=0.54$, $p=0.763$, $df=2,18$</p> <p>Delay: Pre-Injection, $mean=83.6$, $median=92.5$ Early Post-Injection, $mean=77.3$, $median=90.9$ Late Post-Injection, $mean=73.6$, $median=89.2$ $H=1.12$, $p=0.571$, $df=2,18$</p> <p>Response: Pre-Injection, $mean=83.9$, $median=94.1$ Early Post-Injection, $mean=79.3$, $median=91.1$</p>																																																																																								

			Late Post-Injection, <i>mean</i> =76.9, <i>median</i> =85.9 <i>H</i> =1.36, <i>p</i> =0.507, <i>df</i> =2,18 All other neuron ensemble sizes, <i>p</i> >0.05
Fig. 3.4d Change in FR between injection periods for narrow spiking neurons	17 <i>n</i> =13 (arrays per session containing selective neurons)	Wilcoxon signed-ranks test, 1-tailed	Preferred Location, Pre-Injection, <i>mean</i> =0.45, <i>median</i> =0.47 Post-Injection, <i>mean</i> =0.28, <i>median</i> =0.21 <i>Z</i> =1.66, <i>p</i> =0.049 Least-Preferred Location, Pre-Injection, <i>mean</i> =0.21, <i>median</i> =0.13 Post-Injection, <i>mean</i> =0.24, <i>median</i> =0.09 <i>Z</i> =-0.116, <i>p</i> =0.546
Fig. 3.4f Change in FR between injection periods for broad spiking neurons	17 <i>n</i> =27 (arrays per session containing selective neurons)	Wilcoxon signed-ranks test, 1-tailed	Preferred Location, Pre-Injection, <i>mean</i> =0.43, <i>median</i> =0.43 Post-Injection, <i>mean</i> =0.42, <i>median</i> =0.43 <i>Z</i> =0.383, <i>p</i> =0.649 Least-Preferred Location, Pre-Injection, <i>mean</i> =0.23, <i>median</i> =0.25 Post-Injection, <i>mean</i> =0.34, <i>median</i> =0.36 <i>Z</i> =-2.50, <i>p</i> =0.006
Fig. 3.5b Percent of fixation time on target	Ketamine 18 Saline 7	Two-way analysis of variance with interaction	Ketamine: Pre-Injection, <i>mean</i> =6.97, <i>median</i> =3.64 Early Post-Injection, <i>mean</i> =16.92, <i>median</i> =13.07 Late Post-Injection, <i>mean</i> =6.98, <i>median</i> =4.25 Saline: Pre-Injection, <i>mean</i> =7.28, <i>median</i> =1.85 Early Post-Injection, <i>mean</i> =6.65, <i>median</i> =2.15 Late Post-Injection, <i>mean</i> =5.73, <i>median</i> =2.86 Drug: <i>F</i> =1.73, <i>p</i> =0.193, <i>df</i> =1,69 Injection Period: <i>F</i> =1.42, <i>p</i> =0.248, <i>df</i> =2,69 Interaction: <i>F</i> =1.35, <i>p</i> =0.267, <i>df</i> =2,69
Fig. 3.5c Eye data SVM decoding compared between injection periods	16	Kruskal-Wallis one-way analysis of variance	Cue: Pre-Injection, <i>mean</i> =53.9, <i>median</i> =57.6 Early Post-Injection, <i>mean</i> =52.2, <i>median</i> =52.0 Late Post-Injection, <i>mean</i> =57.7, <i>median</i> =59.3 <i>H</i> =4.01, <i>p</i> =0.135, <i>df</i> =2,45 Delay: Pre-Injection, <i>mean</i> =47.8, <i>median</i> =47.8 Early Post-Injection, <i>mean</i> =46.5, <i>median</i> =46.7 Late Post-Injection, <i>mean</i> =52.1, <i>median</i> =51.8 <i>H</i> =4.59, <i>p</i> =0.101, <i>df</i> =2,45
Fig. 3.5c Eye data SVM decoding accuracy compared	16 <i>n</i> =48, data combined between injection periods	Wilcoxon signed-ranks test, 2-tailed	<i>Z</i> =3.18, <i>p</i> =0.002

between cue and delay epochs			
Fig. 3.5d SVM decoding accuracy for eye data compared to decoding accuracy for neural ensembles	16	Kruskal-Wallis one-way analysis of variance	<p>Cue: Eye data <i>mean</i>=53.9, <i>median</i>=57.6 Neural data <i>mean</i>=83.6, <i>median</i>=91 $H=14.78$, $p=0.0001$, $df=1,30$</p> <p>Delay: Eye data <i>mean</i>=47.8, <i>median</i>=47.8 Neural data <i>mean</i>=86.2, <i>median</i>=91.9 $H=22.91$, $p=1.69e-06$, $df=1,30$</p>
Fig. 3.5d Eye data decoding accuracy compared to chance	16	One sample t-test, 2-tailed	<p>Cue: $T=8.38$, $p=4.82e-07$, $df=15$</p> <p>Delay: $T=8.53$, $p=3.87e-07$, $df=15$</p>
Figure. S3.6a Correct trial SVM decoding accuracy compared between injection periods	Pre-injection 13 Early Post-Injection 12 Late Post-Injection 16	Kruskal-Wallis one-way analysis of variance with post hoc testing	<p>Cue: Pre-Injection, <i>mean</i>=94.5, <i>median</i>=95.8 Early Post-Injection, <i>mean</i>=76.9, <i>median</i>=71.4 Late Post-Injection, <i>mean</i>=82.4, <i>median</i>=88.3 $H=11.11$, $p=0.004$, $df=2,38$ Post Hoc Pre-Injection, Early Post-Injection, $p=0.004$ Pre-Injection, Late Post-Injection, $p=0.031$ Early Post-Injection, Late Post-Injection, $p=0.671$</p> <p>Delay: Pre-Injection, <i>mean</i>=93.4, <i>median</i>=95.2 Early Post-Injection, <i>mean</i>=80.5, <i>median</i>=79.5 Late Post-Injection, <i>mean</i>=86.6, <i>median</i>=90.9 $H=8.35$, $p=0.015$, $df=2,38$ Post Hoc Pre-Injection and Early Post-Injection, $p=0.012$ Pre-Injection and Late Post-Injection, $p=0.139$ Early Post-Injection and Late Post-Injection, $p=0.499$</p> <p>Response: Pre-Injection, <i>mean</i>=95.8, <i>median</i>=96.3 Early Post-Injection, <i>mean</i>=87.6, <i>median</i>=92.9 Late Post-Injection, <i>mean</i>=90.4, <i>median</i>=94 $H=5.5$, $p=0.064$, $df=2,38$ Post Hoc Pre-Injection and Early Post-Injection, $p=0.062$ Pre-Injection and Late Post-Injection, $p=0.201$</p>

			Early Post-Injection and Late Post-Injection, $p=0.768$
Figure. S3.6a Correct trial SVM decoding accuracy compared to chance (33%)	Pre-injection 13 Early Post-Injection 12 Late Post-Injection 16	One sample t-test, 2-tailed	Cue: Pre: $T=40.61$, $p=3.21e-14$, $df=12$ Early-Post: $T=10.19$, $p=6.1e-07$, $df=11$ Late-Post: $T=13.38$, $p=9.65e-10$, $df=15$ Delay: Pre: $T=28.01$, $p=2.66e-12$, $df=12$ Early-Post: $T=12.88$, $p=5.6e-08$, $df=11$ Late-Post: $T=18.84$, $p=7.46e-12$, $df=15$ Response: Pre: $T=52.63$, $p=1.46e-15$, $df=12$ Early-Post: $T=15.05$, $p=1.1e-08$, $df=11$ Late-Post: $T=24.81$, $p=1.36e-13$, $df=15$
Figure. S3.6b SVM decoding accuracy compared between correct and all trials	Pre-injection 13 Early Post-Injection 12 Late Post-Injection 16	Wilcoxon signed-ranks test, 1-tailed	Pre-Injection Period: Cue: $Z=1.38$, $p=0.083$ Delay: $Z=0.719$, $p=0.236$ Response: $Z=1.44$, $p=0.075$ Early Post-Injection Period: Cue: $Z=1.53$, $p=0.063$ Delay: $Z=1.76$, $p=0.039$ Response: $Z=2.80$, $p=0.003$ Late Post-Injection Period Cue: $Z=1.52$, $p=0.063$ Delay: $Z=3.07$, $p=0.001$ Response: $Z=3.41$, $p=0.0003$
Figure. S3.7a, b Change in FR for narrow and broad spiking neurons saline-WM	7 Narrow, $n=5$ (arrays per session containing selective neurons) Broad, $n=11$	Wilcoxon signed-ranks test, 1-sided	Narrow: Preferred Location, Pre-Injection, $mean=0.43$, $median=0.47$ Post-Injection, $mean=0.42$, $median=0.48$ $p=0.500$ Least-Preferred Location, Pre-Injection, $mean=0.32$, $median=0.35$ Post-Injection, $mean=0.26$, $median=0.33$ $p=0.500$ Broad: Preferred Location, Pre-Injection, $mean=0.52$, $median=0.51$ Post-Injection, $mean=0.42$, $median=0.45$ $p=0.803$ Least-Preferred Location, Pre-Injection, $mean=0.29$, $median=0.29$ Post-Injection, $mean=0.32$, $median=0.28$ $p=0.422$
Figure. S3.7c Narrow spiking ranked	Narrow, $n=13$	Wilcoxon signed-ranks test, 1-sided	Rank 1 Pre-Injection, $mean=0.343$, $median=0.363$ Post-Injection, $mean=0.212$, $median=0.161$ $Z=1.66$, $p=0.049$

target location responses			<p>Rank 2 Pre-Injection, <i>mean</i>=0.302, <i>median</i>=0.383 Post-Injection, <i>mean</i>=0.245, <i>median</i>=0.255 <i>Z</i>=0.843, <i>p</i>=0.120</p> <p>Rank 3 Pre-Injection, <i>mean</i>=0.264, <i>median</i>=0.323 Post-Injection, <i>mean</i>=0.278, <i>median</i>=0.282 <i>Z</i>=-0.217, <i>p</i>=0.586</p> <p>Rank 4 Pre-Injection, <i>mean</i>=0.246, <i>median</i>=0.224 Post-Injection, <i>mean</i>=0.254, <i>median</i>=0.164 <i>Z</i>=0.232, <i>p</i>=0.592</p> <p>Rank 5 Pre-Injection, <i>mean</i>=0.219, <i>median</i>=0.242 Post-Injection, <i>mean</i>=0.230, <i>median</i>=0.234 <i>Z</i>=0.027, <i>p</i>=0.511</p> <p>Rank 6 Pre-Injection, <i>mean</i>=0.210, <i>median</i>=0.213 Post-Injection, <i>mean</i>=0.246, <i>median</i>=0.194 <i>Z</i>=-0.299, <i>p</i>=0.382</p> <p>Rank 7 Pre-Injection, <i>mean</i>=0.196, <i>median</i>=0.147 Post-Injection, <i>mean</i>=0.274, <i>median</i>=0.298 <i>Z</i>=-0.708, <i>p</i>=0.240</p> <p>Rank 8 Pre-Injection, <i>mean</i>=0.204, <i>median</i>=0.184 Post-Injection, <i>mean</i>=0.312, <i>median</i>=0.278 <i>Z</i>=-0.380, <i>p</i>=0.352</p> <p>Rank 9 Pre-Injection, <i>mean</i>=0.158, <i>median</i>=0.102 Post-Injection, <i>mean</i>=0.182, <i>median</i>=0.072 <i>Z</i>=0, <i>p</i>=0.500</p>
Figure. S3.7d Broad spiking ranked target location responses	Broad, <i>n</i> =27	Wilcoxon signed-ranks test, 1-sided	<p>Rank 1 Pre-Injection, <i>mean</i>=0.388, <i>median</i>=0.388 Post-Injection, <i>mean</i>=0.375, <i>median</i>=0.383 <i>Z</i>=0.436, <i>p</i>=0.332</p> <p>Rank 2 Pre-Injection, <i>mean</i>=0.348, <i>median</i>=0.366 Post-Injection, <i>mean</i>=0.323, <i>median</i>=0.325 <i>Z</i>=0.779, <i>p</i>=0.218</p> <p>Rank 3 Pre-Injection, <i>mean</i>=0.343, <i>median</i>=0.331 Post-Injection, <i>mean</i>=0.358, <i>median</i>=0.395 <i>Z</i>=-0.621, <i>p</i>=0.733</p> <p>Rank 4 Pre-Injection, <i>mean</i>=0.320, <i>median</i>=0.312</p>

			<p>Post-Injection, <i>mean</i>=0.341, <i>median</i>=0.357 <i>Z</i>=-0.349, <i>p</i>=0.364</p> <p>Rank 5 Pre-Injection, <i>mean</i>=0.299, <i>median</i>=0.298 Post-Injection, <i>mean</i>=0.350, <i>median</i>=0.358 <i>Z</i>=-1.34, <i>p</i>=0.09</p> <p>Rank 6 Pre-Injection, <i>mean</i>=0.284, <i>median</i>=0.280 Post-Injection, <i>mean</i>=0.341, <i>median</i>=0.323 <i>Z</i>=-1.01, <i>p</i>=0.156</p> <p>Rank 7 Pre-Injection, <i>mean</i>=0.242, <i>median</i>=0.249 Post-Injection, <i>mean</i>=0.273, <i>median</i>=0.290 <i>Z</i>=-0.711, <i>p</i>=0.238</p> <p>Rank 8 Pre-Injection, <i>mean</i>=0.229, <i>median</i>=0.244 Post-Injection, <i>mean</i>=0.268, <i>median</i>=0.301 <i>Z</i>=-1.318, <i>p</i>=0.094</p> <p>Rank 9 Pre-Injection, <i>mean</i>=0.211, <i>median</i>=0.223 Post-Injection, <i>mean</i>=0.299, <i>median</i>=0.321 <i>Z</i>=-2.30, <i>p</i>=0.011</p>
<p>Figure. S3.8a-f Eyes on screen time compared between injection periods</p>	<p>Ketamine-WM 18</p> <p>Saline-WM 7</p> <p>Ketamine-Perception 4</p>	<p>Kruskal-Wallis one-way analysis of variance with post hoc testing</p>	<p>Ketamine-WM Cue: Pre-Injection, <i>mean</i>=1382.60, <i>median</i>=1388.31 Early Post-Injection, <i>mean</i>=1434.18, <i>median</i>=1439.26 Late Post-Injection, <i>mean</i>=1412.15, <i>median</i>=1411.39</p> <p><i>H</i>=14.16, <i>p</i>=0.0008, <i>df</i>=2,51 Post Hoc Pre-Injection, Early Post-Injection, <i>p</i>=0.0005 Pre-Injection, Late Post-Injection, <i>p</i>=0.180 Early Post-Injection, Late Post-Injection, <i>p</i>=0.114</p> <p>Delay: Pre-Injection, <i>mean</i>=866.65, <i>median</i>=890.28 Early Post-Injection, <i>mean</i>=939.50, <i>median</i>=946.17 Late Post-Injection, <i>mean</i>=901.11, <i>median</i>=938.40</p> <p><i>H</i>=11.15, <i>p</i>=0.004, <i>df</i>=2,51 Post Hoc Pre-Injection, Early Post-Injection, <i>p</i>=0.003 Pre-Injection, Late Post-Injection, <i>p</i>=0.176 Early Post-Injection, Late Post-Injection, <i>p</i>=0.264</p> <p>Saline-WM Cue:</p>

			<p>Pre-Injection, <i>mean</i>=1399.29, <i>median</i>=1407.69 Early Post-Injection, <i>mean</i>=1386.25, <i>median</i>=1377.65 Late Post-Injection, <i>mean</i>=1383.77, <i>median</i>=1380.16 <i>H</i>=0.27, <i>p</i>=0.872, <i>df</i>=2,18</p> <p>Delay: Pre-Injection, <i>mean</i>=875.11, <i>median</i>=863.25 Early Post-Injection, <i>mean</i>=873.23, <i>median</i>=839.04 Late Post-Injection, <i>mean</i>=890.06, <i>median</i>=892.58 <i>H</i>=0.14, <i>p</i>=0.932, <i>df</i>=2,18</p> <p>Ketamine-Perception Cue: Pre-Injection, <i>mean</i>=1397.99, <i>median</i>=1397.98 Early Post-Injection, <i>mean</i>=1448.03, <i>median</i>=1447.44 Late Post-Injection, <i>mean</i>=1436.54, <i>median</i>=1443.50 <i>H</i>=3.85, <i>p</i>=0.146, <i>df</i>=2,9</p> <p>Delay: Pre-Injection, <i>mean</i>=879.42, <i>median</i>=896.63 Early Post-Injection, <i>mean</i>=954.42, <i>median</i>=953.70 Late Post-Injection, <i>mean</i>=942.55, <i>median</i>=945.68 <i>H</i>=1.5, <i>p</i>=0.472, <i>df</i>=2,9</p>
<p>Figure. S3.8g-l Percent of fixations on target location compared between injection periods</p>	<p>Ketamine-WM 18 <i>n</i>=9 target locations</p> <p>Saline-WM 7 <i>n</i>=9 target locations</p> <p>Ketamine-Perception 4 <i>n</i>=9 target locations</p>	<p>Kruskal-Wallis one-way analysis of variance</p>	<p>Ketamine-WM Cue: Pre-Injection, <i>mean</i>=22.5, <i>median</i>=24.2 Early Post-Injection, <i>mean</i>=26.9, <i>median</i>=24.6 Late Post-Injection, <i>mean</i>=24.0, <i>median</i>=24.9 <i>H</i>=0.84, <i>p</i>=0.658, <i>df</i>=2,24</p> <p>Delay: Pre-Injection, <i>mean</i>=26.9, <i>median</i>=26.2 Early Post-Injection, <i>mean</i>=24.9, <i>median</i>=20.8 Late Post-Injection, <i>mean</i>=28.2, <i>median</i>=26.5 <i>H</i>=1.03, <i>p</i>=0.598, <i>df</i>=2,24</p> <p>Saline-WM Cue: Pre-Injection, <i>mean</i>=21.5, <i>median</i>=22.9 Early Post-Injection, <i>mean</i>=20.0, <i>median</i>=21.1 Late Post-Injection, <i>mean</i>=23.0, <i>median</i>=25.2 <i>H</i>=0.79, <i>p</i>=0.673, <i>df</i>=2,24</p> <p>Delay: Pre-Injection, <i>mean</i>=22.0, <i>median</i>=22.5 Early Post-Injection, <i>mean</i>=27.2, <i>median</i>=27.6 Late Post-Injection, <i>mean</i>=35.4, <i>median</i>=36.1 <i>H</i>=3.65, <i>p</i>=0.161, <i>df</i>=2,24</p>

			<p>Ketamine-Perception</p> <p>Cue: Pre-Injection, <i>mean</i>=28.9, <i>median</i>=30.0 Early Post-Injection, <i>mean</i>=22.6, <i>median</i>=21.7 Late Post-Injection, <i>mean</i>=23.1, <i>median</i>=26.9 <i>H</i>=1.03, <i>p</i>=0.599, <i>df</i>=2,24</p> <p>Delay: Pre-Injection, <i>mean</i>=21.7, <i>median</i>=17.3 Early Post-Injection, <i>mean</i>=21.9, <i>median</i>=22.0 Late Post-Injection, <i>mean</i>=20.6, <i>median</i>=20.3 <i>H</i>=0.7, <i>p</i>=0.704, <i>df</i>=2,24</p>
--	--	--	--

Table 3C: Statistics reporting table for chapter 4.

Figure	Subject	Data Counts	Stat Test	Comparison	Stat Values	P-Value
4.1e Percent of Correct Trials	NHP B, NHP T	20 WM Sessions			<u>NHP B</u> mean = 87% median = 85% <u>NHP T</u> mean = 57% median = 56%	
4.2g Difference in Means	NHP B, NHP T	17 WM Sessions	Wilcoxon Signed Rank Test	Correct and incorrect trials	<u>Rank</u> = 161 <u>Correct</u> mean = 253.98 median = 270.93 <u>Incorrect</u> mean = 93.69 median = 71.43	0.001
4.3d Target Decoding	NHP B, NHP T	17 WM sessions	T-Test	Decoding Accuracy for delay vs chance (11%)	$t = 5.14$ <u>Decoding accuracy:</u> mean = 23% median = 26%	9.72E-05
4.3e Supervised Column Decoding	NHP B, NHP T	17 WM sessions	T-Test	Decoding Accuracy for delay vs chance (33%)	$t = 6.06$ <u>Decoding accuracy:</u>	1.66E-05

					mean = 63% median = 74%	
4.3f Unsupervised Column Decoding	NHP B, NHP T	17 WM sessions	T-Test	Decoding Accuracy for delay vs chance (33%)	$t = 7.9$ <u>Decoding accuracy:</u> median = 66%	6.5E-07
4.4g Correct vs Incorrect Correlation	NHP B, NHP T	11 WM Sessions	Paired T Test	Correct and incorrect trials	$t = 4.9643$ <u>Correct mean</u> = 0.45 median = 0.47 <u>Incorrect mean</u> = 0.30 median = 0.30	5.66E-04
4.4h WM vs Perception	NHP B, NHP T	12 WM Sessions, 12 Perception Sessions	Paired T Test	Observed vs correct correlations in WM task vs perception task delay epochs	$t = 7.38$ <u>WM mean</u> = 0.51 median = 0.52 <u>Perception mean</u> = 0.33 median = 0.32	1.3981E-05

Observed vs shuffled correlation	NHP B, NHP T	17 WM sessions	Wilcoxon Signed Rank Test	Observed vs shuffled null	<i>Rank</i> = 163	0.02
			1-way ANOVA		<i>F</i> (1,32) = 22.5 <u>Observed</u> mean = 0.48 median = 0.50 <u>Shuffled</u> mean = 0.35 median = 0.34	4.2E-05
4.5c Epoch Decoding	NHP B, NHP T	17 WM sessions	T-Test	Decoder vs chance (33%)	t = 9.16 <u>Decoding accuracy:</u> mean = 76% median = 87%	9.1585E-08
4.5d Compare Epochs Decoding	NHP B, NHP T	17 WM sessions	1-way ANOVA Tukey Kramer Post Hoc	Epochs Cue-Delay Cue-Nav Cue-All Delay-Nav Delay-All Nav-All	<i>F</i> (3,64) = 3.3 <u>Cue</u> mean = 0.46 median = 0.52 <u>Delay</u> mean = 0.59 median = 0.66 <u>Navigation</u>	0.03 0.02 0.70 0.94 0.25 0.09 0.96

					<u>Ideal trajectories</u> mean = 0.40 median = 0.43 <u>Real trajectories</u> mean = 0.48 median = 0.50	
4.6d Percent of Shared Neurons Delay	NHP B, NHP T	Ideal trajectories = 12 Center trajectories = 100 All trajectories = 100	1-way ANOVA	Shared neurons between overlapping and non overlapping trajectories	$F(2,209)=0.35$ <u>Ideal mean</u> = 0.38 <u>Center mean</u> = 0.40 <u>All mean</u> = 0.37	0.70
4.6e Correlation Between Sequences Delay	NHP B, NHP T	Ideal trajectories = 12 Center trajectories = 100 All trajectories = 100	1-way ANOVA	Correlation between sequences between overlapping and non overlapping trajectories	$F(5,418) = 36.89$ <u>Shared Ideal mean</u> = 0.23 <u>Shared Center mean</u> = 0.29 <u>Shared All mean</u> = 0.21 <u>All Neurons Ideal mean</u> = 0.07 <u>All Neurons Center</u>	2.61E-31

					<p>mean = 0.10</p> <p><u>All Neurons</u> <u>All</u> <u>Trajectories</u></p> <p>mean = 0.07</p>	
			Tukey Kramer Post Hoc	Shared neuron ideal pairs - shared neuron center pairs		0.99
				Shared neuron ideal pairs - shared neuron all pairs		1
				Shared neuron center pairs - shared neuron all pairs		0.15
				All neuron ideal pairs - All neuron center pairs		0.99
				All neuron ideal pairs - All neuron all pairs		1
				All neuron center pairs - All neuron all pairs		0.99
4.7b Percent correct	NHP B, NHP T	18 Ketamine WM sessions	Kruskal Wallis	Working Memory Injection Period	$H(2,51) =$ 18.75	8.49E-05

		4 Ketamine perception sessions		Perception Injection Period	$H(2,9) = 0.13$	7.7E-05
			Tukey-Kramer Post Hoc		Pre, early post	0.54
					Pre, late post	0.008
					Early-post, late-post	0.94
					<u>Pre injection WM</u> mean = 72% median = 77%	
					<u>Early Post-Injection WM</u> mean = 34% median = 28%	
					<u>Late Post-Injection WM</u> mean = 63% median = 66%	
					<u>Pre Injection Perception</u> mean = 79% median = 84%	
					<u>Early Post-Injection Perception</u> mean = 84% median = 90%	

					<u>Late Post-Injection Perception</u> mean = 85% median = 93%	
4.7c Difference in means	NHP B, NHP T	17 Ketamine WM sessions	Kruskal Wallis Tukey Kramer Post Hoc	Injection period	$F(2,47) = 12.05$	0.002
				Pre, Early post injection		0.001
				Pre, Late post injection		0.07
				Early post injection, late post injection		0.43
					<u>Pre injection</u> mean = 161.9 median = 171.6 <u>Early Post-Injection</u> mean = 40.9 median = 40.2 <u>Late Post-Injection</u> mean = 71.99 median = 100.4	

4.7e Correlation	NHP B, NHP T	17 Ketamine WM sessions	1-way ANOVA Tukey Kramer Post Hoc	Injection period	$F(2,48) =$ 3.14	0.05
				Pre, Early post injection		0.04
				Pre, Late post injection		0.39
				Early post injection, late post injection		0.46
					<u>Pre injection</u> mean = 0.39 median = 0.35	
					<u>Early Post- Injection</u> mean = 0.29 median = 0.29	
					<u>Late Post- Injection</u> mean = 0.34 median = 0.31	

S4.9a Trial-Trial Std	NHP B, NHP T	11 WM sessions	1-way ANOVA	Correct, incorrect, correct shuffle, and incorrect shuffle	$f(3,40) =$ 79.1	7.3E-17
			Tukey Kramer Post Hoc	Correct- correct shuffle		3.77E-09
				Correct- incorrect		3.78E-09
				Correct- incorrect shuffle		3.77E-09
				Correct shuffle- incorrect		0.02
				Correct shuffle- incorrect shuffle		0.99
				Incorrect- incorrect shuffle		0.01
S4.9b Difference in Means	NHP T	6 WM sessions	Wilcoxon Signed Rank Test	Correct and incorrect	$Rank = 14$ <u>Correct</u> mean = 191.12 median =168.74 <u>Incorrect</u> mean = 99.71 median = 108.98	0.56

S4.9c Difference in Means	NHP B	11 WM sessions	Wilcoxon Signed Rank Test	Correct and incorrect	<i>Rank = 55</i> <u>Correct</u> mean = 288.26 median = 277.23 <u>Incorrect</u> mean = 90.09 median = 71.43	0.002
S4.10b Compare Epoch Correlation	NHP B, NHP T	17 WM sessions (Sequences for each epoch considered separately)	1-way ANOVA	Observed correct correlations in cue vs delay vs nav vs all	$F(3,64) = 3.3$ <u>Cue</u> mean = 0.44 median = 0.44 <u>Delay</u> mean = 0.48 median = 0.50 <u>Navigation</u> mean = 0.46 median = 0.48 <u>Delay + Nav</u> mean = 0.50 median = 0.54 <u>All</u> mean = 0.46 median = 0.52	0.64

S4.10c Single Contribution vs Multiple Contributions	NHP B, NHP T	17 WM sessions	Paired T Test	Sparse sequences vs allowing each cell to participate in all 3 sequences	$t = -3.15$ <u>Single mean</u> = 0.48 median = 0.50 <u>Multiple mean</u> = 0.37 median = 0.35	0.006
S4.10d Correlation with Cells Removed Correct Trials	NHP B, NHP T	17 WM sessions	1-way ANOVA Tukey Kramer Post Hoc	Percent of Cells removed 10 - 20% 10 - 30% 10 - 40% 10 - 50% 10 - 60% 10 - 70% 10 - 80% 10 - 90% 20 - 30% 20 - 40% 20 - 50% 20 - 60% 20 - 70% 20 - 80% 20 - 90% 30 - 40% 30 - 50% 30 - 60% 30 - 70% 30 - 80% 30 - 90% 40 - 50% 40 - 60% 40 - 70% 40 - 80% 40 - 90% 50 - 60% 50 - 70% 50 - 80% 50 - 90%	$F(9, 144) =$ 6.26 <u>10%</u> <u>Removed</u> mean = 0.48 <u>20%</u> <u>Removed</u> mean = 0.48 <u>30%</u> <u>Removed</u> mean = 0.48 <u>40%</u> <u>Removed</u> mean = 0.46 <u>50%</u> <u>Removed</u> mean = 0.46	6.56E-06 1 1 0.99 0.99 0.71 0.15 0.15 0 1 1 0.99 0.83 0.24 0.24 0.0001 0.99 0.99 0.78 0.20 0.19 0.0001 1 0.96 0.51 0.50 0.0007 0.98 0.61 0.60 0.001

				60 - 70% 60 - 80% 60 - 90%	<u>60%</u> <u>Removed</u> mean = 0.43	0.99 0.99 0.045
				70 - 80% 70 - 80%	<u>70%</u> <u>Removed</u> mean = 0.40	1 0.39
				80 - 90%	<u>80%</u> <u>Removed</u> mean = 0.40 <u>90%</u> <u>Removed</u> mean = 0.34	0.40
S4.11e Difference in Means	NHP B, NHP T	17 WM sessions 12 ODR Sessions	Kruskal Wallis Tukey Kramer Post Hoc	VR and ODR VR-ODR1 VR-ODR2 ODR1-ODR2	$H(2,34) = 27.2$ <u>VR</u> mean = 253.98 median = 270.93 <u>ODR1</u> mean = 91.53 median = 93.22 <u>ODR2</u> mean = 34.85 median = 31.57	1.2E-06 0.01 1.02E-06 0.29

S4.12a Percent Correct	NHP T	8 Ketamine Sessions	2-way ANOVA	Injection period drug (ketamine, saline)	Drug: $F(1,30)=2.8$	0.107
					Injection Period: $F(2,30)=2.9$	0.066
					Interaction $F(2,30)=2.2$	0.135
					<u>Ketamine</u> <u>Pre</u> mean=54, median=60	0.894
					Ket pre- injection, Sal pre-injection	
					<u>Early-Post</u> mean=30, median=24	0.037
					Ket pre- injection, Ket early post- injection	
					<u>Late-Post</u> mean=47, median=56	1
					Ket pre- injection, Sal early post- injection	
					<u>Saline</u> <u>Pre</u> mean=65, median=70	0.961
Ket pre- injection, Ket late post- injection						
<u>Early-Post</u> mean=55, median=56	0.864					
Ket pre- injection, Sal late post- injection						
<u>Late-Post</u> mean=42, median=57	0.027					
Sal pre- injection, Ket early post- injection						
Sal pre- injection, Sal early post- injection						
	0.972					
Sal pre- injection, Ket late post- injection						
	0.581					
Sal pre- injection, Sal late post- injection						
	0.487					

				Ket early post-injection, Sal early post-injection	0.198
				Ket early post-injection, Ket late post-injection	0.205
				Ket early post-injection, Sal late post-injection	0.873
				Sal early post-injection, Ket late post-injection	0.980
				Sal early post-injection, Sal late post-injection	0.904
				Ket late post-injection, Sal late post-injection	0.993

S4.12b Percent Correct	NHP B	9 Ketamine sessions	2-way ANOVA	Injection period drug (ketamine, saline)	Drug: $F(1,33)=19$	0.001
					Injection Period: $F(2,33)=6.7$	0.0034
					Interaction $F(2,33)=9.5$	0.0005
			Tukey Kramer Post Hoc	Ket pre- injection, Sal pre-injection	<u>Ketamine</u> Pre mean=89, median=90	1
				Ket pre- injection, Ket early post- injection	<u>Early-Post</u> mean=39, median=43	0
				Ket pre- injection, Sal early post- injection	<u>Late-Post</u> mean=80, median=83	0.99
				Ket pre- injection, Ket late post- injection	<u>Saline</u> Pre mean=91, median=90	0.76
				Ket pre- injection, Sal late post- injection	<u>Early-Post</u> mean=93 median=92	0.988
				Sal pre- injection, Ket early post- injection	<u>Late-Post</u> mean=84, median=84	0.0001
				Sal pre- injection, Sal early post- injection		1
Sal pre- injection, Ket late post- injection		0.827				
Sal pre- injection, Sal late post- injection		0.98				

				Ket early post-injection, Sal early post-injection	0
				Ket early post-injection, Ket late post-injection	0.0001
				Ket early post-injection, Sal late post-injection	0.0006
				Sal early post-injection, Ket late post-injection	0.74
				Sal early post-injection, Sal late post-injection	0.96
				Ket late post-injection, Sal late post-injection	0.1

S4.12c Difference in Means	NHP T	8 Ketamine Sessions	Kruskal Wallis	Injection period	$H(2,20) = 4.04$ <u>Pre</u> mean=137 median= 94.9 <u>Early-Post</u> mean=9.6 median= 0.59 <u>Late-Post</u> mean=34.9 median= 70.09	0.13
S4.12d Difference in Means	NHP B	9 Ketamine Sessions	Kruskal Wallis Tukey Kramer Post Hoc	Injection Period Pre, early-post Pre, late-post Early-post, late-post	$H(2,24) = 7.24$ <u>Pre</u> mean=180 median= 187.48 <u>Early-Post</u> mean=68 median= 44.63 <u>Late-Post</u> mean=104. median= 100.76	0.03 0.02 0.24 0.53

S4.12e Correlation	NHP T	8 Ketamine Sessions	1-way ANOVA	Injection Period	$F(2,21) = 1.29$ <u>Pre</u> mean=0.35 median= 0.31 <u>Early-Post</u> mean=0.26 median= 0.26 <u>Late-Post</u> mean=0.34 median= 0.32	0.3
S4.12f Correlation	NHP B	9 Ketamine sessions	1-way ANOVA	Injection Period	$F(2,24) = 2.59$ <u>Pre</u> mean=0.43 median= 0.48 <u>Early-Post</u> mean=0.31 median= 0.25 <u>Late-Post</u> mean=0.35 median= 0.35	0.096
S4.12g Difference in Means	NHP B, NHP T	7 Saline Sessions	Kruskal Wallis	Injection Period	$H(2, 18) = 2.07$ <u>Pre</u> mean=165 median= 164 <u>Early-Post</u> mean=136 median= 144 <u>Late-Post</u> mean=96.7 median=	0.36

					106	
S4.12h Correlations	NHP B, NHP T	7 Saline Sessions	Kruskal Wallis	Injection Period	$H(2, 18) = 2.1$ <u>Pre</u> mean=0.23 median= 0.24 <u>Early-Post</u> mean=0.2 median= 0.28 <u>Late-Post</u> mean=0.36 median= 0.299	0.35

« Curriculum Vitae »

Name: Megan Patricia Roussy

Post-secondary Education and Degrees: University of New Brunswick
Fredericton, New Brunswick, Canada
2012-2016 B.A. (Hon.) Psychology
advisor: Dr. K. Troy Harker

The University of Western Ontario
London, Ontario, Canada
2016-2022 Ph.D. Neuroscience
advisors: Dr. Julio C. Martinez-Trujillo and Dr. Lena Palaniyappan

Honours and Awards:

2022 CIHR Canadian Association of Neuroscience Brain Star Award

2021 Neuroscience Travel Award

2019-2022 Alexander Graham Bell Canada Graduate Scholarship (NSERC, CGS)

2019-2020 Ontario Graduate Scholarship (OGS) - *not accepted*

2018 Neuroscience Travel Award

2018-2019 Jonathan & Joshua Memorial Graduate Scholarship in Mental Health Research

2017-2018 Alexander Graham Bell Canada Graduate Scholarship (NSERC, CGS-M)

2015-2016 Dean's Book Award

2016 Dean's Scholar

2016 Norman S. Fraser Prize in Arts

2016 Dr. Florence Snodgrass Graduating Prize in Psychology

2016 Canadian Psychological Association Certificate of Academic Excellence

2015-2016 Fernando Poyatos Scholarship

2015-2016 Roberta Wilson Weiner Scholarship

2015 Snodgrass Honors Prize in Psychology

2014-2015 Marjorie Barberie Logue CFUW Scholarship

2014-2015 Zula V. Hallett Scholarship (Marysville)

2014 Dr. Florence Snodgrass Memorial Prize- Foundations of Biological Psychology

2014 Dr. Florence Snodgrass Memorial Prize- Foundations of Memory and Cognitive Psychology

2013-2014 Maggie Jean Chestnut Scholarship

2012-2016 Dean's List Recipient

2012-2016 Edwin Jacob Special University Scholarship

2012 Alumni Entrance Scholarship

Publications:

[1] **Roussy, M.**, Busch, A., Luna, R., Leavitt, M. L., Mofrad, M. H., Gulli, R. A.,

- Corrigan, B., Mináč, J., Sachs, A. J., Palaniyappan, L., Muller, L†, & Martinez-Trujillo, J. C. (2022). Neural sequences in primate prefrontal cortex encode working memory in naturalistic environments. *bioRxiv*.
- [2] Corrigan, B. W., Gulli, R., Doucet, G., **Roussy, M.**, Luna, R., Pradeepan, K. S., Sachs, A. J., & Martinez-Trujillo, J. C. (2022). Distinct neural codes in primate hippocampus and lateral prefrontal cortex during associative learning in virtual environments. *Neuron*. doi: 10.1016/j.neuron.2022.04.016
- [3] **Roussy, M.**, Corrigan, B., Rogelio Luna, Gulli, R. A., Sachs, A. J., Palaniyappan, L., & Julio C. Martinez-Trujillo. (2022). Stable working memory and perceptual representations in macaque lateral prefrontal cortex during naturalistic vision. *The Journal of Neuroscience*.
- [4] **Roussy, M.**, Mendoza-Halliday, D., & Martinez-Trujillo, J. (2021). Neural substrates of visual perception and working memory: Two sides of the same coin or two different coins? *Frontiers in Neural Circuits*.
- [5] **Roussy, M.**, Luna, R., Duong, L., Corrigan, B., Gulli, R., Nogueira, R., Moreno-Bote, R., Sachs, A., Palaniyappan, L., & Martinez-Trujillo, J. C. (2021). Ketamine disrupts naturalistic coding of working memory in primate lateral prefrontal cortex networks. *Molecular Psychiatry*.
- [6] Xiang, J., Chen, Y., & **Roussy, M.** (2021). Behavioral inflexibility from a neuronal population perspective. *The Journal of Neuroscience*.
- [7] Blonde, J., **Roussy, M.**, Luna, R., Mahmoudian, B., Gulli, R., Barker, K. C., Lau, J. C., & Martinez-Trujillo, J. C. (2018). Customizable cap implants for neurophysiological experimentation. *Journal of Neuroscience Methods*.

Related Work Experience:

- March 8 - May 2021 **Facilitator** - Public deliberation workshops on AI ethical issues
Advisory Council on Artificial Intelligence, Innovation, Science
and Economic Development Canada, Government of Canada
- Sept 2019-April 2020 **Exam Proctor**
University of Western Ontario
Course Title: Introduction to Psychology
- Sept 2018-May 2019 **Teaching Assistant**
University of Western Ontario
Course Title: Interdisciplinary Medical Science Honours Class
- Oct 2017-Sept 2018 **Technical/Research Support (NHP Support Staff)**
Robarts Research Institute, Western University
- April 2017 **Exam Proctor**
University of Western Ontario
Course Title: Introduction to Psychology
- Sept 2016-Jan 2017 **Teaching Assistant**
University of Western Ontario
Course Title: Anatomy and Cell Biology for Rehabilitation
Neuroscience

Presented Conference Talks:

* Denotes Presenter

- [1] ***Roussy, M.** Impairment of mental representations by ketamine in the primate prefrontal cortex. Brain Mind Institute Psychedelics Workshop. 2021. *Local*.
- [2] ***Roussy, M.**, Resilience of Working Memory Coding in the Primate Lateral Prefrontal Cortex in a Naturalistic Environment. Vision Sciences Society. 2020. *International*.
- [3] ***Roussy, M.**, Luna, R., Duong, L., Palaniyappan, L., and Martinez-Trujillo, J. C. Ketamine impairs behavioural performance and neural coding of spatial working memory in the primate lateral prefrontal cortex. Society for Neuroscience, 2018. *International*.

Presented Conference Posters:

- [1] ***Roussy, M.**, Busch, A., Luna, R., Muller, L., & Martinez-Trujillo, J. Temporal structure of persistent activity in macaque lateral prefrontal cortex during a naturalistic working memory task. Vision Sciences Society, 2022. *International*.
- [2] ***Roussy, M.**, Luna, R., Corrigan, B., Sachs, A., Palaniyappan, L., & Martinez-Trujillo, J. Dissociation between eye position and working memory signals during virtual reality tasks in the primate lateral prefrontal cortex. Canadian Association of Neuroscience, 2021. *National*.
- [3] ***Roussy, M.**, Luna, R., Sachs, A. J., L. Palaniyappan, L., & Martinez-Trujillo, J. C. Cell type specific impairment of working memory by ketamine in primate prefrontal cortex. Roberts Research Retreat, 2021. *Local*.
- [4] ***Roussy, M.**, Luna, R., Corrigan, B., Sachs, A., Palaniyappan, L., & Martinez-Trujillo, J. Dissociation between eye position and working memory signals during virtual reality tasks in the primate lateral prefrontal cortex. Vision Sciences Society, 2021. *International*.
- [5] ***Roussy, M.**, Luna, R., Sachs, A. J., L. Palaniyappan, L., & Martinez-Trujillo, J. C. Cell type specific impairment of working memory by ketamine in primate prefrontal cortex. James A.F. Stevenson Research Day, 2020. *Local*.
- [6] ***Roussy, M.**, Coding of spatial working memory in the primate lateral prefrontal cortex in a naturalistic virtual environment. Gordon Research Conference: Neurobiology of Cognition, 2020. *Conference cancelled due to Covid-19 pandemic. *International*.
- [7] ***Roussy, M.**, Khaki, M., Mortazavi, N., Sachs, A. J., Palaniyappan, L., & Martinez-Trujillo, J. C. Cell type specific impairment of naturalistic spatial working memory coding by ketamine in primate lateral prefrontal cortex. Society for Neuroscience, 2019. *International*.
- [8] Khaki, M., ***Roussy, M.**, Mortazavi, N., Luna, R., Sachs, A. J., Palaniyappan, L., & Martinez-Trujillo, J. C. Naturalistic encoding of spatial working memory in the primate lateral prefrontal cortex in a virtual environment. Society for Neuroscience, 2019. *International*.
- [9] ***Roussy, M.**, Luna, R., Palaniyappan., L., & Martinez-Trujillo, J. C. Systemic antagonism of NMDA receptors disrupts neural encoding of spatial working memory

in the primate prefrontal cortex. Gordon Research Conference: Excitatory Synapses and Brain Function, 2019. *International*.

- [10] *Roussy, M., Luna, R., Palaniyappan, L., Martinez-Trujillo, J. C. Encoding of spatial working memory in virtual reality in the primate prefrontal cortex. Vision Science Society, 2019. *International*.
- [11] *Roussy, M., Luna, R., Palaniyappan, L., & Martinez-Trujillo. Ketamine impairs spatial working memory performance and neural encoding in the primate lateral prefrontal cortex. London Health Research Day, 2019. *Local*.
- [12] *Roussy, M., Luna, R., Palaniyappan, L., & Martinez-Trujillo, J. C. The effect of ketamine on 3D spatial working memory in rhesus macaques. Canadian Association of Neuroscience, 2018. *National*.
- [13] *Roussy, M., Mendoza-Halliday, D., Martinez-Trujillo, J. C., & Palaniyappan, L. Oscillatory neural activity for perceived and memorized representations of motion direction in the primate lateral prefrontal cortex. Society for Neuroscience, 2017. *International*.
- [14] *Roussy, M., Martinez-Trujillo, J. C., & Palaniyappan, L. Measuring spatial working memory in 3D space in Rhesus Macaques. Robarts Research Retreat, 2017. *Local*.

Service Roles:

March 2021 - Present	Committee Chair and Project Lead Evaluation and Reports Committee - Canadian Science Policy Centre (CSPC)
Oct 2019-Present	Reviewing Editor/ Writer Dorsal Column Graduate Student Publication
August 2020-2021	Committee Chair Society of Neuroscience Graduate Students - Information Session Committee
Sept 2019-2021	Elected Council Chair Robarts Research Institute Associations of Trainees
Sept 2019-2021	Mentor Society of Neuroscience Graduate Students Mentorship Program